



# **Smart polymer composite materials for water processing**

Ranwen Ou

M. Eng. (Chemical)

Thesis submitted in fulfilment of the requirements for the degree of

Doctor of Philosophy

Supervisors:

Prof. Huanting Wang

Prof. George P. Simon

Department of Chemical Engineering

Monash University

May 2017



# Smart polymer composite materials for water processing

## Copyright Notices

### Notice 1

Under the Copyright Act 1968, this thesis must be used only under the normal conditions of scholarly fair dealing. In particular no results or conclusions should be extracted from it, nor should it be copied or closely paraphrased in whole or in part without written consent of the author. Proper written acknowledgement should be made for any assistance obtained from this thesis.

### Notice 2

I certify that I have made all reasonable efforts to secure copyright permissions for third-party content included in this thesis and have not knowingly added copyright content to my work without the owner's permission.



---

Ranwen Ou

May 2017

## Declaration

This thesis contains no material which has been accepted for the award of any other degree or diploma at any university or equivalent institution and that, to the best of my knowledge and belief, this thesis contains no material previously published or written by another person, except where due reference is made in the text of the thesis.

A solid black rectangular box used to redact the author's signature.

---

Ranwen Ou

May 2017

## Acknowledgements

My deep gratitude goes first to my supervisors, Professor Huanting Wang and Professor George P. Simon, for their expert guidance, continuous support, encouragement and understanding through my Ph.D. study that benefits me much in the completion and success of this study, as well as my future career.

Secondly, I would like to thank our group members for the encouragement, suggestion, comments and discussion on my research and their companionship during my study. They are Dr Jing Wei, Dr. Huacheng Zhang, Dr Yi Feng, Dr. Kha Tu, Dr Xiaocheng Lin, Dr Seungju Kim, Dr Ze-Xian Low, Dr Soo Kwan Leong, Dr. Ezzatollah Shamsaei, Dr. Jue Hou, Dr. Xiao Xie, Li Wan, Xiaofang Chen, Yan Liang, Yaoxin Hu, Kang Liu, Chen Zhao, Nhi Sa Nguyen, Jeffery Chan, Xingya Li, Jun Lu, Yuqi Wang and Zahra Abbasi. Thanks to my friends, especially Qianqian Shi and Zheng Ma, for their encouragement, support and companion.

Thank you for the support of the staff in Department of Chemical Engineering, especially Kim Phu, Lilyanne, Price, and Jill Crisfield.

Thank you for Monash University and Faculty of Engineering to cover the tuition fee and living expense of my Ph.D study. Thank you for the support of Baosteel-Australia Research and Development Center and the Australian Research Council.

Thank you for the technical assistance with the use of electron microscopes of the staff of Monash Centre for Electron Microscopy (MCEM), especially Dr. Xiya Fang.

Importantly, thank you so much for the unconditional support and love from my beloved family, including my parents, Huazhang Ou and Jieying Qian, and my younger brother, Qingwu Ou. Finally, I would like to express a big thank you for my beloved husband and my best friend, Hao Wu, for his endless encouragement, suggestion, care, and love.

*Ranwen Ou*

Monash University

May 2017

## Abstract

Increasing population and improper industrialization practices have led to detrimental surface and underground water contamination at an unprecedented rate. Therefore, more effective, lower-cost, robust methods to purify water are urgently needed, without further stressing the environment or endangering human health by the treatment itself. Stimuli-responsive materials, which can respond to environmental conditions, have recently attracted much attention in water treatment. In this thesis, three types of responsive material for water processing are developed: responsive separation membrane, responsive forward osmosis draw agent, and responsive adsorbent.

Recently, stimuli-responsive surfaces with switchable superwettability have attracted growing interest for controlled oil-water separation. The fabrication of such smart membranes with good mechanical properties, excellent recycling properties, and the ability to separate oil-water emulsions productively and inexpensively is highly desirable. In this thesis, a robust, thermo-responsive polymer membrane is produced by the combination of thermoplastic polyurethane (TPU) microfibre web and poly (N-isopropyl acrylamide) (PNIPAM). The TPU-PNIPAM membrane possesses switchable superhydrophilicity and superhydrophobicity as the temperature of membrane changes from 25 to 45 °C. The composite membrane is able to separate a 1 wt. % oil-in-water emulsion and 1 wt. % water-in-oil emulsion at 25 and 45 °C, respectively, with a high separation efficiency of  $\geq 99.26$  %. Furthermore, the composite membranes show excellent mechanical properties, and they are highly flexible and mechanically tough.

The feasibility of using stimuli responsive polymer hydrogels as draw agent in the forward osmosis (FO) desalination was recently demonstrated by our group for the first time. The swelling pressure of hydrogel, the effective contact area between FO membrane and hydrogel, and the water transport through the draw agent are key factors affecting water flux. In this study, hydrophilic microfibre and hydrophobic microfibre are blended with hydrogel to prepare composite monoliths, respectively, and the relevant FO performance and improvement mechanism are studied. The incorporation of both hydrophilic and hydrophobic microfibres results in enhanced FO water flux of hydrogel monolith. Whilst the addition of hydrophilic microfibres is good for dewatering, the hydrophobic microfibre does reduce the dewatering flux. The 1<sup>st</sup> hour FO water flux and dewatering flux of hydrophilic TPU microfibre- poly (sodium acrylate) (PSA) monolith are 1.81 and 3.51 L m<sup>-2</sup> h<sup>-1</sup>, respectively, twice of those for

PSA particles. The water flux of PSA – hydrophobic polyester microfibre composite (PSA – PET) reaches 5.0 LMH in the first 10 mins, twice as high as the relevant pure hydrogel alone. Conversely, the dewatering flux of PSA-PET decreases to half of those of pure hydrogel. The kinetic swelling studies show that the use of monolithic hydrogels and the addition of hydrophilic microfibrils enhance water diffusion through the draw agent and sustain high swelling pressure, resulting in improved FO performance. On the other hand, the combination of hydrophilic ionic hydrogel and hydrophobic PET microfibre produced pores in the composite hydrogel because of different wettability, with an additional relaxation force preserved in the composites because of the compressed pressure applied during the preparation. Thus, the porous structure improves the water diffusion, while the compressed pressure enhances the polymer chain relaxation rate.

The introduction of responsive ability potentially advances MOFs more flexible for fundamental studies and other applications, such as controllable adsorption and separation, energy storage and clean energy, sensing, catalysis. Ion adsorption is of great environmental, technological, and biological importance, and it has been widely applied in separation, purification, catalysis, food processing, and pharmaceutical industry. Here, an amphoteric MOF-based ion adsorbent has been designed for stimuli-responsive ion sorption, especially for monovalent ions, by integrating weak acid groups with base groups. This is achieved by post-synthesis modification of MIL-121 via in situ polymerization of tertiary amine monomer introduced in the porous framework. The equilibrium NaCl adsorption capacity of the amphoteric MOF is 0.92 meq/g, which occupies 77 % of ion adsorption sites, demonstrating the efficiency of amphoteric MOF ion adsorbent. The adsorbed salt can be recovered and the MOF-based ion adsorbent can be regenerated with excellent cycle performance. Except for NaCl, the amphoteric MIL-121 is also able to adsorb other monovalent and divalent cations. This study indicates that the introduction of stimuli responsiveness advances the water treatment process to a controllable or “smarter” era, aiming at developing a more convenient, efficient, energy-saving, and environmental friendly water processing system.

This study indicates that the introduction of stimuli responsiveness advances the water treatment process to a controllable or “smarter” era, aiming at developing a more convenient, efficient, energy-saving, and environmental friendly water processing system.

## List of Publications

### Journal Publications:

- [1] **Ranwen Ou**, Jing Wei, Lei Jiang, George P. Simon, and Huanting Wang, Robust thermoresponsive polymer composite membrane with switchable superhydrophilicity and superhydrophobicity for efficient oil-water separation. *Environ. Sci. Technol.* **2016**, 50, 906-914
- [2] **Ranwen Ou**, Huacheng Zhang, George P. Simon, Huanting Wang, Microfibre-polymer hydrogel monolith as forward osmosis draw agent. *J. Membr. Sci.* **2016**, 510, 426-436
- [3] **Ranwen Ou**, Huacheng Zhang, George P. Simon, Huanting Wang, Modification of swelling property of ionic hydrogel for forward osmosis application, *Ind. Eng. Chem. Res.*, **2017**, 56 (2), pp 505–512
- [4] **Ranwen Ou**, Huacheng Zhang, Jing Wei, Li Wan, Yaoxin Hu, George P. Simon, and Huanting Wang, Functionalized Metal Organic Framework with Thermoreversible Ion Sorption Property for Efficient Water Desalination, to be submitted.

### Oral Presentations:

- [1] **Ranwen Ou**, Jing Wei, Huanting Wang, Hydrogel composite monolith as forward osmosis draw agent, International Forward Osmosis Summit 2016, Sydney, Australia
- [2] **Ranwen Ou**, Huacheng Zhang, George P. Simon, Huanting Wang, Hydrophilic microfibre-polymer hydrogel monolith as forward osmosis draw agent, 9<sup>th</sup> International Membrane Science and Technology Conference, Adelaide, Australia

### Other Publications during PhD study:

- [1] **Ranwen Ou**, Yaqin Wang, Huacheng Zhang, Huanting Wang, Tongwen Xu, Preparation of high-flux ultrafiltration membranes by blending strongly charged polymer. *J. Appl. Polym. Sci.* 2016, DOI: 10.1002/APP.44570
- [2] Jing Wei, Ze-xian Low, **Ranwen Ou**, George P. Simon, Huanting Wang. Hydrogel-polyurethane interpenetrating network material as an advanced draw agent for forward osmosis process. *Water Res.* **2016**, 96, 292-298.

[3] Seungju Kim, Xiaocheng Lin, **Ranwen Ou**, Huiyuan Liu, Xiwang Zhang, George P. Simon, Christopher D. Easton and Huanting Wang, Highly crosslinked, chlorine tolerant polymer network entwined graphene oxide membrane for water desalination. *J. Mater. Chem. A*, 2017, 5, 1533-1540

[4] Huacheng Zhang, Ye Tian, Jue Hou, Xu Hou, Guanglei Hou, **Ranwen Ou**, Huanting Wang, Lei Jiang, Bioinspired smart gate-location-controllable single nanochannels: experiment and theoretical simulation. *ACS Nano*. 2015, 9 (12), 12264-12273

[5] Li Wan, Jing Wei, Yan Liang, Yaixin Hu, Xiaofang Chen, Ezzatollah Shamsaei, **Ranwen Ou**, Xiwang Zhang, Huanting Wang, ZIF-derived nitrogen-doped carbon / 3D graphene frameworks for all-solid-state supercapacitors. *RSC. Adv.* 2016, 6, 76575-76581

# Table of Contents

Copyright Notices .....	i
Declaration.....	ii
Acknowledgements.....	iii
Abstract.....	iv
List of Publications .....	vi
List of Figures.....	xi
List of Tables .....	xix
Chapter 1 Introduction .....	1
1.1 Research Background .....	1
1.2 Research Aims .....	3
1.3 Thesis Overview .....	5
1.4 References.....	8
Chapter 2 Literature Review .....	10
2.1 Water Treatment .....	10
2.1.1 Water issue.....	10
2.1.2 Conventional water treatment system.....	12
2.1.3 Advanced water treatment technologies .....	14
2.2 Stimuli Responsive Polymeric Materials.....	32
2.2.1 Type of responsive polymers .....	32
2.2.2 Applications .....	39
2.3 Responsive Materials for Water Treatment .....	41
2.3.1 Responsive membrane .....	41
2.3.2 Responsive draw agent.....	51
2.3.3 Responsive adsorbent.....	55
2.4 Summary.....	58
2.5 References.....	59
Chapter 3 Robust thermo-responsive polymer composite membranes with switchable superhydrophilicity and superhydrophobicity for efficient oil-water separation.....	80
Overview .....	80
3.1 Introduction.....	81
3.2 Experimental .....	84
3.2.1 Materials .....	84
3.2.2 Experimental procedures.....	84
3.3 Results and Discussion .....	86
3.3.1 Preparation and morphology .....	86

3.3.2 Mechanical properties .....	90
3.3.3 Wettability.....	92
3.3.4 Swelling behaviour .....	95
3.3.5 Oil water separation capacity .....	96
3.4 Summary .....	102
3.5 References.....	103
Chapter 4 Microfibres-polymer hydrogel monolith as forward osmosis draw agent .....	107
Overview .....	107
4.1 Introduction.....	108
4.2 Experimental .....	110
4.2.1 Materials .....	110
4.2.2 Experimental procedures.....	110
4.3 Results and discussion .....	113
4.3.1 Morphology of composite hydrogels .....	113
4.3.2 Swelling properties of hydrogels .....	113
4.3.3 Water diffusion in composite hydrogels .....	116
4.3.4 Forward osmosis performance of hydrogels .....	117
4.3.5 Swelling mechanism of hydrogels .....	127
4.4 Summary .....	128
4.5 References.....	128
Chapter 5 Improvement of the swelling properties of ionic hydrogels by the incorporation of hydrophobic, elastic microfibres for forward osmosis applications .....	132
Overview .....	132
5.1 Introduction.....	133
5.2 Experimental .....	135
5.2.1 Materials .....	135
5.2.2 Experimental Procedures .....	135
5.3 Results and Discussion .....	138
5.3.1 Morphology of PET-hydrogel composites.....	138
5.3.2 Swelling behaviour of hydrogels .....	140
5.3.3 Forward osmosis and dewatering performance.....	145
5.3.4 Effect of hydrophilic or hydrophobic fibres on FO performance of hydrogels .....	147
5.4 Summary .....	150
5.5 References.....	151
Chapter 6 Functionalized Metal Organic Framework with thermoreversible ion sorption property for efficient water desalination .....	153
Overview .....	153
6.1 Introduction.....	154

6.2 Experimental .....	156
6.2.1 Materials .....	156
6.2.2 Experimental Procedures .....	156
6.3 Results and Discussion .....	158
6.3.1 Modification of amphoteric MOFs .....	158
6.3.2 Morphology salt adsorption of MOFs.....	161
6.3.3 Adsorption and thermal desorption mechanisms .....	162
6.3.4 NaCl adsorption capacity of amphoteric MOFs.....	164
6.3.5 Cycling performance of amphoteric MOFs .....	165
6.3.6 Adsorption of other ions .....	166
6.4 Summary .....	168
6.5 References.....	168
Chapter 7 Conclusion and Future Work .....	173
7.1 Conclusion .....	173
7.2 Further Directions .....	175

## List of Figures

### Chapter 2

2.1 World map of water withdrawal and consumption and sanitation accessibility.....	10
2.2 Schematic illustration of conventional water treatment process.....	12
2.3 Traditional (chlorine) and advanced oxidation process and number of AOP publications over 1975-2000 period.....	16
2.4 Illustration of different membrane filtration processes.....	28
2.5 Scheme of membrane filtration.....	28
2.6 Illustration of reverse osmosis and forward osmosis process.....	31
2.7 Definition of responsive polymeric materials.....	32
2.8 Chemical structures of LCST polymers.....	33
2.9 Chemical structures of moieties for synthesis of photo-responsive polymers.....	35
2.10 Several applications of stimuli responsive material.....	40
2.11 A schematic representation of the thermo-responsive release principle of core-shell microcapsules with a porous membrane and thermo-responsive PNIPAM gates.....	45
2.12 The extended and contracted state of porous and bulk nonporous responsive membrane and their permeation upon solutes.....	46
2.13 Controllable oil water separation using pH responsive membrane.....	48
2.14 Alternative temperature change cleaning procedures of raw ZrO <sub>2</sub> and PNIPAM-g-ZrO <sub>2</sub> membrane.....	50
2.15 Schematic illustration of forward osmosis desalination process.....	51
2.16 Quasi-continuous FO desalination using a semi-IPN hydrogel as the draw agent.....	54

### Chapter 3

3.1 Schematic illustration of robust thermo-responsive composite membrane.....	80
--	----

<b>3.2</b>	The preparation process of TPU microfibre mat by a force spinner.....	85
<b>3.3</b>	(a) The preparation process of a TPU-PNIPAM composite membrane. The TPU microfibre membrane immersed with NIPAM reaction solution (16.7 wt. %) is polymerized at 70 °C for 2 hours. Photographs of twisting test of (b) TPU microfibre membrane and (c) TPU-PNIPAM membrane with 3.6 wt. % PNIPAM loading (TPU-PNIPAM-3.6). (d) Stress-strain curves of TPU microfibre membrane and swollen TPU-PNIPAM-3.6 membrane.....	86
<b>3.4</b>	Contact angle-time curves of TPU film with DDI water and NIPAM solution (16.67 wt. %) as testing medium.....	87
<b>3.5</b>	Schematic diagram of formation of TPU-PNIPAM composite. (a) Free radical polymerization of PNIPAM hydrogel, (b) basic chemistry of TPU, (c) polymerization of PNIPAM hydrogel on the TPU microfibre's surface. The hydrogen bonds formed between urethane groups and acrylamide groups combined two polymers.....	87
<b>3.6</b>	(a) SEM image and (b) diameter distribution of TPU microfibre membrane.....	88
<b>3.7</b>	SEM images of TPU microfibre membrane and TPU-PNIPAM composite membranes (3.6 and 13.4 wt. %). Membrane surfaces of (a) TPU microfibre membrane (558×), (b) TPU-PNIPAM-3.6 (811×) and (c) TPU-PNIPAM-13.4 membrane (683×); microfibre surfaces of (d) TPU microfibrils (71202×), (e) TPU-PNIPAM-3.6 (67286×) and (f) TPU-PNIPAM-13.4 (35187×); microfibre cross-sections of (g) TPU microfibrils (38448×), (h) TPU-PNIPAM-3.6 (43471×) and (i) TPU-PNIPAM-13.4 (2885×) .....	88
<b>3.8</b>	(a) SEM image and (b) pore size distribution of composite membrane with 3.6 wt. % PNIPAM (TPU-PNIPAM-3.6), and (c) SEM image and (d) pore size distribution of TPU-PNIPAM-13.4 membrane.....	89
<b>3.9</b>	Membrane thickness and PNIPAM coating thickness of composite membranes (1.4, 3.6, 7.6, 13.4, and 25.3 wt. % ).....	90
<b>3.10</b>	(a) elongation, (b) tensile strength, (c) Young's modulus, and (d) toughness of TPU microfibre membrane (0 wt. %) and TPU-PNIPAM membranes (1.4, 3.6, 7.6, 13.4, and 25.3 wt. % ).....	91
<b>3.11</b>	Water contact angle images of (a) TPU film and (b) TPU microfibre membrane.....	92

<b>3.12</b>	(a) Water contact angles of swollen TPU-PNIPAM membranes (1.4, 3.6, 7.6, 13.4, and 25.3 wt. %) and the swollen PNIPAM hydrogel (100 wt. %) at room temperature (RT) and 45°C. (b) Schematic diagram of switching wettability of TPU-PNIPAM membrane at different temperatures. (c) A water droplet (1μL) spreading on a swollen TPU-PNIPAM-3.6 membrane within 0.094 s at room temperature. (d) Water contact angle (150.2°) of swollen TPU-PNIPAM-3.6 membrane at 45 °C. (e) Underwater oil contact angle (141.3°) of swollen TPU-PNIPAM-3.6 membrane at room temperature. (f) Underwater oil contact angle of swollen TPU-PNIPAM-3.6 membrane at 45°C. Hexadecane was used for testing the underwater oil contact angle.....	93
<b>3.13</b>	SEM images of composite membranes and the relevant water contact angle. (a) TPU-PNIPAM-1.4, (b) TPU-PNIPAM-3.6, (c) TPU-PNIPAM-7.6, (d) TPU-PNIPAM-13.4, (e) TPU-PNIPAM-25.3. (f) Water contact angle of composite membranes and PNIPAM hydrogel at room temperature and 45 °C.....	94
<b>3.14</b>	Photographs of TPU-PNIPAM-3.6 immersed into DDI water at different temperatures: (a) room temperature, (b) 45 °C.....	94
<b>3.15</b>	Swelling properties of the PNIPAM of TPU-PNIPAM-3.6 membrane. (a) Swelling curve of dry TPU-PNIPAM-3.6 membrane. (b) Swelling ratio of TPU-PNIPAM-3.6 membrane at different temperatures. (c) Deswelling curve of TPU-PNIPAM-3.6 membrane tested at 45 °C DDI water. (d) Reswelling curve of TPU-PNIPAM-3.6 membrane tested at 25°C DDI water.....	95
<b>3.16</b>	(a) Oil intrusion pressure and water flux of TPU-PNIPAM membranes (1.4, 3.6, 7.6, 13.4, and 25.3 wt. %) at room temperature. (b) Water intrusion pressure and oil flux of TPU microfibre membrane and TPU-PNIPAM membranes at 45 °C. Hexadecane was used as the test oil. (c) Separation efficiency of TPU-PNIPAM-3.6 membrane for reversibly oil-water separation at room temperature and 45 °C. The inset shows the 1 wt. % SDS-stabilized silicone oil-water emulsion and the collected water before and after separation at room temperature (left), and the 99 wt. % SDS-stabilized silicone oil-water emulsion and the collected oil before and after separation at 45 °C (right). (d) Separation efficiencies of TPU-PNIPAM-3.6 membrane for separating different 1 wt. % oil-water emulsions at room temperature.....	97

<b>3.17</b>	Controllable oil-water separation using TPU-PNIPAM-3.6 membrane at (a) room temperature and (b) 45 °C respectively (hexadecane: red, water: transparent).....	98
<b>3.18</b>	(a) The variation of flux as a function of time for 24 h separation of 1 wt. % SDS – stabilized hexadecane-water emulsion. (b) The variation of flux as a function of time for 24 h separation of 99 wt. % SDS-stabilized hexadecane-water emulsion. TPU-PNIPAM-3.6 was used in the test of (a) and (b).....	98
<b>3.19</b>	Optical microscopy images and diameter distribution of oil drops in 1 wt. % oil-water emulsion and water drops in 99 wt. % oil-water emulsion.....	100
<b>3.20</b>	Optical microscopy images SDS-stabilized 1 wt. % oil-water emulsions before (a1-e1) and after (a2-e2) filtration.....	101
<b>3.21</b>	Optical microscopy images SDS-stabilized 99 wt. % oil-water emulsions before (a1-b1) and after (a2-b2) filtration.....	102
 <b>Chapter 4</b>		
<b>4.1</b>	Schematic illustration of water transport in TPU-hydrogel composite.....	107
<b>4.2</b>	The preparation process of TPU-hydrogel composites.....	111
<b>4.3</b>	Water flux of PN5S5 hydrogel particle and PN5S5 composite hydrogels with different TPU loadings.....	111
<b>4.4</b>	SEM images of TPU microfibrils and cross-section of composite hydrogels.....	113
<b>4.5</b>	Swelling ratios of pure hydrogel and composite hydrogels.....	114
<b>4.6</b>	(a) Swelling behavior and (b) swelling kinetics of pure hydrogel (PN5S5) and composite hydrogel (TPU-PN5S5) .....	115
<b>4.7</b>	Wettability of TPU microfibrils and water absorption ability of hydrogels.....	116
<b>4.8</b>	(a) The swelling of pure hydrogel (left) and composite hydrogel (right) in aqueous rhodamine B (RhB) solution. (b) The water absorption process of composite hydrogel (50 wt. % water content) tracked by rhodamine B aqueous solution. These images were taken with an optical microscope.....	117
<b>4.9</b>	One hour FO water flux of pure hydrogel particle and composite hydrogels.....	118

<b>4.10</b> SEM images of pure hydrogel particles.....	119
<b>4.11</b> The first 10 min FO water fluxes of PSA particle and wet TPU-PSA composite, with 2000 ppm NaCl solution or pure water as feed.....	120
<b>4.12</b> 24 hours forward osmosis water flux of (a) pure hydrogel particle and (b) composite hydrogels with 50 wt. % initial water content; average dewatering flux of (c) pure hydrogel particle and (d) composite hydrogels as a function of SA content.....	122
<b>4.13</b> Forward osmosis and solar dewatering performance of pure hydrogel particle and composite hydrogels .....	123
<b>4.14</b> Liquid and vapour water recovery of hydrogels in the dewatering process.....	124
<b>4.15</b> Temperature changes of (a) pure hydrogel particle and (b) composite hydrogels under a 1 kW·m <sup>-2</sup> incandescent heat dewatering process.....	124
<b>4.16</b> Reusability of (a) PSA particles and (b) TPU-PSA. 5 cycles of forward osmosis and dewatering performance were tested.....	125
<b>4.17</b> The swelling ratio of PSA and TPU-PSA under different osmotic pressure (different concentration of NaCl solution) .....	126
<b>4.18</b> The proposed swelling mechanisms of (a) pure hydrogel particle and (b) TPU-hydrogel composite.....	127

## **Chapter 5**

<b>5.1</b> Illustration of the swelling pressure improvement of PET-hydrogel composite.....	132
<b>5.2</b> The preparation process of hydrogel-PET microfibre composite.....	137
<b>5.3</b> The solar dewatering setup for measuring the liquid water recovery.....	138
<b>5.4</b> SEM images of (a) PN5S5 hydrogel and (b) PET microfibrils.....	139
<b>5.5</b> (a-c) Surface and (d-f) cross-sectional SEM images of composite hydrogels.....	139
<b>5.6</b> (a) Swelling ratio and (b) swelling kinetics of hydrogels with different loadings of PET microfibrils, and (c) forward osmosis water flux induced by the hydrogel and its composites.....	141

<b>5.7</b>	The optical images of pure PN5S5 hydrogel and PN5S5-PET-0.5/0.5 composite hydrogel (a) before and (b) after swelling in aqueous rhodamine B (RhB) solution.....	142
<b>5.8</b>	(a) Swelling ratio and (b) swelling kinetics of PN5S5-PET-0.5/0.5 hydrogels prepared with different compression pressure, and (c) forward osmosis water flux induced by the hydrogel draw agent.....	143
<b>5.9</b>	The 60 mins forward osmosis water flux of PSA composite with (a) different PET fibres loading, and (b) different compressed pressure loading.....	144
<b>5.10</b>	Plot of swelling ratio of PN5S5 and PN5S5-PET-0.5/0.5-18 as a function of osmotic pressure of NaCl solution at equilibrium.....	144
<b>5.11</b>	(a) 24 hours FO water flux, and (b) dewatering performance of hydrogels.....	145
<b>5.12</b>	The temperature change of pure hydrogel and composite hydrogel during 60 mins solar dewatering under 1 kW/m <sup>2</sup> incandescent lamp.....	146
<b>5.13</b>	The cycle performance of PN5S5-PET-0.5/0.5-18 composite.....	146
<b>5.14</b>	SEM images of (a) PET microfibre and (b) polydopamine coated PET microfibre.....	147
<b>5.15</b>	Wettability of PET microfibre, polydopamine coated PET microfibre and their composite hydrogels.....	147
<b>5.16</b>	Contact angle of PET (a, c) and D-PET (b, d) microfibrils with NIPAM solution (a, b) and SA solution (c, d) as testing medium.....	148
<b>5.17</b>	Optical images of (a, b) PN5S5-PET and (c, d) PN5S5-D-PET hydrogel before and after dropping a drop of 100 ppm RhB solution.....	149
<b>5.18</b>	(a) Forward osmosis water flux and (b) dewatering performance of PN5S5-PET-0.5/0.5-18 and PN5S5-D-PET-0.5/0.5-18.....	149

## **Chapter 6**

<b>6.1</b>	Illustration of reversible ion sorption with functionalized MOF.....	153
<b>6.2</b>	Schematic illustration of the synthesis of amphoteric-functionalized MIL-121 (PDMVBA-p-MIL-121) and its thermoreversible adsorption process.....	155

<b>6.3</b> The SEM images of MIL-121 crystals calcined at different temperatures.....	158
<b>6.4</b> FTIR spectra of MIL-121 powder calcined at different temperatures.....	159
<b>6.5</b> XRD patterns of MIL-121 powders calcined at different temperatures.....	159
<b>6.6</b> The adsorption capacity (1000 ppm NaCl solution) of PDMVBA-p-MIL-121 prepared with MIL-121 powders calcined at different temperatures, and 3 days of impregnation time before polymerization.....	160
<b>6.7</b> The adsorption capacity (1000 ppm NaCl solution) of PDMVBA-p-MIL-121 prepared with different impregnation time before polymerization and MIL-121-300°C.....	160
<b>6.8</b> TEM images of (a) as-prepared MIL-121-300 °C and (b) after kept in water under stirring for one month.....	160
<b>6.9</b> Characterization of MIL-121 and PDMVBA-p-MIL-121. SEM images of (a) MIL-121-300 °C and (b) PDMVBA-p-MIL-121. (c) NaCl adsorption capacity of PDMVBA, MIL-121-300°C and PDMVBA-p-MIL-121. (d) XRD patterns of as-prepared MIL-121, MIL-121-300 °C, and PDMVBA-p-MIL-121 before and after NaCl adsorption. The red arrows on the peaks show the peak shift of pattern MIL-121-300 °C compared with the XRD pattern of MIL-121. (e) FTIR spectra of MIL-121-300 °C, and PDMVBA-p-MIL-121 before and after NaCl adsorption.....	161
<b>6.10</b> The MgCl <sub>2</sub> adsorption capacity of PDMVBA, MIL-121-300°C and PDMVBA-p-MIL-121.....	162
<b>6.11</b> Thermogravimetric analysis curves and the relevant derivative of (a) MIL-121, (b) MIL-121-300°C, (c) PDMVBA-p-MIL-121-300°C, and (d) PDMVBA-p-MIL-121-300°C-NaCl. The TGA was conducted under N <sub>2</sub> gas flow.....	162
<b>6.12</b> The adsorption capacity of PDMVBA-p-MIL-121 at different NaCl concentrations...	165
<b>6.13</b> a) The cycling performance of PDMVBA-p-MIL-121 for thermoreversible sorption of 10000 ppm NaCl solution. The PDMVBA-p-MIL-121 was thermally regenerated at 80 °C in 500 ppm NaCl solution. b) FTIR spectra of PDMVBA-p-MIL-121 before and after NaCl adsorption, and after thermal desorption.....	165

<b>6.14</b> The FTIR spectra of PDMVBA-p-MIL-121 before and after the adsorption of NaCl, and after thermal regeneration.....	166
<b>6.15.</b> The adsorption capacity of PDMVBA-p-MIL-121 for adsorption of different monovalent and divalent cations.....	166

## List of Tables

### Chapter 2

2.1 Redox potential of oxidants.....15

2.2 Specific surface area and applications of adsorbents.....21

### Chapter 3

3.1 Superwetting membranes and relevant properties for oil-water separation published in recent years.....82

### Chapter 4

4.1 Composition of pure hydrogels and composite hydrogels.....110

4.2. The water flux of hydrogel draw agent in recent publications.....121

### Chapter 5

5.1 Composition of pure hydrogel and composite hydrogels.....136

### Chapter 6

6.1 The radius, hydration energy, and solubility of relevant benzoic acid salt of cations.....167



## Chapter 1 Introduction

### 1.1 Research Background

Some 97 % of water on earth exists as ocean saltwater, 0.5 % is brackish water found in surface estuaries and salty underground aquifers, whilst fresh water only constitutes 2.5%. Of this freshwater, less than one percent is usable by humans, because most freshwater is locked into polar icecaps or permanent mountain snow cover.[1] It is estimated that 1.2 billion people lack access to safe drinking water, 2.6 billion have little or no sanitation, and millions of people die annually-3,900 children a day-from severe waterborne diseases.[2] However, increasing population and poor industrialization practices have led to detrimental surface and underground water contamination at an unprecedented rate, worsening this situation. Much effort has been made into the purification of contaminated water, since the total amount of usable freshwater is limited. Even though conventional water treatment methods can address many of these problems, they are often chemically, energetically and operationally intensive. The chemicals used in the treatment will become the contamination sources of freshwater. In addition, developing a conventional water and wastewater treatment facility require considerable infusion of capital and time, which precludes their use in much of the world, especially where water is really needed.[3] More effective, lower-cost, robust methods to purify water are urgently needed, without further stressing the environment or endangering human health by the treatment itself.

Advanced water treatment technology has been developed to deal with this problems. In the past several decades, advanced oxidation process, biological treatment, adsorption / ion exchange process and membrane separation process have attracted intensive attention, and proven to be suitable for practical application.

Advanced oxidation processes (AOPs) deal with the chemically polluted water and wastewater, and has shown great potential for the treatment of ground water, municipal wastewater sludge and volatile organic compounds (VOCs).[4, 5] AOPs are also capable of treating problematic pollutants in water that may not be removed by conventional treatment method effectively, such as persistent organic pollutants, which is toxic, stable and active in the environment. The AOP aims to mineralize the organic pollutant into relatively harmless inorganic molecules, such as carbon dioxide, water, sulphates and nitrate.[6] Biological treatment has been used for consuming biodegradable soluble organic contaminants and

removal of nitrogen and phosphorus in the conventional wastewater treatment system.[7] The practical value of biological water treatment technologies arise for several reasons. Firstly, this process is operationally practical, it can be carried out in situ at the polluted site. Secondly, it is an environmentally friendly technology, without generating secondary pollution. Thirdly, it is cost-effective. The recent development of this utilized technology is concentrated on removal of metal ions and oils.

Membrane filtration has proven to be one of the most promising separation techniques.[8] Membrane separation processes, like microfiltration, ultrafiltration, nanofiltration, reverse osmosis, in water treatment have increased rapidly over the past decade.[9] Microfiltration and ultrafiltration process are widely used in food and beverage processing, biotechnological applications and pharmaceutical industry, water purification and others. [10-12] Nanofiltration and reverse osmosis process are mainly used for water purification. [13, 14] Seawater reverse osmosis (SWRO) plants have been built to undertake seawater desalination to alleviate the water scarcity problem, even though they are energy-intensive. Low-pressure driven membrane processes (microfiltration / ultrafiltration) are highly promising due to their relatively low energy consumption. Forward osmosis (FO), which has been widely investigated for desalination and wastewater treatment, is renowned for little or no operation pressures, high rejection over a wide range of contaminants and lower membrane fouling propensity than pressure-driven membrane processes.[15] Compared to the traditional water treatment methods, membrane filtration technique has the following advantages: (1) it is a simple, low capital cost, low-maintenance process; (2) the systems are compact, and some of them are portable; ultrafiltration setup can be connected to the tap to purify the tap water; (3) it is an environmentally-friendly process, without the need for addition of chemicals during the treatment.

Adsorption is of great environmental, technological, and biological importance, as often stressed. Generally, porous solid materials are used as adsorbent for gas-phase and liquid-phase adsorption, e.g. active carbons, metal oxides, zeolites, clays, and metal organic framework.[16] Adsorption at the liquid/solid interface is of great importance in industry and everyday life, such as in detergents, adhesion, lubrication, flotation of minerals, water treatment, oil recovery, pigments and particle technology. To efficiently decontaminate aqueous wastes, both adsorption and ion exchange are considered to be highly effective and affordable/low-cost methods.

“Smart” or responsive polymer materials respond to surrounding environments by changing their physicochemical properties, such as regulating transport of ions and molecules, changing wettability and adhesion of different species on external stimuli, or converting chemical and biochemical signals into optical, electrical, thermal and mechanical signals, and vice versa.[17] In addition to the fundamental interest, responsive materials are playing an increasingly important role in a variety of applications, such as drug delivery, tissue engineering, biosensors, coatings, as well as the emerging environmental applications.[18] The introduction of a responsive ability or “smartness” endows a designated material or device with multiple synergistic and advanced functions, broaden its applications and promote its performance.

With the rapid development of responsive polymer materials, smart systems have been incorporated with the filtration system for separation and purification purposes, responsive membrane, responsive draw agent and responsive adsorbent have emerged, and gaining increasing concern in the recent decades. The occurrence of smart membrane have realized the controllable separation process, and bridged to anti-fouling membrane and biomimetic membrane. Smart draw agent, which can recover the water with low energy cost, lights the future of forward osmosis desalination process. The responsive adsorbent that can be regenerated and recycled by stimuli, especially physical stimuli, is ideal for resource reclamation from contaminated water or water softening. The smart filtration system with self-cleaning, self-refreshing, energy-saving, or controllable separation abilities will improve the efficiency of many technological processes, and has strong potential for future applications.

## **1.2 Research Aims**

Responsive membrane systems with switchable properties and highly adaptive surfaces have been manufactured in recent decades, but most have been focused on how different responsive interactions within the membranes can be tuned and monitored in controlled environments, such as permeation and pore size. The challenges of responsive membrane for water treatment lie in: (1) how to achieve functionality while maintaining membrane stability and mechanical integrity for the practical application; (2) how to fabricate a membrane which can respond in more complex and less defined situations and mimic the functionalities of living systems. It is thought that responsive membranes will be used in various niche applications in the next 5-10 years, and be more widely use in 10-20 years.[19] It is a challenge, yet highly desirable to explore the field of responsive membrane with better properties and practical applications.

Meanwhile, only a few responsive materials have been investigated as draw agents, including magnetic particles, responsive polyelectrolyte and hydrogel. Responsive hydrogels, which shows great potential for practical application, have been developed by our group.[20, 21] Using responsive FO draw agent shows several advantages, such as the ready recovery of product water and draw agent, and low back diffusion. However, there are still some challenges upon the applications of responsive draw agent: 1) relatively low water flux, 2) incomplete theoretical study, 3) reusability, 4) development of proper FO unit for continuous water production.

Responsive adsorbents have been intensively studied in the past several decades, primarily magnetic responsive adsorbent for easy collection and separation from aqueous solution. Other responsive materials introduced are mainly used to tune the wettability and adhesion of different species for the selective adsorption purpose. The regeneration of adsorbent by stimuli responsiveness can significantly reduce the cost of adsorption process, but investigates rarely. The development of stimuli-responsively regenerable adsorbent with high adsorption and proper reusability is highly desirable.

The development of practical responsive forward osmosis draw agents, responsive separation membranes and responsive adsorbent is thus still at an early stage.

The research aim of this study is to introduce stimuli responsive ability into the water treatment system, and analyze the effect of responsiveness on the performance of the material and process, aiming to improve the performance and understand the improvement mechanisms. More specifically,

#### 1. Development of high efficiency separation membranes for water treatment

- (1) Introducing responsiveness to a membrane/film by incorporating responsive polymer;
- (2) Introducing special wettability into the responsive composite membrane for novel properties;
- (3) Improving the separation performance of responsive membrane;
- (4) Improving the response rate of the responsive membrane;
- (5) Investigating the relationship between surface roughness, special wettability, novel properties, and the performance of the membrane.

#### 2. Development of high-performance smart draw agents for forward osmosis processes

- (1) Introducing special wettability into the smart composite hydrogel for novel properties;
- (2) Improving the water absorbing ability and stimuli response rate of the draw agent;
- (3) Improving the liquid transportation inside the responsive draw agent;
- (4) Investigating the relationship between roughness, special wettability, novel properties, and the forward osmosis performance of the draw agent.
- (5) Investigating the improvement mechanisms by studying swelling behavior.

### 3. Development of responsive adsorbent for efficient solute removal

- (1) Selection of high surface area materials as the base;
- (2) Introduce stimuli-responsiveness into the highly porous material for reversible adsorption and desorption;
- (3) Improving the adsorption performance and kinetics of the responsive adsorbent;
- (4) Investigating the solute adsorbed and desorbed ability of this adsorbent;
- (5) Study the mechanism of reversible adsorption and desorption theoretically.

## 1.3 Thesis Overview

### Abstract

The brief background, research aims, and major findings of this thesis are concluded in this section.

### Chapter 1. Introduction

This section gives brief background on water treatment and responsive materials, research aims and thesis overview.

### Chapter 2. Literature Review

This chapter starts with emphasizing the importance of water treatment by summarizing the current water issue. Traditional and recent water treatment technologies are detailed. Thirdly, the responsive materials and responsive water treatment system are described. Finally, the research aims and significance of this work are presented.

**Chapter 3.** Robust Thermo-responsive polymer composite membrane with switchable superhydrophilicity and superhydrophobicity for efficient oil-water separation

In this work, a robust, thermo-responsive polymer membrane is produced by the combination of an elastic polyurethane (TPU) microfibre web and poly (N-isopropyl acrylamide) (PNIPAM). PNIPAM hydrogel is evenly coated on the surface of TPU microfibrils, and thus, the wettability of TPU-PNIPAM membrane is amplified by taking advantage of the hierarchical structure and increased surface roughness. The TPU-PNIPAM membrane possesses switchable superhydrophilicity and superhydrophobicity as the temperature of membrane changes from 25 to 45 °C. The composite membrane is shown successfully able to separate a 1 wt % oil-in-water emulsion and 1 wt % water-in-oil emulsion at 25 and 45 °C, respectively, with a high separation efficiency of  $\geq 99.26\%$ . Furthermore, the composite membranes show excellent mechanical properties, and they are highly flexible and mechanically tough. The smart composite membranes reported here have great potential for further development for practical high efficiency oil–water separations.

This chapter has been published as a journal article: Ranwen Ou, Jing Wei, Lei Jiang, George P. Simon, and Huanting Wang, *Environ. Sci. Technol.* **2016**, 50, 906-914

#### **Chapter 4.** Microfibre-polymer hydrogel monolith as forward osmosis draw agent

Stimuli-responsive polymer hydrogels have shown great potential for use as draw agent in emerging forward osmosis (FO) technology. The swelling pressure of hydrogel and the effective contact area between FO membrane and hydrogel are key parameters for achieving such a high water flux. In this work, the forward osmosis performance of hydrogels can be significantly improved by producing composite hydrogel monoliths containing thermoplastic polyurethane (TPU) microfibrils. The use of monolithic hydrogels and the addition of microfibrils enhance water diffusion through the draw agent and sustain high swelling pressure, resulting in improved FO performance. As observed in the sigmoidal swelling curves, the swelling kinetics of microfibre-hydrogel composite (TPU microfibre-poly (NIPAM-co—SA), TPU-PN5S5) is faster than that of pure hydrogel (PN5S5), and the time required for the composite to reach swelling equilibrium decreases significantly; the diffusion exponent of TPU-PN5S5 composite increase from 0.73 to 0.81, indicating that addition of microfibrils increases the water diffusion rate. Further studies show that water transports more quickly through the microchannels around TPU microfibrils due to their hydrophilicity and capillary forces. The composite monolith was tested as forward osmosis draw agent, and it was found that the 1st hour FO water flux and dewatering flux of TPU-PSA are 1.81 and 3.51 L m<sup>-2</sup> h<sup>-1</sup>, respectively, twice of those for PSA particles alone.

This chapter has been published as a journal article: Ranwen Ou, Huacheng Zhang, George P. Simon, Huanting Wang, *J. Membr. Sci.* **2016**, 510, 426-436

**Chapter 5.** Modification of the swelling properties of ionic hydrogel for forward osmosis applications

The swelling properties of hydrogels, and the effective contact between forward osmosis membrane and hydrogel, are key parameters for improving the performance of a draw agent. A new strategy is developed here to modify the swelling property of hydrogel by the introduction of structural inhomogeneity and preservation of a compressed pressure in an ionic hydrogel, in order to get increased forward osmosis water flux. That is achieved by the incorporation of an ionic hydrogel with a hydrophobic microfibre under compressed pressure during preparation. The forward osmosis water flux of the composite hydrogels generally increased with increasing microfibre loading and compressed loading. The water flux of poly (NIPAM-co-SA) – polyester microfibre composite (PN5S5 – PET) and poly (sodium acrylate) – polyester microfibre composite (PSA – PET) reached 3.0 and 5.0 LMH in the first 10 mins, respectively, when their swelling ratio is 4. The water flux of composites were twice as high as the relevant, neat hydrogel. The composite hydrogels were also good at maintaining high water flux over long time periods. The water flux of PSA-PET decreased from 3.5 to 1.4 LMH after 24 hour forward osmosis test.

This chapter has been published as a journal article: Ranwen Ou, Huacheng Zhang, George P. Simon, Huanting Wang, *Ind. Eng. Chem. Res.*, **2017**, 56 (2), pp 505–512

**Chapter 6.** Amphoteric Functionalized Metal Organic Framework for Highly Efficient, Reversible Ion Sorption

To explore the emerging stimuli responsive MOFs for advanced adsorption technology, an amphoteric MOF-based ion adsorbent is developed for physical stimuli reversible ion sorption, especially for monovalent ions, by integrating cation sites and anion sites with responsiveness in MOFs. This is illustrated by post-synthesis modification of MIL-121 via in situ polymerization of tertiary amine monomer introduced in the framework. The synergic effect of tertiary amine groups of the polymer and non-coordinating carboxylic acid groups of MIL-121 give rise to the ion adsorption ability and thermal regeneration properties. The equilibrium NaCl adsorption capacity of the amphoteric MOF is 0.92 meq/g, which occupies 77 % of ion adsorption sites, demonstrating the efficiency of amphoteric MOF ion adsorbent. The adsorbed

salt can be recovered and the MOF-based ion adsorbent regenerated by heating at elevated temperature in 500 ppm NaCl solution, with excellent cycle performance. Other than for NaCl, the amphoteric MIL-121 is able to adsorb other monovalent and divalent cations. This study firstly introduces an amphoteric MOF for monovalent ion adsorption, and realizes the thermal regeneration of MOF-based ion adsorbent.

The results presented in this Chapter has been drafted and will be submit as a journal article: Ranwen Ou, Huacheng Zhang, Jing Wei, Li Wan, Yaoxin Hu, George P. Simon, and Huanting Wang, Functionalized Metal Organic Framework with Thermoreversible Ion Sorption Property for Efficient Water Desalination.

## **Chapter 7. Conclusion and Future Work**

This chapter concludes the major finding of this thesis and the suggest Future Work for stimuli responsive materials in water processing.

## **1.4 References**

- [1] S. Diop, P. M'mayi, D. Lisbjerg, R. Johnstone, Vital water graphics: an overview of the state of the world's fresh and marine waters, UNEP/Earthprint, 2002.
- [2] M.A. Montgomery, M. Elimelech, Water and sanitation in developing countries: including health in the equation, *Environmental Science & Technology*, 41 (2007) 17-24.
- [3] M.A. Shannon, P.W. Bohn, M. Elimelech, J.G. Georgiadis, B.J. Mariñas, A.M. Mayes, Science and technology for water purification in the coming decades, *Nature*, 452 (2008) 301-310.
- [4] S. Parsons, Advanced oxidation processes for water and wastewater treatment, IWA publishing, 2004.
- [5] R. Andreozzi, V. Caprio, A. Insola, R. Marotta, Advanced oxidation processes (AOP) for water purification and recovery, *Catalysis today*, 53 (1999) 51-59.
- [6] D.G. Rao, R. Senthilkumar, J.A. Byrne, S. Feroz, Wastewater treatment: advanced processes and technologies, CRC Press, 2012.
- [7] Z. Aksu, Application of biosorption for the removal of organic pollutants: a review, *Process Biochemistry*, 40 (2005) 997-1026.
- [8] H. Bai, Z. Liu, D.D. Sun, A hierarchically structured and multifunctional membrane for water treatment, *Applied Catalysis B: Environmental*, 111 (2012) 571-577.

- [9] J. Mulder, Basic principles of membrane technology, Springer Science & Business Media, 2012.
- [10] L.J. Zeman, A.L. Zydney, Microfiltration and ultrafiltration: principles and applications, M. Dekker, 1996.
- [11] J.K. Bungay, P.M. Bungay, H. Lonsdale, M. de Pinho, Synthetic Membranes:: Science, Engineering and Applications, Springer Science & Business Media, 2012.
- [12] V. Goel, M.A. Accomazzo, A.J. DiLeo, P. Meier, A. Pitt, M. Pluskal, R. Kaiser, Deadend microfiltration: applications, design, and cost, in: Membrane Handbook, Springer, 1992, pp. 506-570.
- [13] B. Van der Bruggen, C. Vandecasteele, Removal of pollutants from surface water and groundwater by nanofiltration: overview of possible applications in the drinking water industry, Environmental pollution, 122 (2003) 435-445.
- [14] A.A. Hussain, A.E. Al-Rawajfeh, Recent patents of nanofiltration applications in oil processing, desalination, wastewater and food industries, Recent Patents on Chemical Engineering, 2 (2009) 51-66.
- [15] T.Y. Cath, A.E. Childress, M. Elimelech, Forward osmosis: principles, applications, and recent developments, Journal of membrane science, 281 (2006) 70-87.
- [16] J. Rouquerol, F. Rouquerol, P. Llewellyn, G. Maurin, K.S. Sing, Adsorption by powders and porous solids: principles, methodology and applications, Academic press, 2013.
- [17] M.A.C. Stuart, W.T. Huck, J. Genzer, M. Müller, C. Ober, M. Stamm, G.B. Sukhorukov, I. Szleifer, V.V. Tsukruk, M. Urban, Emerging applications of stimuli-responsive polymer materials, Nature materials, 9 (2010) 101-113.
- [18] M. Wei, Y. Gao, X. Li, M.J. Serpe, Stimuli-responsive polymers and their applications, Polymer Chemistry, 8 (2017) 127-143.
- [19] A.G. Fane, R. Wang, M.X. Hu, Synthetic Membranes for Water Purification: Status and Future, Angewandte Chemie International Edition, (2015).
- [20] D. Li, X. Zhang, J. Yao, G.P. Simon, H. Wang, Stimuli-responsive polymer hydrogels as a new class of draw agent for forward osmosis desalination, Chemical Communications, 47 (2011) 1710-1712.
- [21] D. Li, H. Wang, Recent developments in reverse osmosis desalination membranes, Journal of Materials Chemistry, 20 (2010) 4551-4566.

## Chapter 2 Literature Review

### 2.1 Water Treatment

#### 2.1.1 Water issue

97 % of water on earth is saltwater in the ocean, 0.5 % is brackish water found in surface estuaries and salty underground aquifers, and freshwater only constitutes 2.5%. Of this freshwater, 68.9 % is locked into polar icecaps or permanent mountain snow cover, 30.8 % is stored underground in the form of groundwater, including soil moisture, swamp water and permafrost, and 0.3 % is in freshwater lakes and rivers. Statistically, less than 1 % freshwater, is usable by humans, which is only 0.01% of all water resources on earth. [1]

The freshwater available for human consumption is between 12,500 km<sup>3</sup> to 14.000 km<sup>3</sup> each year. The water withdrawal and consumption are likely to speed up in the near future, as shown in Figure 2.1a. Global freshwater withdrawal has grown from 3,790 km<sup>3</sup> per year in 1995 to 4,430 km<sup>3</sup> in 2000, and is expected to grow by about 10 - 12 % every 10 years, reaching 5,240 km<sup>3</sup> by 2025. With the rapid population growth, the potential global availability of freshwater drop dramatically from 12,900 m<sup>3</sup> per capita per year (1970) to 9,000 m<sup>3</sup> (1990), to less than 7,000 m<sup>3</sup> in 2000. It is estimated that is projected to 5,100 m<sup>3</sup> by 2025. However, the freshwater resources distribute unevenly on earth that 3 billion people will live in the water scarcity region of 1,700 m<sup>3</sup> per capita per year by 2025.

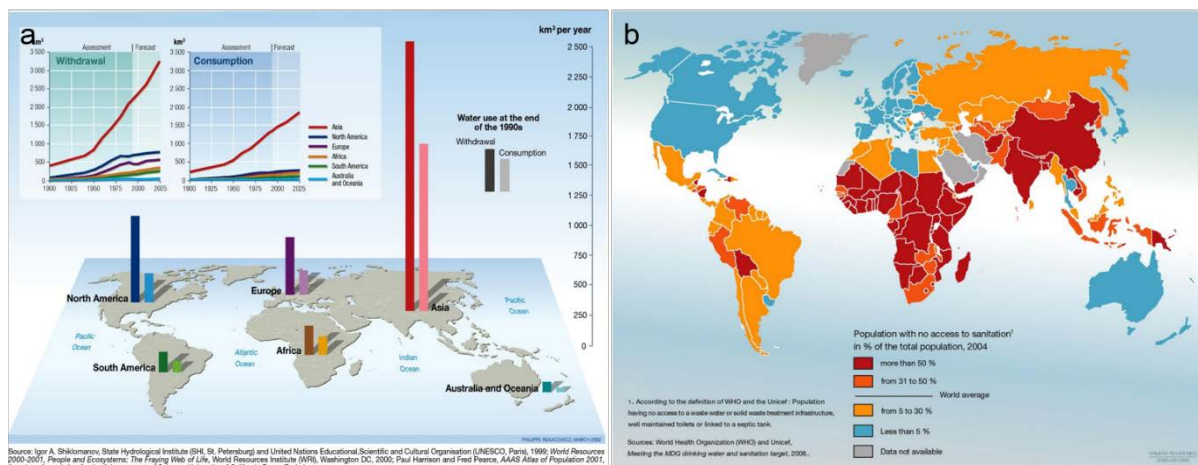


**Figure 2.1** World map of a) water withdrawal and consumption and b) sanitation accessibility.[1]

Despite the water shortage, water quality issue is also a major challenge that humans face.[2-4] Agriculture, industry and domestic usage consume one-third of the total accessible freshwater, resulting in water contaminated with synthetic and geogenic natural chemicals. Here lists some important pollution sources and pollution ways. (1) To maintain and increase the agricultural production, several million tons of chemicals are used to control pests annually.[3, 5] The pesticide can infiltrate into nearby soil or enter aquatic system, which contaminate ground and surface water, and may cause accidental poisoning to human. (2) Elements such as arsenic, fluoride, selenium and uranium, where are contained geologically within aquifers, can be leached into drinking water supplies, with subsequent great negative health effects on humans, such as cancer and fluorosis. (3) Mining activity involves the intense use of chemicals, energy and water, generating enormous amount of waste such as sulfuric acid, cyanide, mercury and copper that may cause chronic neurotoxicity.[6, 7] (4) Spills and hazardous waste sites are a prominent cause of water pollution. Chemicals like uranium, technetium, chromium, chlorinated solvents, nitroaromatic explosives, fuel hydrocarbons and so on are expected to release into the environment and cause long term contamination of drinking water resources, though many of the waste sites are under control.[8-10] (5) Municipal wastewater is another major source of pharmaceutical compounds that is highly bioactive and ecotoxicological.[11, 12] It is estimated that the observed concentration of human pharmaceuticals in raw sewage is up to several micrograms per liter. Importantly, microorganisms and viruses can also be found in the urban wastewater, which directly affect human health, child mortality and malnutrition. In addition, persistent organic pollutants (POPs) contaminate the environment in multiple sources, including waste sites, agriculture, combustion and others. The increasing chemical and organism pollution of freshwater is a key problem for human health.

The lack of ready access to clean water and sanitation has had significant adverse health impact on human.[13] This can lead to water-, sanitation-, and hygiene-related diseases, including diarrhea, intestinal helminths, schistosomiasis, dengue fever, trachoma and so on, which currently affect more than a third of populations. Figure 2.1b shows lack of accessibility to sanitation in the world. It is estimated that 1.2 billion people lack access to safe drinking water, 2.6 billion have little or no sanitation, and millions of people die annually-3,900 children a day-from severe waterborne diseases.[13, 14] According to a study from Pacific Institute, preventable deaths will reach 135 million by 2020 if action is not taken to address the issue of lack of water, sanitation, and hygiene.[15] Water scarcity also limits the food and energy

production, industrial output, and the quality of our environment, affecting the economy. International organizations have been setup to attract global attention and deal with the accessibility of improved sanitation around the world. Reliable detection, wastewater collection and treatment systems are all vital for safe water and human health.

### 2.1.2 Conventional water treatment system

Water treatment processes treat surface / ground water, industrial water and wastewater and make it more acceptable for specific uses. The conventional water treatment processes for treating raw water from surface source are mainly preliminary treatment, coagulation / flocculation, sedimentation / clarification, filtration and disinfection, as shown in Figure 2.2.[16-19]

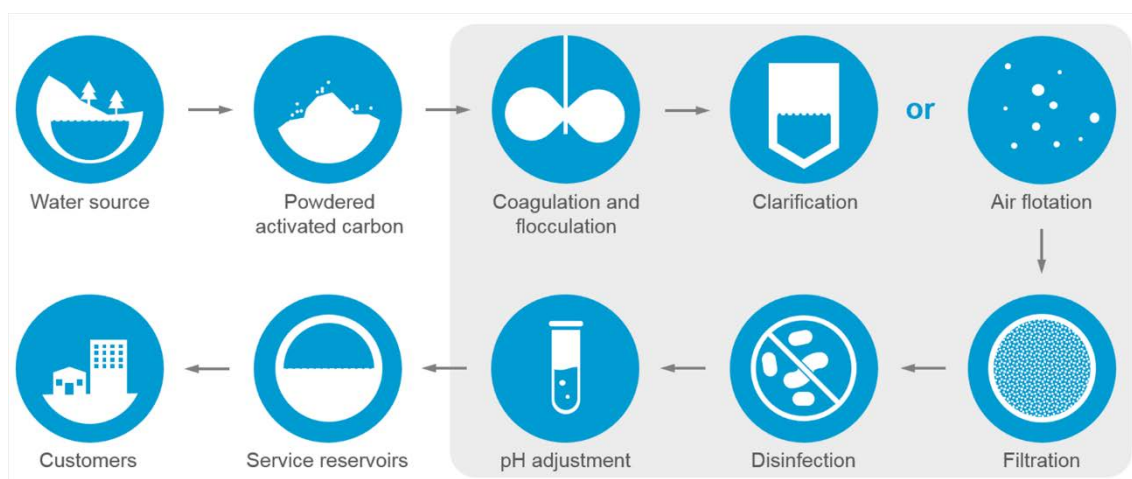


**Figure 2.2** Schematic illustration of conventional water treatment process.

In preliminary treatments, all large objects usually involving sand and grit in the incoming water are removed before entering the remaining treatment stages. Then, activated carbon or pre-chlorination may be applied. Powdered activated carbon is mainly used for the removal of organic matter, while the pre-chlorination is for controlling algae and biological growth.

Coagulation and flocculation aim to remove a large amount of organic compounds, suspended particles, and pathogens attached to dissolved substances.[20] In the coagulation process, coagulants with a positive charge are added to the water, with rapidly mixing, to neutralize the mostly negatively charged dissolved and suspended particles. Coagulants are usually iron or aluminium salts, such as aluminium sulphate, ferric sulphate, ferric chloride, or polymers. With the reaction started, the particles coagulate or flocculate to form larger particles. Mixing speed, mixing intensity and mixing time all affect the efficiency flocculation. During flocculation, the

destabilized particles are further aggregated. The visible floc in the suspension is slowly mixed using turbulence until it is sufficiently large to settle with gravity.

Following flocculation, the flocs are removed during clarification / sedimentation unit where the flow slow down. In the clarification process, most of the flocs are removed by gravitational settling, whilst the suspended particles in water are removed during filtration process. Air flotation may also be used so that the suspended matter such as oil or solids can float to the surface for easy removal via a filtration process.

In the filtration process, the relatively floc – free water flows through the filter by gravity, with the nature of the particles removed from the water depending on the type of filter. Slow sand filtration removes bacteria, protozoa and viruses, which produces essentially clean water. In contrast, rapid sand filtration removes suspended particles, but does not remove bacteria, protozoa or viruses. However, rapid sand filtration is much more commonly used, because the water flow of rapid sand filtration is hundred times higher than the slow sand filtration process, and it require relatively little space to operate. The most popular filter of the conventional treatment process is composed of anthracite coal and sand.

Disinfection aims to kill remaining microorganisms in water, such as bacteria, viruses and other pathogens. Normally, chlorine is used as the dosing chemical added to water.[21, 22] Supplemental chlorine is added to continue disinfection of water while it moves through the distribution network. However, the usage of chlorine to disinfect can lead to several problems. Chlorination of organic materials can generate carcinogenic or harmful chlorinated-organic compounds. Also, the residual chlorine may be able to chlorinate organic material in natural aquatic environment. Ozonation is a popular and safer alternative to chlorination.

After all the above procedures, pH adjustment and fluoridation may be applied to treat the water before storage and distributing to customer.

When treating wastewater, such as sewage, industrial and agricultural wastewater, additional treatment is needed in addition to the above processes. A wastewater treatment plant may include one or more of the following plants: oil-water separator, clarifier, roughing filter, activated sludge, carbon filtration and advanced electro dialysis reversal system.

Centralized municipal wastewater systems can address many of the problems on water contamination and sanitation, but they are often chemically, energetically and operationally intensive. Developing a conventional water and wastewater treatment facility requires

considerable capital and time, which precludes their use in much of the world, especially where water is really needed. It is estimated that global annual infrastructure costs of US\$100 billion over the next 20 years.[3] In addition, the chemicals used in the treatment will become the contaminating sources of freshwater. More effective, lower-cost, robust methods to purify water are urgently needed, without further stressing the environment or endangering human health by the treatment itself, as well as a cheap, fast and reliable detection method for detecting pollutants in natural water.

### 2.1.3 Advanced water treatment technologies

To deal with the rapidly increasing water pollution, new types of pollutants and inaccessibility of sanitation, advanced water treatment technologies have emerged to achieve a more robust, cost-effective and greener water treatment system.[14, 23] In general, four processes have been developed, advanced oxidation process, biological treatment, adsorption or ion exchange process and membrane filtration. In this chapter, more attention is paid to the adsorption / ion exchange process and the membrane filtration process as they are closely related to the works done in the subsequent chapters.

#### *2.1.3.1 Advanced oxidation process*

Advanced oxidation processes (AOPs) have been developed to deal with the chemically polluted water and wastewater, and show great potential for the treatment of ground water, municipal wastewater sludge and volatile organic compounds (VOCs).[23, 24] AOPs are also capable of treating problematic pollutants in water that may not be able to be removed effectively by conventional treatment methods, such as persistent organic pollutants, which are toxic, stable and active in the environment. The AOPs aim is to mineralize the organic pollutant into relatively harmless inorganic molecules, such as carbon dioxide, water, sulphates and nitrate.[25] To date, many AOPs have been developed for water and wastewater treatment, including ultraviolet (UV) photolysis, solar photocatalysis, H<sub>2</sub>O<sub>2</sub>, Fenton's reagent, photocatalysis, ozone, sonolysis, radiation, supercritical water oxidation and so on.

Although there are more than 10 techniques classified as AOPs, these processes produce in situ reactive free radicals, mainly hydroxyl radicals. The degradation of organic pollutants in aqueous solution by AOPs is mainly achieved by a series of hydroxyl radicals initiated reactions. Hydroxyl radicals (HO•) are a powerful oxidant that can be easily produced. As

shown in Table 2.1, the standard redox potential value of hydroxyl radical is 2.80 V, second to fluorine (3.03 V), suggesting that it is possible to complete mineralization most organic matters.

**Table 2.1** Redox potential of oxidants.[23]

Oxidants	Redox potential (V)
Fluorine	3.03
Hydroxyl radical	2.80
Atomic oxygen	2.42
Ozone	2.07
Hydrogen peroxide	1.78
Perhydroxyl radical	1.70
Permanganate	1.68
Hypobromous acid	1.59
Chlorine dioxide	1.57
Hypochlorous acid	1.49
Chlorine	1.36

There have been extensive studies on the development of AOPs over the past 40 years, as shown in Figure 2.3. Figure 2.3a shows the traditional and advanced oxidation processes. Oxidants such as chlorine,  $H_2O_2$  and ozone are applied to oxidize pollution or provide disinfection in conventional oxidation technologies. However, they are not efficient enough when oxidizing more complex and stable materials or complete oxidation of pollutants. Therefore, in the advanced oxidation processes, these oxidants are combined with other reagents or assisted techniques to produce more hydroxyl radicals ( $HO\bullet$ ) during treatment. For example, the combination of ferrous ions ( $Fe^{2+}$ ) and  $H_2O_2$  gives a new oxidant – Fenton's reagent. Oxidants for  $HO\bullet$  generation include  $O_3$ ,  $H_2O_2$ , Fenton,  $TiO_2$  and water, assisted techniques for enhancing the  $HO\bullet$  generation are ultraviolet (UV), sonolysis, microwave, irradiation and supercritical liquid.[26]

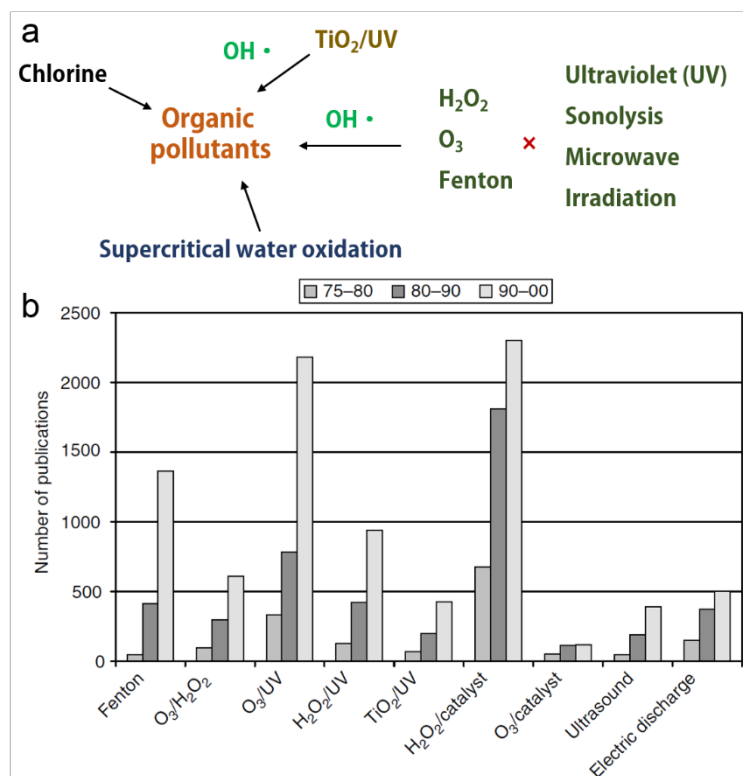


**Figure 2.3** (A) Traditional (chlorine) and advanced oxidation process and (B) number of AOP publications over 1975-2000 period [27].

Ultraviolet (UV) is an electromagnetic radiation with a wavelength shorter than that of visible light but longer than x-rays, which can cause chemical reactions.[28] In advanced oxidation processes (AOPs), UV advances the elimination of organic pollutant by initiating the generation of powerful oxidising agent, such as HO•, from relevant oxidants. (1) H<sub>2</sub>O<sub>2</sub> alone is not sufficient when oxidizing stable and complex organics. Under UV irradiation, every H<sub>2</sub>O<sub>2</sub> decomposes to two hydroxyl radicals, enhancing the degradation performance.[29-31] Since H<sub>2</sub>O<sub>2</sub> is totally soluble in water, the UV/ H<sub>2</sub>O<sub>2</sub> process provides an effective source of hydroxyl radicals, and there is no need for further separation after treatment. (2) Fenton's reagent can degrade a wide range of pollutants to largely harmless or biodegradable products. In an aqueous acidic medium, Fe<sup>2+</sup> is oxidized to Fe<sup>3+</sup>, while H<sub>2</sub>O<sub>2</sub> decompose into HO<sup>-</sup> and HO•. The Fenton reaction stops as soon as all Fe<sup>2+</sup> is consumed, resulting in the cessation of hydroxyl radical generation, and no further degradation of organic pollutants. The photo – Fenton reaction rates can be increased manyfold assisted with UV / visible light irradiation. During the reaction, Fe<sup>2+</sup> ions are regenerated by irradiation from oxidized Fe<sup>3+</sup>, so that HO• is supplied continuously.[32-34] (3) Ozone oxides organic pollutants directly or indirectly via the formation of HO•. Incomplete oxidation with ozone may produces toxic intermediates, sometimes even more toxic than the initial compounds. Thus, UV / O<sub>3</sub> is developed to degrade

organic pollutants more effectively through the generation of HO• from aqueous ozone produced H<sub>2</sub>O<sub>2</sub>. [35, 36] UV / O<sub>3</sub> / H<sub>2</sub>O<sub>2</sub> is also used for treatment of organic compounds.

Photocatalysis is to accelerate a catalytic reaction involving light absorption by a catalyst. [37] Photocatalysis can degrade a wide range of refractory organics into biodegradable compounds, or even mineralize them. [38] Mild operating conditions, complete mineralization of organic pollutants and the low operating cost made this process feasible for water treatment. In the photocatalytic reaction, the catalyst absorbs a photon to excite an electron (e<sup>-</sup>) from valence band (VB) to conduction band (CB), at the same time creating holes (h<sup>+</sup>) in the valence band. [39] Those holes act as oxidizing agents, which generate free radicals able to undergo further reactions. When h<sup>+</sup> comes into contact with water molecules, HO• and H<sup>+</sup> are produced. On the other hand, electrons can react with dissolved oxygen to generate O<sub>2</sub><sup>-•</sup> ions, then the peroxide radicals react with water molecules, H<sup>+</sup> and h<sup>+</sup> to eventually form HO•. Semiconductors, such as TiO<sub>2</sub>, ZnO, Fe<sub>2</sub>O<sub>3</sub>, CdS, GaP and ZnS, have been shown to be suitable photocatalysts because of the appropriate positioning of VB and CB bands for adsorption of light. Among the semiconductor catalysts studied, titanium dioxide (TiO<sub>2</sub>) is the most popular and exhibits best performance for photocatalytic water treatment. TiO<sub>2</sub> shows good chemical and thermal stability, and it remains stable after repeated catalytic cycles under a photon energies of 300 – 390 nm. [40, 41] In addition, development of catalyst with broader photoactivity range and feasible photocatalytic system are challenges that attract intensive attention.

Sonolysis –, microwave – assisted oxidation processes and supercritical water oxidation process are also well studied. [42-46] Sonolysis of water produces H• and HO• by thermal dissociation of water. Sound waves are also used to enhance the performance of Fenton process, ozonation process and the activity of catalyst or photocatalyst. It is observed that microwave can greatly enhance the efficiency of AOPs, but the performance is not as good as using ultraviolet. By taking advantage of the unique properties of supercritical water, organic pollutants is mineralized through adding oxygen into the water.

Advanced oxidation processes provide a promising technology for the treatment of wastewater containing organic pollutants, and have demonstrated their ability to solve this problems in a greener, cost-efficient, practical way.

### 2.1.3.2 Biological treatment

Biological treatment has been used for consuming biodegradable soluble organic contaminants and removal of nitrogen and phosphorus in the conventional wastewater treatment system.[47] The practical value of biological water treatment technologies arises for several reasons.[25] Firstly, this process is very practical, it can be carried out in situ at the polluted site. Secondly, it is an environmentally friendly technology, without generating secondary pollution. Thirdly, it is cost-effective. The recent development of this utilized technology is concentrated on removal of metal ions and oils.

Mining activity mobilize more than  $5 \times 10^{10}$  metric tons of geological materials annually in our world,[1] and can also cause significant environmental problems, constituting the most common metal pollution in fresh water. Biological treatments have been proven successful for efficient removal of metal ions from contaminated water.[48-50] Generally, metal ions can be treated by biosorption, bioaccumulation and phytoremediation.

Biosorption is the uptake of toxicants by dead/inactive biomaterials or by materials derived from biological sources. Depending on the biosorbent used in the process, the mechanism of metal removal can be physical adsorption, ion exchange, complexation, chelation and micro-precipitation.[51] Several bacterial, fungal biomass and seaweed show good biosorption capacity of relevant metal ions. For example, the biosorption capacities of a bacterial biomass, *Corynebacterium glutamicum*, for adsorbing lead and nickel are 568 and 111 mg/g, respectively. [49, 52] A kind of seaweed, *Ascophyllum nodosum*, adsorbs 215 mg/g cadmium and 136 mg/g nickel.[53, 54] In addition, as an industrial waste, crab shell performs very good, the relevant adsorption capacity of cadmium, cobalt, copper, lead, nickel and zinc are 199, 510, 244, 870, 170 and 124 mg/g, respectively.[55-60] However, most research focus on the biosorption of metal ion, but few reports desorption and regeneration of biomaterials, which indicates the industrial applicability of the process.

Bioaccumulation is the uptake of metal ions by living cells. In this process, metal ions are bound onto the cell by rapid sorption, then accumulated inside the cell by metabolism.[61] Bioaccumulation is usually conducted in batch systems. Thus, additional processes, such as harvesting, drying, processing and storing, are reduced.[62, 63] However, it is not feasible to treat solutions with high pollutants loading. The uptake capacity of bioaccumulation is about one tenth of the biosorption process.

Phytoremediation uses living plants to clean up chemically contaminated soil, air and water.[64] Four different processes mediated by plants are developed for treating metal polluted soil, sediment and water, including rhizofiltration, phytostabilization, phytovolatilization and phytoextraction. Rhizofiltration uses hydroponically cultivated plants to absorb and concentrate metals in their roots and shoots in the metal contaminated water.[65] Phytostabilization reduces the migration of pollutants in the soil. Phytovolatilization removes pollutants from soil or water and release it to air by transforming them to a volatile form. Phytoextraction concentrates the pollutants into the plant biomass from environment. The phytoremediation process is cost-effective, easily monitored, but it is a long term remediation method. Over the past 20 years, this technology has been employed to deal with organic and inorganic contaminants all over the world.

The increasing amounts of oily wastewater from oil fields, oil mills, petroleum industry, frequent oil spill accident, and domestic households poses a major threat to the environment. The oil water mixtures can be separated by gravity separation and filtration. The oil water emulsions can be treated by centrifugation or ultrafiltration. However, dissolved oil in water is difficult to remove, and causes serious issues of toxicity. Biological treatment has been proven to treat it effectively by degrading the hydrocarbon to CO<sub>2</sub>, H<sub>2</sub>O and biomass. Oil bioremediation can be achieved by direct addition of microorganisms into the pollution sites, and / or addition of nitrogen and phosphorous to initiate the growth of microorganisms.[66, 67] Microorganisms have been studied to treat drilling fluid contaminated waste water, edible oil contaminated wastewater and petroleum contaminated wastewater. To treat the drilling fluid, suitable carbon source is added after the dilution of wastewater with water, followed by inoculating of metal treating and oil utilizing microorganisms. The resultant water can be reused after separation the slurry or further treatment. This method removes metal and oil contaminants at the same time. To treat petroleum contaminated wastewater, oleophilic oil-eating microbes are used to break complex petroleum into fatty acids or carboxylic acids.[68] If proper nutrients are introduced, these microorganisms can remove the oil completely.

There is no doubt that biological treatment is a promising alternative of conventional wastewater treatment methods. With proper handling, microorganisms can not only survive in tough environment, but also remove problematic organic and inorganic waste from water. More pilot scale experiments are needed to be carried out to make biological treatment more reliable for treating real wastewater.

### 2.1.3.3 Adsorption or ion-exchange process

Adsorption and ion exchange processes are two of the most important water treatment technologies that have been employed in many environmental applications, such as removal of organic contaminants, taste and odor regulation, removal of sulfur compounds, toxic / heavy metal removal, nitrogen and phosphorus removal, treatment of nuclear waste solutions, produce high quality water, and so on.[69, 70] Adsorption is the adhesion of atoms, ions or molecules onto the external and/or internal surface of a porous solid. Ion exchange is also a sorption process using a porous solid, but only for ions, and for the sorption of every ion, there is another ion(s) with equivalent charge released to the solution from the ion exchanger.

#### *Adsorption*

Adsorption is a process of enrichment of material on an interface.[71] It is of great environmental, technological and biological importance, as it has been widely used in separation, purification, catalysis, food processing, and pharmaceutical industries. Adsorption is a consequence of surface energy.[72, 73] For solids, matter on the surface have more energy than that inside the bulk, this excess energy is called “surface energy”. These surfaces are available to rearrange or react to reduce their surface energy according to the Second Law of Thermodynamics. Thus, it is more favourable to use adsorbents with high specific surface areas, for example, industry uses adsorbents of fine particle size and a specific surface area larger than 100 m<sup>2</sup>/g. To date, porous solid materials such as activated carbons, metal oxides, zeolites, clays, and metal organic framework have been used as adsorbents for various applications, as shown in Table 2.2.[74]

*Activated carbon.* The surface area of activated carbon normally ranges from 300 to 1500 m<sup>2</sup>/g, with a pore volume between 0.7-1.8 cm<sup>3</sup>/g. The manufacture of activated carbon uses carbonaceous material as a source, including wood, peat, coal, nutshells and so on. The preparing process involves carbonization and activation.[75, 76] During the carbonization process, the source material is heated up to 400-600 °C in an oxygen deficient atmosphere to convert it into carbon or a carbon-containing residue. Activation aims to improve the accessibility of pore structure by chemical activation or thermal activation. It also helps to open and widen the micropores.

Activated carbon has been extensively used for the water treatment.[77] Organic compounds like aromatic solvents, chlorinated aromatics, chlorophenols, polynuclear aromatics, pesticides and herbicides, chlorinated nonaromatics, high molecular weight hydrocarbons and surfactants,

and inorganic compounds such as chlorine, bromine, iodine, fluorine, antimony, arsenic, bismuth, chromium, tin, silver, mercury, cobalt and zirconium can be efficiently adsorbed by activated carbon. The adsorption with activated carbon is preferred for water treatment under some circumstances: non-biodegradable compounds, solid residue lower than 50 ppm, oil residue lower than 10 ppm, organics concentration <5000 ppm and inorganics concentration <1000 ppm.

**Table 2.2** Specific surface area and applications of adsorbents.

Adsorbents	Specific surface area (m <sup>2</sup> /g)	Applications
Activated carbon	300~1500	Organic compounds: aromatic solvents, high molecular weight hydrocarbons Inorganic compounds: cation and anion ions
Metal oxides	Alumina 200~400 Silica 300~850	Gas
Clays	Smectite ~30 Laponite ~300	Decolouration, dye, radioactive material, metal ions
Zeolites	LTA 150~450 FAU 500~900	Gas separation, catalysis, drying
Mesoporous silica	MCM-41 >1000 SBA-15 500~1000	Organics: pharmaceuticals, cyanuric acid, phenols, dyes
Metal organic framework	100~5000	Metal ions, dyes, gas

*Metal oxides.* Some metal oxides can be fabricated to obtain high specific surface area. The metal oxides studied as adsorbent are alumina, magnesia, silica, titanium dioxide, ferric oxide, chromium and so on. Among them, alumina and silica are notable adsorbents, having a specific surface area of 200-400 m<sup>2</sup>/g and 300-850 m<sup>2</sup>/g, respectively. Metal oxides are usually used for gas adsorbent, desiccant, gas sensor, catalyst or catalyst support, pigments and fillers, [78-81] but they are not readily applied for water treatment.

*Clays.* Clay combines clay minerals and trace amount of metal oxides and organic matter, plastic when hydrated and harden when drying.[82, 83] As the mineralogical constituents of clay, clay minerals are hydrous phyllosilicates with coordinating cations such as Al<sup>3+</sup>, Mg<sup>2+</sup>, Fe<sup>3+</sup> or Fe<sup>2+</sup>, and a particle size range of 1 nm to 1 μm. Based on the clay minerals, layer silicate includes Kaolinite, Smectites, Vermiculites, Palygorskites and so on. Kaolinite is the most well-known type of clay, which is relatively thick and rigid, with a BET surface area in the range of 10-20 m<sup>2</sup>/g. For Smectite, the surface area of montmorillonite is about 30 m<sup>2</sup>/g, while

that of laponite can be up to 300 m<sup>2</sup>/g.[84] Due to their inertness, stability and low cost, clays have been used in many industrial applications that are directly related to the adsorbent properties. In the water treatment process, clays can be used for decolouration, dye adsorption, radioactive materials adsorption and heavy metal adsorption.[85-87]

*Zeolites.* Zeolites are microporous, aluminosilicate minerals, have a general formula of  $M_{x/n}[(AlO_2)_x(SiO_2)_y] \cdot mH_2O$ .  $[(AlO_2)_x(SiO_2)_y]$  constitutes the zeolite framework, while M is the exchangeable cation, such as Na<sup>+</sup>, K<sup>+</sup>, Ca<sup>2+</sup> and Mg<sup>2+</sup>. The zeolites can be divided to zeolite A, zeolite X, zeolite Y and Pentasil zeolites with more specific formula. Zeolites can be obtained naturally or synthesized from alumina, silica and base. The synthesis of zeolite involves the formation of poorly ordered aluminosilicate hydrogel, the growth of oligomer precursors and the development of crystallinity.[88] The synthetic zeolites are uniform and phase pure. The effective pore volume for N<sub>2</sub> of Ca<sub>6</sub>A (zeolite A) is about 0.30 cm<sup>3</sup>/g, those of NaX (Si/Al=1.25, zeolite X) and Silicalite I (Pentasil zeolites) are 0.35 and 0.19 cm<sup>3</sup>/g, respectively. The zeolites are of great fundamental and technological importance, have been applied for catalysis, gas separation and drying. In liquid adsorption application, zeolite can adsorb Ca<sup>2+</sup> and Mg<sup>2+</sup> in replace of Na<sup>+</sup> to soften water.

*Mesoporous silica.* Mesoporous silica such as MCM-41 and SBA-15 comprises uniform ordered pores / channels, high pore volume and high surface area, which is a promising adsorbent for water treatment and catalysis.[89, 90] The pore/ channel size can be tuned by using surfactants of different length or by varying synthesis conditions. Functionalized mesoporous silica has also been made to extend the applications of this adsorbent. Mesoporous silica has been investigated for the removal of organics in aqueous solution, including pharmaceuticals, cyanuric acid, phenols and dyes.

*Metal organic framework.* Metal organic frameworks (MOFs) are an emerging class of porous materials built from organic linkers and inorganic metal nodes or metal-based clusters through coordination bonds, and are well known for high surface area, uniform pore size, controllable structures, and readily tailorable functions.[91-93] Highly porous and flexible MOFs have shown great potential as high-performance adsorbents in the development of advanced adsorption technology. Compared to the other adsorbents, MOFs show several advantages:[94-96] 1) it has relatively high surface area, which can be up to 5000 m<sup>2</sup>/g, so that it is possible to adsorb large amount of molecules per volume unit. 2) It has flexible and designable chemical

structure that can be functionalized by organic or inorganic compounds. 3) The high surface area may also advance the MOF adsorption process faster.

The current research on MOFs focus has been mainly involved gas storage, gas separation and purification, catalysis, drug delivery and sensor.[97] However, MOF-based materials have recently been explored for adsorbing organic compounds, cations and anions in liquid phase. In general, the uniform framework structure and high surface area endow the MOF-based ion adsorbents with superior ion adsorption kinetics and remarkable uptake capacity. To date, the research has been mainly focused on the adsorption properties of pristine MOFs. On the other hand, the MOF-based ion adsorbents have been mainly used to adsorb metal pollutants in oxo-hydroxo anion forms such as perchlorate, chromate, selenite and arsenate in water treatment and purification processes. In addition, the regeneration of spent MOFs usually requires the use of chemicals via ion exchange process.

#### *Ion-exchange process*

Ion exchange processes are one of the most important scientific developments of the 20<sup>th</sup> century, and have been applied for water softening, environmental remediation, wastewater treatment, hydrometallurgy, chromatography, biomolecular separation and catalysis.[70] As the key component of ion exchange process, ion exchangers are insoluble solid materials carrying exchangeable cations or ions.[98] The ion exchanger can be natural or artificial materials, inorganic or polymeric materials. With the development of ion exchange technology, the artificial polymeric resin has become the most popular and practical ion exchangers, and widely applied. The synthetic resin is well known for high capacity, wide versatility, low cost, and designable structure. Here, the species and applications of polymeric resin is introduced. The polymeric resin is composed of a crosslinked network of hydrocarbon chains and functional groups with ionic charges at various positions. A proper crosslinking density makes the resin insoluble in water and ensure the swelling. Polystyrene divinylbenzene is commonly used as the matrix (hydrocarbon chains) of resin. Others, phenol-formaldehyde matrix and acrylic/methacrylic acid – divinylbenzene matrix are also used. The polymeric resin can be classified into four types according to the functional groups: strong acid cation resins, strong base anion resins, weak acid cation resins and weak base anion resins.[77]

*Strong acid cation resins.* These resins are functionalized with sulfonic acid groups ( $-\text{SO}_3\text{H}$ ) or sodium sulfonate groups ( $-\text{SO}_3\text{Na}$ ), which can fully dissociate in water to form highly ionized ion exchange sites.  $\text{Na}^+$  and  $\text{H}^+$  are highly exchangeable over the whole pH range.

Strong acid cation resin can exchange with all kinds of cations in water, including monovalent and multivalent ions. The sodium form is preferred for water softening, while the hydrogen form is for preparing ultrapure water. The regeneration of resins is achieved by washing it with strong acid or sodium chloride solution.

*Weak acid cation resins.* The functional group of these resins is carboxylic acid group (-COOH), which can partially dissociate in water to behave like weak organic acid. Thus, weak acid cation resins can only exchange with multivalent cations, such as  $Mg^{2+}$  and  $Ca^{2+}$ . Because of the good affinity between -COOH and  $H^+$ , these resins can be regenerated easier with lower amount of acids.

As a kind of weak acid cation resin, heavy metal selective chelating resin can form complexes with heavy metal ions, so that they are much more selective in heavy metal. Functional groups with two or more chelating sites are usually used to decorate the resin, such as iminodiacetic acid group, iminodiacetate, aminophosphonate, 8-hydroxyquinoline and picolylamine. The relative selectivity of a commercial chelating resin for mercury is 2800 times as that of calcium.

*Strong base anion resins.* These resins are decorated with quaternary ammonium groups, and are used in hydroxide form. The hydroxyl groups are fully dissociated in water, and can exchange with all anions in water under an entire pH range. The regeneration of strong base anion resins are treated with concentrated sodium hydroxide solutions.

*Weak base anion resins.* These kind of resins are functionalized with weak base such as primary, secondary and tertiary amine. They can only exchange with strong acid in water, and the exchange capacity is greatly affected by pH. Weak base anion resins are more readily regenerated with lower concentration base solution compared to that of strong base anion resins.

#### 2.1.3.4 Membrane separation technology

Membranes are a selective barrier that allow the permeation of some matter but block others.[99, 100] There are both biological and synthetic membranes. Biological membranes include cell membranes, nuclear membranes and tissue membranes. Synthetic membranes are man-made and used in laboratories and industry. With regards membrane technology for water treatment, only synthetic membranes are discussed in this study.

Synthetic membranes can be subdivided into symmetric and asymmetric membranes. The development of asymmetric membrane is the breakthrough for industrial applications.[101] Thinner membrane generates higher permeation. Asymmetric membranes are composed of a

dense and thin selective layer (high rejection and permeation) and a porous support layer (good mechanical property). The modern membrane separation industry started in 1960s with the development of interfacial polymerization and multilayer composite coating. The Loeb-Sourirajan process made defect-free, high flux reverse osmosis membranes with 10 times higher flux than any membrane at that time.[102, 103] During 1970s and 1980s, microfiltration, ultrafiltration, reverse osmosis and electrodialysis processes were all established. In 1980s, membrane processes were applied for industrial gas separation. More recently from mid-1990s, microfiltration / ultrafiltration processes have been developed as reliable and economical systems for the treatment of municipal water sources and for sewage treatment integrated in membrane bioreactor. Nowadays, membrane technology is very promising for water treatment which has been widely applied.

### *Fabrication*

Either inorganic or organic materials can be used for preparing membranes. The manufacturing technique aims to fabricate membranes with certain structure or morphology for a specific separation. Among the techniques developed, some of them are more important and have been commonly used, including sintering, track-etching, phase inversion, sol-gel process, vapor deposition and solution coating.

*Sintering.* The sintering method is a two steps process involves compressing powders and sintering at elevated temperatures.[104, 105] The material used in this process normally has outstanding chemical, thermal and mechanical stability, such as powders of polymers, metals, graphite and glass. The sintering temperature depends on the material used. During sintering, the interfaces between powders “melt” to form a continuous and porous membrane. The pore sizes of this membrane is about 0.1-10  $\mu\text{m}$ , and depends on the particle size of powders, while the porosity is 10 to 20 %. The sintering method can prepared microfiltration membranes.

*Track-etching.* Using this method, a porous membrane with an assembly of parallel cylindrical pores of uniform dimension can be fabricated. The preparation method starts with a dense film, followed by a high energy particle radiation vertically applied on the film, and etching with acid or alkaline solution.[106-108] The radiation particles create tracks in the matrix, and then the acid or alkaline etches along these tracks to form uniform cylindrical pores. The radiation time determines the porosity, while the etching time determines the pore diameter. The surface porosity of membranes obtained using this method is low, usually not higher than 10%. The pore size ranges from 0.02 to 10  $\mu\text{m}$ .

*Phase inversion.* Phase inversion is the most commonly used and versatile technique for fabricating filtration membranes. Phase inversion is a process to transform polymer from liquid state to solid state, which includes a range of different techniques, such as solvent evaporation, evaporation-controlled precipitation, thermal precipitation, precipitation in vapor phase and immersion precipitation.[99] Solvent evaporation is to evaporate the solvent of the liquid polymer solution cast on a suitable support, in an inert and dry atmosphere to obtain a dense and homogeneous membrane. In the vapor phase precipitation process, the casted liquid polymer film is precipitated in an atmosphere with saturated nonsolvent vapor. The membrane forms due to the penetration of nonsolvent into the polymer film, resulting in the formation of porous membrane. Most of the membranes prepared in lab or for commercialization are phase inversion membranes obtained by immersion precipitation. In this process, a casted liquid polymer solution film is immersed in a nonsolvent / coagulation bath.[109-111] The exchange of solvent and nonsolvent precipitates the polymer to be a porous membrane. Solvent/nonsolvent pair is an important factors affecting the membrane structure. Water is often used as a nonsolvent. Polymer concentration, evaporation time, humidity, temperature and casting solution composition are also parameters determining the membrane performance. The obtained membrane can be used directly or for post treatment.

*Coating.* As mentioned above, thinner membrane generates higher water flux. To increase the water flux, composite membranes with a porous support layer and a very thin selective layer are desired. Thus, the support layer and selective layer can be optimized independently for optimal performance, such as permeation, selectivity, stability and mechanical properties. The support layers are often asymmetric membranes obtained from phase inversion. Coating procedures such as dip coating,[112, 113] spray coating, spin coating,[114, 115] grafting, plasma polymerization, interfacial polymerization and in situ polymerization[116, 117] can be applied to prepare these membranes.

In the case of dip-coating, an asymmetric membrane is firstly immersed in a low concentration coating solution containing polymer, monomer or crosslinker, and then coated membrane is placed in oven to evaporate the solvent and crosslink it.[113] Membranes prepared by dip-coating are used in reverse osmosis, gas separation and pervaporation. In the interfacial polymerization process, the reaction occurs on the active surface of support layer between two very active monomers dissolved in two immiscible solvents. Amine and acid chloride / isocyanate are usually used as the active monomer pair. A polymer film thinner than 50 nm can be obtained through this technique.

### *Characterization of membranes*

The properties of membrane determines its applications. Membranes need to be characterized for a specific process. Based on the morphology and structure, there are porous and nonporous membranes.

*Porous membrane.* The characterization of porous membrane includes structure related parameters and permeation related parameters. The structure related characterization includes the determination of pore size, pore distribution, selective layer thickness and the surface porosity. These can be characterized by scanning electron microscopy, permeation measurement, solute rejection measurement, bubble point method, mercury intrusion porometry and so on. The permeation related parameters are flux and molecular weight cut-off (MWCO). Normally, dead end cells are used to measure the flux by applying a certain pressure. In the molecular weight cut-off measurement, a series of molecules with increased molecular weight are permeated through the relevant membrane. Cut-off is the molecular weight that is  $\geq 90\%$  rejected by the membrane.

*Nonporous membrane.* Nonporous membrane separates molecular size substances. Normally, gas permeability is used for the characterization. Other physical properties such as glass transition temperature, crystallinity and density are used for better understanding concerning permeability through the nonporous polymeric membrane. The thickness of selective layers can be determined by plasma etching. Surface properties of the selective layer can also be determined by electron spectroscopy, X-ray photoelectron spectroscopy, secondary ion mass spectrometry and auger electron spectroscopy.

### *Types of membrane processes*

Membrane filtration has been proven to be one of the most promising separation techniques. Separation occurs when an appropriate driving force is applied. The driving forces are pressure difference, concentration difference, osmotic pressure difference, temperature difference and electrical potential difference. According to the pore size and rejection of relevant membrane, membrane processes for water treatment can be divided into microfiltration, ultrafiltration, nanofiltration, reverse osmosis and forward osmosis (Figure 2.4),[99] they have increased rapidly over the past decade. Figure 2.5 shows the process of membrane filtration, the membrane selectively retains some solutes, while water permeates through under applied pressure or osmotic pressure.

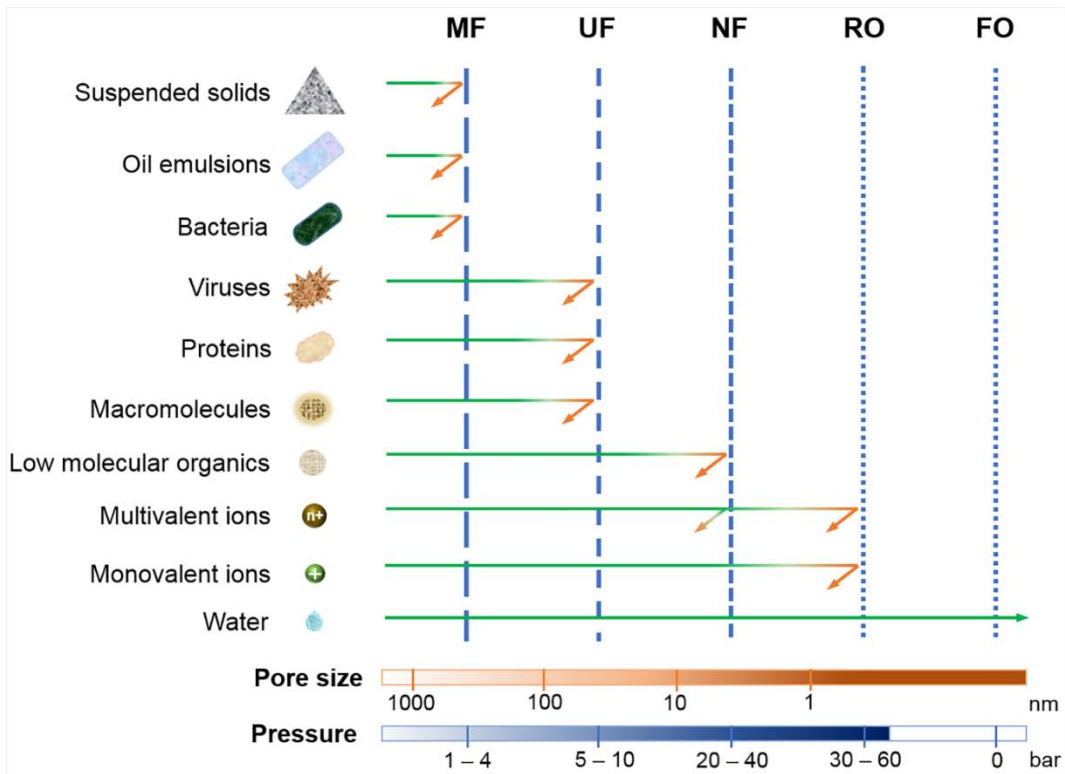


**Figure 2.4** Illustration of different membrane filtration processes.

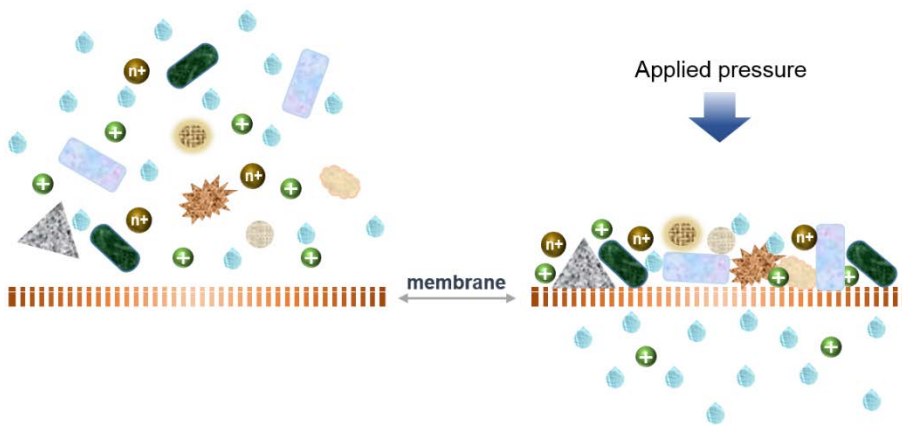


**Figure 2.5** Schematic of membrane filtration.

*Microfiltration (MF)*. The pore sizes of microfiltration membrane is between 10 to 0.05  $\mu\text{m}$ , the applied pressure ranges from 1 to 4 bar, normally lower than 2 bar.[99] Microfiltration membranes are suitable for filtering out suspended solids, emulsions and bacteria.

Microfiltration membranes can be prepared from organic or inorganic materials by sintering, sol/gel process, anodic oxidation, stretching, track-etching and phase inversion. Organic materials include polymers, such as polytetrafluoroethylene (PTFE), poly (vinylidene fluoride) (PVDF), cellulose esters and polycarbonates. Inorganic materials are mainly ceramics such as

alumina, zirconia, titania and silicium carbide. Inorganic membranes are more favorable than polymer ones, due to the outstanding chemical and thermal resistances.

In terms of industrial applications, microfiltration is mainly used to separate impurities with a particle size large than 0.1  $\mu\text{m}$  from liquid. A number of applications of microfiltration have been proven to be efficient:[118-120] 1) sterilization and clarification of beverages and pharmaceuticals under mild conditions, 2) cell harvesting, 3) metal recovery as colloidal oxides and hydroxides, 4) removal of large particles during water treatment or ultrapure water production, 5) wastewater treatment, 6) oil-water emulsion separation and so on.

*Ultrafiltration (UF)*. The pore sizes of ultrafiltration membrane are between 1 nm to 0.05  $\mu\text{m}$ . Compared to microfiltration membrane, ultrafiltration membranes have a much denser selective layer, resulting in a much higher hydrodynamic resistance. Thus, the applied pressure (driving force) of ultrafiltration process is higher, between 1 to 10 bar. Ultrafiltration membrane is typically used for retaining macromolecules and colloids from a solution.

Ultrafiltration membranes are mostly an asymmetric polymer membrane prepared by the phase inversion process.[121] Some of the polymeric materials used for UF membrane preparation are polysulfone, poly (ether sulfone), sulfonated polysulfone, poly (vinylidene fluoride), polyacrylonitrile, cellulosics, polyimide, polyetheretherketone and so on. Some inorganic materials such as alumina and zirconia can also be used for UF membrane preparation. Ultrafiltration membranes are often used as porous support for preparing membranes for nanofiltration, reverse osmosis, forward osmosis and gas separation. Applications can be found in the field such as dairy and food industry, oil water emulsion separation, electropaint recovery, textile industry, pharmaceutical industry, paper industry, leather industry and water treatment.[122, 123]

*Nanofiltration (NF)*. The pore sizes of nanofiltration membrane should be less than 10 nm, the applied pressure ranges from 10 to 40 bar. Nanofiltration membrane is permeable to solvent but reject solutes, which separates small organic molecules and multivalent inorganic salts from a solvent. High pressures applied in this process are due to the high hydrodynamic resistance caused by dense selective layer and the osmotic pressure of the feed solution.

Water flux and selectivity are both vital factors determining the performance of nanofiltration membranes. For a given material, the flux is inversely proportional to the membrane thickness. Both integral asymmetric membrane and thin film composite membrane are used as nanofiltration membrane.[124, 125] The materials suitable for preparing integral asymmetric

membrane by phase inversion are cellulose esters, aromatic polyamides, polybenzimidazole, polybenzimidazolone, polyamidehydrazide and polyimides, which show high selectivity towards salt. The thin film composite membrane is manufactured by coating a thin layer on a porous support which is mainly ultrafiltration membrane obtained from phase inversion. Coating techniques include dip coating, in situ polymerization, interfacial polymerization and plasma polymerization, and interfacial polymerization are the most preferred.

Nanofiltration membranes are not sufficient to retain monovalent ions such as  $\text{Na}^+$  and  $\text{Cl}^-$ , but can be effectively remove multivalent ions and low molecular compounds. The main applications of nanofiltration membrane are desalination of brackish water, removal of micropollutants, water softening, wastewater treatment and dyes removal.[126, 127]

*Reverse osmosis (RO)*. The pore sizes of reverse osmosis membrane is about 1 nm or lower, the applied pressure ranges from 30 to 60 bar. Only solvent permeates through the reverse osmosis membrane, indicating that RO process separates all solutes include monovalent ions from solvent. The rejection of monovalent ions in RO process can be greater than 98 %.

Reverse osmosis membrane are also integral asymmetric membrane and composite membrane.[128] To increase the permeation, the dense selective layer should be thinner. The RO membrane materials are cellulose triacetate, aromatic polyamide, polyamide and poly(ether urea), similar with those of nanofiltration. Most composite membranes are prepared by forming a dense thin film by interfacial polymerization on an ultrafiltration membrane.[129]

RO process are used for solvent purification and solute concentration. The main applications are desalination of brackish and seawater, production of ultrapure water, food and milk concentration in industry.[130, 131]

*Forward osmosis (FO)*. The pore size of forward osmosis membrane is similar to that of the RO membrane, less than 1 nm that only solvent permeates. Osmosis is the movement of solvent molecules across a semipermeable membrane from a region of lower solute chemical potential to a region of higher solute chemical potential. Osmotic pressure is the minimum pressure applied to prevent transport of solvent across the membrane. In the FO process, a semipermeable membrane is placed between a draw solution with higher osmotic pressure and a feed solution with lower osmotic pressure, as shown in Figure 2.6.[132] The osmotic pressure difference between draw solution and feed solution acts as the driving force of this process instead of pressure. In contrast, RO and other pressure driven processes need an applied pressure to overcome the osmotic pressure of feed and the hydrodynamic resistance of the

membrane. Thus, the forward osmosis process has great potential to reduce the energy cost for water treatment.

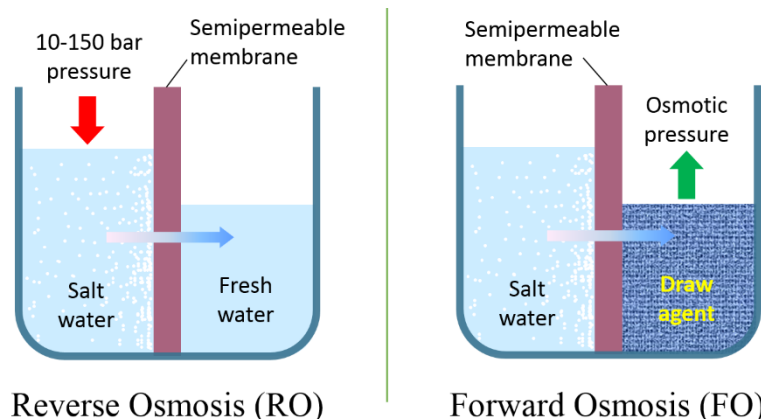


**Figure 2.6** Illustration of the reverse osmosis and forward osmosis processes.

In the 1970s, RO membranes were used for the study of forward osmosis process. However, the water flux is much lower than expected. Until the 1990s, Hydration Technologies Inc. developed a commercial FO membrane made of cellulose triacetate (CTA). The desired FO membrane would have these characteristics: [133-135] 1) a dense selective layer for high solute rejection, 2) a thin support layer with minimum porosity for low internal concentration polarization, 3) hydrophilicity for higher permeation and fewer fouling problem, and 4) high mechanical strength and chemical stability. Except for the FO membrane, the draw solution is the other vital component determining the performance of the process. Some key characteristics of a good draw solution are: 1) high osmotic pressure to generate high water flux, 2) minimal reverse draw solute, 3) low toxicity, 4) easy recovery of water and regeneration, and 5) low cost. There are many different draw solutions studied, including salts, fertilizers, saccharide, hydrogel, hydrophilic particles, polyelectrolyte, hydrogel etc. A proper draw solution not only promotes the performance of FO process, but also reduces the cost of it.

The forward osmosis process has been studied for a series of applications in water purification, pharmaceutical industry, food processing and power generation. With regards to waste water treatment and water purification, it can be applied for concentration of dilute industrial wastewater,[136, 137] landfill leachate and digested sludge liquids,[138] and designing hydration bags.[139] Forward osmosis process is ideal for seawater desalination if proper draw solution found.[140, 141] In food processing, FO is studied to concentrate beverages and liquid foods. In the pharmaceutical industry, FO can not only be used to concentrate sensitive products, but also for designing osmotic pumps for the controlled release of drugs.[142, 143]

## 2.2 Stimuli Responsive Polymeric Materials

“Smart” or responsive polymer materials respond to their surrounding environment by changing their physicochemical properties, such as regulating the transport of ions and molecules, changing wettability and adhesion of different species on external stimuli, or converting chemical and biochemical signals into optical, electrical, thermal and mechanical signals, and vice versa (Figure 2.7).[144] In addition to the fundamental interest, responsive materials are playing an increasingly important role in a variety of applications, such as drug delivery, tissue engineering, biosensors and coatings, as well as emerging environmental applications.[145] The introduction of responsive ability or “smartness” endows a material or device with multiple synergistic and advanced functions, broadening its applications and improving its performance.

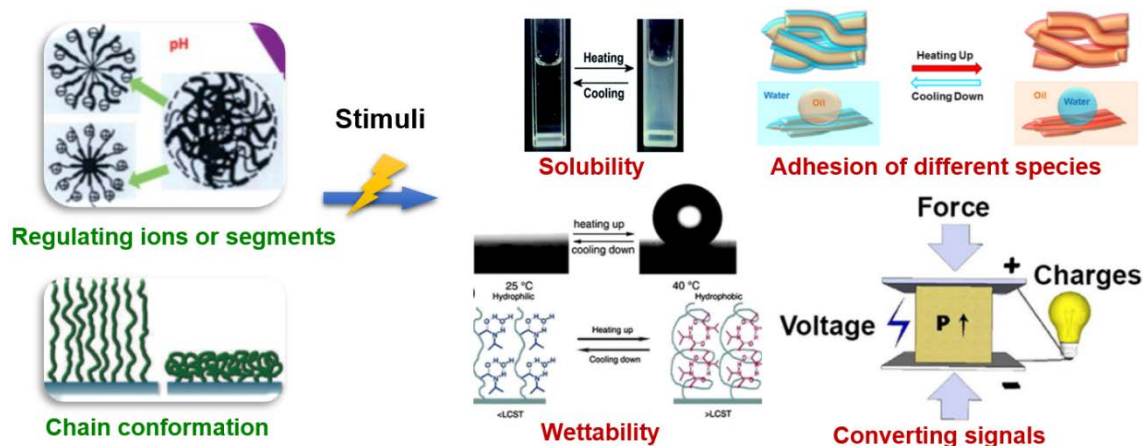


**Figure 2.7** Definition of responsive polymeric materials.

### 2.2.1 Type of responsive polymers

Stimuli responsive materials have been made which respond to a range different stimuli source have been developed, including temperature, pH, light, electricity, magnetic field, ultrasound, and biological matters.

#### *Thermo-responsive*

These materials respond significantly to small temperature changes. Poly (N-isopropyl acrylamide) (PNIPAM), as the most studied thermo-responsive polymer, decreases water solubility as temperature increases, the temperature that changes the polymer solubility dramatically called lower critical solution temperature (LCST).[146, 147] This type of swelling behaviour is known as inverse (or negative) temperature-dependence. Figure 2.8 shows the chemical structures of LCST polymers. Polymers with LCST are made of polymer chains that

either possess moderately hydrophobic groups or contain a mixture of hydrophilic and hydrophobic segments. For PNIPAM, at lower temperatures, hydrogen bonding between hydrophilic segments (amide groups) of the polymer chain and water molecules dominate, leading to enhanced dissolution in water.[148] As the temperature increases, hydrophobic interactions among hydrophobic segments (isopropyl groups) become strengthened, while hydrogen bonding becomes weaker, resulting in shrinkage of the polymer chains.

The LCST of polymers can be altered by incorporating hydrophilic or hydrophobic segments.[149] For example, the LCST of PNIPAM decreases when copolymerized with hydrophobic monomer, and increases with hydrophilic monomer. However, the introduction of other monomers may affect the sensitivity of the thermo-responsive copolymer. By controlling the polymer topology, the kinetics of the coil-to-globule transition can also be controlled. NIPAM copolymers grafted with oligoNIPAM or PEG show a fast response to temperature changes. The grafted short chain of oligoNIPAM in the former case contributes to rapid dehydration while PEG provides the water channel for fast rehydration.[150, 151] There are other polymers exhibit inverse-temperature dependence, most notable are poly (N-vinylcaprolactam) (PVCL), poly (organophosphazene) (PPZ), PEG, poly (ethylene oxide) (PEO), and poly (propylene oxide) (PPO).[146]

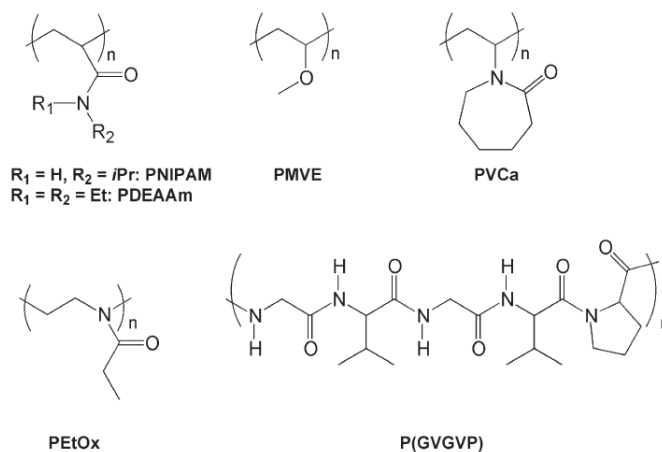


**Figure 2.8** Chemical structures of LCST polymers. [146]

In contrast, positive temperature polymers are defined by their upper critical solution temperature (UCST). This kind of polymer swells at high temperature. At relatively lower temperature, a complex structure with hydrogen bonds is formed, when temperature increases, this structure dissociates due to the breaking of hydrogen bonds, thus the polymer swells rapidly above UCST. The combination of acrylamide and acrylic acid is positively temperature dependent.[152]

### *pH-responsive*

pH-responsive polymers undergo structural and property changes such as surface activity, chain conformation, solubility and configuration in response to solution pH. The pH-sensitive polymers contain pendant acidic or basic groups that either accept or release protons in response to changes in environmental pH. In general, pH-responsive polymers made with basic monomers act as cationic polymer in acidic condition, while those made with acidic monomers act as anionic polymer in basic conditions.

The pH-responsive acidic polymers may have acidic group such as carboxylic groups, sulfonic acid, phosphoric acid, boronic acid, or aminoacid.[153] Poly (acrylic acid) (PAA) and poly (methacrylic acid) (PMAA) are the most widely reported pH-responsive polymers with carboxylic groups. The most studied responsive polymers made with sulfonic acid are poly (2-acrylamido-2-methylpropane sulfonic acid) (PAMPS) and poly (4-styrenesulfonic acid) (PSSA).[154] The pH-responsive basic polymers contain tertiary amine groups, morpholino, pyrrolidine, piperazine, pyridine, imidazole groups, or dendrimers. The most preferred basic pH-responsive polymers are tertiary amine methacrylate based polymers, such as poly [(2-dimethylamino) ethyl methacrylate] (PDMA), poly [(2-diethylamino) ethyl methacrylate] (PDEA) and poly [(2-diisopropylamino) ethyl methacrylate] (PDPA).

The presence of ionizable groups on polymer chains results in swelling of the hydrogels much beyond that can be achievable by non-electrolyte polymer hydrogels.[155] Since the swelling of polyelectrolyte hydrogels is mainly due to the electrostatic repulsion among charges present on the polymer chain, the extent of swelling is influenced by any condition that reduces the electrostatic repulsion, such as pH, ionic strength, and type of counter ions.[156]

### *Photo-responsive*

Light is an inexpensive and sustainable source of energy. It is straightforward and non-invasive to use light to induce responsive behaviour. Photo-responsive polymers are macromolecules that change their physiochemical properties in response to light irradiation of appropriate wavelength and intensity.[157, 158] Their response leads to a light triggered self-assembly, surface modification or patterning, swelling behaviour, shape change and fluorescence emission of a material, opening a door for their use in reversible optical storage, polymer viscosity control, photomechanical transduction/actuation, protein bioactivity modulation, tissue engineering and drug delivery.[159] Typically, these changes are caused by

the light-induced structural transformations of specific functional groups along the polymer backbone or side chains. Chemical structures of photo-responsive moieties are shown in Figure 2.9. The most extensively studied photo-responsive polymers are azobenzene-based and spiroopyran-based polymers.

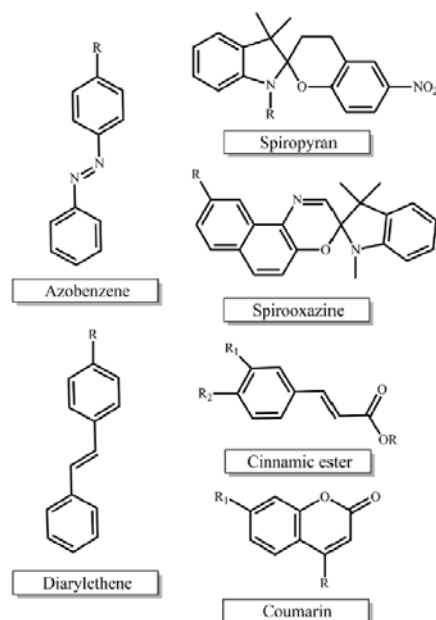


**Figure 2.9** Chemical structures of moieties for synthesis of photo-responsive polymers.[160]

Azobenzene is a chromophore with cis-to-trans isomerisation under irradiation, accompanied by a fast and complete change in electronic structure, geometric shape and polarity. The more stable trans-azobenzene is nonpolar, while the cis-form is polar.[158] By incorporating azobenzene derivatives, functionalities such as switchable shape, polarity and self-assembly can be introduced into the material.[161] Azo chromophores have been introduced into many polymeric systems, such as epoxy based polymer, polypeptides, poly (N-hydroxypropyl methacrylamide), PAA, PNIPAM etc. That endows the material photo-switchable morphology,[162] surface properties[163] and polymeric aggregates[164] in solution. In addition, azobenzene groups can also be used to control the assembly of supramolecular polymers, generate a photomechanical effect and cause macroscopic motion.[165]

Spiropyran is a phytochrome that isomerized between spiroopyran- (SP) and merocyanine- (MC) forms under stimuli. Spiropyran is relatively nonpolar and has no charge, while merocyanine is polar and zwitterionic. Spiropyran is isomerized to merocyanine under UV light irradiation, and merocyanine changes to spiroopyran upon visible light irradiation or heat.[166] Spiropyran has been introduced to prepare photo-responsive polymers with PAA,[167] PHPMA[168] and PNIPAM.[169]

Other than photo-responsive behaviour based on light-induced isomerisation, another mechanism can also be stimulated by polarity changes from cleavage of photo-labile esters that give birth corresponding alcohol and acid components, such as pyrenylmethyl chromophores and pyrenylmethyl esters.

### *Electro-responsive*

Electro-responsive polymers change their size and shape by swelling or shrinking in response to an applied electric field. Transforming the electric signal into a physical response by a polymer generally relies on the collapse of a gel, electrochemical reactions, electrically activated complex formation, ionic polymer-metal interactions, electrorheological effects, or changes in electrophoretic mobility.[170] These polymers can be ionic or dielectric. The responsive mechanism of ionic polymer is that the mobility of free ions driven by electric field changes the local ion concentrations in a solution or within a material, resulting in gel deformation. The deformation of dielectric material is induced by electrostatic forces between two electrodes.

Polyelectrolyte hydrogels are ionic electro-responsive polymers. Under electric fields, the mobile, charged ions migrate toward cathode or anode, resulting in anisotropic swelling or deswelling of the gel. Natural polymers such as chitosan, chondroitin sulfate, hyaluronic acid and alginate, and synthetic polymers based on vinylalcohol, allylamine sulfonic acid, aniline, 2-hydroxyethyl methacrylate, methacrylic acid, acrylic acid and vinyl sulfonic acid have been employed as an electro-responsive polymer.[171] In addition, an interpenetrating polymer network hydrogel and copolymer hydrogel combining natural and synthetic component has also been developed.[172] The bending rate and angle of the responsive polymer hydrogel is characterized for different ionic strengths of the medium and magnitude of applied voltage to determine the responsive ability. Ionic electro-responsive polymers require low actuation voltages, but also exhibit low deformations and response rates, and they are usually performed under wet conditions. Ionic polymer-metal composites show large bending strains under low actuation voltages, which is very promising for actuators and sensors developments.

Dielectric polymers exhibit fast response and high deformations with high actuation fields, and they are operated in dry conditions.[173] Poly (vinylidene fluoride)-based, polyacrylates based-, and silicone-based non-ionic polymers with the presence of additional charge carrier or polar component have been employed as electro-responsive materials.[174]

### *Magneto-responsive*

Magneto-responsive polymers can be prepared by introducing magnetic components within a crosslinked network by physically entrapping or covalently immobilizing these units. The distortion of shape and size occurs reversibly in the presence of non-uniform magnetic field. Potential applications of these materials are using as soft biomimetic actuators, sensors, cancer therapy agents, artificial muscles, switches, separation media, membranes and drug delivery systems. The physical combination of magnetic (nano) particles and polymers has been well documented, [175-177] such as PNIPAM and Fe<sub>3</sub>O<sub>4</sub>. These magnetic particles can be Fe<sub>3</sub>O<sub>4</sub> and ferromagnetic cobalt nanoparticles. Over last decade, organometallic polymers have attracted great attention by combining the valuable properties of metals and organic polymers, opening new avenues in multi-responsive or multi-functional. Some examples of organometallic polymers are oxanorbornene-based cobalt-containing diblock copolymer, norbornene-based triblock copolymer comprising cobalt, pyrene and PEG-folate as pendant groups and poly(4-(phenylethynyl)styrene)-b-PEO-b-poly(4-(phenylethynyl)styrene) (PPES-b-PEO-b-PPES) triblock copolymers functionalized with Co<sub>2</sub>(CO)<sub>8</sub>. [178-180] The development and exploration of all-organic magneto-responsive materials will pioneer a new realm.

### *Ultrasound-responsive*

Ultrasound is a high frequency sound waves that can be generated by mechanical oscillations of a piezoelectric material, produced by applying an alternating current. Ultrasound has been proven to be an effective stimuli that can be applied on demand and on site. The interaction between ultrasound and a certain substance can induce thermal and cavitation effect. Thermal effect is caused by the transfer of acoustic energy to the substance, resulting in temperature rise. The cavitation effect generates gas bubbles in the substance as a result of the ultrasound vibration. [181, 182] Transient bubble collapse generates local shock, which is considered the main source for chemical and mechanical effects of ultrasonic energy.

Unlike polymers that can be triggered by other stimuli, ultrasound responsive polymers do not have a specific or common characteristic. Generally, those materials which respond to ultrasound are gels and other non-swollen macroscopic solids, polymeric micelles or layer-by-layer coated microbubbles. The characterization of the ultrasound responsiveness of a polymer is normally proceeded in an applications. The most studied application is ultrasound-induced drug release. The drug release rate of copolymers from biodegradable polymeric materials,

such as polyglycolides, polylactides, and poly [bis(p-carboxyphenoxy)alkane] anhydrides, and sebacic acid and non-biodegradable ethylene-vinyl acetate, have been studied, and demonstrated that the release kinetics enhanced significantly with increasing ultrasound intensity.[183-185] This is due to the acceleration of the degradation of biodegradable polymers by ultrasound. Ultrasound can also be used to destabilize the supramolecular polymer assemblies and coat stabilized microbubbles on a polymer.

### *Biologically responsive*

The biologically responsive materials respond to biological small molecules or biomacromolecules. The responsiveness arises from the interaction between biological species and the functional groups of responsive material, or the conjugation of synthetic polymer and biological component.[171] Taking advantage of responding to natural systems, the biologically responsive materials are promising for controlled drug delivery, bio-sensing / diagnostics, smart films / matrices for tissue engineering, or in situ construction of structural networks. The biological stimuli can be that they are glucose-, enzyme-, antigen- and redox / thiol- responsive.

Glucose-responsive polymers are of great importance in developing smart delivery systems for insulin delivery which is triggered by a rise in blood glucose levels, aiming to treat diabetes mellitus. The glucose-responsive materials are mainly based on the glucose oxidase (GOx)-based reaction of glucose with oxygen. Glucose responsiveness is caused by the interaction of the responsive polymer with the byproducts (gluconic acid and H<sub>2</sub>O<sub>2</sub>) from the enzymatic oxidation of glucose. Thus, a pH responsive polymer is usually loaded or conjugated with GOx to prepare a glucose-responsive polymer. pH-responsive polymers like poly(acrylic acid),[186] poly(methacrylic acid),[187] and some polybase such as poly(2-hydroxyethyl methacrylate), poly(N-isopropyl acrylamide) and their copolymer [188-190] have been integrated with GOx to obtain glucose-responsive polymers. Poly(ethylene glycol) (PEG) and chitosan have also been studied to increase the biocompatibility.[191, 192] The glucose responsiveness can also be achieved by the binding of glucose with concanavalin A (ConA) [193] and the reversible covalent bond of glucose and boronic acids.[194] In the glycopolymer-ConA complex, ConA tends to crosslink or aggregate the glycopolymers, however, the binding of saccharide and ConA can disrupt the aggregation, resulting in the release of insulin. Boronic acids can reversibly complex with sugars, and are able to change their water solubility under different pH or diol concentrations.

Enzyme-responsive materials are usually applied for the in situ formation of hydrogels by an enzyme triggered reaction, which shows potential in tissue engineering and drug delivery. They can be fabricated by incorporating functional groups that react under enzymatic conditions. [195] Proteases are widely employed as the enzyme in the reactions. Antigen-responsive polymers swell and deswell upon the addition of antigen. This kind of materials are prepared by incorporating antigen and antibody in a polymer, while the binding of antigen and antibody crosslinks the polymers. When the antigen is added into the system, it binds with antibody of the polymer, triggering swelling.[196] Redox / thiol-responsive polymers contain disulfide linkages in the backbone or in the side chain. Disulphide bonds can be reversibly converted to thiols upon various reducing agents, changing the solubility and swelling state of the polymer. By taking advantage as the most abundant reducing agent in most cells, glutathione (GSH) has been utilized to design redox / thiol-responsive drug delivery system to release therapeutics in the cell.[197, 198]

### 2.2.2 Applications

The development of stimuli responsive materials is driven by a desire to mimic nature. To date, this kind of material shows great potential and increasing importance in a diverse range of applications (Figure 2.10), such as controlled drug delivery, diagnostics, tissue engineering, sensors and biosensors, environmental remediation, chemo-mechanical actuators, as well as microelectromechanical systems, textiles and coatings.[144, 145] Stimuli responsive materials can not only applied itself as a functional material in a process, but can also be used to multifunctionalize some other kinds of raw materials for advanced applications. The application of stimuli responsive materials can be different due to different environmental stimuli.

Thermo-responsive polymers have been applied for the development of polymeric temperature sensors, to control the proximity of side-chain functionalities, to control the osmotic pressure of a polymer solution so that induce a reversible movement of water through a semi-permeable membrane, for the collection of water from fogs and recovery, for passive cooling building over water absorption and release upon different temperatures,[202] and for the preparation of hydrogels for a specific use.[140]

Due to the pH variations along the gastrointestinal (GI) tract, pH-responsive polymers are very promising for biology applications.[203] In the GI tract, the pH value of stomach is around 2, and pH 7 within colon, then up to pH 8.2 in duodenum. Thus, one of the most favourable

applications is drug delivery. Other applications also show great potential for practical usage, such as non-viral gene carriers for incorporating naked DNA into the cells, and biosensors for accurate dosing during drug delivery or else.

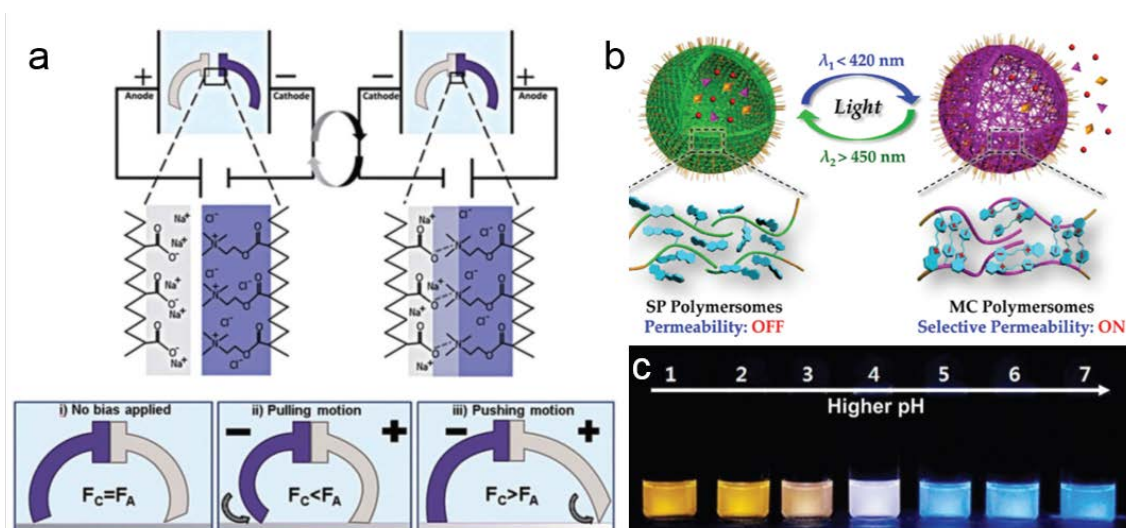


**Figure 2.10** Several applications of stimuli responsive material. (a) Charged gel walker, (b) drug delivery, (c) sensor.[199-201]

The photo-responsive materials have been studied extensively for various applications due to the intrinsic advantages of light over other kinds of stimuli, such as non-invasive, straight forward, remote control, sustainable, accurate on site dosing etc.[204, 205] It has been used for controlled drug delivery, fabricating functional micropatterns onto substrates by selective light exposure, preparation of hydrogel that may further suitable for drug / gene delivery, photography, paints / coatings, scaffolds, biosensors or actuators, and manufacture of photodegradable materials, photo-switchable liquid crystalline elastomers (LCEs) for remote actuation etc.

Electro-responsive polymers show expanding scientific and technological importance for applications in biomechanics, robotics and artificial muscle actuation, sensing, energy transduction, sound dampening, chemical separations, controlled drug delivery, optical systems, and energy harvesting.

The study of magneto-responsive materials is mainly focus on the synthesis. The applied external magnetic field can adaptively change the physical properties of magneto-responsive materials, resulting in shape distortion. It attracts significant attention for use as soft biomimetic

actuators, sensors, cancer therapy agents, artificial muscles, switches, separation media, membranes and drug delivery.

The most favourable applications of biologically responsive materials are controlled drug delivery, but are used in other applications like biosensing / diagnostics, cell support, injectable scaffolds, and tissue engineering.

As a bridge connecting synthetic materials and devices and nature, most of the applications of stimuli responsive materials are bio-related. The exploration of the fundamental science and advanced applications of stimuli responsive material will lead to new, relevant processes in a “smarter” new era.

## **2.3 Responsive Materials for Water Treatment**

Recently, responsive materials have been introduced in the water treatment process, responsive membrane, responsive forward osmosis draw agent and responsive adsorbent have emerged, and gaining increasing concern in recent decades. The development of smart membranes has been realized for the controllable separation process, and to produce anti-fouling membrane and biomimetic membrane. Smart draw agents, which can recover water with lower energy cost, lights the future of forward osmosis desalination process. The responsive adsorbent that can be regenerated and recycled by stimuli, especially by physical stimuli, is ideal for resource reclamation from contaminated water or water softening. Such smart water treatment systems with self-cleaning, self-refreshing, energy-saving, or controllable separation abilities will improve the efficiency of many technological processes, and they have strong potential for future applications.

### **2.3.1 Responsive membrane**

As the responsive material provides the membrane with responsiveness, it responds to external stimuli, and thus the flux, solute selectivity and wettability become tunable via changes in conformation of polymer chains. It is envisaged that combining various stimuli-induced molecular level changes with versatility of membrane design would unlock the potential of smart responsive membranes not only with better performance but also with unprecedented functionalities for a wider range of applications. [206] For example, as has been learnt from low-fouling surfaces in nature, the “self-cleaning” membrane could be fabricated with tunable

or responsive properties, because the change in configuration between hydrophilic and hydrophobic state can lead to desorption of absorbed solutes.

Stimuli-responsive membranes have a large number of previously established applications and many more potential applications, where they are key components in complex technical systems such as sensors, separation processes, and drug delivery devices. Increasing demand has driven the development of responsive membranes. There are four essential elements of smart membranes: [207] (1) responsivity of smart membranes changes in environmental stimuli; (2) stability of the smart membrane processes; (3) reversibility of the response of smart membranes to the environmental stimuli; (4) reproducibility of smart membrane materials and processes.

### *Fabrication*

According to the stimuli source, there are mainly seven types of responsive membranes, including thermally responsive, pH-responsive, photo-responsive, electric field-responsive, magnetic field-responsive, glucose-responsive and ionic strength-responsive membrane. Responsive membranes responding to different stimuli often have similar fabrication methods. [208] They can generally be fabricated by 1) processing the stimuli responsive materials (polymers or copolymers) into membranes, or 2) modification of existing membranes by physical / chemical methods to introduce stimuli responsive materials.

The membrane processing approach enables the stimuli responsive membranes with desired mechanical properties, pore structure, barrier structure and layer thickness to be made. The membrane processing methods for the preparation of membranes from stimuli responsive materials include radiation induced in situ formation, solvent casting, interpenetrating networks (IPNs) and phase inversion. In the radiation-based method, a mixture solution with monomers and crosslinkers is coated on a porous film, followed by radiation to initiate the polymerization, resulting in a film formed. In the solvent casting method, stimuli responsive polymers are dissolved in solvent before casting on a flat glass plate, and allowing solvent evaporation. The free-standing membranes obtained are dried and crosslinked. For preparation of interpenetrating networks, a stimuli responsive monomer is polymerized within a crosslinked network in the presence of crosslinker and initiator. The IPNs membrane shows good mechanical strength due to the high levels of crosslinking. Phase inversion can also be applied to prepare responsive membrane by immersing the casting solution of stimuli responsive polymer in an appropriate non-solvent to enable the membrane formation.

By surface modification, the useful properties of base membrane are preserved, and responsive properties are introduced to the membrane. There are two modification approaches employed for membrane functionalization, the “grafting to” and “grafting from” technique.[209] Grafting is an important and widely used method to incorporate functional moieties to the membrane. The “grafting to” technique incorporates terminal functionalized small molecules or large macromolecules onto the membrane surface. The “grafting to” functionalization can be achieved by physical adsorption or chemical grafting. By physical adsorption, a stimuli responsive polymer coating is formed on the membrane, which is done by soaking a raw membrane in a polymer solution and allowing it to dry before annealing to strengthen the attachment of coating to membrane. By chemical grafting, terminal functionalized molecules / macromolecules are activated by accelerator or catalyst to immobilize the (macro) molecules on to the membrane surface. The “grafting from” technique initiates the polymerization of stimuli responsive monomer and / or crosslinker on the membrane surface, thus the polymer chains grow from initiator site on membrane surface. The “grafting from” technique includes two steps: immobilization of initiator onto the membrane surface, and activation of the initiator to trigger the polymerization of monomer. According to different activation approach, this modification methods can be divided to photo-initiated (UV and non-UV) grafting, redox-initiated grafting, plasma-initiated grafting, thermal grafting, atom transfer radical polymerization (ATRP) and reversible addition-fragmentation chain transfer (RAFT) polymerization.

#### *Fundamental study*

The current research of responsive membranes is mainly focussed on fundamental studies, including the change of flux and solute selectivity, and the on-off state for different stimuli. Stimuli responsive membranes can be classified as porous and non-porous membranes, according to their morphology.

*Porous membrane.* Reber et al. prepared thermally responsive ion track membranes by chemically grafting poly (N-isopropyl acrylamide) (PNIPAM) hydrogel onto the single/multi-pore ion track membranes of poly (ethylene terephthalate) (PET).[210] It was found that the incorporation of the hydrogel into the pores does not influence the phase transition temperature. The bovin insulin permeation in the open state was 35 times above the level of the closed state. In the open state, the transport rates of the solvent and the solute were identical implying that the free space in the open pores was larger than the size of the permeating bovine albumin

molecules (about 7.3 nm) and is not molecular selective. Choi et al. developed a temperature-responsive membrane by grafting PNIPAM onto porous PP films for separations based on solute hydrophobicity. [211] The water permeability of the membrane was temperature-dependent, lower water flux at temperatures below LCST, and higher water fluxes at temperature above LCST. Solutions containing hydrophobic and hydrophilic solutes were supplied continuously to the feed side, while the membrane temperature was altered. It was found that above LCST, only the hydrophobic solutes were adsorbed onto the membranes, while the hydrophilic solutes permeated through the pores. By changing the temperature to below LCST, the adsorbed hydrophobic solutes desorbed from the membranes. Thus, with stepwise temperature change below and above LCST, specific solutes could be concentrated and purified on the permeate side. Ito et al. designed nanopores, pH-responsive membranes by self-assembly of ionizable polypeptide brushes on a gold-coated porous membrane.[212] At low pH, poly (L-glutamic acid) (PLGA) chains are protonated and folded forming  $\alpha$ -helical structures that lie on the surface; at higher pH, they are deprotonated forming extended random structures that extend into the solution. It was observed that the modified membranes were dependent on pH, with high permeation at low pH and low permeation at near neutral pH. Chung et al. grafted copolymerization of spiropyran-containing methacrylate (SPMMA) and acrylamide (AM) on to the surface of a porous polytetrafluoroethylene (PTFE) membranes.[213] It was found that the permeability of a water-methanol mixture through the modified membranes was increased by UV irradiation, but decreased by visible light irradiation. Chu et al. fabricated a temperature-responsive core-shell microcapsule with a porous outer membrane and PNIPAM gates by using plasma-graft pore-filling polymerization.[214] As shown in **Figure 2.11**, at low graft yields, the release rate was higher at temperatures above the LCST than at temperatures below the LCST, due to pore opening controlled by the PNIPAM gates. In contrast, at high graft yields, the release rate was lower at temperatures above the LCST than at temperatures below the LCST, because the pores were fully blocked and a PNIPAM layer covered the entire capsule surface.

*Non-porous membrane.* Yamakawa et al. Prepared temperature-responsive charged membranes from the polymer mixture of poly (vinyl alcohol) (PVA), in situ polymer of N-isopropyl acrylamide (NIPAM) and PVA, and a polyanion (poly (vinyl alcohol-co-2-acrylamido-2-methylpropane sulfonic acid)).[215] The permeation experiments in a dialysis system consisting of the membrane and mixed KCl and CaCl<sub>2</sub> solutions show that the transport

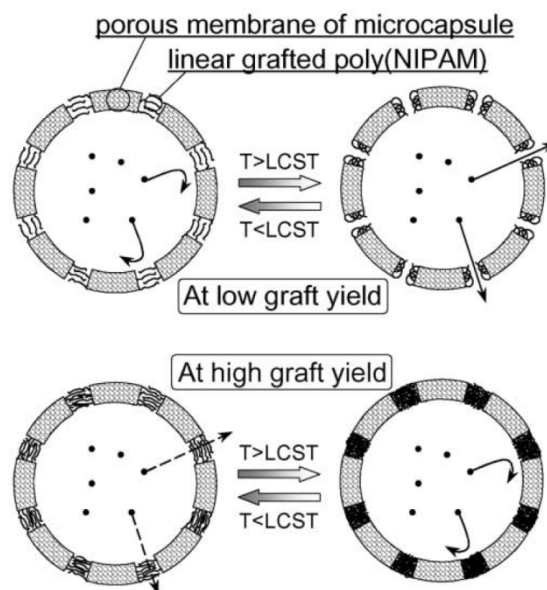


**Figure 2.11.** A schematic representation of the thermo-responsive release principle of core-shell microcapsules with a porous membrane and thermo-responsive PNIPAM gates. [214]

modes of  $\text{Ca}^{2+}$  ions through the membrane are controlled by temperature changes in two ways: downhill transport (from high to low concentration) occurred at temperatures below the LCST of PNIPAM, and uphill transport (from low to high concentration) occurred at temperatures above the LCST. Park et al. prepared an organic-inorganic composite IPN membrane using tetraethylorthosilicate (TEOS) as inorganic network and chitosan as organic filling.[216] Chitosan is positively charged and swells in an acidic medium and shrinks in a basic solution because of the ionisation of its amino groups. According to the swelling behaviour, an increase in pH from 2.5 to 7.5 yielded an increase in the rate of drug permeation because of the shrinking of the incorporated chitosan in TEOS IPN, while a decrease in pH resulted in low permeation rate. Anzai et al. reported a photo-responsive membrane made by dissolving poly (vinyl chloride) (PVC) and azobezene-modified crown ethers (Bis (2, 3-benzo-1, 4, 7, 10, 13-pentaoxa-2-cyclopentadecaen-15-ylmethyl) azobenzene-4, 4'-dicarboxylate) in solvent, and casting onto a glass plate, following by evaporating the solvent.[217] The photo-controlled permeation of alkali cations through the composite membrane was investigated. Before UV irradiation, the permeation selectivity of the membrane for the cations were  $\text{K}^+ > \text{Rb}^+ > \text{Na}^+ > \text{Cs}^+$ ; on UV irradiation, the permeation of the  $\text{K}^+$  was accelerated, while others were little affected.

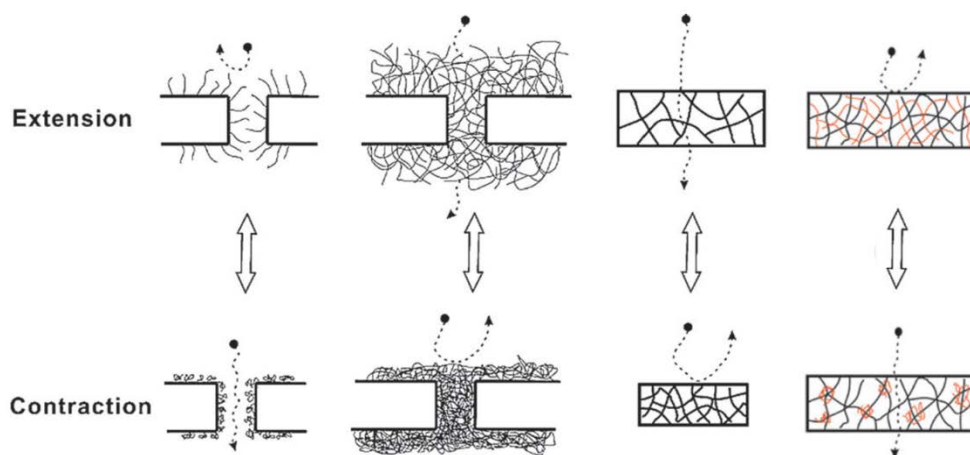


**Figure 2.12** The extended and contracted state of porous responsive membrane and their permeation upon solutes.

To date, most of the studies on responsive membrane have focused on investigating the change of permeation flux and pore size of the membrane under stimuli. Generally speaking, as shown in Figure 2.12, for porous responsive membranes prepared by grafting method, there are two distinct behaviours: at low graft yields, the permeation flux was higher in the contracted state than the extended state due to pore opening; In contrast, at high graft yields, the permeation flux was lower (or no flux) in the contracted state than the extended state, because the pores were fully blocked and the responsive polymer covered the entire pore surface. Researchers applied this responsive membrane in drug release because of this unique property. Apart from the permeation flux and pore size, the change of hydrophilicity under stimuli has also been studied. In the extended state, the membrane is hydrophilic; while in the contracted state, it is hydrophobic. This property has been studied for concentrating and purifying the hydrophilic and hydrophobic solutes. In addition, some of the responsive membranes also possess ion-selectivity. These membranes may find use in self-regulating systems.

### *Applications*

In the water treatment process, stimuli responsive membranes have been used for controllable separation and addressing membrane fouling.

*Controllable separation.* Controllable oil water separation is the most studied controllable separation process so far. Che et al. developed a CO<sub>2</sub> responsive PMMA-co-PDEAEMA polymer nanofibre membrane.[218] This smart nanostructured electrospun polymer membrane is capable of switching oil / water wettability by bubbling and removing CO<sub>2</sub>. After CO<sub>2</sub>

bubbling, water penetrated the membrane while oil was retained. In contrast, upon exposure and dried in  $N_2$ , oil penetrated while water retained the membrane. The water flux was estimated to be 9500 LMH, while oil flux was as high as 17000 LMH. Kwon et al. fabricated a POSS + PDMS – based membrane for on demand electric field actuated separation of oil water emulsion driven by gravity.[219] Before applying an electric field, both oil and water were retained above the membrane, in the “off” state. However, when a voltage was applied to the membrane, water permeated through the membrane and oil was retained. The separation efficiency was  $\geq 99.9\%$  for oil water emulsions. Cheng et al. reported a pH controllable oil water separating membrane, which was fabricated by assembling responsive thiol molecules on the  $Cu(OH)_2$  nanorod structured copper mesh.[220] In non-alkaline solution, the membrane exhibited superhydrophobicity, permeating oil. It became superhydrophilic in alkaline solution, permeating water phase. Hu et al. prepared a photothermal-responsive ultrathin Au nanorods / poly (N-isopropyl acrylamide –co – acrylamide) cohybrid single-walled carbon nanotube (SWNT) nanoporous membrane.[221] The membrane exhibits hydrophilic and underwater oleophobicity, with a maximum separation water flux of 36000 LMH, which it can be modulated by light illumination during the process of separation. Zhang et al. developed a pH responsive membrane obtained by grafting a block copolymer, comprising blocks of pH responsive poly (2-vinylpyridine) and oleophilic/ hydrophobic polydimethylsiloxane (P2VP-b-PDMS), on non-woven textiles.[222] As illustrated in Figure 2.13, oil penetrated the original membrane after wetting with acidic solution (pH=2), water penetrated the membrane and oil retained. Cao et al. fabricated a thermo- and pH- dual responsive membrane for controllable oil water separation.[223] This membrane is synthesized by coating poly (dimethylamino ethyl methacrylate) (PDMAEMA) on a copper mesh via photo initiated free radical polymerization. Controllable separation can be achieved by adjusting the temperature or pH. Water permeated through the membrane under 55 °C (pH 7) and pH less than 13 ( $T = 25\text{ °C}$ ), while oil was retained. When the temperature is above 55 °C or pH is larger than 13, oil permeated through the mesh.

By introducing stimuli responsive ability, controllable oil water separation has been proven in three different manners upon giving stimuli: 1) selective separation of oil or water from oil water mixture / emulsion by changing membrane wettability and adhesion of different species, 2) “on” and “off” state management, 3) tuning the flux of separation by changing wettability.

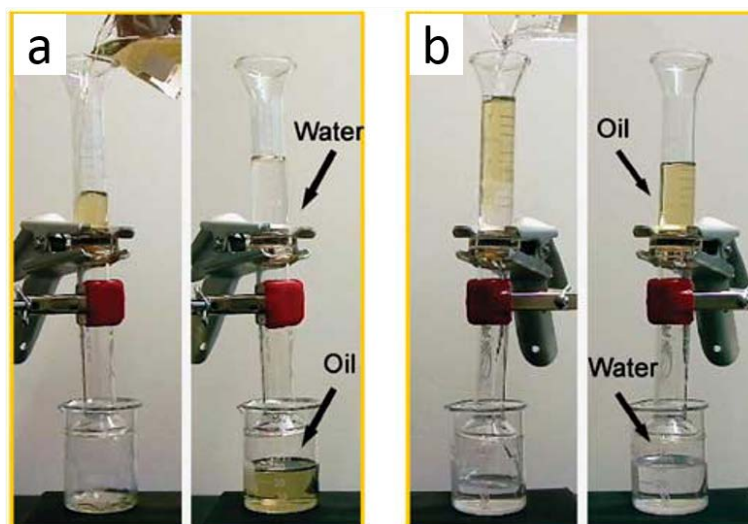


**Figure 2.13** Controllable oil water separation using pH responsive membrane.[222]

Responsive membranes have also been used for selective separation of proteins and metal ions. The membrane with controllable selectivity for protein separation was fabricated by grafting polymerization of sulfobetaine (SB) monomer near the surface of a PVP coated PVDF membrane.[224] After immersing in NaCl solution at 60°C, the protein mixture of BSA and Lys could be separated efficiently. However, after the immersion of membrane in pure water, both the flux and selectivity declined obviously. Le et al. prepared an electrochemical-pH-switchable PAA film for the removal of metal ions from aqueous waste in a lab-made semi-pilot system.[225] Metal ions were adsorbed by the PAA film via chelating. The adsorbed ions can be released in an electrochemically switchable process, when water electrolysis provides hydronium ions to regenerate the acidic form of PAA. A PNIPM functionalized PET track-etched UF membrane is fabricated via surface-initiated atom transfer radical polymerization by Frost et al.[226] The hydrodynamic pore diameter of this membrane could be switched from 21nm at 23 °C to 69 nm at 45 °C, while the rejection of monomodal 21 nm silica nanoparticles could be switched from 99% at 23 °C to only 35% at 45 °C.

*Addressing membrane fouling.* Due to the complexity of water or wastewater, membrane fouling often limits the membrane processes for water treatment. Membrane cleaning methods such as backflushing, air sparging, pumping cleaning solutions or acid / base solutions have been used in industry. However, these methods not only shorten the service life of the membrane, but also increase the operating cost. It is estimated that the membrane cleaning process takes 50 % of the total cost of membrane based process.[227, 228] It is of environmental, practical and capital importance to overcome the membrane fouling issue. To address the membrane fouling by introducing stimuli responsive materials, it is achieved by

improving the hydrophilicity of membrane or the oscillation between swollen and collapsed conformations of the responsive polymer, resulting in desorption of adsorbed fouling.

Han et al. fabricated a pH responsive membrane by blending pH responsive copolymers, poly (methyl methacrylate-co-acrylic acid) (PMMA-AA) or poly (methyl methacrylate-co-4-vinyl pyridine) (PMMA-4VPy), with polyethersulfone (PES), and forming via phase inversion.[229] The protein (BSA) ultrafiltration experiments showed that the membrane exhibited excellent anti-fouling property, which is due to the increased hydrophilicity of membrane and the same negatively charge of BSA and PAA in neutral solution. Cheng et al. prepared a pH sensitive hollow fibre membrane by blending PES with an amphiphilic copolymer poly (styrene- acrylic acid-N-vinylpyrrolidone) (PSt-AA-NVP).[230] The anti-fouling performance and flux recovery ratios increased after blending with PSt-AA-NVP that was because pH induced phase separation of the copolymer, resulting in the surface aggregation of AA and NVP chains, preventing the protein adsorption onto the membrane surface. Yu et al. modified a thin film composite reverse osmosis membrane by depositing thermo-responsive polymer, poly (N-isopropyl acrylamide-co-acrylamide) (PNIPAM-co-AM), on membrane surface. This membrane exhibited significantly enhanced antifouling properties and cleaning efficiency.[231] The enhanced antifouling performance was because of the improved wettability of membrane surface. The improved cleaning efficiency of the modified membrane was due to the phase transition of the thermo-responsive polymer coating layer. Meng et al. modified the TFC-RO membrane by redox initiated grafting of a zwitterionic polymer poly (4-(2-sulfoethyl)-1-(4-vinylbenzyl) pyridinium betaine) (PSVBP) to obtain a salt-responsive membrane.[232] The incorporation of PSVBP improved the antifouling property by increasing the hydrophilicity and negatively charged density on the membrane surface. On the other hand, the improved cleaning efficiency was attributed to the state transition of the salt-responsive polymer, facilitating the removal of foulants on membrane surface. Zhou et al. designed a thermo-responsive membrane by chemically grafting PNIPAM brushes onto the surface of zirconium oxide ( $ZrO_2$ ) membranes.[233] Following the temperature change ( $35\text{ }^\circ\text{C} / 25\text{ }^\circ\text{C}$ ) cleaning method (Figure 2.14), a flux recovery of about 80 % was achieved for PNIPAM-g- $ZrO_2$  membrane, while that of  $ZrO_2$  membrane was only about 14 % at  $25\text{ }^\circ\text{C}$ . The hydrophilicity and rapid stretching of PNIPAM chains were responsible for the loosening and shaking off adsorbed BSA on membrane surface.

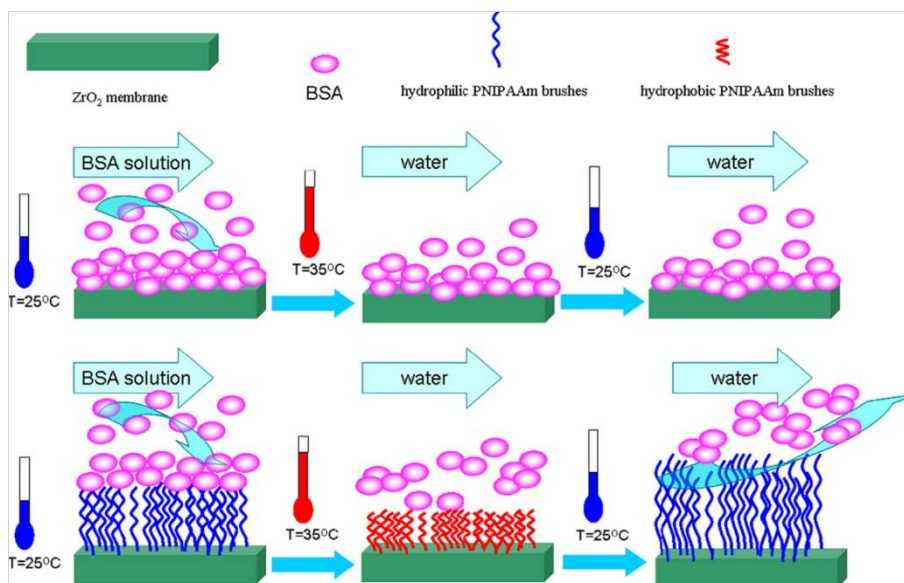


**Figure 2.14** Alternative temperature change cleaning procedures of raw  $ZrO_2$  and PNIPAM-g- $ZrO_2$  membrane.[233]

The incorporation of stimuli responsive ability to address the membrane fouling issue is relatively new. However, this process shows great potential in practical application as the research listed above.

Responsive membrane systems with switchable properties and highly adaptive surfaces have been manufactured in recent decades, but most of it has been focused on how the different responsive interactions within the membranes can be tuned and monitored in controlled environments. The challenges of responsive membrane lie in: (1) how to achieve functionality while maintaining membrane stability and mechanical integrity for the practical application; (2) how to fabricate a membrane which can respond in more complex and less defined situations and mimic the functionalities of living systems; (3) the development of piezoelectric membranes that vibrate under an AC field. It is thought that responsive membranes will be used in various niche applications in the next 5-10 years, and be more widely use in 10-20 years. It is a challenge, yet highly desirable, to explore the field of responsive membrane with better properties and practical applications.

## 2.3.2 Responsive draw agent

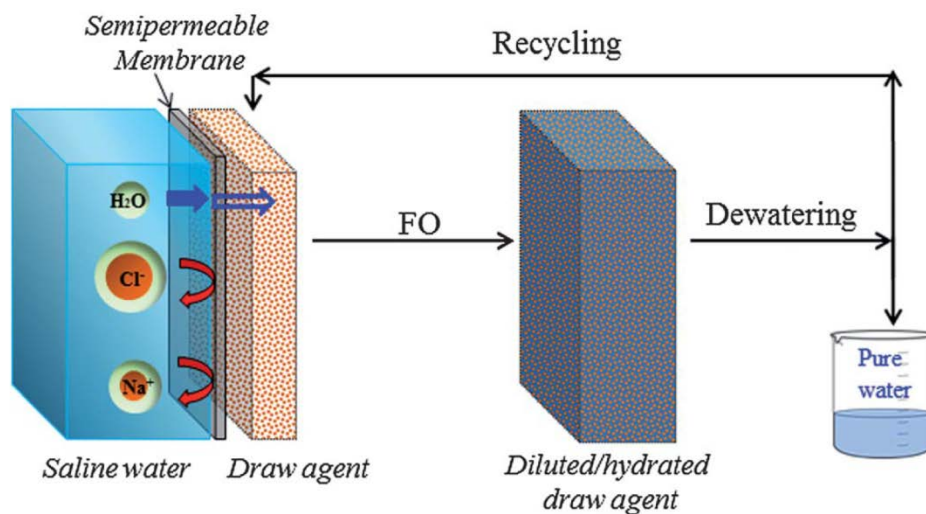


**Figure 2.15** Schematic illustration of forward osmosis desalination process.

Forward osmosis (FO) is a process in which a semi-permeable membrane is used as a separation medium, and the differential of osmotic pressure of draw and feed acts as driving force, as shown in Figure 2.15. Forward osmosis process has attracted rapidly-growing research interest because it shows great potential in reducing energy costs in desalination and water treatment. Semipermeable membrane and draw agents play a vital role in the FO process. When selecting a draw agent, it should possess a sufficiently high osmotic pressure, relative to the feed solution; it should be able to be easily recovered and regenerated at low energy cost; it should allow for reuse in the FO process and retain its high performance in the long-term operation; it should be low or no toxicity, chemical stability, and good compatibility with the FO membrane. Smart draw agents have been considered as a low energy cost material in the forward osmosis process, attracting increasing attention in recently years. To date, there are mainly three types of such responsive draw agents reported, including functionalized magnetic nanoparticles, responsive polyelectrolyte solutions, and stimuli-responsive polymer hydrogels.

*Magnetic particles.* Warne et al. and Adham et al. suggested using functionalized magnetic nanoparticles as draw agents in the forward osmosis process.[234] Chung's group fabricated a series of highly hydrophilic magnetic nanoparticles (MNPs) coated with different polymers to balance the FO performance and the reusability. The MNPs modified with 2-pyrrolidone, triethylene glycol and PAA yield 2.4-7.5 LMH water permeation with DI water as feed, however, the MNPs aggregated after recycling, and lower flux was obtained by recycled particles.[235] After combining the MNPs with PNIPAM and triethylene glycol, excellent

stability and recycle capacity were obtained, and the flux was maintained after 5 cycles, although the FO flux is only 1.2 LMH when DI water used as feed.[236] In future work, they modified MNPs with PAA or PAA/PNIPAM, which generated 2.6-5.5 LMH water flux when DI water as feed, with constant fluxes after recycling.[237] Regardless of the low water flux, the long-term stability and large-scale production of magnetic nanoparticles still needs to be addressed.

*Responsive polyelectrolytes.* The pH sensitive polyelectrolyte (poly (sodium acrylate), PSA) has been reported in the forward osmosis process by Chung's group. The water flux generated by the 0.6 g/ml PSA 1200 solution was ~5 LMH. However, the diluted PSA solution was recovered by ultrafiltration process under 10 bar, it is an energy-consuming process.[238] Linear poly (N-isopropyl acrylamide-co-sodium acrylate) (PNIPAM-SA) was also used as draw agent. Even though thermo-responsive polyelectrolytes can be easily recovered by heat ultrafiltration at 2 bar, the flux generated was only 0.35 LMH owing to the low proportion of ionic groups in the polyelectrolyte network (4 wt. % SA).[148] Cai et al. reported a CO<sub>2</sub> switchable dual responsive polymers as a forward osmosis draw solute.[239] After purging with CO<sub>2</sub>, the low molecular weight responsive polymer (poly [2-(dimethylamino) ethyl methacrylate], PDMAEMA) became polyelectrolytes with high osmolality and used as draw solutes for seawater desalination. When PDMAEMA with a molecular weight of 4000 g/mol was used, the 0.6 g/g polymer solution generated > 2 LMH water flux against seawater as feed. After removal of CO<sub>2</sub> by purging inert gas, these polymer precipitated above their LCST, realizing the water recovery and draw solute reuse. Recently, a thermo-responsive copolymer, poly (sodium styrene-4-sulfonate-co-N-isopropylacrylamide) (PSSS-PNIPAM), was employed as draw solute in forward osmosis for seawater desalination. A water flux of 4 LMH has been obtained with simulated seawater as the feed solution; the draw solution was regenerated with membrane distillation (MD) at a temperature above the lower critical solution temperature. [240] A series of oligomeric poly (tetrabutylphosphonium styrenesulfonate) (PSSP) were also evaluated as FO draw solutes.[241] When 20 wt. % polymer solution was used as draw solute and 2000 ppm NaCl solution used as a feed, the water flux was about 6 LMH. More than 99.5% of PSSPs in diluted solutions can be recovered by only thermal treatment and without any further significant decrease in the water permeation flux. More recently, ionic liquids have also been explored as a responsive draw agent.[242] Although the separation of polyelectrolytes from water has been investigated, little attention has been paid

to the quality of the water product. The polyelectrolytes are likely to contaminate the product water, especially the polymers with small molecular weight.

*Responsive hydrogels.* Cross-linked poly (N-isopropyl acrylamide) (PNIPAM) and its copolymer have been applied as smart draw agents in forward osmosis water treatment. Cross-linked poly (N-isopropyl acrylamide) (PNIPAM) is a classical thermo-sensitive hydrogel with both hydrophilic groups and hydrophobic groups in the network, which switches between hydrophilicity and hydrophobicity at temperatures lower and higher than its lower critical solution temperature (LCST). In 2011, our group successfully demonstrated the feasibility by using smart draw agents in FO desalination for the first time. In the first study, PAM (polyacrylamide), PSA, PNIPAM, and PNIPAM-co-SA hydrogels were used for purifying brackish water (2000 ppm NaCl solution). The result showed that the FO water flux increased with increasing ionic group content in the network, and decreased with increasing time; the water recovery increased with increasing amount of NIPAM and higher water content of the hydrogels. The average water flux of PNIPAM-co-SA in the first hour was 0.55 LMH, the swollen hydrogel with 66.7 % water content released 17 % water after 2 minutes dewatering at 50 °C.[234] To improving the FO performance, we fabricated a hydrogel and carbon particles composite, the water flux of composite PSA-NIPAM-C in the first 0.5 hour was 0.77 LMH and almost 100 % water was recovered after 1 h exposure to solar irradiation of 1 kWm<sup>-2</sup>. [243] The hydrogels were also composited with reduced graphene oxide (rGO) to improve the swelling properties. When the water flux was tested using deionized water as the feed solution, the incorporation of 1.2 wt. % rGO led to an increase in the water flux by 164 % and 325 % for the PSA composite and PSA-NIPAM composite, respectively. Adding small amounts of rGO also increased the water recovery by a factor of two in the solar dewatering process.[244] In addition, in other work the hydrogel had magnetic nanoparticles incorporated. The result indicated that the magnetic heating was an effective and rapid method for dewatering of hydrogels. Significantly enhanced liquid water recovery (53 %) was achieved under magnetic heating, as opposed to only around 7 % liquid water recovery obtained via convection heating.[245] In addition to these factors, the effect of particle size on the performance of FO process has been investigated. The result showed that reducing the hydrogel particle size resulted in an increase in the rate of swelling, generating higher water flux.[246] The dual-functionality hydrogels consist of a water-absorptive layer (PSA-NIPAM particles) and a dewatering layer (PNIPAM particles) were applied to improve the dewatering rate. The dewatering flux rose from 10 to 25 LMH when the solar concentrator increased the input energy

from 0.5 to 2 kW / m<sup>2</sup>. [247] According to our previous study, the swelling pressure of hydrogel, the effective contact area between FO membrane and draw agent, and the water transport among the hydrogel are key factors affecting the FO water flux. Cai et al. reported thermally responsive hydrogels with a semi-interpenetrating network (semi-IPN) structure as the FO draw agent. The SI-0.2PSA generated 0.2 LMH water flux, which was higher than the PNIPAM (0.13 LMH) for the first hour FO process. At 40 °C, the semi-IPN hydrogels rapidly release nearly 100 % of the water absorbed during the FO drawing process carried out at room temperature. They also designed a quasi-continuous FO desalination unit, as show in Figure 2.16. [248] Recently, functionalized thermo-responsive microgels have been employed as draw agents in a laboratory scale FO desalination system. The microgel-based FO process showed a high water flux up to 9 LMH and a high water recovery ability of 72.4 %. [249] Thermal responsive polyionic liquid hydrogels, tetrabutylphosphonium p-styrenesulfonate (P4444 SS) and tributylhexylphosphonium p-styrenesulfonate (P4446 SS), with a LCST of about 44 °C were developed by Cai et al. for FO desalination. [250] The initial water flux of P4444 SS was higher than 2 LMH, and decreased to about 0.5 LMH after 7 hours, when 2000 ppm NaCl solution used as feed. The water and draw agent were recovered at 60 °C.

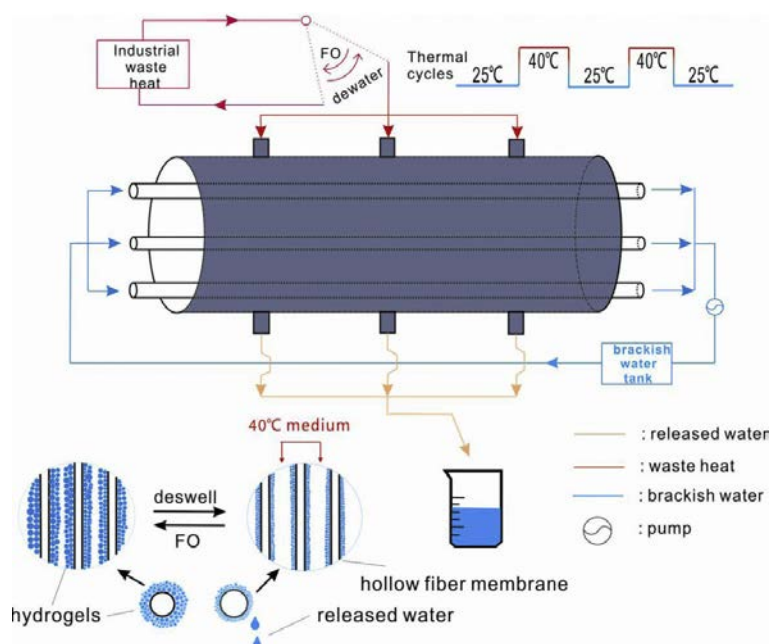


**Figure 2.16** Quasi-continuous FO desalination using a semi-IPN hydrogel as draw agent. [248]

Using responsive FO draw agent shows several advantages, such as easy recovery of product water and draw agent, and low back diffusion. However, there are still some challenges upon their applications: 1) relatively low water flux, 2) incomplete theoretical study, 3) reusability, 4) development of proper FO unit for continuous water production.

### 2.3.3 Responsive adsorbent

Adsorption is one of the most widely applied water treatment technologies due to their simple operation, relatively low cost, high efficiency, flexibility, and insensitivity to toxic substance. Developing regenerable, low cost, and environmentally-friendly adsorbents are always desired in view of practical water treatment applications. Stimuli responsive materials have been incorporated into adsorption materials for regeneration, selective adsorption and high adsorption capacity. To date, responsive hydrogel, magnetic composite and responsive material modified particles are the main responsive adsorbent studied and applied.

*Responsive hydrogel.* Shirsath et al. synthesize a poly (acrylic acid)-bentonite-FeCo (PAA-B-FeCo) hydrogel nanocomposite as a responsive adsorbent for removal of organic pollutant from water.[251] Temperature and pH affect the adsorption performance of PAA-B-FeCo that the optimum condition was operated at 35 °C and pH 11. Aburto et al. synthesized a stimuli responsive chitosan hydrogel (IH<sub>DBTS</sub>) by crosslinking of chitosan with glutaraldehyde in the presence of dibenzothiophene sulfone (DBTS) as template.[252] This hydrogel is temperature responsive, with a LCST of 50 °C. IH<sub>DBTS</sub> selectively adsorbed DBTS due to the conformational memory at the temperature of LCST. Yamashita et al. prepared an interpenetrating network (IPN) gel of PNIPAM and PSA for heavy metal ions removal.[253] The IPN gel adsorbed Cu<sup>2+</sup> ion below LCST but not above. However, at elevated temperature, water was released from hydrogel but Cu<sup>2+</sup> ions still trapped inside. Desorption of heavy metal ions can be triggered by acidic treatment. Lu et al. prepared sodium alginate beads by post crosslinking sodium alginate with glutaraldehyde in the presence of acetic acid and hydrochloric acid in acetone.[254] The sodium alginate beads could adsorb cationic dye and heavy metal ions, with and adsorption capacity of Cu<sup>2+</sup>, Ag<sup>+</sup>, Fe<sup>3+</sup> and methylene blue were 55, 83, 136, 573 mg/g, respectively. These adsorption performances were affected by the solution pH. The adsorption capacity of sodium alginate beads in the neutral state was twice as high as that in the acidic state, because the high pH dissociated carboxylic ions to provide high charge density and it interrupted the hydrogen bonding interaction. Nanostructured zwitterionic (ZI) hybrid hydrogel was prepared with monomer N, N-dimethyl-N-methacryloyloxyethyl-N-(3-sulfopropyl) ammonium (DMMSA) for protein separation of Lys and BSA.[255] This pH responsive hydrogel showed a minimum adsorption of Lys at pH 10.7, and that of BSA was observed at pH 4.8, indicating the feasibility of protein separation. Adsorption and desorption carried out in pH 6.0 buffer solution revealed nice cycle performance.

*Magnetic composite particles.* The magnetic composite particles have an advantage of easy collection / separation from solution by giving magnetic field. However, it is not responsible for the regeneration of adsorbent. Iron oxide has been incorporated into activated carbon to introduce the magnetic ability for easy collection. The study of Oliveira et al. showed that the composite exhibited same high adsorption capacities for phenol, chloroform, chlorobenzene and drimaren red dye in aqueous solution. Iron oxide has also been introduced to clay (bentonite) to obtain a magnetic composite for removing divalent metal ions in water, with adsorption capacities in a range of 40-75 mmol/g for  $\text{Ni}^{2+}$ ,  $\text{Cu}^{2+}$ ,  $\text{Cd}^{2+}$  and  $\text{Zn}^{2+}$ . [256] Xie et al. introduced a facile method to prepare  $\text{Fe}_3\text{O}_4 @$  polydopamine (PDA)-Ag core-shell microspheres for fast adsorption of Methylene blue (MB). [257] The as-prepared  $\text{Fe}_3\text{O}_4 @$  PDA-Ag exhibited good acid stability, high cyclic stability, magnetic separation, fast regeneration ability by using  $\text{NaBH}_4$  as the desorption agent. Magnetic  $\text{Fe}_3\text{O}_4 @$  carbon nanofibres with hierarchical porous fabricated by using electrospun polyacrylonitrile / polybenzoxazine nanofibres as a composite carbon source exhibited efficient adsorption for organic dyes. [258] The  $\text{Fe}_3\text{O}_4 @$  CNFs showed fast dyes adsorption kinetics and magnetic separation from water in a minute. Magnetic  $\text{Fe}_3\text{O}_4 @$  graphene composite (FGC) was also evaluated as adsorbent for methylene blue and Congo red removal. [259] The maximum adsorption capacities of MB and CR on FGC were 45 and 34 mg/g, respectively. Iron oxide / carbon nanotubes magnetic composites were also fabricated for heavy metal removal, such as chromium, europium,  $\text{Ni}^{2+}$  and  $\text{Sr}^{2+}$ . [260] What's more, natural polymer such as alginate and chitosan has already been composited with iron oxide, and applied for metal ions adsorption. [261, 262]

*Surface modified particles.* A pH- and temperature- responsive magnetic composite (poly (N-isopropyl acrylamide) grafted chitosan/ $\text{Fe}_3\text{O}_4$  composite particles, CN-MCP) was fabricated by Yang et al. as a high selective adsorbent for nonylphenol in water. [263] CN-MCP showed high adsorption capacity for removing nonylphenol: 1) 123 mg/g at pH 9 and 20 °C due to the charge attraction and binding between CN-MCP and nonylphenol; 2) 116 mg/g at pH 5 and 40 °C, because of their hydrophobic interaction. CN-MCP exhibited fast and highly efficient antibiotics adsorption, high stability, reusability and easy separation Liu et al. manufactured a pH- responsive and magnetic composite composed of graphene oxide (GO)/nanoscale zero-valent iron (nZVI) was used for antibiotics adsorption and oxidation degradation. [264]. After removal of antibiotics, the GO/nZVI composite was put into alkaline solution (pH>9) for adsorbent regeneration and antibiotics degradation by ozonization. Ammonium-functionalized hollow polymer particles ( $\text{HPP-NH}_3^+$ ) developed by Qin et al. were studied as a pH-responsive

adsorbent for selective removal of acid dye in water.[265] With the solution pH decreased from 9 to 2, the adsorption capacity of HPP-  $\text{NH}_3^+$  increased significantly from 59 to 406 mg/g, demonstrating the feasibility of easy regeneration under mild condition (pH 10 weak alkaline solution). The dye removal efficiency can be still as high as above 98 % after 5 adsorption – desorption cycles. Xu et al. fabricated a thermal responsive magnetic molecularly imprinted polymers (TMMIPs) by coating magnetic nanoparticle cores with thermo-responsive polymer and applied it for selective removal of sulfamethazine (SMZ) in aquatic environments.[266] TMMIPs could be collected by magnetic field and regenerated by changing the temperature of aqueous solution at 45 °C. A thermo-responsive composite synthesized by grafting poly (oligoethylene glycol) methacrylate (POEGMA) on cationic agarose adsorbent was used for size selective protein adsorption.[267] The adsorption capacity of POEGMA-g-Q increased with increasing temperature and reached maximum value around their LCST. This adsorbent has also been demonstrated for size selective adsorption upon temperature changes. In Dong's study, thermosensitive polymer composed of 4-vinylpyridine and NIPAM was imprinted on hollow porous polystyrene particles for selective recognition, controlled adsorption and release of bisphenol A (BPA).[268] The adsorption capacity of T-MIPs was temperature related, higher under 33 °C, and decreased rapidly at 50 °C. These composite particles were employed for removal of BPA from seawater and yogurt samples.

In addition, MOF-based adsorbents have been studied for water treatment such as removal of metal ions, toxic anions and dye. They showed remarkable adsorption capacity and superior adsorption kinetics, owing to their high surface area and accessibility of adsorption sites. Recently, photo-responsive metal organic frameworks have been fabricated for on command cargo release in water, indicating that responsive MOF-based possesses great potential for efficient and environmental friendly water treatment.[269]

Responsive adsorbents have been intensively studied in the past several decades, primarily magnetic responsive adsorbent for easy collection and separation from aqueous solution. Other responsive materials introduced are mainly used to tune the wettability and adhesion of different species for the selective adsorption purpose. The regeneration of adsorbent by stimuli responsiveness can significantly reduce the cost of adsorption process. The development of stimuli-responsive regenerable adsorbents with high adsorption and proper reusability are highly desirable.

## 2.4 Summary

Increasing population and improper industrialization practices have led to detrimental surface and underground water contamination at an unprecedented rate, endangering human health. Conventional water treatment systems can address many of these problems, but they are always chemically, operationally and energetically intensive, and require considerable infusion of capital and time, which precludes their use in much of the world, especially where water is really needed. There is a pressing need to develop a more effective, lower-cost, robust methods for water treatment and purification, without further stressing the environment by the treatment itself.

Advanced water treatment technologies have been developed to deal with this situation, they are mainly advanced oxidation process, biological treatment, adsorption / ion exchange process and membrane separation process. These advanced water treatment technologies deal with a range of contaminants that conventional water treatment system cannot address, such as persistence organic substances, toxic / heavy metals and radioactive metals, or deal with it in a more efficient way. The previous investigations have demonstrated the feasibility of these technologies and promoted their industry applications. However, further developments are needed to overcome the problems encountered, such as developing robust materials, stabilizing the treatment performance for real applications, maintaining the reusability, building practical and reliable systems and so on.

Stimuli responsive materials that change their physical and / or chemical properties in response to environmental stimuli, have been recently incorporated into the water treatment materials and include responsive membranes, responsive forward osmosis draw agents and responsive adsorbents. These responsive water treatment materials show great potential to overcome many problems found on the advanced water treatment technologies, such as membrane fouling and the energetic and chemical regeneration. The main use of responsiveness in membranes are controlling separation and addressing fouling. By the oscillation of chain conformation and wettability, selective permeation, tunable permeation flux and on-off state management can be achieved, as well as the releasing of adsorbed foulants. Responsive draw agents that release water and achieve regeneration by giving environmental stimuli, are very promising for reducing energy consumption of the forward osmosis process. Responsive adsorbents show great potential in practical application because of easy collection, easy regeneration and accessibility of raw adsorbent modification. However, the development

of these three kinds of responsive materials are still in an initial stage, with further development for advanced functionalities and applications desired for achieving a smart water treatment system with highly improved treatment efficiency and / or biomimetic nature.

In the following chapters, thermo-responsive oil water separation membrane (Chapter 3), responsive microfibrils-hydrogel composite draw agent (Chapter 4 & 5), and thermo-responsive MOF-based adsorbent (Chapter 6) are fabricated and evaluated for water processing.

## 2.5 References

- [1] S. Diop, P. M'mayi, D. Lisbjerg, R. Johnstone, Vital water graphics: an overview of the state of the world's fresh and marine waters, UNEP/Earthprint, 2002.
- [2] C.J. Vörösmarty, P.B. McIntyre, M.O. Gessner, D. Dudgeon, A. Prusevich, P. Green, S. Glidden, S.E. Bunn, C.A. Sullivan, C.R. Liermann, Global threats to human water security and river biodiversity, *Nature*, 467 (2010) 555-561.
- [3] R.P. Schwarzenbach, T. Egli, T.B. Hofstetter, U. von Gunten, B. Wehrli, Global water pollution and human health, *Annual Review of Environment and Resources*, 35 (2010) 109-136.
- [4] F.R. Rijsberman, Water scarcity: fact or fiction?, *Agricultural water management*, 80 (2006) 5-22.
- [5] R.E. Galt, Beyond the circle of poison: significant shifts in the global pesticide complex, 1976–2008, *Global Environmental Change*, 18 (2008) 786-799.
- [6] Y. Chen, F. Parvez, M. Gamble, T. Islam, A. Ahmed, M. Argos, J.H. Graziano, H. Ahsan, Arsenic exposure at low-to-moderate levels and skin lesions, arsenic metabolism, neurological functions, and biomarkers for respiratory and cardiovascular diseases: review of recent findings from the Health Effects of Arsenic Longitudinal Study (HEALS) in Bangladesh, *Toxicology and applied pharmacology*, 239 (2009) 184-192.
- [7] M. Amini, K.C. Abbaspour, M. Berg, L. Winkel, S.J. Hug, E. Hoehn, H. Yang, C.A. Johnson, Statistical modeling of global geogenic arsenic contamination in groundwater, *Environmental science & technology*, 42 (2008) 3669-3675.
- [8] L. Giusti, A review of waste management practices and their impact on human health, *Waste management*, 29 (2009) 2227-2239.
- [9] D.L. Baun, T.H. Christensen, Speciation of heavy metals in landfill leachate: a review, *Waste management & research*, 22 (2004) 3-23.

- [10] T.H. Christensen, P. Kjeldsen, P.L. Bjerg, D.L. Jensen, J.B. Christensen, A. Baun, H.-J. Albrechtsen, G. Heron, Biogeochemistry of landfill leachate plumes, *Applied geochemistry*, 16 (2001) 659-718.
- [11] D.W. Kolpin, E.T. Furlong, M.T. Meyer, E.M. Thurman, S.D. Zaugg, L.B. Barber, H.T. Buxton, Pharmaceuticals, hormones, and other organic wastewater contaminants in US streams, 1999– 2000: A national reconnaissance, *Environmental science & technology*, 36 (2002) 1202-1211.
- [12] T. Ternes, A. Joss, Human pharmaceuticals, hormones and fragrances, IWA publishing, 2007.
- [13] M.A. Montgomery, M. Elimelech, Water and sanitation in developing countries: including health in the equation, *Environ. Sci. Technol*, 41 (2007) 17-24.
- [14] M.A. Shannon, P.W. Bohn, M. Elimelech, J.G. Georgiadis, B.J. Marinas, A.M. Mayes, Science and technology for water purification in the coming decades, *Nature*, 452 (2008) 301-310.
- [15] P.H. Gleick, *Dirty-water: Estimated Deaths from Water-related Diseases 2000-2020*, Citeseer, 2002.
- [16] P. Vesilind, *Wastewater treatment plant design*, IWA publishing, 2004.
- [17] C.R. Schulz, D.A. Okun, D. Donaldson, J. Austin, *Surface water treatment for communities in developing countries*, (1992).
- [18] M. Hammer, J.(1975). *Water and Waste Water Technology*, in, John Wiley.
- [19] E. Washington, DC:“Primer for Municipal Waste water Treatment Systems.” Document no, in, EPA 832-R-04-001, 2004.
- [20] W.J. Weber, *Physicochemical processes for water quality control*, Wiley Interscience, 1972.
- [21] K. Christman, The history of chlorine, *Water World*, 14 (1998) 66-67.
- [22] C. HOWLETT, CHLORINE-THE ISSUE, THE REALITY AND THE SOLUTION, in: ABSTRACTS OF PAPERS OF THE AMERICAN CHEMICAL SOCIETY, AMER CHEMICAL SOC PO BOX 57136, WASHINGTON, DC 20037-0136, 1995, pp. 120-ENVR.
- [23] S. Parsons, *Advanced oxidation processes for water and wastewater treatment*, IWA publishing, 2004.
- [24] R. Andreozzi, V. Caprio, A. Insola, R. Marotta, Advanced oxidation processes (AOP) for water purification and recovery, *Catalysis today*, 53 (1999) 51-59.
- [25] D.G. Rao, R. Senthilkumar, J.A. Byrne, S. Feroz, *Wastewater treatment: advanced processes and technologies*, CRC Press, 2012.

- [26] J.J. Pignatello, E. Oliveros, A. MacKay, Advanced oxidation processes for organic contaminant destruction based on the Fenton reaction and related chemistry, *Critical reviews in environmental science and technology*, 36 (2006) 1-84.
- [27] H. Suty, C. De Traversay, M. Cost, Applications of advanced oxidation processes: present and future, *Water Science and Technology*, 49 (2004) 227-233.
- [28] J.R. Bolton, C.A.C. Cotton, *The ultraviolet disinfection handbook*, American Water Works Association, 2011.
- [29] G. Ruppert, R. Bauer, G. Heisler, UV-O<sub>3</sub>, UV-H<sub>2</sub>O<sub>2</sub>, UV-TiO<sub>2</sub> and the photo-Fenton reaction-comparison of advanced oxidation processes for wastewater treatment, *Chemosphere*, 28 (1994) 1447-1454.
- [30] J.C. Kruithof, P.C. Kamp, B.J. Martijn, UV/H<sub>2</sub>O<sub>2</sub> treatment: A practical solution for organic contaminant control and primary disinfection, *Ozone: Science and Engineering*, 29 (2007) 273-280.
- [31] S.R. Cater, M.I. Stefan, J.R. Bolton, A. Safarzadeh-Amiri, UV/H<sub>2</sub>O<sub>2</sub> treatment of methyl tert-butyl ether in contaminated waters, *Environmental science & technology*, 34 (2000) 659-662.
- [32] H. Shemer, Y.K. Kunukcu, K.G. Linden, Degradation of the pharmaceutical metronidazole via UV, Fenton and photo-Fenton processes, *Chemosphere*, 63 (2006) 269-276.
- [33] J. Chen, L. Zhu, Heterogeneous UV-Fenton catalytic degradation of dyestuff in water with hydroxyl-Fe pillared bentonite, *Catalysis Today*, 126 (2007) 463-470.
- [34] J. Chen, L. Zhu, Catalytic degradation of Orange II by UV-Fenton with hydroxyl-Fe-pillared bentonite in water, *Chemosphere*, 65 (2006) 1249-1255.
- [35] A. Chin, P. Bérubé, Removal of disinfection by-product precursors with ozone-UV advanced oxidation process, *Water Research*, 39 (2005) 2136-2144.
- [36] M.S. Lucas, J.A. Peres, G.L. Puma, Treatment of winery wastewater by ozone-based advanced oxidation processes (O<sub>3</sub>, O<sub>3</sub>/UV and O<sub>3</sub>/UV/H<sub>2</sub>O<sub>2</sub>) in a pilot-scale bubble column reactor and process economics, *Separation and Purification Technology*, 72 (2010) 235-241.
- [37] J. Verhoeven, Glossary of terms used in photochemistry (IUPAC Recommendations 1996), *Pure and Applied Chemistry*, 68 (1996) 2223-2286.
- [38] M.N. Chong, B. Jin, C.W. Chow, C. Saint, Recent developments in photocatalytic water treatment technology: a review, *Water research*, 44 (2010) 2997-3027.
- [39] M.A. Lazar, S. Varghese, S.S. Nair, Photocatalytic water treatment by titanium dioxide: recent updates, *Catalysts*, 2 (2012) 572-601.

- [40] A. Mills, S. Le Hunte, An overview of semiconductor photocatalysis, *Journal of photochemistry and photobiology A: Chemistry*, 108 (1997) 1-35.
- [41] S. Malato, P. Fernández-Ibáñez, M.I. Maldonado, J. Blanco, W. Gernjak, Decontamination and disinfection of water by solar photocatalysis: recent overview and trends, *Catalysis Today*, 147 (2009) 1-59.
- [42] Y. Shiyong, W. Ping, Y. Xin, W. Guang, W. ZHANG, S. Liang, A novel advanced oxidation process to degrade organic pollutants in wastewater: Microwave-activated persulfate oxidation, *Journal of environmental sciences*, 21 (2009) 1175-1180.
- [43] T. Velegraki, I. Poulios, M. Charalabaki, N. Kalogerakis, P. Samaras, D. Mantzavinos, Photocatalytic and sonolytic oxidation of acid orange 7 in aqueous solution, *Applied Catalysis B: Environmental*, 62 (2006) 159-168.
- [44] H. Destailats, A. Colussi, J.M. Joseph, M.R. Hoffmann, Synergistic effects of sonolysis combined with ozonolysis for the oxidation of azobenzene and methyl orange, *Journal of Physical Chemistry A*, 104 (2000) 8930-8935.
- [45] P.E. Savage, Organic chemical reactions in supercritical water, *Chemical reviews*, 99 (1999) 603-622.
- [46] H. Barner, C. Huang, T. Johnson, G. Jacobs, M. Martch, W. Killilea, Supercritical water oxidation: an emerging technology, *Journal of hazardous materials*, 31 (1992) 1-17.
- [47] Z. Aksu, Application of biosorption for the removal of organic pollutants: a review, *Process Biochemistry*, 40 (2005) 997-1026.
- [48] B. Volesky, Biosorbents for metal recovery, *Trends in Biotechnology*, 5 (1987) 96-101.
- [49] K. Vijayaraghavan, M.W. Lee, Y.-S. Yun, Evaluation of fermentation waste (*Corynebacterium glutamicum*) as a biosorbent for the treatment of nickel (II)-bearing solutions, *Biochemical Engineering Journal*, 41 (2008) 228-233.
- [50] B. Volesky, Z. Holan, Biosorption of heavy metals, *Biotechnology progress*, 11 (1995) 235-250.
- [51] F. Veglio, F. Beolchini, Removal of metals by biosorption: a review, *Hydrometallurgy*, 44 (1997) 301-316.
- [52] S. Choi, Y.-S. Yun, Lead biosorption by waste biomass of *Corynebacterium glutamicum* generated from lysine fermentation process, *Biotechnology letters*, 26 (2004) 331-336.
- [53] Z. Holan, B. Volesky, Biosorption of lead and nickel by biomass of marine algae, *Biotechnology and Bioengineering*, 43 (1994) 1001-1009.
- [54] Z. Holan, B. Volesky, I. Prasetyo, Biosorption of cadmium by biomass of marine algae, *Biotechnology and bioengineering*, 41 (1993) 819-825.

- [55] H. An, B. Park, D. Kim, Crab shell for the removal of heavy metals from aqueous solution, *Water Research*, 35 (2001) 3551-3556.
- [56] M.Y. Lee, K.J. Hong, T. Kajiuchi, J.W. Yang, Determination of the efficiency and removal mechanism of cobalt by crab shell particles, *Journal of Chemical Technology and Biotechnology*, 79 (2004) 1388-1394.
- [57] M.-Y. Lee, S.-H. Lee, H.-J. Shin, T. Kajiuchi, J.-W. Yang, Characteristics of lead removal by crab shell particles, *Process biochemistry*, 33 (1998) 749-753.
- [58] K. Vijayaraghavan, J.R. Jegan, K. Palanivelu, M. Velan, Nickel recovery from aqueous solution using crab shell particles, *Adsorption Science & Technology*, 23 (2005) 303-312.
- [59] K. Vijayaraghavan, K. Palanivelu, M. Velan, Biosorption of copper (II) and cobalt (II) from aqueous solutions by crab shell particles, *Bioresource technology*, 97 (2006) 1411-1419.
- [60] K. Vijayaraghavan, H.Y.N. Winnie, R. Balasubramanian, Biosorption characteristics of crab shell particles for the removal of manganese (II) and zinc (II) from aqueous solutions, *Desalination*, 266 (2011) 195-200.
- [61] G. Dönmez, Z. Aksu, The effect of copper (II) ions on the growth and bioaccumulation properties of some yeasts, *Process Biochemistry*, 35 (1999) 135-142.
- [62] Z. Aksu, G. Dönmez, The use of molasses in copper (II) containing wastewaters: effects on growth and copper (II) bioaccumulation properties of *Kluyveromyces marxianus*, *Process Biochemistry*, 36 (2000) 451-458.
- [63] Z. Aksu, G. Dönmez, Combined effects of molasses sucrose and reactive dye on the growth and dye bioaccumulation properties of *Candida tropicalis*, *Process Biochemistry*, 40 (2005) 2443-2454.
- [64] S.D. Cunningham, D.W. Ow, Promises and prospects of phytoremediation, *Plant physiology*, 110 (1996) 715.
- [65] M.N. Vara Prasad, H.M. de Oliveira Freitas, Metal hyperaccumulation in plants: biodiversity prospecting for phytoremediation technology, *Electronic Journal of Biotechnology*, 6 (2003) 285-321.
- [66] M. Benka-Coker, A. Olumagin, Waste drilling-fluid-utilising microorganisms in a tropical mangrove swamp oilfield location, *Bioresource technology*, 53 (1995) 211-215.
- [67] O.O. Amund, C. Igiri, Biodegradation of petroleum hydrocarbons under tropical estuarine conditions, *World Journal of Microbiology and Biotechnology*, 6 (1990) 255-262.
- [68] M.P. Díaz, K.G. Boyd, S.J. Grigson, J.G. Burgess, Biodegradation of crude oil across a wide range of salinities by an extremely halotolerant bacterial consortium MPD-M, immobilized onto polypropylene fibers, *Biotechnology and bioengineering*, 79 (2002) 145-153.

- [69] A. Dąbrowski, Adsorption—from theory to practice, *Advances in colloid and interface science*, 93 (2001) 135-224.
- [70] S.D. Alexandratos, Ion-exchange resins: a retrospective from industrial and engineering chemistry research, *Industrial and Engineering Chemistry Research*, 48 (2009) 388.
- [71] W.L. McCabe, J.C. Smith, P. Harriott, *Unit operations of chemical engineering*, McGraw-Hill New York, 1993.
- [72] A. Anson, J. Jagiello, J.B. Parra, M.L. Sanjuan, A.M. Benito, W.K. Maser, M.T. Martínez, Porosity, surface area, surface energy, and hydrogen adsorption in nanostructured carbons, *The Journal of Physical Chemistry B*, 108 (2004) 15820-15826.
- [73] S.J. Gregg, K.S.W. Sing, H. Salzberg, Adsorption surface area and porosity, *Journal of The Electrochemical Society*, 114 (1967) 279C-279C.
- [74] J. Rouquerol, F. Rouquerol, P. Llewellyn, G. Maurin, K.S. Sing, *Adsorption by powders and porous solids: principles, methodology and applications*, Academic press, 2013.
- [75] F. Rodríguez-Reinoso, Production and applications of activated carbons, *Handbook of porous solids*, (2002) 1766-1827.
- [76] H. Marsh, F.R. Reinoso, *Activated carbon*, Elsevier, 2006.
- [77] V.J. Inglezakis, S.G. Pouloupoulos, *Adsorption, ion exchange and catalysis*, Elsevier, 2006.
- [78] S.-W. Bian, J. Baltrusaitis, P. Galhotra, V.H. Grassian, A template-free, thermal decomposition method to synthesize mesoporous MgO with a nanocrystalline framework and its application in carbon dioxide adsorption, *Journal of Materials Chemistry*, 20 (2010) 8705-8710.
- [79] M. Bhagiyalakshmi, J.Y. Lee, H.T. Jang, Synthesis of mesoporous magnesium oxide: its application to CO<sub>2</sub> chemisorption, *International Journal of Greenhouse Gas Control*, 4 (2010) 51-56.
- [80] J. Rouquerol, K.S. Sing, P. Llewellyn, *Adsorption by metal oxides, Adsorption by Powders and Porous Solids: Principles, Methodology and Applications*, (2013) 393.
- [81] R.M. Cornell, U. Schwertmann, *The iron oxides: structure, properties, reactions, occurrences and uses*, John Wiley & Sons, 2003.
- [82] H. Van Olphen, Thermodynamics of interlayer adsorption of water in clays. I.—Sodium vermiculite, *Journal of Colloid Science*, 20 (1965) 822-837.
- [83] A.R. Khokhlov, Physics of finely divided matter, *Physics-Uspekhi*, 30 (1987) 196-196.
- [84] F. Bergaya, The meaning of surface area and porosity measurements of clays and pillared clays, *Journal of Porous Materials*, 2 (1995) 91-96.

- [85] A. Günay, B. Ersoy, S. Dikmen, A. Evcin, Investigation of equilibrium, kinetic, thermodynamic and mechanism of Basic Blue 16 adsorption by montmorillonitic clay, *Adsorption*, 19 (2013) 757-768.
- [86] E. Errais, J. Duplay, M. Elhabiri, M. Khodja, R. Ocampo, R. Baltenweck-Guyot, F. Darragi, Anionic RR120 dye adsorption onto raw clay: Surface properties and adsorption mechanism, *Colloids and Surfaces A: Physicochemical and Engineering Aspects*, 403 (2012) 69-78.
- [87] J.U.K. Oubagaranadin, Z. Murthy, Adsorption of divalent lead on a montmorillonite– illite type of clay, *Industrial & Engineering Chemistry Research*, 48 (2009) 10627-10636.
- [88] A. Baiker, H. Blaser, G. Ertl, H. Knözinger, J. Weitkamp, *Handbook of Heterogeneous Catalysis*, Ertl, G., Knözinger, H., Weitkamp, J., Eds, (1997) 2422.
- [89] C. Kresge, M. Leonowicz, W. Roth, J. Vartuli, J. Beck, Ordered mesoporous molecular sieves synthesized by a liquid-crystal template mechanism, *nature*, 359 (1992) 710-712.
- [90] D. Zhao, J. Feng, Q. Huo, N. Melosh, G.H. Fredrickson, B.F. Chmelka, G.D. Stucky, Triblock copolymer syntheses of mesoporous silica with periodic 50 to 300 angstrom pores, *science*, 279 (1998) 548-552.
- [91] X. Zhao, X. Bu, T. Wu, S.-T. Zheng, L. Wang, P. Feng, Selective anion exchange with nanogated isorecticular positive metal-organic frameworks, *Nature communications*, 4 (2013).
- [92] A.J. Howarth, M.J. Katz, T.C. Wang, A.E. Platero-Prats, K.W. Chapman, J.T. Hupp, O.K. Farha, High Efficiency Adsorption and removal of selenate and selenite from water using metal–organic frameworks, *Journal of the American Chemical Society*, 137 (2015) 7488-7494.
- [93] H. Furukawa, K.E. Cordova, M. O’Keeffe, O.M. Yaghi, The chemistry and applications of metal-organic frameworks, *Science*, 341 (2013) 1230444.
- [94] J.-R. Li, J. Sculley, H.-C. Zhou, Metal–organic frameworks for separations, *Chem. Rev*, 112 (2012) 869-932.
- [95] X. Li, H. Xu, F. Kong, R. Wang, A Cationic Metal–Organic Framework Consisting of Nanoscale Cages: Capture, Separation, and Luminescent Probing of Cr<sup>2O7</sup>– through a Single-Crystal to Single-Crystal Process, *Angewandte Chemie International Edition*, 52 (2013) 13769-13773.
- [96] H. Fei, C.S. Han, J.C. Robins, S.R. Oliver, A Cationic Metal–Organic Solid Solution Based on Co (II) and Zn (II) for Chromate Trapping, *Chemistry of Materials*, 25 (2013) 647-652.
- [97] S.L. James, Metal-organic frameworks, *Chemical Society Reviews*, 32 (2003) 276-288.
- [98] A.A. Zagorodni, *Ion exchange materials: properties and applications*, Elsevier, 2006.

- [99] J. Mulder, Basic principles of membrane technology, Springer Science & Business Media, 2012.
- [100] R.W. Baker, Membrane technology and applications, John Wiley & Sons, Ltd, (2004) 96-103.
- [101] R. Zsigmondy, W. Bachmann, Ueber neue filter, Zeitschrift für anorganische und allgemeine Chemie, 103 (1918) 119-128.
- [102] M. So, F. Eirich, H. Strathmann, R. Baker, Preparation of asymmetric loeb-sourirajan membranes, Journal of Polymer Science Part C: Polymer Letters, 11 (1973) 201-205.
- [103] S. Loeb, The Loeb-Sourirajan membrane: How it came about, in, ACS Publications, 1981.
- [104] S. Liu, K. Li, R. Hughes, Preparation of porous aluminium oxide ( $Al_2O_3$ ) hollow fibre membranes by a combined phase-inversion and sintering method, Ceramics international, 29 (2003) 875-881.
- [105] X. Tan, Y. Liu, K. Li, Preparation of LSCF ceramic hollow-fiber membranes for oxygen production by a phase-inversion/sintering technique, Industrial & engineering chemistry research, 44 (2005) 61-66.
- [106] Z. Siwy, P. Apel, D. Dobrev, R. Neumann, R. Spohr, C. Trautmann, K. Voss, Ion transport through asymmetric nanopores prepared by ion track etching, Nuclear Instruments and Methods in Physics Research Section B: Beam Interactions with Materials and Atoms, 208 (2003) 143-148.
- [107] E. Ferain, R. Legras, Track-etched membrane: dynamics of pore formation, Nuclear Instruments and Methods in Physics Research Section B: Beam Interactions with Materials and Atoms, 84 (1994) 331-336.
- [108] J. Quinn, J. Anderson, W. Ho, W. Petzny, Model pores of molecular dimension: the preparation and characterization of track-etched membranes, Biophysical journal, 12 (1972) 990-1007.
- [109] H.Y. Wang, T. Kobayashi, N. Fujii, Molecular imprint membranes prepared by the phase inversion precipitation technique, Langmuir, 12 (1996) 4850-4856.
- [110] H. Strathmann, K. Kock, The formation mechanism of phase inversion membranes, Desalination, 21 (1977) 241-255.
- [111] C. Smolders, A. Reuvers, R. Boom, I. Wienk, Microstructures in phase-inversion membranes. Part 1. Formation of macrovoids, Journal of Membrane Science, 73 (1992) 259-275.

- [112] B. McCool, N. Hill, J. DiCarlo, W. DeSisto, Synthesis and characterization of mesoporous silica membranes via dip-coating and hydrothermal deposition techniques, *Journal of membrane science*, 218 (2003) 55-67.
- [113] Y. Lu, R. Ganguli, C.A. Drewien, M.T. Anderson, C.J. Brinker, W. Gong, Y. Guo, H. Soyez, B. Dunn, M.H. Huang, Continuous formation of supported cubic and hexagonal mesoporous films by sol-gel dip-coating, *Nature*, 389 (1997) 364-368.
- [114] J. Le Roux, D. Paul, Preparation of composite membranes by a spin coating process, *Journal of membrane science*, 74 (1992) 233-252.
- [115] S. Mintova, T. Bein, Microporous Films Prepared by Spin-Coating Stable Colloidal Suspensions of Zeolites, *Advanced Materials*, 13 (2001) 1880-1883.
- [116] M. Ulbricht, H. Matuschewski, A. Oechel, H.-G. Hicke, Photo-induced graft polymerization surface modifications for the preparation of hydrophilic and low-protein-adsorbing ultrafiltration membranes, *Journal of Membrane Science*, 115 (1996) 31-47.
- [117] H. Iwata, M. Oodate, Y. Uyama, H. Amemiya, Y. Ikada, Preparation of temperature-sensitive membranes by graft polymerization onto a porous membrane, *Journal of membrane science*, 55 (1991) 119-130.
- [118] L.J. Zeman, A.L. Zydney, *Microfiltration and ultrafiltration: principles and applications*, M. Dekker, 1996.
- [119] J.K. Bungay, P.M. Bungay, H. Lonsdale, M. de Pinho, *Synthetic Membranes:: Science, Engineering and Applications*, Springer Science & Business Media, 2012.
- [120] V. Goel, M.A. Accomazzo, A.J. DiLeo, P. Meier, A. Pitt, M. Pluskal, R. Kaiser, Deadend microfiltration: applications, design, and cost, in: *Membrane Handbook*, Springer, 1992, pp. 506-570.
- [121] A.R. Cooper, *Ultrafiltration membranes and applications*, Springer Science & Business Media, 2013.
- [122] A.-S. Jönsson, G. Trägårdh, Ultrafiltration applications, *Desalination*, 77 (1990) 135-179.
- [123] M. Cheryan, *Ultrafiltration and microfiltration handbook*, CRC press, 1998.
- [124] Y. Song, F. Liu, B. Sun, Preparation, characterization, and application of thin film composite nanofiltration membranes, *Journal of applied polymer science*, 95 (2005) 1251-1261.
- [125] C. Wu, S. Zhang, D. Yang, X. Jian, Preparation, characterization and application of a novel thermal stable composite nanofiltration membrane, *Journal of Membrane Science*, 326 (2009) 429-434.

- [126] B. Van der Bruggen, C. Vandecasteele, Removal of pollutants from surface water and groundwater by nanofiltration: overview of possible applications in the drinking water industry, *Environmental pollution*, 122 (2003) 435-445.
- [127] A.A. Hussain, A.E. Al-Rawajfeh, Recent patents of nanofiltration applications in oil processing, desalination, wastewater and food industries, *Recent Patents on Chemical Engineering*, 2 (2009) 51-66.
- [128] D. Li, H. Wang, Recent developments in reverse osmosis desalination membranes, *Journal of Materials Chemistry*, 20 (2010) 4551-4566.
- [129] K.P. Lee, T.C. Arnot, D. Mattia, A review of reverse osmosis membrane materials for desalination—development to date and future potential, *Journal of Membrane Science*, 370 (2011) 1-22.
- [130] S. Sourirajan, *Reverse osmosis*, London, UK: Logos Press Ltd., 1970.
- [131] G.-d. Kang, Y.-m. Cao, Development of antifouling reverse osmosis membranes for water treatment: a review, *Water research*, 46 (2012) 584-600.
- [132] T.Y. Cath, A.E. Childress, M. Elimelech, Forward osmosis: principles, applications, and recent developments, *Journal of membrane science*, 281 (2006) 70-87.
- [133] C. Klaysom, T.Y. Cath, T. Depuydt, I.F. Vankelecom, Forward and pressure retarded osmosis: potential solutions for global challenges in energy and water supply, *Chemical society reviews*, 42 (2013) 6959-6989.
- [134] J. Wei, C. Qiu, C.Y. Tang, R. Wang, A.G. Fane, Synthesis and characterization of flat-sheet thin film composite forward osmosis membranes, *Journal of Membrane Science*, 372 (2011) 292-302.
- [135] S. Zhao, L. Zou, C.Y. Tang, D. Mulcahy, Recent developments in forward osmosis: opportunities and challenges, *Journal of Membrane Science*, 396 (2012) 1-21.
- [136] D.K. Anderson, *Concentration of dilute industrial wastes by Direct osmosis*, University of Rhode Island, 1977.
- [137] F. Votta, *Concentration of Industrial Waste by Direct Osmosis*, (1974).
- [138] R. York, R. Thiel, E. Beaudry, Full-scale experience of direct osmosis concentration applied to leachate management, in: *Proceedings of the Seventh International Waste Management and Landfill Symposium (Sardinia'99)*, S. Margherita di Pula, Cagliari, Sardinia, Italy, 1999.
- [139] N.A. Thompson, P.G. Nicoll, Forward osmosis desalination: a commercial reality, in: *IDA World Congress—Perth Convention and Exhibition Centre (PCEC)*, Perth, Western Australia September, 2011, pp. 4-9.

- [140] D. Li, X. Zhang, J. Yao, G.P. Simon, H. Wang, Stimuli-responsive polymer hydrogels as a new class of draw agent for forward osmosis desalination, *Chemical Communications*, 47 (2011) 1710-1712.
- [141] J.R. McCutcheon, R.L. McGinnis, M. Elimelech, A novel ammonia—carbon dioxide forward (direct) osmosis desalination process, *Desalination*, 174 (2005) 1-11.
- [142] Y.-C. Su, L. Lin, A water-powered micro drug delivery system, *Journal of Microelectromechanical Systems*, 13 (2004) 75-82.
- [143] J.R. Herron, E.G. Beaudry, C.E. Jochums, L.E. Medina, Osmotic concentration apparatus and method for direct osmotic concentration of fruit juices, in, *Google Patents*, 1994.
- [144] M.A.C. Stuart, W.T. Huck, J. Genzer, M. Müller, C. Ober, M. Stamm, G.B. Sukhorukov, I. Szleifer, V.V. Tsukruk, M. Urban, Emerging applications of stimuli-responsive polymer materials, *Nature materials*, 9 (2010) 101-113.
- [145] M. Wei, Y. Gao, X. Li, M.J. Serpe, Stimuli-responsive polymers and their applications, *Polymer Chemistry*, 8 (2017) 127-143.
- [146] D. Schmaljohann, Thermo- and pH-responsive polymers in drug delivery, *Advanced drug delivery reviews*, 58 (2006) 1655-1670.
- [147] B. Jeong, S.W. Kim, Y.H. Bae, Thermosensitive sol–gel reversible hydrogels, *Advanced drug delivery reviews*, 64 (2012) 154-162.
- [148] R. Ou, Y. Wang, H. Wang, T. Xu, Thermo-sensitive polyelectrolytes as draw solutions in forward osmosis process, *Desalination*, 318 (2013) 48-55.
- [149] R. Yoshida, K. Sakai, T. Okano, Y. Sakurai, Modulating the phase transition temperature and thermosensitivity in N-isopropylacrylamide copolymer gels, *Journal of Biomaterials Science, Polymer Edition*, 6 (1995) 585-598.
- [150] Y. Kaneko, S. Nakamura, K. Sakai, T. Aoyagi, A. Kikuchi, Y. Sakurai, T. Okano, Rapid deswelling response of poly (N-isopropylacrylamide) hydrogels by the formation of water release channels using poly (ethylene oxide) graft chains, *Macromolecules*, 31 (1998) 6099-6105.
- [151] R. Yoshida, K. Uchida, Y. Kaneko, K. Sakai, Comb-type grafted hydrogels with rapid de-swelling response to temperature changes, *Nature*, 374 (1995) 240.
- [152] T. Aoki, M. Kawashima, H. Katono, K. Sanui, N. Ogata, T. Okano, Y. Sakurai, Temperature-responsive interpenetrating polymer networks constructed with poly (acrylic acid) and poly (N, N-dimethylacrylamide), *Macromolecules*, 27 (1994) 947-952.
- [153] G. Kocak, C. Tuncer, V. Bütün, pH-Responsive polymers, *Polymer Chemistry*, 8 (2017) 144-176.

- [154] L. Gabaston, S. Furlong, R. Jackson, S. Armes, Direct synthesis of novel acidic and zwitterionic block copolymers via TEMPO-mediated living free-radical polymerization, *Polymer*, 40 (1999) 4505-4514.
- [155] Y. Qiu, K. Park, Environment-sensitive hydrogels for drug delivery, *Advanced drug delivery reviews*, 53 (2001) 321-339.
- [156] B. Firestone, R. Siegel, Kinetics and mechanisms of water sorption in hydrophobic, ionizable copolymer gels, *Journal of applied polymer science*, 43 (1991) 901-914.
- [157] S. Dai, P. Ravi, K.C. Tam, Thermo-and photo-responsive polymeric systems, *Soft Matter*, 5 (2009) 2513-2533.
- [158] G.S. Kumar, D. Neckers, Photochemistry of azobenzene-containing polymers, *Chemical Reviews*, 89 (1989) 1915-1925.
- [159] A. Tiwari, H. Kobayashi, *Responsive Materials and Methods: State-of-the-art Stimuli-responsive Materials and Their Applications*, John Wiley & Sons, 2013.
- [160] T. Manouras, M. Vamvakaki, Field responsive materials: photo-, electro-, magnetic-and ultrasound-sensitive polymers, *Polymer Chemistry*, 8 (2017) 74-96.
- [161] N. Viswanathan, D. Kim, S. Tripathy, Surface relief structures on azo polymer films, *Journal of Materials Chemistry*, 9 (1999) 1941-1955.
- [162] A. Natansohn, P. Rochon, Photoinduced motions in azo-containing polymers, *Chemical reviews*, 102 (2002) 4139-4176.
- [163] K.G. Yager, C.J. Barrett, All-optical patterning of azo polymer films, *Current opinion in solid state and materials science*, 5 (2001) 487-494.
- [164] K.G. Yager, C.J. Barrett, Novel photo-switching using azobenzene functional materials, *Journal of Photochemistry and Photobiology A: Chemistry*, 182 (2006) 250-261.
- [165] M.S. Vollmer, T.D. Clark, C. Steinem, M.R. Ghadiri, Photoswitchable Hydrogen-Bonding in Self-Organized Cylindrical Peptide Systems, *Angewandte Chemie International Edition*, 38 (1999) 1598-1601.
- [166] R. Klajn, Spiropyran-based dynamic materials, *Chemical Society Reviews*, 43 (2014) 148-184.
- [167] M. Moniruzzaman, C. Sabey, G. Fernando, Photoresponsive polymers: an investigation of their photoinduced temperature changes during photoviscosity measurements, *Polymer*, 48 (2007) 255-263.
- [168] Č. Koňák, R.C. Rathi, P. Kopečková, J. Kopeček, Photoregulated association of water-soluble copolymers with spirobenzopyran-containing side chains, *Macromolecules*, 30 (1997) 5553-5556.

- [169] A. Ivanov, N. Ereemeev, P.-O. Wahlund, I.Y. Galaev, B. Mattiasson, Photosensitive copolymer of N-isopropylacrylamide and methacryloyl derivative of spirobenzopyran, *Polymer*, 43 (2002) 3819-3823.
- [170] G. Filipcsei, J. Feher, M. Zrinyi, Electric field sensitive neutral polymer gels, *Journal of Molecular Structure*, 554 (2000) 109-117.
- [171] D. Roy, J.N. Cambre, B.S. Sumerlin, Future perspectives and recent advances in stimuli-responsive materials, *Progress in Polymer Science*, 35 (2010) 278-301.
- [172] S.J. Kim, H.I. Kim, S.R. Shin, S.I. Kim, Electrical behavior of chitosan and poly (hydroxyethyl methacrylate) hydrogel in the contact system, *Journal of applied polymer science*, 92 (2004) 915-919.
- [173] L.J. Romasanta, M. Lopez-Manchado, R. Verdejo, Increasing the performance of dielectric elastomer actuators: A review from the materials perspective, *Progress in Polymer Science*, 51 (2015) 188-211.
- [174] A. Gugliuzza, E. Drioli, A review on membrane engineering for innovation in wearable fabrics and protective textiles, *Journal of membrane science*, 446 (2013) 350-375.
- [175] B. Brugger, W. Richtering, Magnetic, Thermosensitive Microgels as Stimuli-Responsive Emulsifiers Allowing for Remote Control of Separability and Stability of Oil in Water-Emulsions, *Advanced Materials*, 19 (2007) 2973-2978.
- [176] J. Zhang, S. Xu, E. Kumacheva, Polymer microgels: reactors for semiconductor, metal, and magnetic nanoparticles, *Journal of the American Chemical Society*, 126 (2004) 7908-7914.
- [177] M. Zrinyi, Intelligent polymer gels controlled by magnetic fields, *Colloid & Polymer Science*, 278 (2000) 98-103.
- [178] S. Mukherjee, H. Dinda, L. Shashank, I. Chakraborty, R. Bhattacharyya, J. Das Sarma, R. Shunmugam, Site-specific amphiphilic magnetic copolymer nanoaggregates for dual imaging, *Macromolecules*, 48 (2015) 6791-6800.
- [179] Y. Zha, H.D. Thaker, R.R. Maddikeri, S.P. Gido, M.T. Tuominen, G.N. Tew, Nanostructured block-random copolymers with tunable magnetic properties, *Journal of the American Chemical Society*, 134 (2012) 14534-14541.
- [180] Z.M. Al-Badri, R.R. Maddikeri, Y. Zha, H.D. Thaker, P. Dobriyal, R. Shunmugam, T.P. Russell, G.N. Tew, Room temperature magnetic materials from nanostructured diblock copolymers, *Nature communications*, 2 (2011) 482.
- [181] P. Marmottant, S. Hilgenfeldt, Controlled vesicle deformation and lysis by single oscillating bubbles, *Nature*, 423 (2003) 153-156.

- [182] I. Lentacker, B.G. De Geest, R.E. Vandenbroucke, L. Peeters, J. Demeester, S.C. De Smedt, N.N. Sanders, Ultrasound-responsive polymer-coated microbubbles that bind and protect DNA, *Langmuir*, 22 (2006) 7273-7278.
- [183] I. Lavon, J. Kost, Mass transport enhancement by ultrasound in non-degradable polymeric controlled release systems, *Journal of controlled release*, 54 (1998) 1-7.
- [184] J. Kost, K. Leong, R. Langer, Ultrasonic modulated drug delivery systems, in: *Polymers in Medicine II*, Springer, 1986, pp. 387-396.
- [185] J. Kost, K. Leong, R. Langer, Ultrasound-enhanced polymer degradation and release of incorporated substances, *Proceedings of the National Academy of Sciences*, 86 (1989) 7663-7666.
- [186] Y. Ito, M. Casolaro, K. Kono, Y. Imanishi, An insulin-releasing system that is responsive to glucose, *Journal of controlled release*, 10 (1989) 195-203.
- [187] C.M. Hassan, F.J. Doyle, N.A. Peppas, Dynamic behavior of glucose-responsive poly (methacrylic acid-g-ethylene glycol) hydrogels, *Macromolecules*, 30 (1997) 6166-6173.
- [188] K. Podual, F.J. Doyle, N.A. Peppas, Dynamic behavior of glucose oxidase-containing microparticles of poly (ethylene glycol)-grafted cationic hydrogels in an environment of changing pH, *Biomaterials*, 21 (2000) 1439-1450.
- [189] K. Podual, F.J. Doyle, N.A. Peppas, Glucose-sensitivity of glucose oxidase-containing cationic copolymer hydrogels having poly (ethylene glycol) grafts, *Journal of Controlled Release*, 67 (2000) 9-17.
- [190] K. Podual, F. Doyle, N. Peppas, Preparation and dynamic response of cationic copolymer hydrogels containing glucose oxidase, *Polymer*, 41 (2000) 3975-3983.
- [191] N. Kashyap, B. Viswanad, G. Sharma, V. Bhardwaj, P. Ramarao, M.R. Kumar, Design and evaluation of biodegradable, biosensitive in situ gelling system for pulsatile delivery of insulin, *Biomaterials*, 28 (2007) 2051-2060.
- [192] V. Ravaine, C. Ancla, B. Catargi, Chemically controlled closed-loop insulin delivery, *Journal of Controlled Release*, 132 (2008) 2-11.
- [193] M. Brownlee, A. Cerami, A glucose-controlled insulin-delivery system: semisynthetic insulin bound to lectin, *Science*, 206 (1979) 1190-1191.
- [194] T.D. James, S. Shinkai, Artificial receptors as chemosensors for carbohydrates, in: *Host-guest chemistry*, Springer, 2002, pp. 159-200.
- [195] S. Toledano, R.J. Williams, V. Jayawarna, R.V. Ulijn, Enzyme-triggered self-assembly of peptide hydrogels via reversed hydrolysis, *Journal of the American Chemical Society*, 128 (2006) 1070-1071.

- [196] T. Miyata, N. Asami, T. Urugami, Preparation of an antigen-sensitive hydrogel using antigen– antibody bindings, *Macromolecules*, 32 (1999) 2082-2084.
- [197] D.P. Jones, J.L. Carlson, P.S. Samiec, P. Sternberg, V.C. Mody, R.L. Reed, L.A.S. Brown, Glutathione measurement in human plasma: evaluation of sample collection, storage and derivatization conditions for analysis of dansyl derivatives by HPLC, *Clinica chimica acta*, 275 (1998) 175-184.
- [198] V. Bulmus, M. Woodward, L. Lin, N. Murthy, P. Stayton, A. Hoffman, A new pH-responsive and glutathione-reactive, endosomal membrane-disruptive polymeric carrier for intracellular delivery of biomolecular drugs, *Journal of Controlled Release*, 93 (2003) 105-120.
- [199] X. Wang, J. Hu, G. Liu, J. Tian, H. Wang, M. Gong, S. Liu, Reversibly switching bilayer permeability and release modules of photochromic polymersomes stabilized by cooperative noncovalent interactions, *Journal of the American Chemical Society*, 137 (2015) 15262-15275.
- [200] K. Paek, H. Yang, J. Lee, J. Park, B.J. Kim, Efficient colorimetric pH sensor based on responsive polymer–quantum dot integrated graphene oxide, *ACS nano*, 8 (2014) 2848-2856.
- [201] D. Morales, E. Palleau, M.D. Dickey, O.D. Velev, Electro-actuated hydrogel walkers with dual responsive legs, *Soft Matter*, 10 (2014) 1337-1348.
- [202] R. Hoogenboom, Temperature-responsive polymers: properties, synthesis and applications, *Smart polymers and their applications*. Elsevier, Cambridge, (2014) 15-44.
- [203] S. Dai, P. Ravi, K.C. Tam, pH-Responsive polymers: synthesis, properties and applications, *Soft Matter*, 4 (2008) 435-449.
- [204] T. Shimoboji, Z.L. Ding, P.S. Stayton, A.S. Hoffman, Photoswitching of ligand association with a photoresponsive polymer– protein conjugate, *Bioconjugate chemistry*, 13 (2002) 915-919.
- [205] J. He, X. Tong, Y. Zhao, Photoresponsive nanogels based on photocontrollable cross-links, *Macromolecules*, 42 (2009) 4845-4852.
- [206] A.G. Fane, R. Wang, M.X. Hu, *Synthetic Membranes for Water Purification: Status and Future*, *Angewandte Chemie International Edition*, (2015).
- [207] C. Liangyin, X. Rui, J. Xiaojie, Stimuli-responsive membranes: smart tools for controllable mass-transfer and separation processes, *Chinese Journal of Chemical Engineering*, 19 (2011) 891-903.
- [208] D. Wandera, S.R. Wickramasinghe, S.M. Husson, Stimuli-responsive membranes, *Journal of Membrane Science*, 357 (2010) 6-35.
- [209] B. Zhao, W.J. Brittain, Polymer brushes: surface-immobilized macromolecules, *Progress in Polymer Science*, 25 (2000) 677-710.

- [210] N. Reber, A. Küchel, R. Spohr, A. Wolf, M. Yoshida, Transport properties of thermo-responsive ion track membranes, *Journal of Membrane Science*, 193 (2001) 49-58.
- [211] Y.-J. Choi, T. Yamaguchi, S.-i. Nakao, A novel separation system using porous thermosensitive membranes, *Industrial & engineering chemistry research*, 39 (2000) 2491-2495.
- [212] Y. Ito, Y.S. Park, Y. Imanishi, Nanometer-sized channel gating by a self-assembled polypeptide brush, *Langmuir*, 16 (2000) 5376-5381.
- [213] D.J. Chung, Y. Ito, Y. Imanishi, Preparation of porous membranes grafted with poly (spiropyran-containing methacrylate) and photocontrol of permeability, *Journal of applied polymer science*, 51 (1994) 2027-2033.
- [214] L.-Y. Chu, S.-H. Park, T. Yamaguchi, S.-i. Nakao, Preparation of thermo-responsive core-shell microcapsules with a porous membrane and poly (N-isopropylacrylamide) gates, *Journal of Membrane Science*, 192 (2001) 27-39.
- [215] T. Yamakawa, S. Ishida, M. Higa, Transport properties of ions through temperature-responsive charged membranes prepared using poly (vinyl alcohol)/poly (N-isopropylacrylamide)/poly (vinyl alcohol-co-2-acrylamido-2-methylpropane sulfonic acid), *Journal of membrane science*, 250 (2005) 61-68.
- [216] S.-B. Park, J.-O. You, H.-Y. Park, S.J. Haam, W.-S. Kim, A novel pH-sensitive membrane from chitosan—TEOS IPN; preparation and its drug permeation characteristics, *Biomaterials*, 22 (2001) 323-330.
- [217] J.i. Anzai, A. Ueno, H. Sasaki, K. Shimokawa, T. Osa, Photocontrolled permeation of alkali cations through poly (vinyl chloride)/crown ether membrane, *Die Makromolekulare Chemie, Rapid Communications*, 4 (1983) 731-734.
- [218] H. Che, M. Huo, L. Peng, T. Fang, N. Liu, L. Feng, Y. Wei, J. Yuan, CO<sub>2</sub>-Responsive Nanofibrous Membranes with Switchable Oil/Water Wettability, *Angewandte Chemie*, 127 (2015) 9062-9066.
- [219] G. Kwon, A. Kota, Y. Li, A. Sohani, J.M. Mabry, A. Tuteja, On-demand separation of oil-water mixtures, *Advanced Materials*, 24 (2012) 3666-3671.
- [220] Z. Cheng, J. Wang, H. Lai, Y. Du, R. Hou, C. Li, N. Zhang, K. Sun, pH-controllable on-demand oil/water separation on the switchable superhydrophobic/superhydrophilic and underwater low-adhesive superoleophobic copper mesh film, *Langmuir*, 31 (2015) 1393-1399.

- [221] L. Hu, S. Gao, X. Ding, D. Wang, J. Jiang, J. Jin, L. Jiang, Photothermal-responsive single-walled carbon nanotube-based ultrathin membranes for on/off switchable separation of oil-in-water nanoemulsions, *ACS nano*, 9 (2015) 4835-4842.
- [222] L. Zhang, Z. Zhang, P. Wang, Smart surfaces with switchable superoleophilicity and superoleophobicity in aqueous media: toward controllable oil/water separation, *NPG Asia Materials*, 4 (2012) e8.
- [223] Y. Cao, N. Liu, C. Fu, K. Li, L. Tao, L. Feng, Y. Wei, Thermo and pH dual-responsive materials for controllable oil/water separation, *ACS applied materials & interfaces*, 6 (2014) 2026-2030.
- [224] Q. Li, Q.-y. Bi, H.-H. Lin, L.-X. Bian, X.-L. Wang, A novel ultrafiltration (UF) membrane with controllable selectivity for protein separation, *Journal of membrane science*, 427 (2013) 155-167.
- [225] X.T. Le, P. Viel, P. Jegou, A. Sorin, S. Palacin, Electrochemical-switchable polymer film: An emerging technique for treatment of metallic ion aqueous waste, *Separation and Purification Technology*, 69 (2009) 135-140.
- [226] S. Frost, M. Ulbricht, Thermoresponsive ultrafiltration membranes for the switchable permeation and fractionation of nanoparticles, *Journal of membrane science*, 448 (2013) 1-11.
- [227] R.D. Wesson, E.S. Dow, S.R. Williams, Responsive Membranes/Material-Based Separations: Research and Development Needs, *Responsive Membranes and Materials*, (2012) 385-393.
- [228] J. Vrouwenvelder, J. Van Paassen, L. Wessels, A. Van Dam, S. Bakker, The membrane fouling simulator: a practical tool for fouling prediction and control, *Journal of Membrane Science*, 281 (2006) 316-324.
- [229] Z. Han, C. Cheng, L. Zhang, C. Luo, C. Nie, J. Deng, T. Xiang, C. Zhao, Toward robust pH-responsive and anti-fouling composite membranes via one-pot in-situ cross-linked copolymerization, *Desalination*, 349 (2014) 80-93.
- [230] C. Cheng, L. Ma, D. Wu, J. Ren, W. Zhao, J. Xue, S. Sun, C. Zhao, Remarkable pH-sensitivity and anti-fouling property of terpolymer blended polyethersulfone hollow fiber membranes, *Journal of membrane science*, 378 (2011) 369-381.
- [231] S. Yu, X. Liu, J. Liu, D. Wu, M. Liu, C. Gao, Surface modification of thin-film composite polyamide reverse osmosis membranes with thermo-responsive polymer (TRP) for improved fouling resistance and cleaning efficiency, *Separation and purification technology*, 76 (2011) 283-291.

- [232] J. Meng, Z. Cao, L. Ni, Y. Zhang, X. Wang, X. Zhang, E. Liu, A novel salt-responsive TFC RO membrane having superior antifouling and easy-cleaning properties, *Journal of Membrane Science*, 461 (2014) 123-129.
- [233] S. Zhou, A. Xue, Y. Zhang, M. Li, J. Wang, Y. Zhao, W. Xing, Fabrication of temperature-responsive ZrO<sub>2</sub> tubular membranes, grafted with poly (N-isopropylacrylamide) brush chains, for protein removal and easy cleaning, *Journal of Membrane Science*, 450 (2014) 351-361.
- [234] D. Li, H. Wang, Smart draw agents for emerging forward osmosis application, *Journal of Materials Chemistry A*, 1 (2013) 14049-14060.
- [235] M.M. Ling, K.Y. Wang, T.-S. Chung, Highly water-soluble magnetic nanoparticles as novel draw solutes in forward osmosis for water reuse, *Industrial & Engineering Chemistry Research*, 49 (2010) 5869-5876.
- [236] M. MingáLing, Facile synthesis of thermosensitive magnetic nanoparticles as “smart” draw solutes in forward osmosis, *Chemical communications*, 47 (2011) 10788-10790.
- [237] M.M. Ling, T.-S. Chung, Surface-dissociated nanoparticle draw solutions in forward osmosis and the regeneration in an integrated electric field and nanofiltration system, *Industrial & Engineering Chemistry Research*, 51 (2012) 15463-15471.
- [238] Q. Ge, J. Su, G.L. Amy, T.-S. Chung, Exploration of polyelectrolytes as draw solutes in forward osmosis processes, *Water research*, 46 (2012) 1318-1326.
- [239] Y. Cai, W. Shen, R. Wang, W.B. Krantz, A.G. Fane, X. Hu, CO<sub>2</sub> switchable dual responsive polymers as draw solutes for forward osmosis desalination, *Chemical Communications*, 49 (2013) 8377-8379.
- [240] D. Zhao, P. Wang, Q. Zhao, N. Chen, X. Lu, Thermoresponsive copolymer-based draw solution for seawater desalination in a combined process of forward osmosis and membrane distillation, *Desalination*, 348 (2014) 26-32.
- [241] J.-j. Kim, H. Kang, Y.-S. Choi, Y.A. Yu, J.-C. Lee, Thermo-responsive oligomeric poly (tetrabutylphosphonium styrenesulfonate) s as draw solutes for forward osmosis (FO) applications, *Desalination*, 381 (2016) 84-94.
- [242] Y. Zhong, X. Feng, W. Chen, X. Wang, K.-W. Huang, Y. Gnanou, Z. Lai, Using UCST ionic liquid as a draw solute in forward osmosis to treat high-salinity water, *Environmental science & technology*, 50 (2015) 1039-1045.
- [243] D. Li, X. Zhang, J. Yao, Y. Zeng, G.P. Simon, H. Wang, Composite polymer hydrogels as draw agents in forward osmosis and solar dewatering, *Soft Matter*, 7 (2011) 10048-10056.

- [244] Y. Zeng, L. Qiu, K. Wang, J. Yao, D. Li, G.P. Simon, R. Wang, H. Wang, Significantly enhanced water flux in forward osmosis desalination with polymer-graphene composite hydrogels as a draw agent, *Rsc Advances*, 3 (2013) 887-894.
- [245] A. Razmjou, M.R. Barati, G.P. Simon, K. Suzuki, H. Wang, Fast deswelling of nanocomposite polymer hydrogels via magnetic field-induced heating for emerging FO desalination, *Environmental science & technology*, 47 (2013) 6297-6305.
- [246] A. Razmjou, G.P. Simon, H. Wang, Effect of particle size on the performance of forward osmosis desalination by stimuli-responsive polymer hydrogels as a draw agent, *Chemical Engineering Journal*, 215 (2013) 913-920.
- [247] A. Razmjou, Q. Liu, G.P. Simon, H. Wang, Bifunctional polymer hydrogel layers as forward osmosis draw agents for continuous production of fresh water using solar energy, *Environmental science & technology*, 47 (2013) 13160-13166.
- [248] Y. Cai, W. Shen, S.L. Loo, W.B. Krantz, R. Wang, A.G. Fane, X. Hu, Towards temperature driven forward osmosis desalination using Semi-IPN hydrogels as reversible draw agents, *Water research*, 47 (2013) 3773-3781.
- [249] Y. Hartanto, S. Yun, B. Jin, S. Dai, Functionalized thermo-responsive microgels for high performance forward osmosis desalination, *water research*, 70 (2015) 385-393.
- [250] Y. Cai, R. Wang, W.B. Krantz, A.G. Fane, Exploration of using thermally responsive polyionic liquid hydrogels as draw agents in forward osmosis, *RSC Advances*, 5 (2015) 97143-97150.
- [251] S. Shirsath, A. Hage, M. Zhou, S. Sonawane, M. Ashokkumar, Ultrasound assisted preparation of nanoclay Bentonite-FeCo nanocomposite hybrid hydrogel: a potential responsive sorbent for removal of organic pollutant from water, *Desalination*, 281 (2011) 429-437.
- [252] J. Aburto, S. Le Borgne, Selective adsorption of dibenzothiophene sulfone by an imprinted and stimuli-responsive chitosan hydrogel, *Macromolecules*, 37 (2004) 2938-2943.
- [253] K. Yamashita, T. Nishimura, M. Nango, Preparation of IPN-type stimuli-Responsive heavy-Metal-Ion adsorbent gel, *Polymers for Advanced Technologies*, 14 (2003) 189-194.
- [254] T. Lu, T. Xiang, X.-L. Huang, C. Li, W.-F. Zhao, Q. Zhang, C.-S. Zhao, Post-crosslinking towards stimuli-responsive sodium alginate beads for the removal of dye and heavy metals, *Carbohydrate polymers*, 133 (2015) 587-595.
- [255] T. Chakrabarty, M. Kumar, V.K. Shahi, pH responsive hybrid zwitterionomer for protein separation: smart nanostructured adsorbent, *Industrial & Engineering Chemistry Research*, 51 (2012) 3015-3022.

- [256] L.C. Oliveira, R.V. Rios, J.D. Fabris, K. Sapag, V.K. Garg, R.M. Lago, Clay–iron oxide magnetic composites for the adsorption of contaminants in water, *Applied Clay Science*, 22 (2003) 169-177.
- [257] Y. Xie, B. Yan, H. Xu, J. Chen, Q. Liu, Y. Deng, H. Zeng, Highly regenerable mussel-inspired Fe<sub>3</sub>O<sub>4</sub>@ polydopamine-Ag core–shell microspheres as catalyst and adsorbent for methylene blue removal, *ACS applied materials & interfaces*, 6 (2014) 8845-8852.
- [258] T. Ren, Y. Si, J. Yang, B. Ding, X. Yang, F. Hong, J. Yu, Polyacrylonitrile/polybenzoxazine-based Fe<sub>3</sub>O<sub>4</sub>@ carbon nanofibers: hierarchical porous structure and magnetic adsorption property, *Journal of Materials Chemistry*, 22 (2012) 15919-15927.
- [259] Y. Yao, S. Miao, S. Liu, L.P. Ma, H. Sun, S. Wang, Synthesis, characterization, and adsorption properties of magnetic Fe<sub>3</sub>O<sub>4</sub>@ graphene nanocomposite, *Chemical Engineering Journal*, 184 (2012) 326-332.
- [260] C. Chen, J. Hu, D. Shao, J. Li, X. Wang, Adsorption behavior of multiwall carbon nanotube/iron oxide magnetic composites for Ni (II) and Sr (II), *Journal of hazardous materials*, 164 (2009) 923-928.
- [261] S.-F. Lim, Y.-M. Zheng, S.-W. Zou, J.P. Chen, Characterization of copper adsorption onto an alginate encapsulated magnetic sorbent by a combined FT-IR, XPS, and mathematical modeling study, *Environmental science & technology*, 42 (2008) 2551-2556.
- [262] Y.-C. Chang, D.-H. Chen, Preparation and adsorption properties of monodisperse chitosan-bound Fe<sub>3</sub>O<sub>4</sub> magnetic nanoparticles for removal of Cu (II) ions, *Journal of Colloid and Interface Science*, 283 (2005) 446-451.
- [263] Y. Zhen, Z. Ning, Z. Shaopeng, D. Yayi, Z. Xuntong, S. Jiachun, Y. Weiben, W. Yuping, C. Jianqiang, A pH-and temperature-responsive magnetic composite adsorbent for targeted removal of nonylphenol, *ACS applied materials & interfaces*, 7 (2015) 24446-24457.
- [264] W. Liu, J. Ma, C. Shen, Y. Wen, W. Liu, A pH-responsive and magnetically separable dynamic system for efficient removal of highly dilute antibiotics in water, *Water research*, 90 (2016) 24-33.
- [265] Y. Qin, L. Wang, C. Zhao, D. Chen, Y. Ma, W. Yang, Ammonium-functionalized hollow polymer particles as a pH-responsive adsorbent for selective removal of acid dye, *ACS Applied Materials & Interfaces*, 8 (2016) 16690-16698.
- [266] L. Xu, J. Pan, J. Dai, X. Li, H. Hang, Z. Cao, Y. Yan, Preparation of thermal-responsive magnetic molecularly imprinted polymers for selective removal of antibiotics from aqueous solution, *Journal of hazardous materials*, 233 (2012) 48-56.

- [267] M.F.X. Lee, E.S. Chan, K.C. Tam, B.T. Tey, Thermo-responsive adsorbent for size-selective protein adsorption, *Journal of Chromatography A*, 1394 (2015) 71-80.
- [268] R. Dong, J. Li, H. Xiong, W. Lu, H. Peng, L. Chen, Thermosensitive molecularly imprinted polymers on porous carriers: preparation, characterization and properties as novel adsorbents for bisphenol A, *Talanta*, 130 (2014) 182-191.
- [269] X. Meng, B. Gui, D. Yuan, M. Zeller, C. Wang, Mechanized azobenzene-functionalized zirconium metal-organic framework for on-command cargo release, *Science Advances*, 2 (2016) e1600480.

## Chapter 3 Robust thermo-responsive polymer composite membranes with switchable superhydrophilicity and superhydrophobicity for efficient oil-water separation

### Overview

To address the worldwide issue of increasing oily wastewater and oil spill accidents, stimuli-responsive surfaces with switchable superwettability have attracted growing interest for the required controlled oil-water separation. However, the fabrication of such smart membranes with good mechanical properties, excellent recycling properties, and the ability to separate oil-water emulsions in a productive and inexpensive way remains desirable yet challenging. In this chapter, a robust, thermo-responsive polymer membrane is produced by the combination of a thermoplastic polyurethane (TPU) microfibre web and poly (N-isopropylacrylamide) (PNIPAM). PNIPAM hydrogel is evenly coated on the surface of TPU microfibrils, and thus the wettability of TPU-PNIPAM membrane is amplified by taking advantage of the hierarchical structure and increased surface roughness. The TPU-PNIPAM membrane possesses switchable superhydrophilicity and superhydrophobicity as the temperature of membrane changes from 25 to 45 °C (Figure 3.1). The composite membrane is shown successfully able to separate a 1 wt. % oil-in-water emulsion and 1 wt. % water-in-oil emulsion at 25 and 45 °C, respectively, with a high separation efficiency of  $\geq 99.26$  %. Furthermore the composite membranes show excellent mechanical properties, and they are highly flexible and mechanically tough.

This chapter has been published as a journal article: Ranwen Ou, Jing Wei, Lei Jiang, George P. Simon, and Huanting Wang, *Environ. Sci. Technol.* **2016**, 50, 906-914

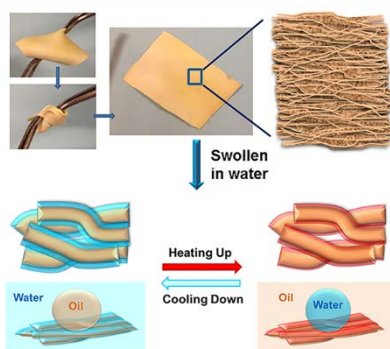


**Figure 3.1** Schematic illustration of robust thermo-responsive composite membrane.

### 3.1 Introduction

The ability to separate oil-water mixtures has recently attracted worldwide attention because of increasing amounts of oil-polluted wastewater, frequent oil spill accidents and the ongoing development of petroleum industry.[1, 2] In general, immiscible oil-water mixtures are separated using conventional separation techniques, such as gravity separation and oil-absorbing materials. In the case of the separation of oil-water emulsions, the conventional separation processes (air flotation, coagulation and flocculation) are costly, energy intensive and are not effective.[3-5] Pressure-driven membranes, especially ultrafiltration (UF) membranes, have been successfully used for the separation of oil-water emulsions. However, the size-sieving mechanism of UF membrane limits the practicality of this process, due to the resultant high energy consumption, low flux and rapid decrease in permeability with usage.[6-10] Recently, a series of superwetting membranes have been produced for efficient oil-water separation, including polymer-coated copper meshes, hydrogel-coated copper meshes, surface-modified copper meshes and polymer networks,[11-16] all taking advantage of surface chemistry and roughness.[17] It has been shown that a superhydrophilic / superoleophobic membrane is suitable for separating oil-in-water emulsions, while a superhydrophobic / superoleophilic membrane separates water-in-oil emulsions.[16, 18] The oil-water separation process with a superwetting membrane has been proven to be energy-efficient and cost-effective, as the membrane separates the oil-water mixture or oil-water emulsion according to the different interfacial effects of oil and water on the superwetting surface. For example, the superwetting membrane prepared by Kota et al. allowed for the removal of dispersed-phase droplets that were considerably smaller than the membrane pore size.[12] It is important to be able to prepare a responsive membrane with switchable superwettability, not only for controllable oil-water separation, but also for fabricating intelligent materials. Stimuli-responsive surfaces have been used to prepare smart membrane for some years, but to date there are only a few works that have been reported on responsive membranes with switchable underwater superoleophilicity and superoleophobicity, and fewer membranes with switchable superhydrophilicity and superhydrophobicity, for oil-water separation. The membranes reported to date with such switchable underwater superoleophilicity and superoleophobicity are pH-sensitive.[19-23] For those with switchable superhydrophilicity and superhydrophobicity, they are photo-induced or pH-responsive. Recently, an aligned ZnO nanorod arrays-coated mesh film was fabricated by Tian et al., which was shown able to be switchable between superhydrophilicity and superhydrophobicity, occurring by photo-

stimulation.[24] The other membranes with switchable superhydrophilicity and superhydrophobicity for oil-water separation are pH-responsive and can be controlled using solutions with different pH values. [25, 26] Some responsive membranes exhibit stimuli-responsive ability, but they are not capable of switching between superwettabilities. For example, a PDMAEMA hydrogel-coated copper mesh has been reported which was both thermo- and pH-responsive; however, it is solely superoleophobic under water without switchable superwettability.[27] A PVCL-co-PSF copolymer membrane shows thermo-responsive, but it is hydrophilic with a contact angle of 49.5 °C at room temperature.[28] Table 3.1 shows some attractive superwetting membranes published in recent years. For example, single-walled carbon nanotube network films and ammonia-modified PVDF membrane were found to be able to separate 99 % oil-water emulsion, and a PAA-g-PVDF membrane was able to efficiently separate a 1 % oil-water emulsion;[2, 16] what's more, a superamphiphilic PVDF membrane could separate oil-in-water and water-in-oil emulsions.[29] However, the responsive membranes with switchable superwettability were applied to separate  $\geq 10$  % oil-water mixtures and not emulsions.

Apart from oil-water separation properties, the mechanical properties and durability of membranes are other key factors important for practical application.[2] For instance, polymeric UF membranes are mainly prepared via phase inversion; however, the porous structure formed in the phase inversion process greatly weakens the mechanical properties of the membranes, and thus restricts their applicability. To meet the mechanical requirements for practical ultrafiltration, support materials (glass, metal, polymer, non-woven fabrics) have been applied to improve their mechanical property, although it may decrease the permeation flux.[8, 10, 30, 31]

Here, for the first time, a robust, thermo-responsive poly (N-isopropylacrylamide) (PNIPAM) hydrogel-coated thermoplastic polyurethane (TPU) microfibre membrane is fabricated for efficient oil-water emulsion separation. The membrane is superhydrophilic at room temperature (25 °C) and becomes superhydrophobic at a temperature above the lower critical solution temperature of PNIPAM (LCST, 32°C). TPU was selected for its high elongation, tensile strength, toughness, wear resistance and good flexibility over a wide temperature range. PNIPAM is a thermally responsive polymer that switches between hydrophilicity and hydrophobicity at temperatures lower and higher than its LCST. The force-spinning method was used to produce a non-woven TPU microfibre mesh or web, and is a rapid and productive technique to produce a micro- or nanoscale fibre mats in less than a minute. It works by

producing a jet of polymer in solution due to a high-speed, rotating nozzle and produces the fibre mesh without the need for a high-voltage power source and the limitation of solution conductivity, as is required, for example, by electrospinning.[32-35]

**Table 3.1** Superwetting membranes and relevant properties for oil-water separation published in recent years.

Year	Materials	Pore Size	wettability	Oil-water mixture concentration	Separation efficiency/ % or residual oil/ ppm	Remarks (flux, intrusion pressure (IP) or mechanical properties)	Ref.
2011	Hydrogel-coated mesh	50 $\mu\text{m}$	Superhydrophilic	30 v/v % hexane water mixture	99.8%	2.0 kPa (IP)	[15]
2012	Aligned ZnO nanorod array-coated mesh	25-270 $\mu\text{m}$	Photo-responsive, superhydrophilicity and superhydrophobicity	30 v/v % oil-water mixture	> 95%	--	[24]
2012	Fluorodecyl POSS+X-PEGDA coated mesh/ fabric	30.5-138 $\mu\text{m}$	Superhydrophilic and superoleophobic	10 v/v % water-in-hexadecane emulsion	>99%	--	[12]
2012	P2VP-b-PDMS-grafted textile	--	pH responsive, underwater superoleophilicity and superoleophobicity	--	--	--	[23]
2013	Single-walled carbon nanotube network films	10-200 nm	Superoleophilic	99.13 v/v % toluene-water emulsion	Oil purity 99.97%	3100 $\text{lm}^{-2}\text{h}^{-1}\text{bar}^{-1}$	[13]
2013	Ammonia modified PVDF membrane	--	Superhydrophobic	99.01 v/v % isooctane-water	Oil purity 99.98%	900 LMH, tensile strength 2.0 MPa, elongation 29.2 %	[2]
2013	Zeolite-coated mesh	5-42 $\mu\text{m}$	Underwater superoleophobic	50 v/v % diesel-water mixture	2.5 ppm	25 $\text{Lm}^{-2}\text{s}^{-1}$ , 729 Pa (IP)	[36]
2013	$\text{Cu}(\text{OH})_2$ nanowire-haired membrane	1-75 $\mu\text{m}$	Superhydrophilic	10 v/v % hexane-water emulsion	25 ppm	150000 LMH	[18]
2013	Chromic acid-treated PU foam with FAS modification	Hundreds micron	superhydrophobic	Crude oil-water mixture	98 %	--	[37]
2014	PVDF membrane	--	superamphiphilic	3.2 % and 99.13 % toluene-water emulsion	--	Water flux 9860 LMH, Oil flux 1820 LMH with 0.09 MPa	[29]
2014	Dual-scaled porous nitrocellulose membranes	450 nm	Underwater superoleophobic	46.7 v/v % gasoline-water mixture	99.92 %	679 Pa (IP)	[38]
2014	PDMAEMA hydrogel coated mesh	40 $\mu\text{m}$	Thermo- & pH-responsive, underwater superoleophobic	30 v/v % gasoline-water mixture	99.97 %	Water and oil permeate through the mesh orderly	[27]
2014	PAA-g-PVDF membrane	--	Superhydrophilic	1 % hexadecane-water emulsion	40 ppm	130 LMH	[16]
2015	PNIPAM-coated TPU microfibre membrane	3-27 $\mu\text{m}$	Thermo-responsive, switchable superhydrophilicity and superhydrophobicity	1 wt. % silicone oil-water emulsion and 99 wt. % silicone oil-water emulsion	99.45 % (55 ppm) at RT, 99.95 % (4.8 ppm) at 45 °C	Toughness 7536 $\text{kJ/m}^3$ , elongation 288 %. RT: 3646 LMH (water flux), 1.37kPa(IP); 45 °C: 503 LMH (oil flux), 0.89 kPa (IP)	This paper

The TPU-PNIPAM composite membrane has excellent mechanical strength, elasticity and switchable superhydrophilicity and superhydrophobicity, and shows a high efficiency in separating SDS-stabilized oil-in-water and water-in-oil micro-emulsions, but not mixtures, at room temperature and at an elevated temperature, respectively.

## 3.2 Experimental

### 3.2.1 Materials

The following chemicals were used as supplied: thermoplastic polyurethane (TPU, TETON\*206) particles were kindly provided by Urethane Compounds Pty. Ltd. Tetrahydrofuran (THF) was purchased from Merck (Kenilworth, NJ, USA). N-isopropyl acrylamide (NIPAM), N, N-methylene bis (acrylamide) (MBA), and ammonium persulfate (APS) were purchased from Sigma-Aldrich (St Louis, MO, USA). Distilled deionized (DDI) water was used in all experiments.

### 3.2.2 Experimental procedures

*Fabrication of TPU-PNIPAM membrane:* Thermoplastic polyurethane particles (12 g) were dissolved in tetrahydrofuran (THF, 88 g) under stirring to obtain a 12 wt. % polymer solution. N-isopropylacrylamide (NIPAM, 2g, monomer), N, N'-methylenebisacrylamide (MBA, 0.04 g, crosslinker) and ammonium persulfate (APS, 0.02 g, initiator) were dissolved in DDI water to form a 16.67 wt. % NIPAM reaction solution. As shown in Figure 3.2, the polymer solution was spun into TPU microfibre mat by a force spinner (Cyclone L-1000M, FibeRio<sup>®</sup> Technology Corporation, USA), with an operating condition of 5000 rpm and 30 seconds. Five microfibre mats were obtained and stacked up to form a TPU microfibre membrane. The as-prepared TPU microfibre membrane was then cut into a certain shape before wetting with NIPAM reaction solution. Free-radical polymerization of the NIPAM monomer solution was applied to coat the PNIPAM hydrogel on the TPU microfibrils' surface. After 2 hours reaction at 70 °C, TPU-PNIPAM membranes were obtained. The PNIPAM hydrogel loading of TPU-PNIPAM membranes was controlled by changing the amount of NIPAM reaction solution added to the TPU microfibre membranes. The TPU-PNIPAM membranes were washed with 25 °C water and 45 °C water more than 10 times to rinse the excess monomer before use.

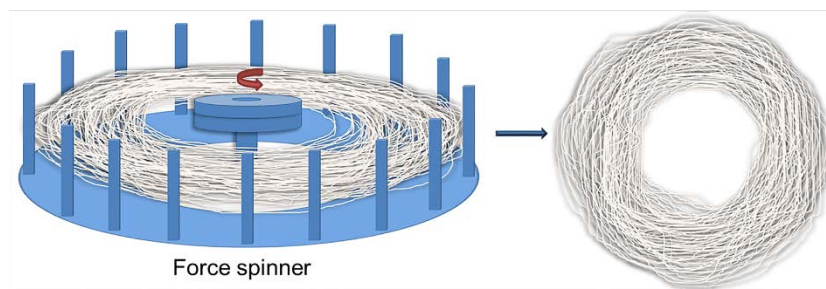


**Figure 3.2** The preparation process of TPU microfibre mat by a force spinner.

*Instruments and Characterization:* Scanning electron microscopy was undertaken with a Nova NanoSEM 450 FESEM, FEI, USA. Optical microscopy images were taken on an Olympus SZX16 Stereo Microscope. The contact angle of the membranes was determined using a contact angle goniometer (Dataphysics OCA15, Dataphysics, Germany). The average value was obtained from more than 5 measurements per sample. The mechanical properties of the membranes were measured using Mini-Instron (Micro Tester 5848, 100 N load cell, Instron Calibration Laboratory, U.K.). The swelling properties of PNIPAM of composite membrane were tested and calculated according to [39, 40]. The swelling ratio was calculated based on the PNIPAM hydrogel amount of the composite membrane, but not the composite membrane.

*Preparation of oil-water emulsions:* 1 wt. % silicone oil-water emulsion was prepared by mixing silicone oil and water in a ratio of 1:99 w/w with 1 mg/mL sodium dedecyl sulfate (SDS) under strong magnetic stirring and shaken to obtain a milky solution. 99 wt. % silicone oil-water emulsion was prepared by mixing silicone oil and water in a ratio of 99:1 w/w with 1 mg/mL SDS under strong stirring and shaking. Oil-water emulsions with different oils (hexadecane, paraffin, olive oil and fish oil) were prepared in a similar fashion. The SDS-stabilized oil water emulsions were stable more than a month.[16]

*Oil-water separation Experiment:* The as-prepared membrane was fixed between two glass tubes with an inner diameter of 12.86 mm. At room temperature, the 1 wt. % silicone oil-water emulsion was poured into the upper tube, and the separation was achieved by gravity only. At 45 °C, the swollen membrane was immersed in the 45 °C water to deswell and the excess water on the membrane surface was removed using tissue paper. The 99 wt. % silicone oil-water emulsion was heated to 45 °C and was poured into the separation setup in an oven set to 45 °C to achieve separation.

The oil concentration in collected water and the water concentration in the collected oil after separation were determined using a UV-Vis spectrophotometer (UV mini 1240) by testing the

light scattering data. The standard oil-water emulsion and the collected samples were sonicated for 0.5 hour to obtain a homogeneous solution before test. The separation efficiency was calculated by the following equation (1):

$$S = \frac{C_0 - C_1}{C_0} \times 100\% \quad (1)$$

where  $C_0$  (10000 mg/L) is the original oil concentration or water concentration in the feed.  $C_1$  is the oil or water concentration in permeate after filtration.

### 3.3 Results and Discussion

#### 3.3.1 Preparation and morphology

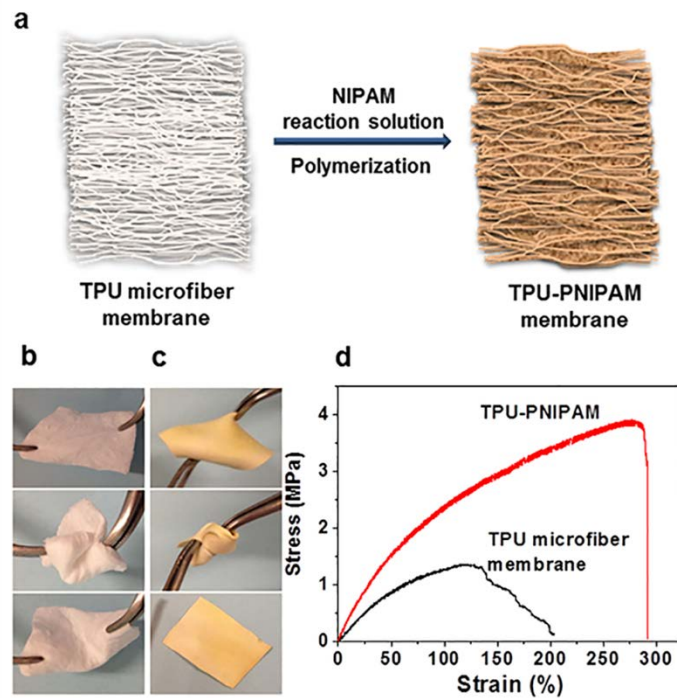


**Figure 3.3** (a) The preparation process of a TPU-PNIPAM composite membrane. The TPU microfibre membrane immersed with NIPAM reaction solution (16.7 wt. %) is polymerized at 70 °C for 2 hours. Photographs are shown of twisting test of (b) TPU microfibre membrane and (c) TPU-PNIPAM membrane with 3.6 wt. % PNIPAM loading (TPU-PNIPAM-3.6). (d) Stress-strain curves of TPU microfibre membrane and swollen TPU-PNIPAM-3.6 membrane.

The TPU microfibre membranes were prepared using force spinning, as shown in Figure 3.2. The PNIPAM-coated TPU microfibre (TPU-PNIPAM) membranes were made using a single step free-radical polymerization (Figure 3.3a). The TPU microfibre can be easily wetted by NIPAM monomer solution, as shown in Figure 3.4. The schematic diagram of formation of

TPU-PNIPAM composite is shown in Figure 3.5. As shown in Figure 3.3b-c, the TPU-PNIPAM membrane shows excellent mechanical properties, and can be readily stretched and twisted without failure, showing significant recovery on removal of deformation. The composite membrane has significantly enhanced stretchability, as compared with the TPU membrane. In this study, TPU-PNIPAM membranes with different amounts of PNIPAM (1.4, 3.6, 7.6, 13.4, and 25.3 wt. %) were prepared. As an example of the nomenclature used, a membrane contains 1.4 wt. % PNIPAM hydrogel is denoted as TPU-PNIPAM-1.4. The TPU microfibrils' diameter is 1-30  $\mu\text{m}$ , and 92 % of them distributes in 1-15  $\mu\text{m}$  (Figure 3.6).

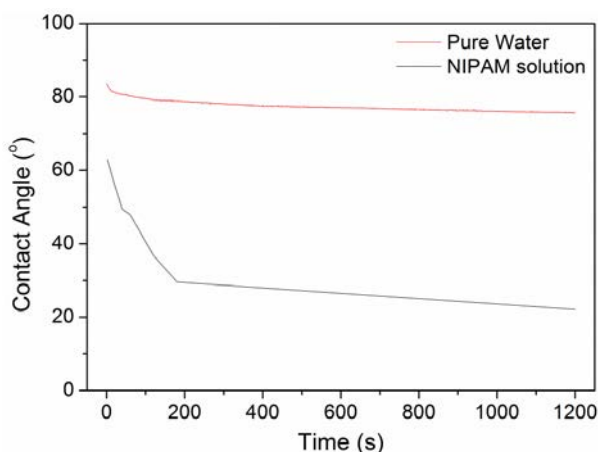


**Figure 3.4** Contact angle-time curves of TPU film with DDI water and NIPAM solution (16.67 wt. %) as testing medium.

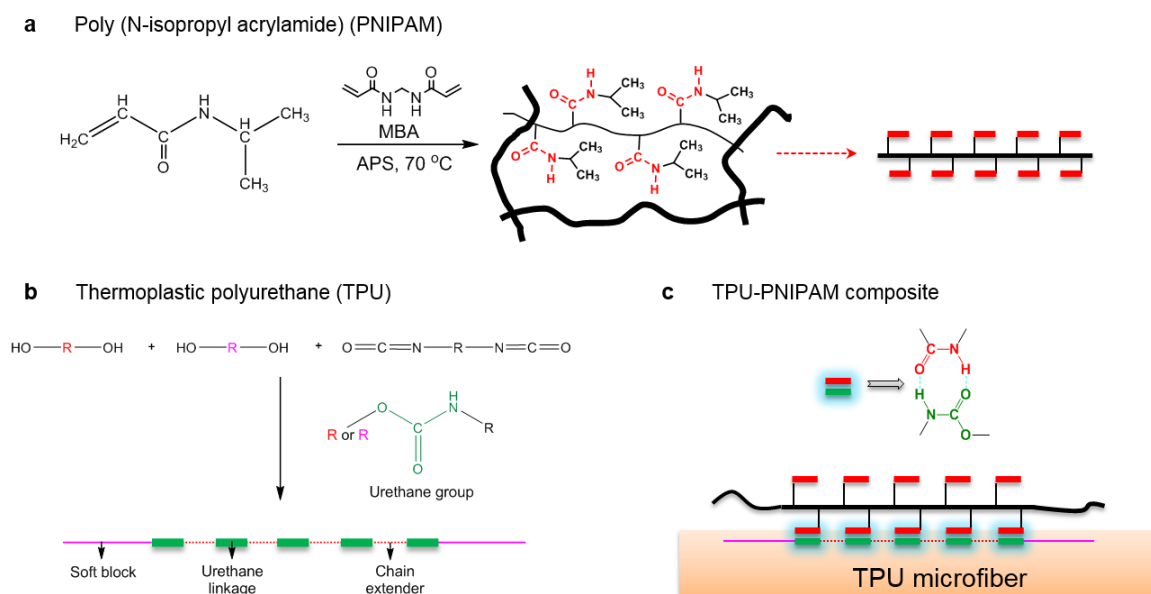


**Figure 3.5** Schematic diagram of formation of TPU-PNIPAM composite. (a) Free radical polymerization of PNIPAM hydrogel, (b) basic chemistry of TPU, (c) polymerization of

PNIPAM hydrogel on the TPU microfibre's surface. The hydrogen bonds form between the urethane and acrylamide groups in two polymers.

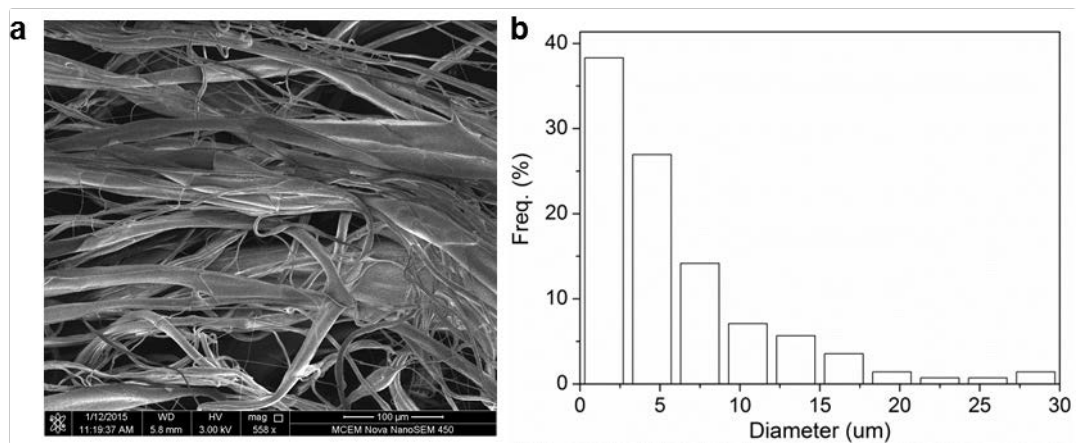


**Figure 3.6** (a) SEM image and (b) diameter distribution of TPU microfibre membrane. The diameter distribution was measured using Nano Measurer 1.2.

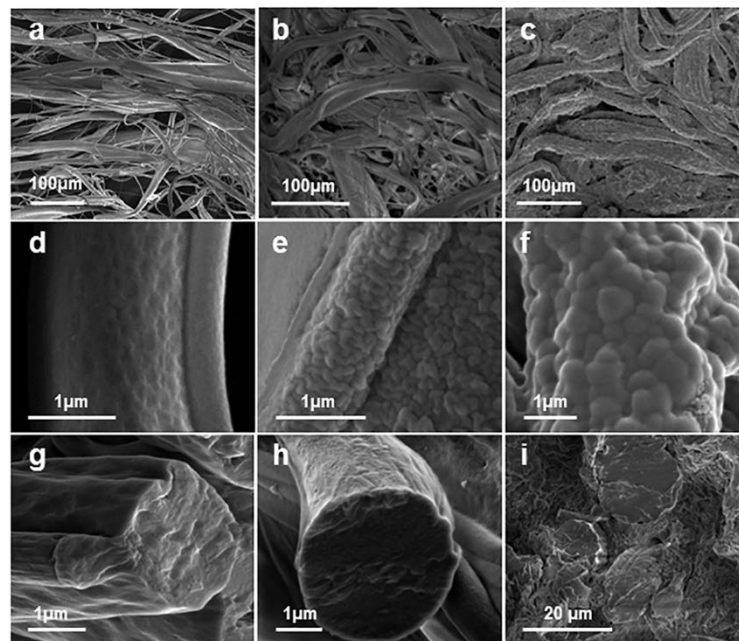


**Figure 3.7** SEM images of TPU microfibre membrane and TPU-PNIPAM composite membranes (3.6 and 13.4 wt. %). Membrane surfaces of (a) TPU microfibre membrane (558 $\times$ ), (b) TPU-PNIPAM-3.6 (811 $\times$ ) and (c) TPU-PNIPAM-13.4 membrane (683 $\times$ ); microfibre surfaces of (d) TPU microfibrs (71202 $\times$ ), (e) TPU-PNIPAM-3.6 (67286 $\times$ ) and (f) TPU-PNIPAM-13.4 (35187 $\times$ ); microfibre cross-sections of (g) TPU microfibrs (38448 $\times$ ), (h) TPU-PNIPAM-3.6 (43471 $\times$ ) and (i) TPU-PNIPAM-13.4 (2885 $\times$ ).

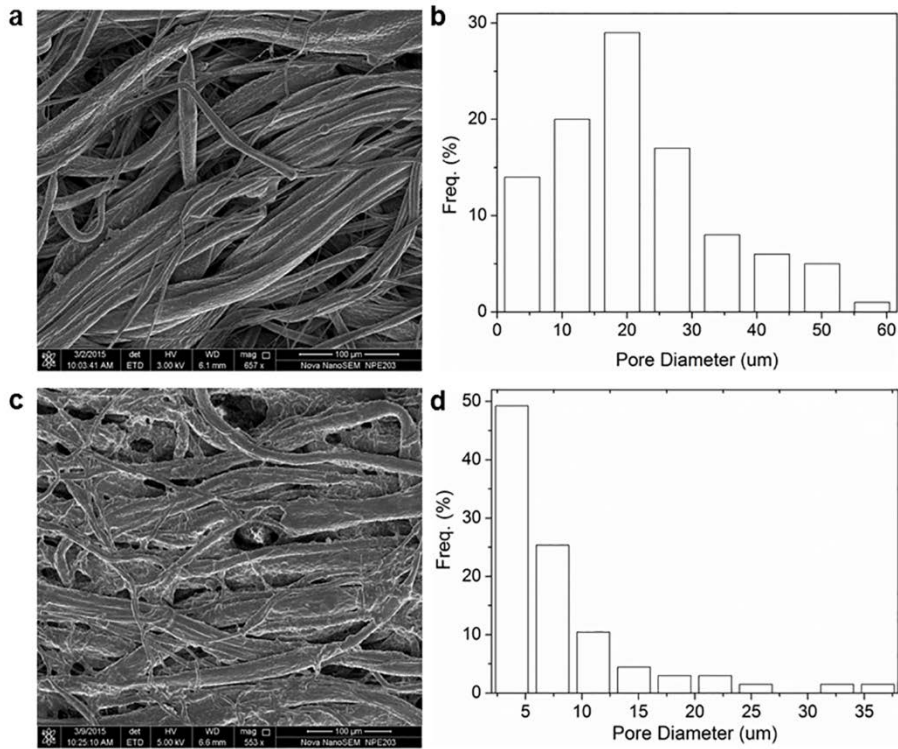


**Figure 3.8** (a) SEM image and (b) pore size distribution of composite membrane with 3.6 wt. % PNIPAM (TPU-PNIPAM-3.6), and (c) SEM image and (d) pore size distribution of TPU-PNIPAM-13.4 membrane.

Figure 3.7 shows the SEM images of TPU microfibre membrane, TPU-PNIPAM-3.6 and TPU-PNIPAM-13.4 membrane, which were taken after 10 times of cyclic heating. The SEM images of microfibre surface and cross-section (Figure 3.7d-i) indicate that PNIPAM was evenly coated on the TPU microfibres, and its surface roughness increased with greater PNIPAM loading. These membranes showed similar morphologies before the cyclic heating, as shown in Figure 3.8. In addition, within the TPU microfibre membrane, the microfibres were loosely packed whilst in the TPU-PNIPAM membrane the microfibres were bound by the PNIPAM hydrogel phase. In the latter instance, the pore size of the TPU-PNIPAM membranes was greatly decreased, as shown in Figure 3.7a-c, with the pore size was found to decrease with increasing PNIPAM loading (Figure 3.8). The pore size distributions of dry TPU-PNIPAM-3.6 and TPU-PNIPAM-13.4 membrane were 3-27  $\mu\text{m}$ , and 2-15  $\mu\text{m}$ , respectively. Figure 3.9 shows the thickness of the composite membranes and their PNIPAM hydrogel coating thickness. The PNIPAM coating thickness of TPU-PNIPAM with a hydrogel loading of 1.4, 3.6, 7.6, 13.4, and 25.3 wt. % were 106, 160, 227, 3061, and 10124 nm, respectively. With the hydrogel loading increased, the PNIPAM coating thickness increased. The membrane thickness of TPU-PNIPAM with a hydrogel loading of 1.4, 3.6, 7.6, 13.4, and 25.3 wt. % were

1.47, 0.64, 0.63, 0.54, and 1.13 mm, respectively. It decreased with increasing hydrogel loading when the loading amount was lower than 13.4 wt. %. The results of SEM images, PNIPAM coating thickness, and membrane thickness indicated that TPU microfibrils were bound by the PNIPAM hydrogel, and increasing space between microfibrils was filled by the hydrogel with greater hydrogel loading. However, there was not sufficient PNIPAM hydrogel in the TPU-PNIPAM-1.4 to bind the TPU microfibrils, resulting in a thick membrane with large pores.

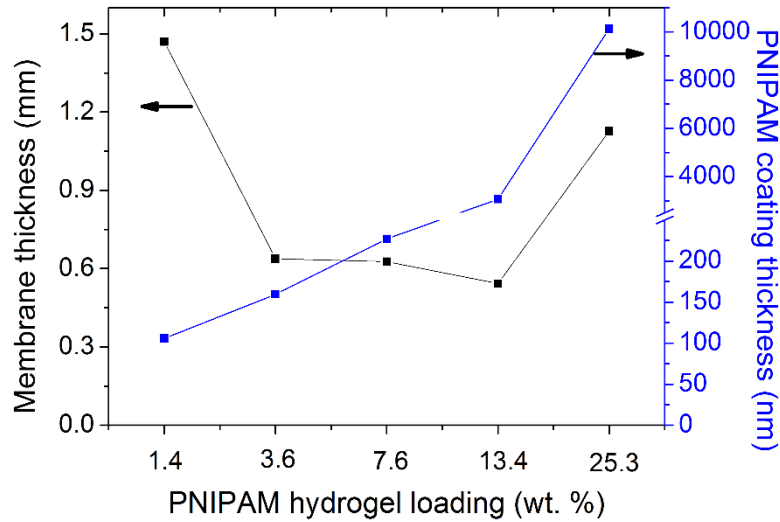


**Figure 3.9** Membrane thickness and PNIPAM coating thickness of composite membranes (1.4, 3.6, 7.6, 13.4, and 25.3 wt. %).

### 3.3.2 Mechanical properties

The mechanical properties of swollen TPU-PNIPAM membranes increased with increasing hydrogel loading initially, however when the hydrogel loading was greater than 3.6 wt. %, it decreased (Figure 3.10). The elongation and toughness of the dry composite membranes follow a similar trend, and TPU-PNIPAM-3.6 reaches the maximum as well. However, the tensile strength and Young's modulus of the dry composite membranes show different trends: TPU-PNIPAM-7.6 exhibits the largest tensile strength, and the Young's modulus of the composite membranes with the 7.6, 13.4 and 25.3 wt. % hydrogel loading are 10 times higher than those of others. For TPU-PNIPAM-1.4 and TPU-PNIPAM-3.6, the microfibrils are coated with the hydrogel uniformly; as the hydrogel loading become greater, the hydrogel coating surface becomes rougher, and thicker hydrogel starts to fill up the space between TPU microfibrils (Figure 3.7i). The dry TPU-PNIPAM-3.6 is flexible and stretchable; whereas the dry TPU-PNIPAM-7.6 becomes hard. Since the dry PNIPAM hydrogel is itself hard and brittle, the dry composite membrane with a hydrogel loading higher than 3.6 wt. % also

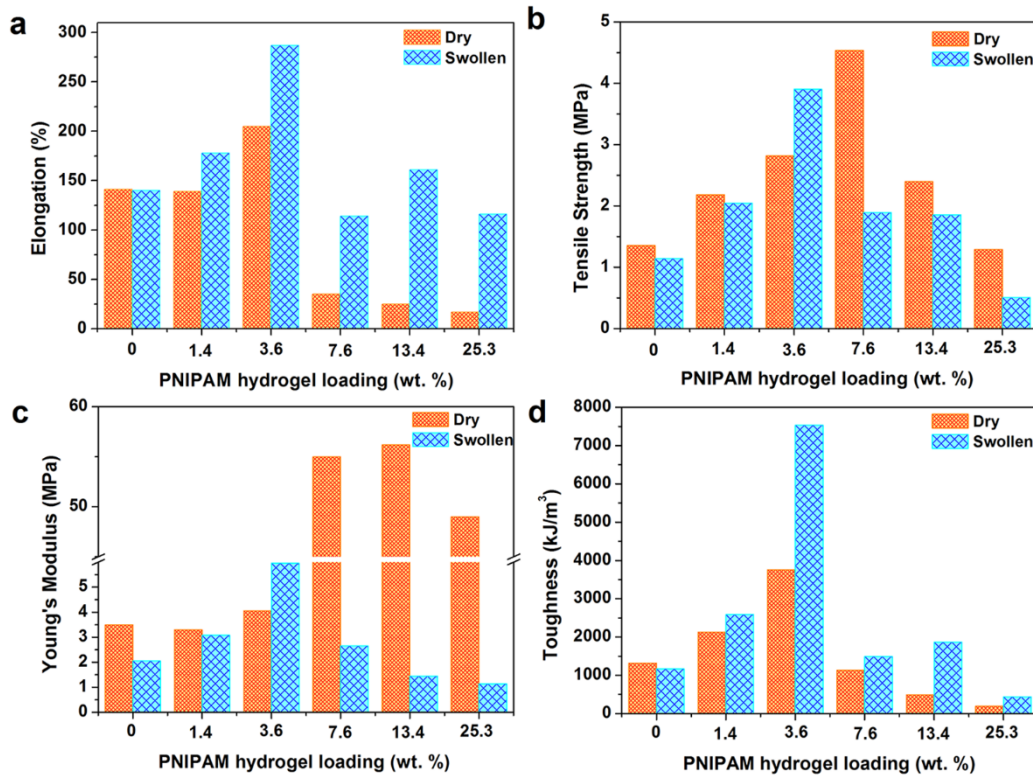


**Figure 3.10** (a) elongation, (b) tensile strength, (c) Young's modulus, and (d) toughness of TPU microfibre membrane (0 wt. %) and TPU-PNIPAM membranes (1.4, 3.6, 7.6, 13.4, and 25.3 wt. %).

becomes harder and more brittle with increasing hydrogel loading, resulting in the decreased tensile strength and elongation, and high Young's modulus and low toughness observed. The swollen TPU-PNIPAM-3.6 membrane is flexible and tough and reaches the optimal values of mechanical properties among the composite membranes. The stress-strain curves of TPU microfibre membrane and swollen TPU-PNIPAM-3.6 membrane (Figure 3.3d) indicate that the mechanical properties of TPU-PNIPAM-3.6 membrane were significantly enhanced. The elongation, tensile strength, Young's modulus and toughness of TPU-PNIPAM-3.6 are 2.04, 2.88, 1.71 and 5.70 times of those of the TPU microfibre membrane alone (uncoated). The elongation and tensile strength of TPU-PNIPAM-3.6 are as high as 288 % and 3.90 MPa, which are much better than those of the other reported oil water separation membranes.[2, 39, 40] For example, the ammonia modified PVDF oil water separation membrane prepared by Zhang et al. exhibited an elongation of 29.2% and a tensile strength of 2.0 MPa, which showed good flexibility and mechanical stability in the oil water separation process.[2] The toughness of dry TPU microfibre membrane is 1321 kJ/m<sup>3</sup>; however, the toughness of swollen TPU-PNIPAM-3.6 is 7536 kJ/m<sup>3</sup>, which is comparable with natural rubber (10000 kJ/m<sup>3</sup>). The images in

Figure 3.3b-c show the twisting test of TPU microfibre membrane and TPU-PNIPAM-3.6 membrane. Both two membranes had good flexibility that could not only withstand bending, but also complex twisting, while TPU-PNIPAM-3.6 showed greater elasticity and recovery.

### 3.3.3 Wettability

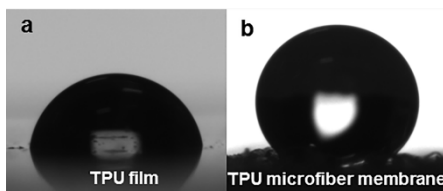


**Figure 3.11** Water contact angle images of (a) TPU film and (b) TPU microfibre membrane. The water contact angle of TPU film was  $82.0^\circ$ , and that of TPU microfibre membrane was  $148.3^\circ$ .

The water contact angle of TPU thin film was  $82.0^\circ$ , after spinning the TPU into microfibres, the water contact angle of TPU microfibre membrane increased to  $148.3^\circ$  (Figure 3.11) because of the resultant surface roughness of TPU. Figure 3.12 shows the wettability of PNIPAM hydrogel and TPU-PNIPAM membranes. As shown in Figure 3.12a, compared to swollen PNIPAM, the water contact angles of swollen TPU-PNIPAM membranes were lower at room temperature and increased at  $45^\circ\text{C}$ , demonstrating that the TPU-PNIPAM-3.6 membrane exhibited switchable superwettability. At room temperature, with increasing hydrogel loading, the contact angles of composite membranes increase; meanwhile the hydrogel fills the space between TPU microfibres instead of coating on the surface alone (Figure 3.13), and the membrane roughness decreased, resulting in a similar wettability to the PNIPAM hydrogel. At  $45^\circ\text{C}$ , the contact angles of composite membrane initially increase and then decrease with increasing hydrogel loading, while TPU-PNIPAM-3.6 shows the highest value. The thermo-responsive properties of PNIPAM can be explained by the reversible formation of intermolecular hydrogen bonding between amide groups of PNIPAM chains and water molecules, and intramolecular hydrogen bonding between amide groups of PNIPAM chains below and above the LCST.[17, 41, 42] At temperatures below LCST, the stretching PNIPAM chains are wrapped by the water molecules, showing hydrophilicity; while at temperatures above LCST, the collapsed PNIPAM chains are wrapped by isopropyl groups, showing hydrophobicity (Figure 3.12b). Nevertheless, the synergism of integrating TPU microfibres and PNIPAM amplifies these properties to superhydrophilicity and superhydrophobicity.

Figure 3.12c-f show that TPU-PNIPAM-3.6 membrane was superhydrophilic, with a water drop spreading in a timeframe of less than 0.094 s, and underwater demonstrated oleophobic behaviour ( $141.3^\circ$ ) at room temperature; but became superhydrophobic ( $150.2^\circ$ ) and underwater superoleophilic, with an oil drop spreading time of 70 s at  $45^\circ\text{C}$ . TPU-PNIPAM-3.6 submerged under water at room temperature, and floated on the surface of water without a water droplet on the membrane surface at  $45^\circ\text{C}$  (Figure 3.14).

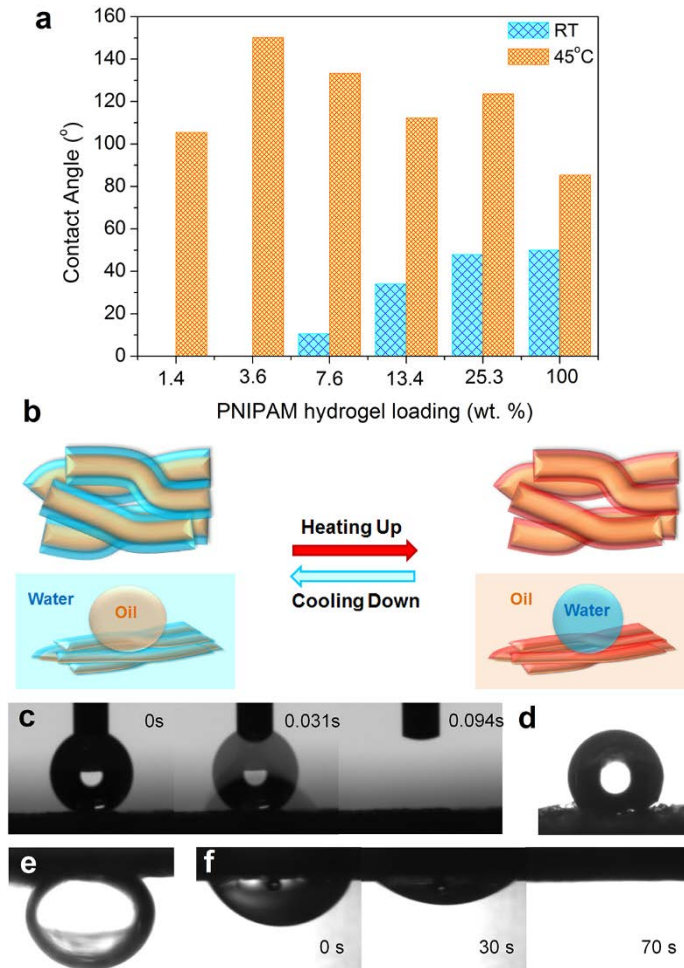


**Figure 3.12** (a) Water contact angles of swollen TPU-PNIPAM membranes (1.4, 3.6, 7.6, 13.4, and 25.3 wt. %) and the swollen PNIPAM hydrogel (100 wt. %) at room temperature (RT) and  $45^\circ\text{C}$ . (b) Schematic diagram of switching wettability of TPU-PNIPAM membrane at different temperatures. (c) A water droplet ( $1\mu\text{L}$ ) spreading on a swollen TPU-PNIPAM-3.6 membrane within 0.094 s at room temperature. (d) Water contact angle ( $150.2^\circ$ ) of swollen TPU-PNIPAM-3.6 membrane at  $45^\circ\text{C}$ . (e) Underwater oil contact angle ( $141.3^\circ$ ) of swollen TPU-PNIPAM-3.6 membrane at room temperature. (f) Underwater oil contact angle of swollen TPU-PNIPAM-3.6 membrane at  $45^\circ\text{C}$ . Hexadecane was used for testing the underwater oil contact angle.

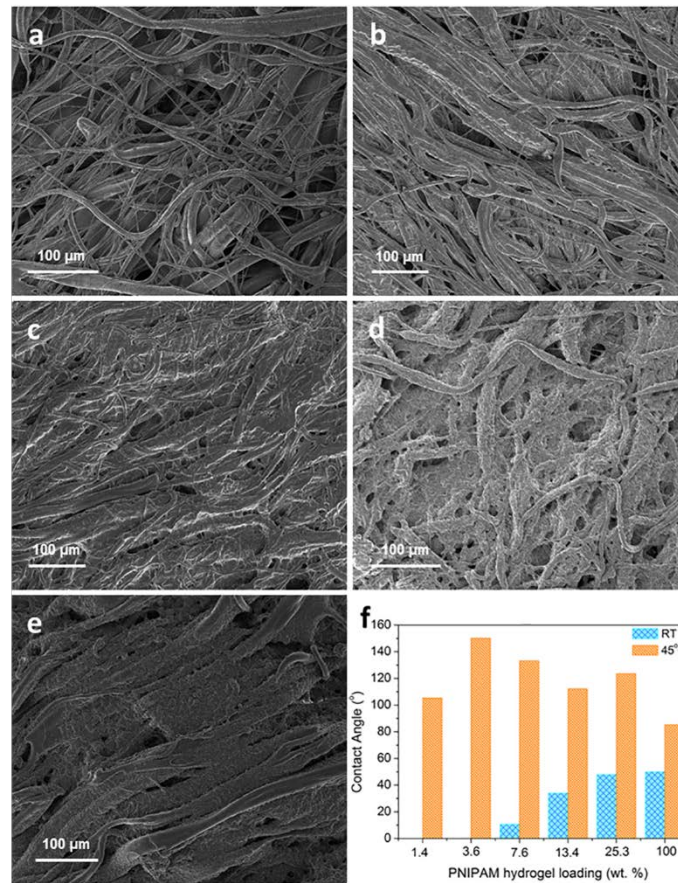


**Figure 3.13** SEM images of composite membranes and the relevant water contact angle. (a) TPU-PNIPAM-1.4, (b) TPU-PNIPAM-3.6, (c) TPU-PNIPAM-7.6, (d) TPU-PNIPAM-13.4, (e) TPU-PNIPAM-25.3. (f) Water contact angle of composite membranes and PNIPAM hydrogel at room temperature and 45 °C.

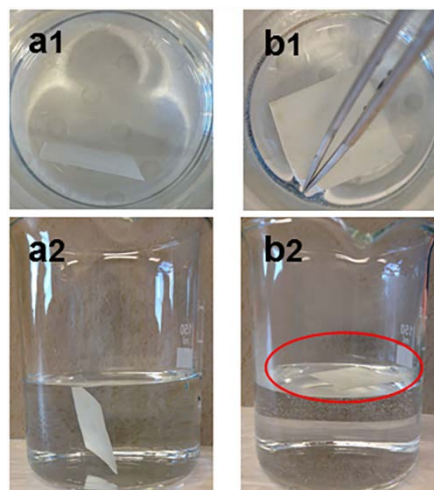


**Figure 3.14** Photographs of TPU-PNIPAM-3.6 immersed into DDI water at different temperatures: (a) room temperature, (b) 45 °C. (a1) and (b1) show the top view of the process, while (a2) and (b2) show the front view.

## 3.3.4 Swelling behaviour

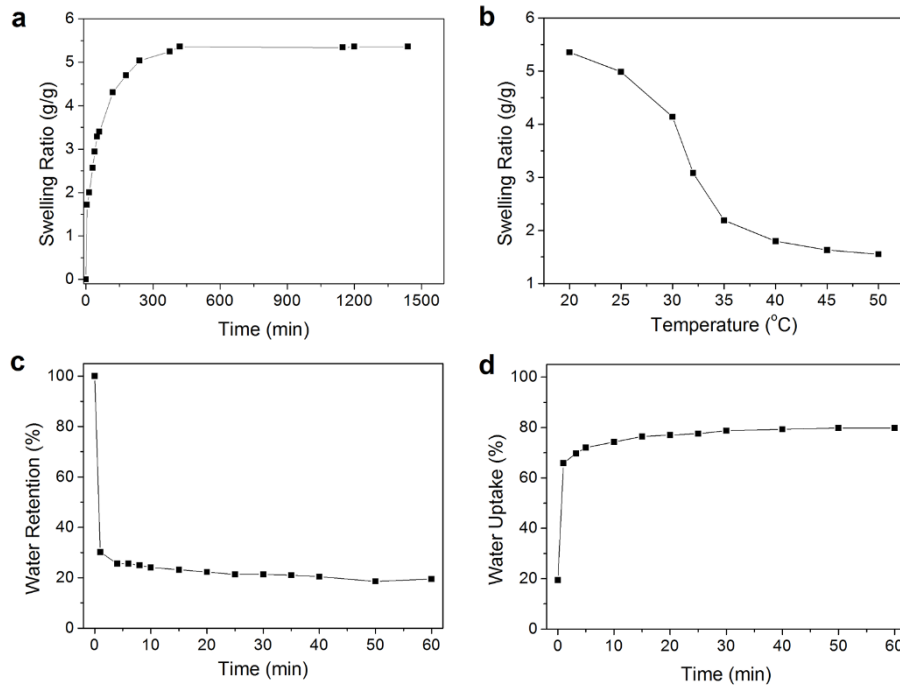


**Figure 3.15** Swelling properties of the PNIPAM of TPU-PNIPAM-3.6 membrane. (a) Swelling curve of dry TPU-PNIPAM-3.6 membrane. (b) Swelling ratio of TPU-PNIPAM-3.6 membrane at different temperatures. (c) Deswelling curve of TPU-PNIPAM-3.6 membrane tested at 45 °C DDI water. (d) Reswelling curve of TPU-PNIPAM-3.6 membrane tested at 25 °C DDI water.

Apart from the wettability, the degree of swelling also plays an important role in the potential use of the hydrogel. It has been recognized that PNIPAM hydrogels would possess low reswelling and deswelling rates at temperatures below or over its LCST, which is responsible for the formation of a dense, hydrophobic layer at the surface of the hydrogels due to the occurrence of volume-phase transition (VPT) that retards the collective diffusion of water molecules in the swelled and/or deswelled hydrogels.[39, 40, 43, 44] Figure 3.15 shows the swelling properties of the PNIPAM phase of the TPU-PNIPAM-3.6 membrane. It took 400 minutes for dry TPU-PNIPAM-3.6 membrane to achieve a swelling equilibrium in DDI water (Figure 3.15a). Even though the swelling ratio of the PNIPAM was 5.36 g/g, the appearance of the membrane changed little because of the small amount of hydrogel loading. The LCST of TPU-PNIPAM-3.6 membrane is the same as PNIPAM hydrogel, some 32-33 °C (Figure 3.15b). Importantly, the deswelling and reswelling equilibrium of TPU-PNIPAM-3.6 membrane could be achieved in less than 3 minutes by immersing it into 45 °C and 25 °C DDI water, respectively, as shown in Figure 3.15c-d. The rapid deswelling and reswelling properties could be a result of the morphology of hydrogel nanoparticles on the microfibrils surface and the consequent

large surface area. The excellent mechanical properties, suitable pore sizes, switchable superhydrophilicity and superhydrophobicity, rapid deswelling and reswelling property make clear the appropriate application of these TPU-PNIPAM membranes for separating oil-in-water emulsion and water-in-oil emulsion at room temperature (25 °C) and 45 °C, respectively.

### 3.3.5 Oil water separation capacity

To study the oil-water separation ability of TPU-PNIPAM membranes, oil intrusion pressure and water intrusion pressure, the relevant water flux and oil flux were all tested, and the results shown in Figure 3.16a-b. The intrusion pressure indicates the maximum height of oil / water that the TPU-PNIPAM membrane can support at room temperature / 45 °C, which is calculated by the following equation (2):

$$P = \rho g h_{\max} \quad (2)$$

where  $\rho$  is the density of the oil / water,  $g$  is gravitational acceleration, and  $h_{\max}$  is the maximum height of oil / water the membranes can support. The fluxes were calculated by measuring the volume of liquid permeated through the membranes over a period of time due to gravity only. Both intrusion pressure and flux were tested more than 5 times to obtain the average value. At room temperature, TPU-PNIPAM membranes are hydrophilic, the oil intrusion pressures of TPU-PNIPAM-1.4, TPU-PNIPAM-3.6, TPU-PNIPAM-7.6, and TPU-PNIPAM-13.4 membrane are 0.35, 1.37, 1.53, and 3.26 kPa, respectively, and the relevant water fluxes are 3288, 3646, 1657, and 41 LMH. With increasing hydrogel loading, the pore size of the composite membranes becomes smaller, which is responsible for the increasing oil intrusion pressure and decreasing water flux. At 45 °C, the TPU-PNIPAM membranes are hydrophobic, the water intrusion pressure firstly increased and then decreased, while the oil flux decreased with increasing hydrogel loading of the composite membranes. Only TPU-PNIPAM-3.6 exhibited proper water intrusion pressure at 45 °C (0.89 kPa), which was slightly higher than that of TPU microfibre membrane alone (0.80 kPa). TPU-PNIPAM-1.4 showed low water intrusion pressure, because the microfibrils were loosely piled, with huge gaps among the membrane (Figure 3.13a), Conversely, coating with PNIPAM decreased the water contact angle of TPU microfibre membrane from 148.3 ° to 105 °. Coating with PNIPAM hydrogel provides the TPU microfibrils with switchable hydrophilicity and hydrophobicity, but only TPU-PNIPAM-3.6 possesses switchable superhydrophilicity and superhydrophobicity (Figure 3.12a). The increasing hydrogel loading decreased the pore size, as well as the surface roughness, resulting in decreasing contact angle and water intrusion pressure. The oil fluxes of

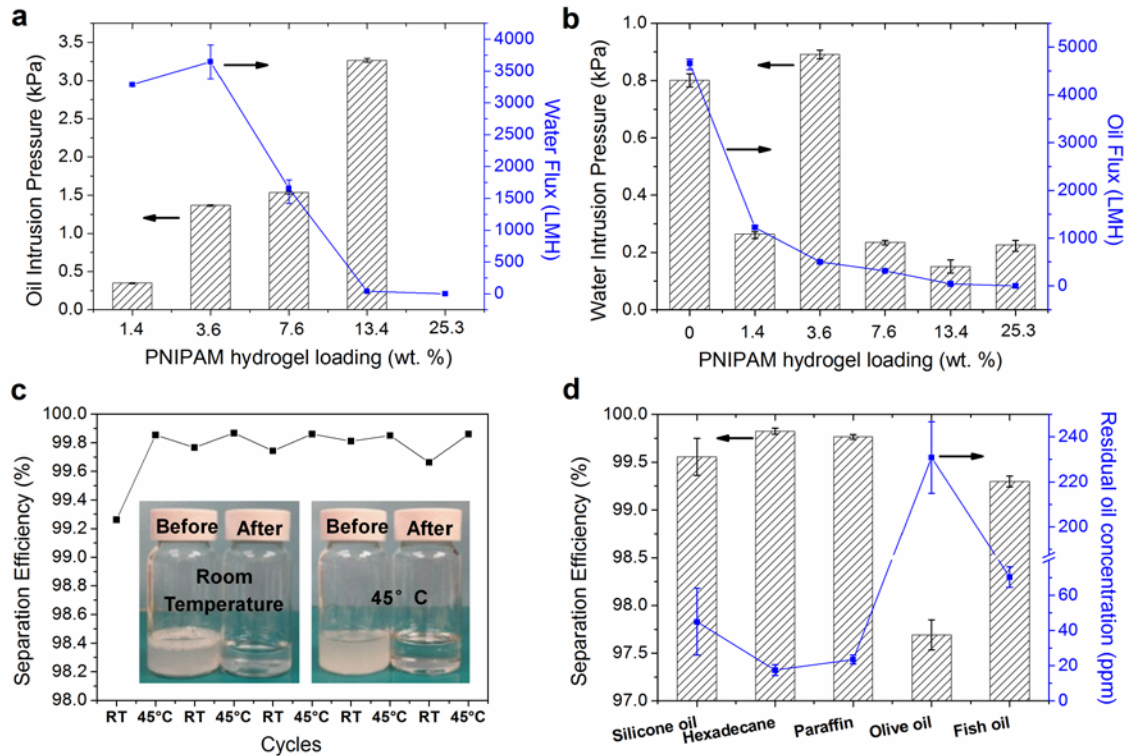


**Figure 3.16** (a) Oil intrusion pressure and water flux of TPU-PNIPAM membranes (1.4, 3.6, 7.6, 13.4, and 25.3 wt. %) at room temperature. (b) Water intrusion pressure and oil flux of TPU microfibre membrane and TPU-PNIPAM membranes at 45 °C. Hexadecane was used as the test oil. (c) Separation efficiency of TPU-PNIPAM-3.6 membrane for reversibly oil-water separation at room temperature and 45 °C. The inset shows the 1 wt. % SDS-stabilized silicone oil-water emulsion and the collected water before and after separation at room temperature (left), and the 99 wt. % SDS-stabilized silicone oil-water emulsion and the collected oil before and after separation at 45 °C (right). (d) Separation efficiencies of TPU-PNIPAM-3.6 membrane for separating different 1 wt. % oil-water emulsions at room temperature.

TPU microfibre membrane and TPU-PNIPAM-3.6 membrane were 4659 and 503 LMH, respectively. The loosened structure of TPU microfibre membrane reduced the water intrusion pressure but enhanced the oil flux. Combining the results of room temperature oil intrusion pressures and 45 °C water intrusion pressures of the membranes, TPU-PNIPAM-3.6 is the membrane that can best be applied to controllable separation of oil-in-water emulsion and water-in-oil emulsion at different temperatures, which is consistent with the contact angle data in Figure 3.12. The illustration of controllable separation of oil-water mixture with TPU-PNIPAM-3.6 membrane is shown in Figure 3.17. Water selectively permeated through the membrane and oil (hexadecane, red) was retained above the membrane at room temperature. Likewise oil permeated through the membrane, but the permeation of oil was blocked when

the membrane surface was covered by water at 45 °C, thus both oil and water were retained. Figure 3.18 shows the variation of flux during 24 hours separation of SDS-stabilized hexadecane-water emulsions. The diameter distribution of oil drops in 1 wt. % hexadecane-water emulsion is 2-15  $\mu\text{m}$ , and that of water drops in 99 wt. % hexadecane-water emulsion is 3-30  $\mu\text{m}$  (Figure 3.19). For separating 1 wt. % hexadecane-water emulsion at room temperature, the initial flux was 3700 LMH. It dropped to about 2400 LMH after 1 hour and was remained in the following 23 hours. The flux of separating 99 wt. % hexadecane-water emulsion at 45 °C showed a similar trend. After 2 hours, the flux dropped from 670 to 480 LMH, and it remained constant for the subsequent 22 hours. No external force was employed during the separation process.



**Figure 3.17** Controllable oil-water separation using TPU-PNIPAM-3.6 membrane at (a) room temperature and (b) 45 °C respectively (hexadecane: red, water: transparent). Oil-water separation at 45 °C was conducted in a 45 °C oven.

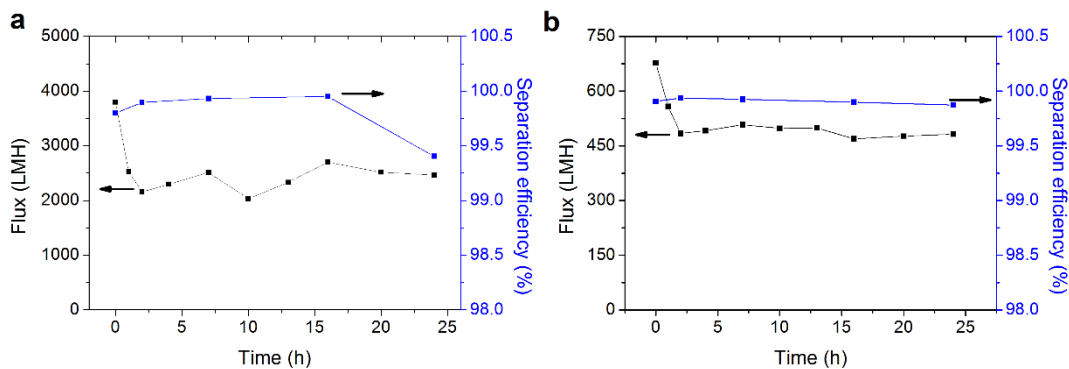


**Figure 3.18** (a) The variation of flux as a function of time for 24 h separation of 1 wt. % SDS-stabilized hexadecane-water emulsion. (b) The variation of flux as a function of time for 24 h separation of 99 wt. % SDS-stabilized hexadecane-water emulsion. TPU-PNIPAM-3.6 was used in the test of (a) and (b).

Silicone oil, with a density approaching that of water, was used to prepare the emulsion with water for testing the oil-water emulsion separation capability of TPU-PNIPAM-3.6 membrane. 1 wt. % silicone oil-water emulsion contains 1 wt. % silicone oil, 99 wt. % DDI water and 1 mg/mL sodium dedecyl sulfate (SDS), it is oil-in-water emulsion. Similarly, 99 wt. % silicone oil-water emulsion contains 99 wt. % silicone oil, 1 wt. % DDI water and 1 mg/mL SDS, and thus is a water-in-oil emulsion. The silicone oil-water emulsions were much more stable than the hexadecane-water emulsions. The diameter of silicone oil drops in water is 2-25  $\mu\text{m}$ , and that of water drops in silicone oil is 5-30  $\mu\text{m}$  (Figure 3.19). The TPU-PNIPAM-3.6 membrane was able to demonstrate excellent ability to separate oil-water emulsions. At room temperature, 1 wt. % silicone oil-water emulsion was separated, and the separation efficiency was higher than 99.26 %; at 45 °C, 99 wt. % silicone oil-water emulsion was separated, and the separation efficiency was 99.85 %. TPU-PNIPAM-3.6 showed switchable superhydrophilicity and superhydrophobicity, it separated oil-in-water and water-in-oil emulsions at temperatures below and above LCST respectively. However, the TPU microfibre membrane showed hydrophobicity, it separated a water-in-oil emulsion only. The TPU microfibre membrane was applied to separate 99 wt. % silicone oil-water emulsion, and the separation efficiency was 99.78 %. For separating water-in-oil emulsion, even though TPU-PNIPAM-3.6 was swollen in 45 °C water, it showed similar separation efficiency with the dry TPU microfibre membrane. The separation efficiencies of TPU-PNIPAM-3.6 membrane for reversely separating 1 wt. % and 99 wt. % silicone oil-water emulsions at room temperature and 45 °C individually are shown in Figure 3.16c. It was found that the separation efficiencies were stable both at room temperature and 45 °C, demonstrating that the TPU-PNIPAM-3.6 membrane is stable and shows excellent separation ability under switching temperatures. The inset of Figure 3.16c shows photographs of oil-water emulsions and the collected liquids, before and after separation, which also indicates that the TPU-PNIPAM-3.6 membrane separated emulsions successfully. Other than for silicone oil-water emulsions, the TPU-PNIPAM-3.6 membrane was able to separate other oil-water emulsions with high separation efficiency (Figure 3.16d). The optical microscopy images of emulsions before and after filtration are shown in Figure 3.20 and Figure 3.21.

In conclusion, the TPU microfibre-PNIPAM hydrogel composite membrane (e.g., TPU-PNIPAM-3.63) exhibit excellent oil-water emulsion separation performance: (1) it separates water-in-oil and oil-in-water emulsions effectively and efficiently under switching temperatures, with an separation efficiency of  $\geq 99.26\%$ , while the TPU microfibre membrane

without hydrogel coating separates water-in-oil emulsion only; (2) the swollen TPU-PNIPAM-3.6 (45 °C) shows a similar separation efficiency with the dry TPU microfibre membrane; and (3) other oil-water emulsions can also be separated by TPU-PNIPAM, and excellent separation efficiencies were achieved.

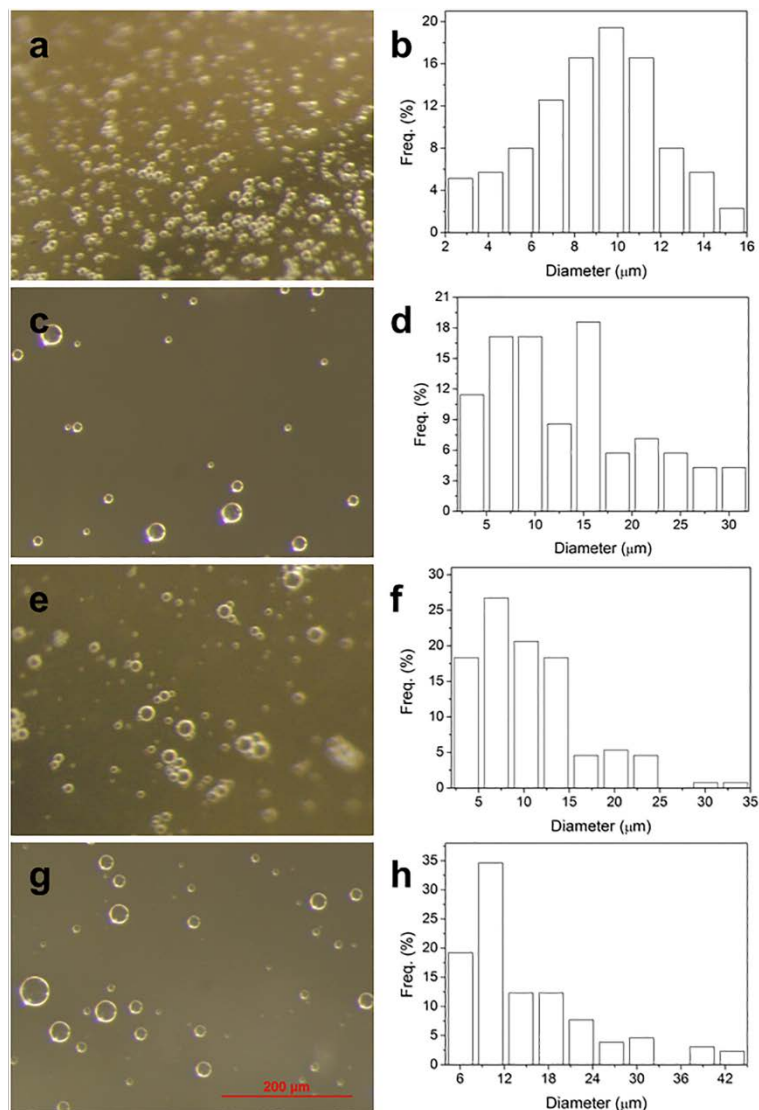


**Figure 3.19** Optical microscopy images and diameter distribution of oil droplets in 1 wt. % oil-water emulsion and water droplets in 99 wt. % oil-water emulsion. (a) Oil droplets in 1 wt. % SDS-stabilized hexadecane-water emulsion; (b) diameter distribution of oil droplets in 1 wt. % SDS-stabilized hexadecane-water emulsion; (c) water drops in 99 wt. % SDS-stabilized hexadecane-water emulsion; (d) diameter distribution of water droplets in 99 wt. % SDS-stabilized hexadecane-water emulsion. (e) Oil droplets in 1 wt. % SDS-stabilized silicone oil-water emulsion; (f) diameter distribution of oil droplets in 1 wt. % SDS-stabilized silicone oil-water emulsion; (g) water droplets in 99 wt. % SDS-stabilized silicone oil-water emulsion; (h) diameter distribution of water droplets in 99 wt. % SDS-stabilized silicone oil-water emulsion.

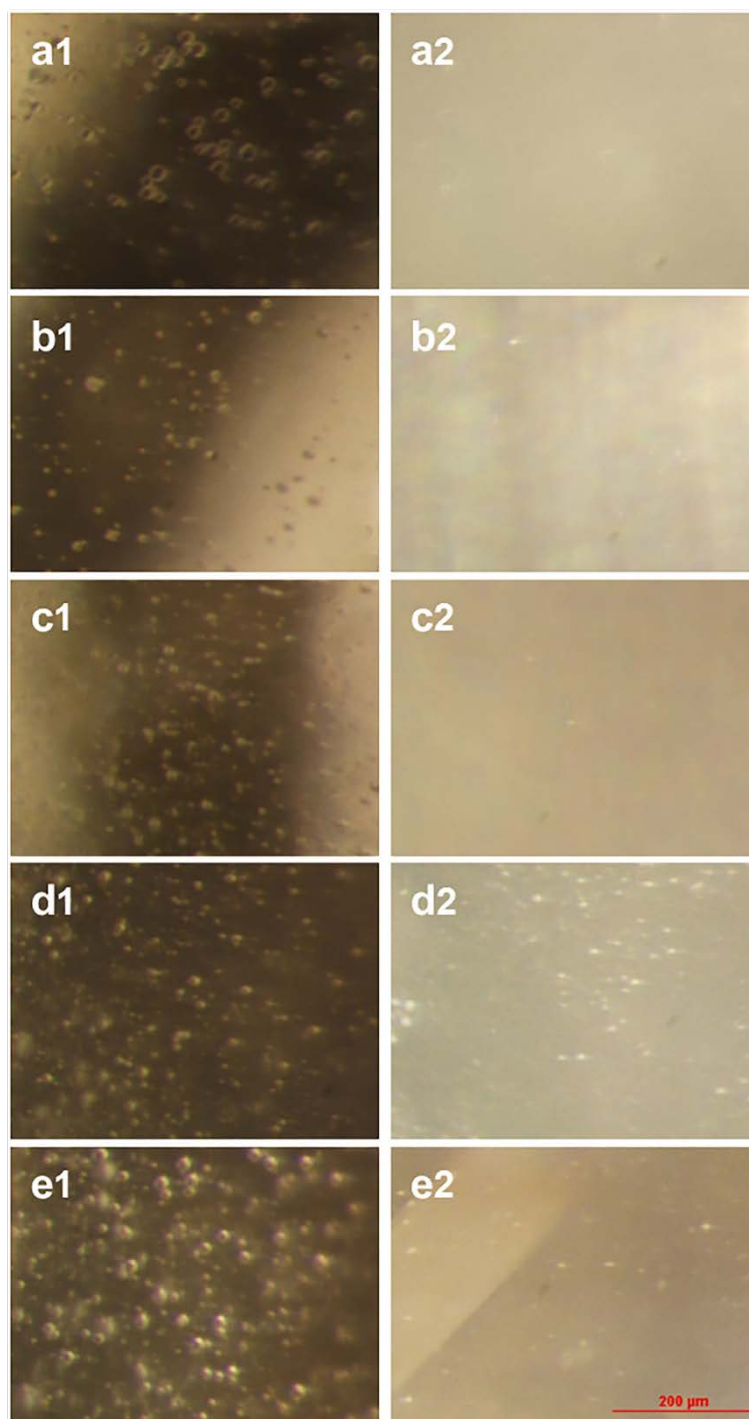


**Figure 3.20** Optical microscopy images SDS-stabilized 1 wt. % oil-water emulsions before (a1-e1) and after (a2-e2) filtration. (a) 1 wt. % silicone oil-water emulsion, (b) 1 wt. % hexadecane-water emulsion, (c) 1 wt. % paraffin-water emulsion, (d) 1 wt. % olive oil-water emulsion, (e) 1 wt. % fish oil-water emulsion.

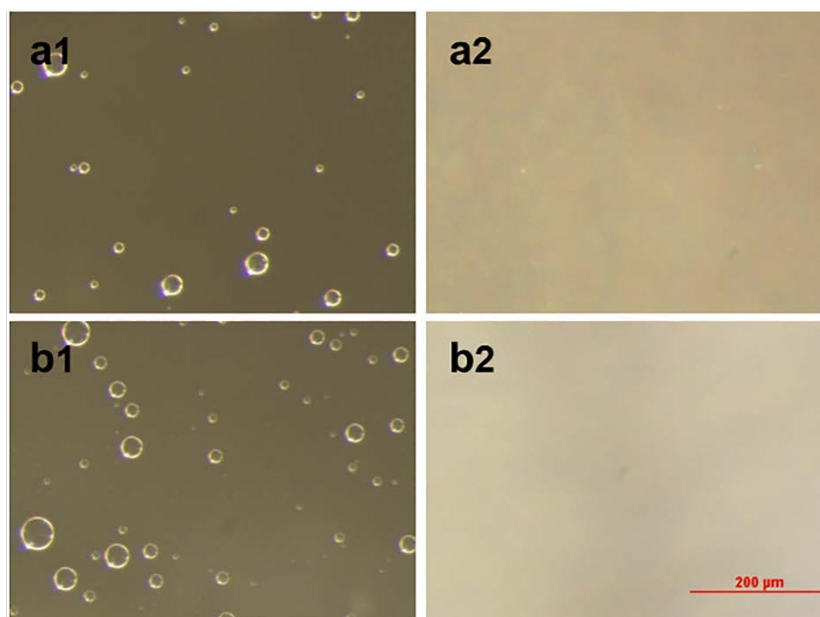


**Figure 3.21** Optical microscopy images SDS-stabilized 99 wt. % oil-water emulsions before (a1-b1) and after (a2-b2) filtration. (a) 99 wt. % hexadecane-water emulsion, (b) 99 wt. % silicone oil-water emulsion

### 3.4 Summary

In conclusion, a robust thermo-responsive polymer membrane with switchable superhydrophilicity and superhydrophobicity was successfully fabricated by combining a thermoplastic polyurethane (TPU) microfibrils and poly (N-isopropylacrylamide) (PNIPAM) nanoparticles. Among the polymer composite membranes prepared, the TPU-PNIPAM-3.6 material performed best, exhibiting excellent mechanical properties with an elongation of 288 % and a toughness of  $7536 \text{ kJ/m}^3$ , comparable with natural rubber ( $10000 \text{ kJ/m}^3$ ). The water contact angles of TPU-PNIPAM-3.6 membrane switched between  $0^\circ$  (room temperature) and  $150.2^\circ$  ( $45^\circ\text{C}$ ), and the PNIPAM hydrogel of the composite membrane reached deswelling and reswelling equilibrium in 3 minutes. Driven by gravity only, the TPU-PNIPAM-3.6 membrane could separate 1 wt. % silicone oil-water emulsion at room temperature with a separation efficiency of  $\geq 99.26\%$ , and separate 99 wt. % silicone oil-water emulsions at  $45^\circ\text{C}$  with a separation efficiency of  $\geq 99.85\%$ . This membrane is thus a good candidate for not only oil-water emulsion separation, but also for fabricating smart materials for rapidly responsive drug delivery systems and sensors. In addition, other polymeric micro- or nanofibrils membranes could be used as the substrates for fabricating superwetting materials, which broadens the methods of preparation of such materials.

### 3.5 References

- [1] P. Kajitvichyanukul, Y. Hung, L. Wang, *Advanced Physicochemical Treatment Processes; Handbook of Environment Engineering*, in, The Humana Press Inc.: Totowa, NJ, 2006.
- [2] W. Zhang, Z. Shi, F. Zhang, X. Liu, J. Jin, L. Jiang, Superhydrophobic and Superoleophilic PVDF Membranes for Effective Separation of Water - in - Oil Emulsions with High Flux, *Advanced Materials*, 25 (2013) 2071-2076.
- [3] B. Chakrabarty, A. Ghoshal, M. Purkait, Ultrafiltration of stable oil-in-water emulsion by polysulfone membrane, *Journal of Membrane Science*, 325 (2008) 427-437.
- [4] A. El-Kayar, M. Hussein, A. Zatout, A. Hosny, A. Amer, Removal of oil from stable oil-water emulsion by induced air flotation technique, *Separations Technology*, 3 (1993) 25-31.
- [5] G. Kwon, A. Kota, Y. Li, A. Sohani, J.M. Mabry, A. Tuteja, On - Demand Separation of Oil - Water Mixtures, *Advanced Materials*, 24 (2012) 3666-3671.
- [6] P. Lipp, C. Lee, A. Fane, C. Fell, A fundamental study of the ultrafiltration of oil-water emulsions, *Journal of Membrane Science*, 36 (1988) 161-177.
- [7] M. Padaki, R.S. Murali, M. Abdullah, N. Misdan, A. Moslehyani, M. Kassim, N. Hilal, A. Ismail, Membrane technology enhancement in oil–water separation. A review, *Desalination*, 357 (2015) 197-207.
- [8] M.M. Pendergast, E.M. Hoek, A review of water treatment membrane nanotechnologies, *Energy & Environmental Science*, 4 (2011) 1946-1971.
- [9] D. Rana, T. Matsuura, Surface modifications for antifouling membranes, *Chemical reviews*, 110 (2010) 2448-2471.
- [10] B. Van der Bruggen, C. Vandecasteele, T. Van Gestel, W. Doyen, R. Leysen, A review of pressure - driven membrane processes in wastewater treatment and drinking water production, *Environmental progress*, 22 (2003) 46-56.
- [11] L. Feng, Z. Zhang, Z. Mai, Y. Ma, B. Liu, L. Jiang, D. Zhu, A super - hydrophobic and super - oleophilic coating mesh film for the separation of oil and water, *Angewandte Chemie International Edition*, 43 (2004) 2012-2014.
- [12] A.K. Kota, G. Kwon, W. Choi, J.M. Mabry, A. Tuteja, Hygro-responsive membranes for effective oil–water separation, *Nature communications*, 3 (2012) 1025.
- [13] Z. Shi, W. Zhang, F. Zhang, X. Liu, D. Wang, J. Jin, L. Jiang, Ultrafast Separation of Emulsified Oil/Water Mixtures by Ultrathin Free - Standing Single - Walled Carbon Nanotube Network Films, *Advanced Materials*, 25 (2013) 2422-2427.

- [14] C. Wang, T. Yao, J. Wu, C. Ma, Z. Fan, Z. Wang, Y. Cheng, Q. Lin, B. Yang, Facile approach in fabricating superhydrophobic and superoleophilic surface for water and oil mixture separation, *ACS applied materials & interfaces*, 1 (2009) 2613-2617.
- [15] Z. Xue, S. Wang, L. Lin, L. Chen, M. Liu, L. Feng, L. Jiang, A Novel Superhydrophilic and Underwater Superoleophobic Hydrogel - Coated Mesh for Oil/Water Separation, *Advanced Materials*, 23 (2011) 4270-4273.
- [16] W. Zhang, Y. Zhu, X. Liu, D. Wang, J. Li, L. Jiang, J. Jin, Salt - Induced Fabrication of Superhydrophilic and Underwater Superoleophobic PAA - g - PVDF Membranes for Effective Separation of Oil - in - Water Emulsions, *Angewandte Chemie International Edition*, 53 (2014) 856-860.
- [17] T. Sun, G. Wang, L. Feng, B. Liu, Y. Ma, L. Jiang, D. Zhu, Reversible switching between superhydrophilicity and superhydrophobicity, *Angewandte Chemie International Edition*, 43 (2004) 357-360.
- [18] F. Zhang, W.B. Zhang, Z. Shi, D. Wang, J. Jin, L. Jiang, Nanowire - Haired Inorganic Membranes with Superhydrophilicity and Underwater Ultralow Adhesive Superoleophobicity for High - Efficiency Oil/Water Separation, *Advanced Materials*, 25 (2013) 4192-4198.
- [19] Z. Cheng, H. Lai, Y. Du, K. Fu, R. Hou, C. Li, N. Zhang, K. Sun, pH-induced reversible wetting transition between the underwater superoleophilicity and superoleophobicity, *ACS applied materials & interfaces*, 6 (2013) 636-641.
- [20] G. Ju, M. Cheng, F. Shi, A pH-responsive smart surface for the continuous separation of oil/water/oil ternary mixtures, *NPG Asia Materials*, 6 (2014) e111.
- [21] B. Wang, Z. Guo, pH-responsive bidirectional oil–water separation material, *Chemical Communications*, 49 (2013) 9416-9418.
- [22] B. Wang, Z. Guo, W. Liu, pH-responsive smart fabrics with controllable wettability in different surroundings, *RSC Advances*, 4 (2014) 14684-14690.
- [23] L. Zhang, Z. Zhang, P. Wang, Smart surfaces with switchable superoleophilicity and superoleophobicity in aqueous media: toward controllable oil/water separation, *NPG Asia Materials*, 4 (2012) e8.
- [24] D. Tian, X. Zhang, Y. Tian, Y. Wu, X. Wang, J. Zhai, L. Jiang, Photo-induced water–oil separation based on switchable superhydrophobicity–superhydrophilicity and underwater superoleophobicity of the aligned ZnO nanorod array-coated mesh films, *Journal of Materials Chemistry*, 22 (2012) 19652-19657.

- [25] Z. Cheng, J. Wang, H. Lai, Y. Du, R. Hou, C. Li, N. Zhang, K. Sun, pH-Controllable On-Demand Oil/Water Separation on the Switchable Superhydrophobic/Superhydrophilic and Underwater Low-Adhesive Superoleophobic Copper Mesh Film, *Langmuir*, 31 (2015) 1393-1399.
- [26] W. Zhang, Y. Cao, N. Liu, Y. Chen, L. Feng, A novel solution-controlled hydrogel coated mesh for oil/water separation based on monolayer electrostatic self-assembly, *RSC Advances*, 4 (2014) 51404-51410.
- [27] Y. Cao, N. Liu, C. Fu, K. Li, L. Tao, L. Feng, Y. Wei, Thermo and pH dual-responsive materials for controllable oil/water separation, *ACS applied materials & interfaces*, 6 (2014) 2026-2030.
- [28] M. Sinha, M. Purkait, Preparation of a novel thermo responsive PSF membrane, with cross linked PVCL-co-PSF copolymer for protein separation and easy cleaning, *RSC Advances*, 5 (2015) 22609-22619.
- [29] M. Tao, L. Xue, F. Liu, L. Jiang, An intelligent superwetting PVDF membrane showing switchable transport performance for oil/water separation, *Advanced Materials*, 26 (2014) 2943-2948.
- [30] P. Sukitpaneenit, T.-S. Chung, Molecular elucidation of morphology and mechanical properties of PVDF hollow fiber membranes from aspects of phase inversion, crystallization and rheology, *Journal of Membrane Science*, 340 (2009) 192-205.
- [31] C. Zhao, J. Xue, F. Ran, S. Sun, Modification of polyethersulfone membranes—a review of methods, *Progress in Materials Science*, 58 (2013) 76-150.
- [32] M.R. Badrossamay, H.A. McIlwee, J.A. Goss, K.K. Parker, Nanofiber assembly by rotary jet-spinning, *Nano letters*, 10 (2010) 2257-2261.
- [33] T.B. Mîndru, L. Ignat, I.B. Mîndru, M. Pinteala, Morphological aspects of polymer fiber mats obtained by air flow rotary-jet spinning, *Fibers and Polymers*, 14 (2013) 1526-1534.
- [34] K. Sarkar, C. Gomez, S. Zambrano, M. Ramirez, E. de Hoyos, H. Vasquez, K. Lozano, Electrospinning to forcesspinning™, *Materials Today*, 13 (2010) 12-14.
- [35] I. Sebe, B. Szabó, Z.K. Nagy, D. Szabo, L. Zsidai, B. Kocsis, R. Zelkó, Polymer structure and antimicrobial activity of polyvinylpyrrolidone-based iodine nanofibers prepared with high-speed rotary spinning technique, *International journal of pharmaceutics*, 458 (2013) 99-103.
- [36] Q. Wen, J. Di, L. Jiang, J. Yu, R. Xu, Zeolite-coated mesh film for efficient oil–water separation, *Chemical Science*, 4 (2013) 591-595.

- [37] X. Zhang, Z. Li, K. Liu, L. Jiang, Bioinspired Multifunctional Foam with Self - Cleaning and Oil/Water Separation, *Advanced Functional Materials*, 23 (2013) 2881-2886.
- [38] X. Gao, L.P. Xu, Z. Xue, L. Feng, J. Peng, Y. Wen, S. Wang, X. Zhang, Dual - Scaled Porous Nitrocellulose Membranes with Underwater Superoleophobicity for Highly Efficient Oil/Water Separation, *Advanced Materials*, 26 (2014) 1771-1775.
- [39] T.a. Asoh, T. Kaneko, M. Matsusaki, M. Akashi, Rapid and Precise Release from Nano - Tracted Poly (N - isopropylacrylamide) Hydrogels Containing Linear Poly (acrylic acid), *Macromolecular bioscience*, 6 (2006) 959-965.
- [40] Q. Zheng, S. Zheng, From poly (N - isopropylacrylamide) - block - poly (ethylene oxide) - block - poly (N - isopropylacrylamide) triblock copolymer to poly (N - isopropylacrylamide) - block - poly (ethylene oxide) hydrogels: Synthesis and rapid deswelling and reswelling behavior of hydrogels, *Journal of Polymer Science Part A: Polymer Chemistry*, 50 (2012) 1717-1727.
- [41] Z. Ahmed, E.A. Gooding, K.V. Pimenov, L. Wang, S.A. Asher, UV resonance Raman determination of molecular mechanism of poly (N-isopropylacrylamide) volume phase transition, *The Journal of Physical Chemistry B*, 113 (2009) 4248-4256.
- [42] S.-Y. Lin, K.-S. Chen, R.-C. Liang, Thermal micro ATR/FT-IR spectroscopic system for quantitative study of the molecular structure of poly (N-isopropylacrylamide) in water, *Polymer*, 40 (1999) 2619-2624.
- [43] A. Gutowska, Y.H. Bae, J. Feijen, S.W. Kim, Heparin release from thermosensitive hydrogels, *Journal of controlled release*, 22 (1992) 95-104.
- [44] M.H. Stenzel, T.P. Davis, Star polymer synthesis using trithiocarbonate functional  $\beta$  - cyclodextrin cores (reversible addition - fragmentation chain - transfer polymerization), *Journal of Polymer Science Part A: Polymer Chemistry*, 40 (2002) 4498-4512.

## Chapter 4 Microfibres-polymer hydrogel monolith as forward osmosis draw agent

### Overview

The swelling pressure of hydrogel and the contact of membrane–hydrogel are key parameters for achieving high water flux. In this work, the forward osmosis performance of hydrogels can be significantly improved by producing composite hydrogel monoliths containing thermoplastic polyurethane (TPU) microfibres. The use of monolithic hydrogels and the addition of microfibres enhance water diffusion through the draw agent and sustain high swelling pressure, resulting in improved FO performance. As observed in the sigmoidal swelling curves, the swelling kinetics of microfibre-hydrogel composite (TPU microfibre-poly (NIPAM-co-SA), TPU-PN5S5) is more rapid than that of pure hydrogel (PN5S5), and the time required for the composite to reach swelling equilibrium decreases significantly; the diffusion exponent of TPU-PN5S5 composite increases from 0.73 to 0.81, indicating that addition of microfibres increases the water diffusion rate. Further studies show that water transports more quickly through the microchannels around TPU microfibres due to their hydrophilicity and capillary forces, as illustrated in Figure 4.1. The composite monolith was tested as forward osmosis draw agent, and it was found that the 1st hour FO water flux and dewatering flux of TPU-PSA are 1.81 and 3.51  $\text{L}\cdot\text{m}^{-2}\cdot\text{h}^{-1}$ , respectively, twice of those for PSA particles alone.

This chapter has been published as a journal article: Ranwen Ou, Huacheng Zhang, George P. Simon, Huanting Wang, *J. Membr. Sci.* **2016**, 510, 426-436

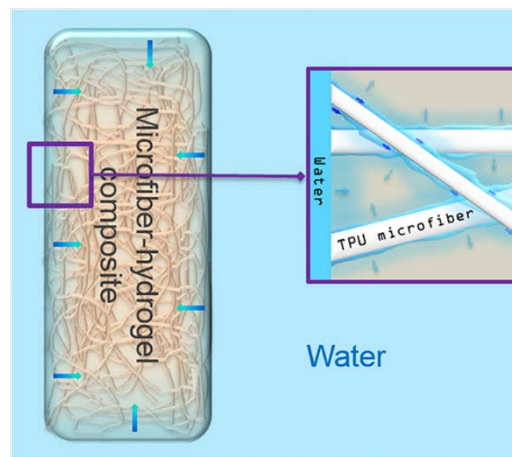


**Figure 4.1** Schematic illustration of water transport in TPU-hydrogel composite.

## 4.1 Introduction

Polymer hydrogels are three-dimensional networks of hydrophilic polymers, which can become highly swollen in water or biological fluids. [1, 2] The unique properties of polymer hydrogels, such as absorption, swelling and de-swelling behavior, hydrophilicity, and biocompatibility, [3, 4] have been applied in many areas such as hygiene, pharmaceutical, drug delivery, bio-sensors, artificial skin and muscles, the oil industry, agriculture, water treatment, and textile manufacture. [5-8] Recently, our group have successfully demonstrated the feasibility of using stimuli responsive polymer hydrogels as draw agent in the forward osmosis (FO) desalination for the first time.[9] The FO process shows low membrane fouling propensity and has potential to reduce water desalination and treatment costs.[10]

In the FO process, a draw agent is used to withdraw pure water from feed solution, while a semipermeable membrane blocks the solute from the feed. Dry particles of cross-linked poly (N-isopropyl acrylamide) (PNIPAM), poly (sodium acrylate) (PSA), and their copolymer have been used for purifying brackish water. However, the properties of hydrogel draw agents need to be improved to increase water flux for practical application. Thus, much effort has been poured into investigating the relationship of water flux and hydrogel properties, and improving the water flux. Research has shown that the swelling pressure of hydrogel, the contact of FO membrane-hydrogel, and water transport through the draw agent are key factors affecting water flux.[11-14] The contact of FO membrane-hydrogel indicates the percentage of contact area between hydrogel and FO membrane to the FO membrane area.

A number of strategies, such as reducing the particle size of hydrogels and compressing hydrogel particles into a monolith, have been demonstrated to improve the contact of FO membrane-hydrogel and the water transport of draw agent. [12, 13, 15-18] In particular, the addition of graphene into hydrogels greatly increased the softness of the composite hydrogels, decreased the retractive force of polymer chains, and improved the inter-particle and particle-membrane contacts, leading to significantly improved FO water fluxes.[13]

To maintain water flux in the FO process, the swelling pressure and water transport (or swelling rate) of hydrogel draw agent need to be sustained. It is well known that the swelling pressure of polymer hydrogels originates from polymer-water mixing, elastic reaction force of the network, and osmotic pressure of ionizable groups.[14, 19] One effective methodology to increase the swelling pressure of hydrogels is to increase the amount of ionic group in hydrogel, which increases the osmotic pressure. For instance, the water flux of the copolymer hydrogel

of NIPAM and SA increases with increasing the amount of ionic SA. [9, 20] On the other hand, significant efforts have been made to improve the polymer-water mixing rate and thus the swelling and deswelling properties of hydrogels. By introducing porosity in hydrogel, the interfacial contact between hydrogel and water is enhanced, giving rise to increased swelling and deswelling rates. [21-23] Introduction of structural inhomogeneity in hydrogels is another effective way to improve water diffusion. [24-26] In such hydrogels, the hydrophilic component acts as a tunnel across the dense and hydrophobic layer at the surface of hydrogels, accelerating water diffusion; the improvement of response rate of PNIPAM hydrogel can be achieved by forming comb-type grafted networks to enhance mobility of grafted chains. [27, 28] These strategies are potentially useful for designing high-performance draw agents for FO applications.

In this work, a new and effective method to sustain the swelling pressure is developed and demonstrated by incorporating hydrophilic microfibrils into a polymer hydrogel monolithic draw agent. The incorporated microfibrils provide a hydrophilic microfibril surface and microchannel around the hydrogel phase, to advantageously directly transport water to the inner part of hydrogel monolith, increasing the water diffusion, easing the restriction that polymer chain relaxation causes, and maintaining the low swelling ratio of hydrogel contacted with membrane. The microfibril-polymer monolith can be readily prepared by dispersion of hydrophilic microfibrils in aqueous monomer solution, and subsequent polymerization of monomers, and this preparation process allows for tuning of compositions of hydrogels (content of ionic monomer) and loading of microfibrils. In this study, thermoplastic polyurethane (TPU) was chosen as microfibril material for its good elasticity, high wear resistance, good oil and grease resistance and low cost. The TPU microfibrils used in this experiment were prepared by force spinning, which is a fast and efficient technique to produce micro- and nano-scale fibres. [29, 30] The swelling behavior and mechanisms of pure hydrogels and composite hydrogels are studied. The composite hydrogel is applied as a draw agent in FO process to quantify the improvement in the swelling pressure and water flux.

## 4.2 Experimental

### 4.2.1 Materials

N-isopropyl acrylamide (NIPAM, 97 %), Sodium acrylate (SA, 97 %), N, N-methylenebis (acrylamide) (MBA, 99 %), ammonium persulfate (APS,  $\geq 98$  %), and N, N, N', N'-tetramethyl ethylenediamine (TEMED, 99 %) were purchased from Sigma-Aldrich Australia. Thermoplastic polyurethane (TPU, TETON\*206) was kindly provided by Urethane Compounds Pty. Ltd Australia. Tetrahydrofuran (THF) was purchased from Merck. Pure water was used in all experiments. All the chemicals mentioned above were used without further purification.

### 4.2.2 Experimental procedures

*Preparation of pure hydrogel:* A 16.67 wt. % monomer solution was prepared by dissolving monomer (NIPAM, SA), cross-linker (MBA), and initiator (APS) in deionized water. The weight ratio of monomer, cross-linker, and initiator was fixed at 50:1:0.5. The composition of NIPAM and SA is shown in Table 4.1. A drop of TEMED was added into the monomer solution under mild shaking to accelerate the initiation of the polymerization reaction. The hydrogels were formed within a few minutes, followed by rinsing with deionized water and drying in a 60 °C oven. The dry hydrogel was ground into particles for use as a draw agent. The average particle sizes of PNIPAM, PN7S3, PN5S5, PN3S7, and PSA were 20.9, 23.5, 12.8, 21.7, and 39.8  $\mu\text{m}$ , respectively.

**Table 4.1** Composition of pure hydrogels and composite hydrogels.

<b>Pure hydrogels</b>	N-isopropyl acrylamide (wt. %)	Sodium acrylate (wt. %)	<b>Composite hydrogels</b>	TPU microfibre (wt. %)	N-isopropyl acrylamide (wt. %)	Sodium acrylate (wt. %)
PNIPAM	100	0	TPU-PNIPAM	50	50	0
PN7S3	70	30	TPU-PN7S3	50	35	15
PN5S5	50	50	TPU-PN5S5	50	25	25
PN3S7	30	70	TPU-PN3S7	50	15	35

*Preparation of TPU microfibre-hydrogel composite:* TPU was dissolved in THF to form a 12 wt. % polymer solution. The solution was spun into a TPU microfibre mat by a force spinner (Cyclone L-1000M, FibeRio® Technology Corporation, USA). At a rotational speed of 5000

rpm, 1 g of microfibre was formed in less than 30 seconds. The diameter distribution of TPU microfibre used in this study is 0.5-50  $\mu\text{m}$ .

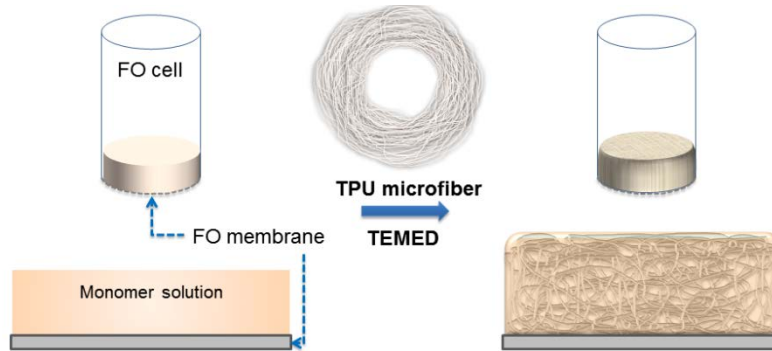


**Figure 4.2** The preparation process of TPU-hydrogel composites.

To make the composite, a drop of TEMED was added to the monomer solution. After mild shaking, the TPU microfibre was immersed into the solution and a few minutes later, the composite monolith was formed. The composite hydrogel was washed with pure water before use. For the composites used as draw agent, in order to get better contact of composite - FO membrane, the composite monolith was prepared on the membrane in the FO cell. The preparation process of TPU microfibre-hydrogel composite draw agent is shown in Figure 4.2. The FO performances of PN5S5 particles and TPU-PN5S5 composites with 0, 30, 50, and 70 wt. % TPU microfibre loading were tested (Figure 4.3), the results suggest that those with 50 wt. % TPU microfibre loading performed the best. Thus the TPU-hydrogel with 50 wt. % TPU loading, as shown in Table 4.1, was used in the following study as comparison with hydrogel particles.

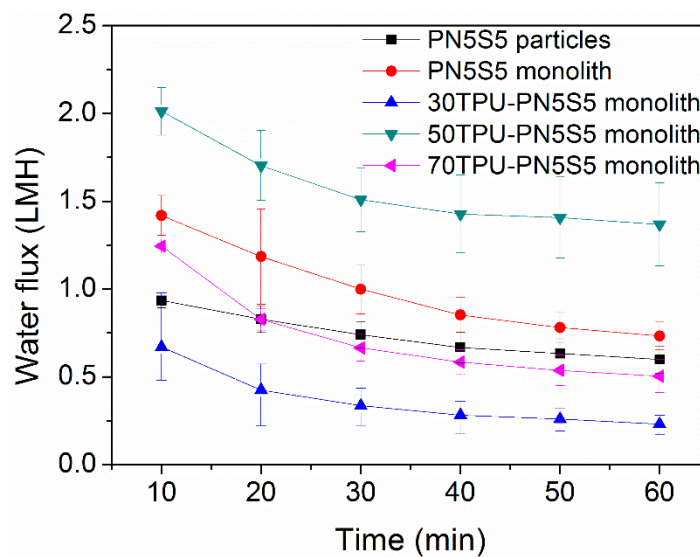


**Figure 4.3** Water flux of PN5S5 hydrogel particle and PN5S5 composite hydrogels with different TPU loadings.

*Characterization:* The morphology of pure hydrogel particles and TPU microfibre-hydrogel composites was observed by a scanning electron microscope (Nova NanoSEM 450 FESEM, FEI, USA). The diameters of TPU microfibrils were determined by the Nano Measurer 1.2. A contact angle goniometer (Dataphysics OCA15, Dataphysics, Germany) was used to determine the wettability of TPU microfibre mat and hydrogels. An industrial incandescent lamp (IR 250 C, 230 V, 250 W, Philips) was used as the light source for dewatering the hydrogel draw agents, as part of the FO process, and a radiometer (FZ-A) was used to determine the light intensity.

The swelling ratio and FO water flux were measured and calculated as in our previous study. [13, 17] The swelling ratio  $Q$  (g/g) was determined by weighing the dry hydrogels and swollen hydrogels over a period of time; the swollen hydrogels were kept in deionized water for 3 days and the water was replaced with fresh deionized water every day.

Forward osmosis tests were carried out in a homemade FO cell, as shown in Figure 4.2. The active surface of the FO membrane (CTA membrane, Hydration Technologies Inc., Albany, OR) was faced to feed solution. 0.5 g of dry pure hydrogel particle was used in the test. 1 g of TPU-hydrogel composite composed of 0.5 g of TPU microfibrils and 0.5 g of hydrogel, with different initial water contents was used as draw agent in the test. 2000 ppm NaCl solution was used as feed water in the measurements. The FO water flux,  $F$  ( $L \cdot m^{-2} \cdot h^{-1}$ , or LMH), was determined by the weight change of the FO cell over a period of time. The effective area of the FO membrane was  $4.91 \text{ cm}^2$ .

In the dewatering process, the FO cell with swollen hydrogel was put under an incandescent lamp. The light intensity on the hydrogel surface was fixed at  $1 \text{ kW} \cdot \text{m}^{-2}$  and the weight loss as a function of time recorded. The averaging dewatering flux ( $F_d$ , LMH) was calculated by equation:

$$F_d = \frac{V}{A \times t} \quad (1)$$

where  $V$  (L) is the volume loss of hydrogel in the dewatering process over a period of time  $t$  (h). The FO cell was moved to dewater directly, so the effective area  $A$  ( $\text{m}^2$ ) is  $4.91 \text{ cm}^2$ .

### 4.3 Results and discussion

#### 4.3.1 Morphology of composite hydrogels

The morphology of TPU microfibrils and composite hydrogels was observed using scanning electron microscopy, with the results shown in Figure 4.4. Figure 4.4a demonstrates that the diameter of TPU microfibril is unevenly distributed, their diameter ranging from 0.5 to 50  $\mu\text{m}$ . Figure 4.4b-f show the cross-section of TPU-hydrogel composites. In such dry composites, the TPU microfibrils are dispersed within the hydrogel, and a gap can be seen between the microfibril and hydrogel.

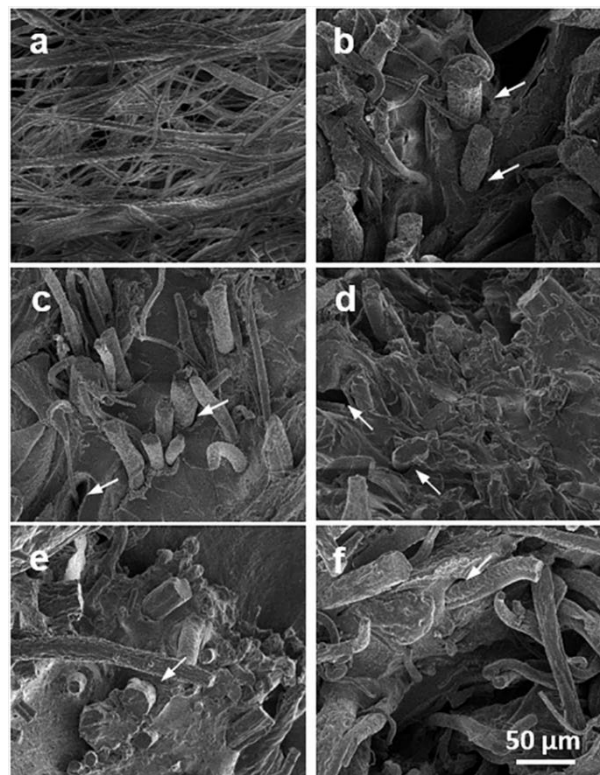


**Figure 4.4** SEM images of TPU microfibrils and cross-section of composite hydrogels. (a) TPU microfibrils, (b) TPU-PNIPAM composite, (c) TPU-PN7S3 composite, (d) TPU-PN5S5 composite, (e) TPU-PN3S7 composite, and (f) TPU-PSA composite. The gaps between the microfibril and the hydrogel are indicated by arrows.

#### 4.3.2 Swelling properties of hydrogels

The swelling ratio of the composite hydrogels is half of that of corresponding pure hydrogels, as shown in Figure 4.5. Since the composite hydrogels contain 50 wt. % TPU microfibril and 50 wt. % hydrogel, and TPU microfibril does not swell in water to the same degree as a hydrogel,

blending with TPU microfibre decreases the swelling ratio of the composites in a proportionate manner.

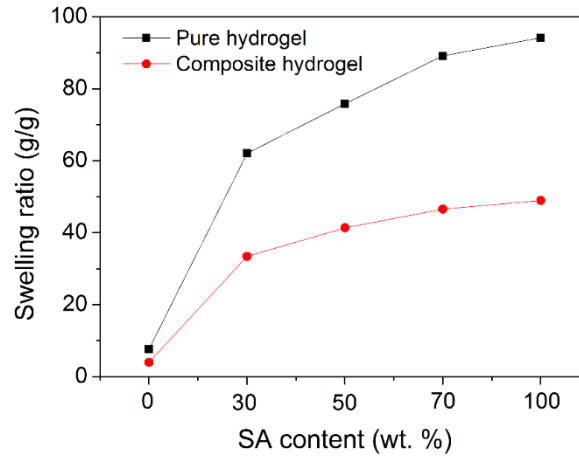


**Figure 4.5** Swelling ratios of pure hydrogel and composite hydrogels.

Swelling is a continuous process of solvent transition from an unsolvated glassy or partially rubbery state, to a fully relaxed rubbery region. [19] The swelling of hydrogel includes the diffusion of water and the relaxation of polymer chains with the incoming water makes them more mobile. A comprehensive, but simple equation can be used to describe the diffusion mechanism in hydrogels, the so-called power law: [31, 32]

$$\frac{M_t}{M_\infty} = kt^n \quad (2)$$

where  $M_t$  and  $M_\infty$  are the amount of water absorbed at time  $t$  and infinite time, respectively.  $k$  is the characteristic constant of the water-polymer system, while  $n$  is the diffusional exponent, indicating the mechanism of diffusion. For slab samples (monoliths in this study), if the polymer chain relaxation rate is much faster than the water diffusion rate, it is Fickian diffusion or Case I diffusion ( $n = 0.5$ ). Fickian diffusion is a diffusion-controlled swelling process, [33] whilst if the water diffusion rate is very rapid compared to the relaxation rate of increasingly-solvated polymer chains, it is non-Fickian diffusion or Case II diffusion ( $n = 1$ ), and is a relaxation-controlled swelling process. Anomalous diffusion dominates when the diffusion and relaxation rate are comparable or  $0.5 < n < 1$ . These three models describe the relationship between solvent diffusion rate and polymer chain relaxation rate, as well as the kinetics of hydrogel swelling. Depending on different applications, the polymeric hydrogels can be designed with suitable swelling behavior and swelling kinetics. For the hydrogel used as a draw agent, faster swelling is desired. Theoretically, an improvement of the solvent diffusion rate of more Fickian diffusion or increasing the polymer chain relaxation rate of more non-Fickian diffusion enhances the swelling kinetics of hydrogel.

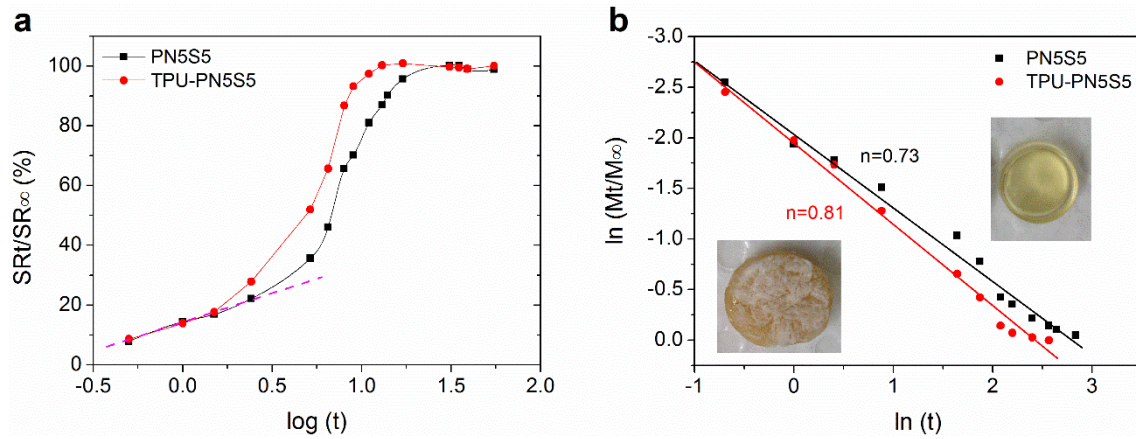


**Figure 4.6** (a) Swelling behavior and (b) swelling kinetics of pure hydrogel (PN5S5) and composite hydrogel (TPU-PN5S5). SR in (a) is short for swelling ratio. Two circular slabs (PN5S5 and TPU-PN5S5) with the same amount of PN5S5 hydrogel and similar thickness (4 mm) were used in this study. The insets are the images of samples used.

After TPU microfibres were incorporated, the swelling rate of composite hydrogel was clearly enhanced (Figure 4.6). In the swelling process, the water diffuses into the polymer, which changes the polymer chains from a glassy to rubbery state, with increasing mobility of the macromolecules and volume expansion. [31] The effect of the TPU microfibre on the swelling kinetics of hydrogels was then investigated. Pure hydrogel, PN5S5, and composite hydrogel, TPU-PN5S5 circular slabs were swollen in water from glassy state (dry sample).

The time-dependence of the degree of swelling hydrogels can be seen as sigmoidal curves (Figure 4.6a). [34] The curves can be divided into three parts: [35] firstly, the swelling is restricted by the rigid and glassy inner core in the direction normal to the front surface; secondly, the rigid core changes from the glassy to rubbery state after the fronts meet, permitting swelling in all directions, and thus accelerating the swelling kinetics; [36] thirdly, once the hydrogels approach their equilibrium swelling ratios, they show slower rates of swelling. Since the thickness of PN5S5 and TPU-PN5S5 are both 4 mm, the initial parts of the swelling curves are very similar, as shown in Figure 4.6a. However, the acceleration of swelling kinetics of TPU-PN5S5 occurs earlier than those of PN5S5, which means it takes a shorter time for TPU-PN5S5 to transition from the glassy to rubbery state. The diffusion exponent,  $n$ , of TPU-PN5S5 increased from 0.73 (PN5S5) to 0.81 after blending with TPU microfibre, as shown in Figure 4.6b, indicating the solvent diffusion rate of the composite was higher. Thus, the polymer molecular relaxation rate of PN5S5 is greater than the solvent diffusion rate, [37, 38] so the increase of water diffusion rate in TPU-PN5S5 leads to an earlier occurrence of the acceleration

swelling process. Due to the benefit of the increased rate of water diffusion, the composite reached equilibrium swelling after 11 h, while the pure hydrogel equilibrium took 17 h.

### 4.3.3 Water diffusion in composite hydrogels

In the following section, the mechanism of the water diffusion improvement by incorporating TPU microfibrils will be discussed. Figure 4.7 shows the wettability of TPU microfibre and the water absorbing ability of hydrogels, which indicates the enhanced absorbing ability of composite hydrogels is related to the wettability of TPU microfibrils. The dry TPU microfibrils are hydrophobic, as shown in Figure 4.7a, the water contact angle of dry TPU microfibre changing only slightly after 5 minutes test. However, when the microfibrils become totally wet, the water droplet spread on the microfibrils in less than 0.1 second, demonstrating that the wet TPU microfibre is hydrophilic.

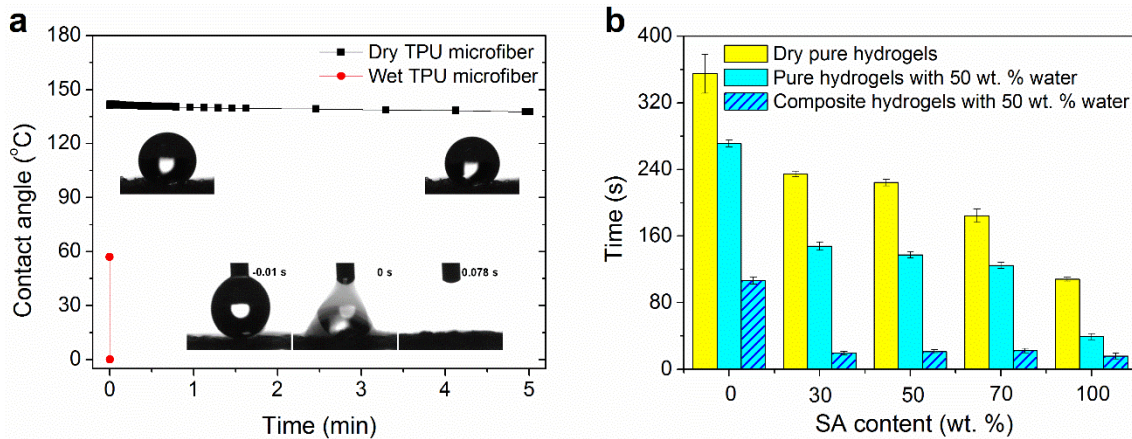


**Figure 4.7** Wettability of TPU microfibrils and water absorption ability of hydrogels. (a) Plot of contact angle *versus* time of dry TPU microfibril and wet TPU microfibril. (b) Time needed for absorbing a 3  $\mu\text{L}$  water droplet by dry pure hydrogels, wet pure hydrogel and wet composite hydrogels. The wet hydrogels contained 50 wt. % water. Contact angle goniometer was used to control the volume of water droplets and observe the absorbing process.

To test the water absorbing ability of hydrogels, a 3  $\mu\text{L}$  water droplet was dropped on the surface of pure hydrogels and composite hydrogels (slabs), and the time required for the water droplet to be absorbed recorded. The results in Figure 4.7b show that: 1) the absorption time decreases with increasing the SA content of hydrogels; 2) the water absorption ability of wet composite hydrogel is much better than that of dry pure hydrogels or pure hydrogels containing 50 wt. % water. The water absorption ability of composite hydrogels is much greater than that

of the neat hydrogels. This may be caused by the hydrophilicity of the wet TPU microfibres, or the capillary effect generated by the channels around microfibres.

To better observe the effect of TPU microfibres, a rhodamine B aqueous solution was used to track water transport in the pure hydrogel and composite, and the relevant images are shown in Figure 4.8. Figure 4.8a indicates that water can transport faster in the composite than pure hydrogel. In Figure 4.8b, before the dye solution was dropped on the hydrogel, the TPU microfibres could not be seen clearly by an optical microscope. After 50 seconds, the pink microfibres became more visible inside the hydrogel, whilst the color of hydrogel became lighter. This indicates that the RhB solution was more easily transported into the inner part of composite hydrogel through the microchannels around TPU the microfibres.

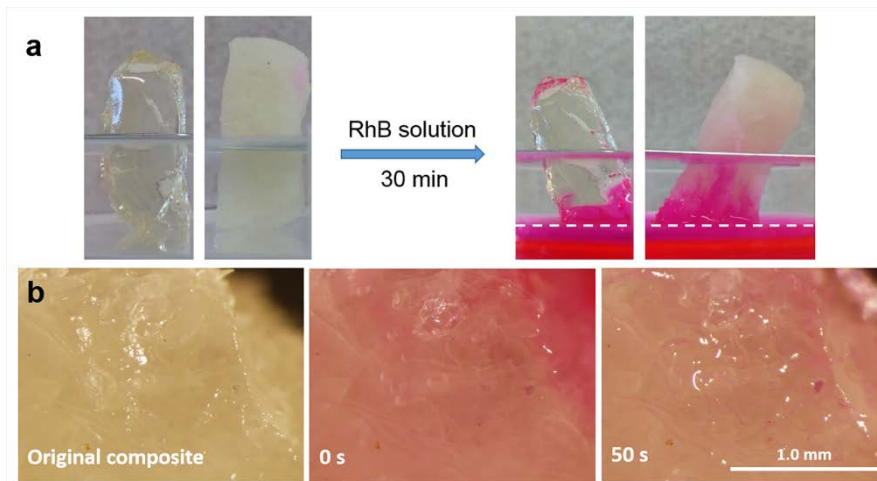


**Figure 4.8** (a) The swelling of pure hydrogel (left) and composite hydrogel (right) in aqueous rhodamine B (RhB) solution. (b) The water absorption process of composite hydrogel (50 wt. % water content) tracked by rhodamine B aqueous solution. These images were taken with an optical microscope.

#### 4.3.4 Forward osmosis performance of hydrogels

To investigate the effect of the water diffusion improvement of composite hydrogel on the swelling pressure, the composite hydrogels were tested as draw agents in FO, and compared with the relevant hydrogel particles shown in our previous study. Figure 4.3 demonstrates that TPU-PN5S5 with 50 wt. % TPU loading performed better than PN5S5 monolith, while PN5S5 monolith performed better than PN5S5 particles. In order to compare the forward osmosis performance of composite hydrogel monolith and pure hydrogel particles, the first hour FO water flux of dry pure hydrogel particle and composite monolith with different water content (0, 33.3, 50, 60, and 66.7 wt. %) were measured, as shown in Figure 4.9. Generally, the water

flux of both pure and composite hydrogel increased with increasing amount of sodium acrylate in the hydrogels, and this is consistent with their water absorption ability. There is an ionic –COONa group in sodium acrylate, so the copolymer PNIPAM-SA with greater amount of sodium acrylate possesses higher osmotic pressure, generating higher water flux.

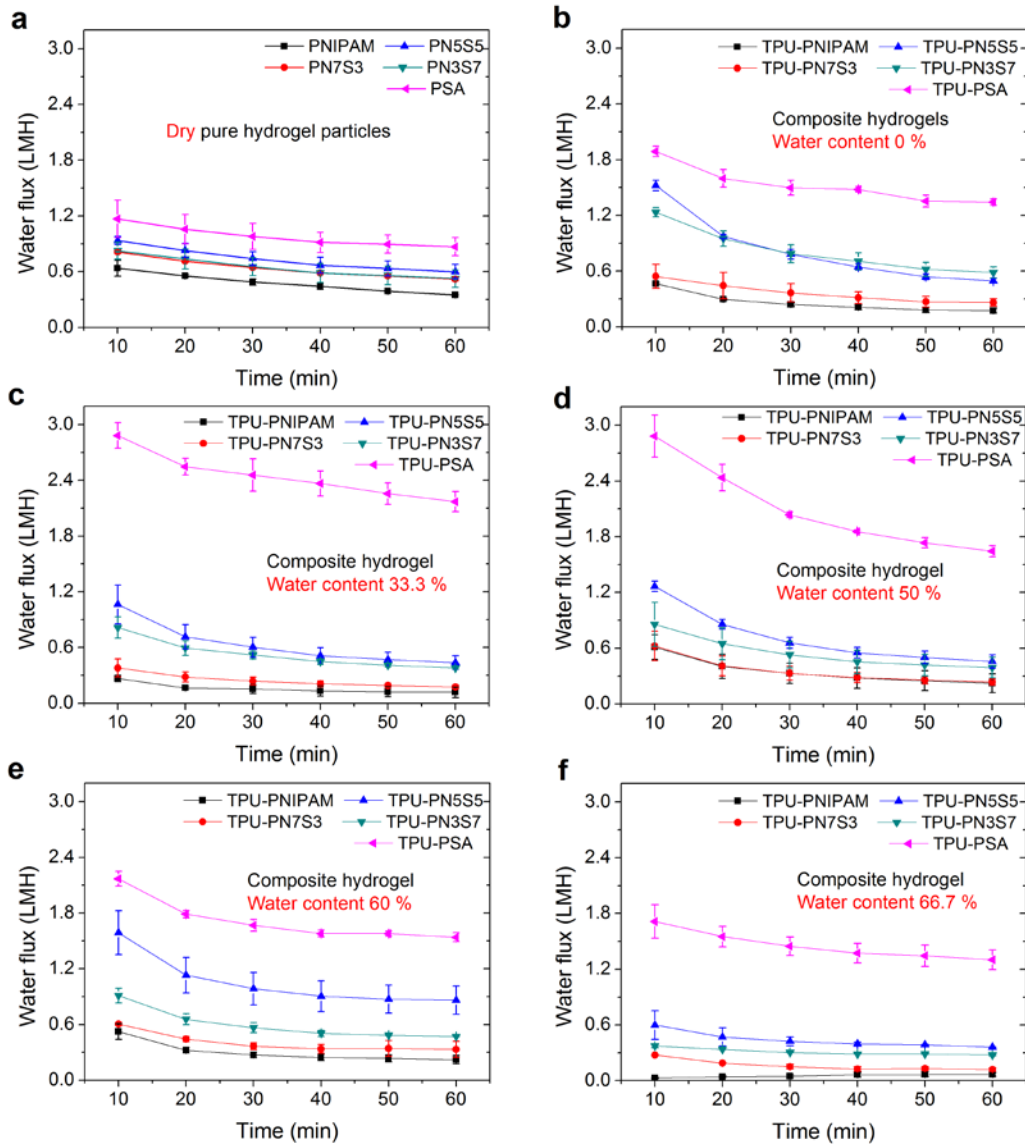


**Figure 4.9** One hour forward osmosis water flux of pure hydrogel particle and composite hydrogels. (a) Dry pure hydrogel particle, and composite hydrogels with an initial water content of (b) 0, (c) 33.3, (d) 50, (e) 60, and (f) 66.7 wt.%. 2000 ppm NaCl solution was used as feed. 0.5 g dry pure hydrogel particle and 1 g composite hydrogel (composed of 0.5 g hydrogel and 0.5 g TPU microfibre) were used in the test.

However, PN5S5 and TPU-PN5S5 performed better than PN3S7 and TPU-PN3S7, respectively. The study of Hartanto et al. showed that the addition of higher amount of acrylic acid in PNIPAM-AA hydrogel resulted in higher water flux, but the addition of excess acrylic

acid from 50 % to 70 % appears to have limited impact on the water flux. [15] Note that the FO water flux depends on not only the osmotic pressure of hydrogel, but also on the contact of membrane–hydrogel. Figure 4.10 shows that the particle size of PN5S5 is smaller than that of PN3S7, thus, the PN5S5 particle generated higher flux due to better contact. The average particle size of PNIPAM, PN7S3, PN5S5, PN3S7, and PSA were 20.9, 23.5, 12.8, 21.7, and 39.8  $\mu\text{m}$ , respectively, determined by Nano Measurer 1.2. Importantly, the TPU-hydrogel composite was monolithic. Higher water fluxes of TPU-PN5S5 may be caused by better contact of the membrane and composite than that of TPU-PN3S7.

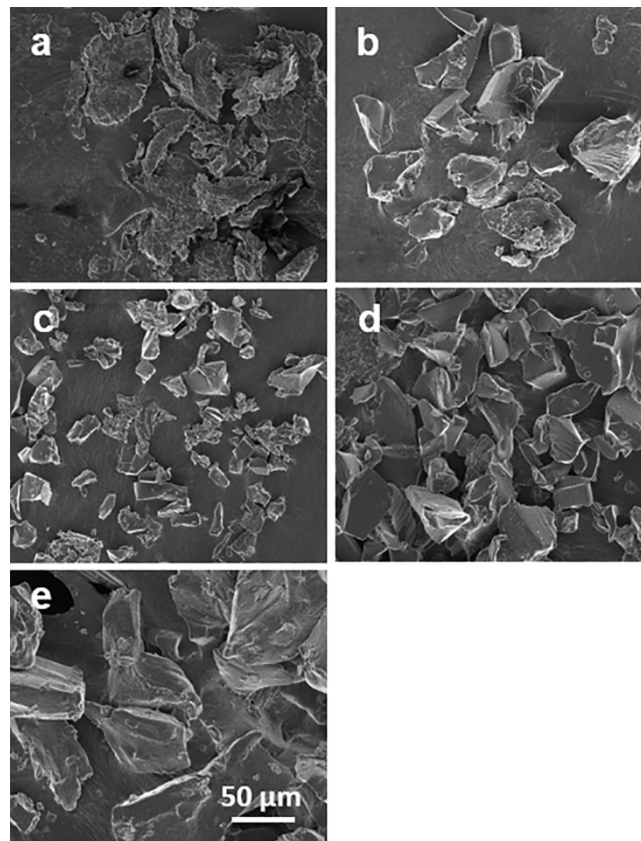


**Figure 4.10** SEM images of pure hydrogel particles. (a) PNIPAM, (b) PN7S3, (c) PN5S5, (d) PN3S7, and (e) PSA.

Compared to dry pure hydrogel particles, composite hydrogels performed better in the FO process. In the first 10 minutes of the FO test, the water flux of PNIPAM, PN7S3, PN5S5, PN3S7, and PSA particle were 0.64, 0.81, 0.94, 0.83, and 1.17 LMH, respectively; while those of relevant dry composite hydrogels were 0.46, 0.54, 1.52, 1.23, and 1.89 LMH, individually. Among the hydrogels, TPU-PSA exhibited greatly enhanced water flux compared to other composites and PSA particles. With the increased initial water content, the first 10 minutes water flux of TPU-PSA increased from 1.89 LMH to 2.88 LMH (33.3 and 50 wt. % water

content), and then gradually decreased to 1.71 LMH (66.7 wt. % water content). Other composite hydrogels with 0-60 wt. % water content generated similar water flux, however, when it was increased to 66.7 wt. %, the water flux decreased obviously to lower than 0.6 LMH. Theoretically, the composite hydrogel with a smaller amount of water should generate higher water flux because ionization of charged groups results in a higher osmotic pressure and thus higher swelling pressure. However, with regards to the water flux of the composite hydrogel, there is a balance between swelling pressure and membrane–hydrogel contact. Higher swelling pressure generates higher water fluxes; on the other hand, better contact with the membrane also produces higher water flux. The composite hydrogels with greater water content were softer and flatter, while those with less water content was harder and curved (not flat), which indicates that better contact between FO membrane and composite hydrogel can be obtained by increasing its water content. As a result, the water flux of composite hydrogel with a larger amount of water changed slightly or even became higher. When 2000 ppm NaCl solution was used as feed, TPU-PSA with an initial water content of 50 wt. % generated 2.88 LMH water flux in the first 10 minutes, and 1.77 LMH after 1 hour. In contrast, those of the PSA particles were 1.16 and 0.87 LMH, respectively.

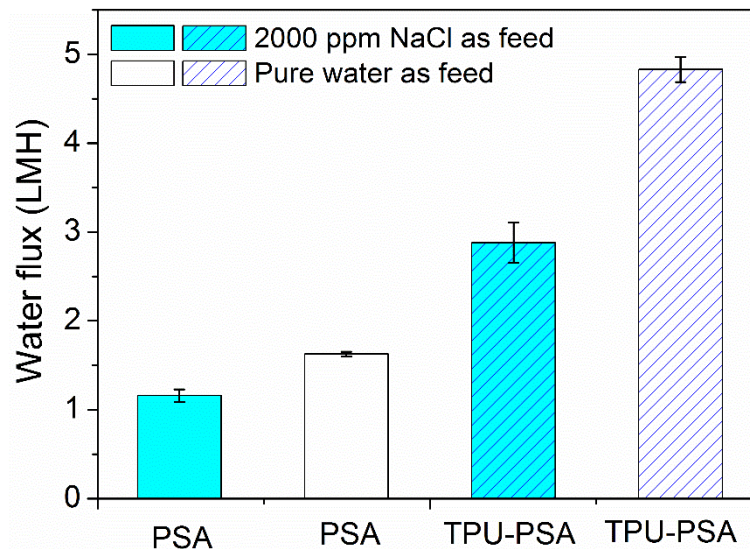


**Figure 4.11** The first 10 min FO water fluxes of PSA particle and wet TPU-PSA composite, with 2000 ppm NaCl solution or pure water as feed.

When pure water was used as feed, the FO water flux of PSA and TPU-PSA were also tested, as shown in Figure 4.11. The first 10 minute water fluxes of dry PSA particles were 1.17 and 1.63 LMH when 2000 ppm NaCl solution and pure water were used as feed, respectively. By blending with 50 wt. % TPU microfibres, the water flux of wet TPU-PSA (50 wt. % water content) increased to 2.88 and 4.83 LMH, respectively.

Figure 4.12a-b shows the 24 hours FO performance of hydrogels. For pure hydrogel particle, PSA showed highest water flux. It generated 1.17 LMH water flux in the first 10 minutes, 0.53 LMH after 5 hours, and 0.27 LMH after 24 hours. In the test, TPU-PSA monolith showed the highest FO water flux among 10 hydrogels. It generated a water flux of 2.77 LMH, 1.28 LMH and 0.80 LMH in the first 10 minutes, after 5 hours, and after 24 hours, respectively. These values are about twice as large as those of PSA hydrogel particles. In previous study, the water flux of hydrogel particles dropt very fast to below 1 LMH in less than 5 hours. For example, as shown in Table 4.2, it takes 1, 3, 5, and 4 hours for PSA, [9] PSA-C, [17], PSA-rGO [13] hydrogel particles, and MCG-NP50-AA50 microgels [15] to drop down to less than 1 LMH, respectively. However, TPU-PSA maintained a water flux of > 1 LMH in the first 12 hours, which benefits from the good water transport system.

**Table 4.2.** The water flux of hydrogel draw agent in recent publications.

Draw agent	Water flux (LMH)		Ref.
	1 <sup>st</sup> hour	5 <sup>th</sup> hour	
PSA particles	0.96	0.58	[9]
PSA-Carbon paticles	1.05	0.80	[17]
PSA-rGO	3.1	0.95	[13]
PNIPAM-SA-iron oxide	1.48	0.70	[18]
PNIPAM-SA microgels	4	--	[15]
PNIPAM-SI-0.5 PVA	0.24	0.08	[16]
TPU-PSA	2.17	1.28	This work

After the FO process, all the water absorbed by the hydrogels was dewatered using an industrial incandescent lamp ( $1 \text{ kW} \cdot \text{m}^{-2}$  sunlight), and the average dewatering flux is shown in Figure 4.12c-d. In a practical application, the dewatering could be achieved by combining the solar energy and industrial waste heat. As shown in Figure 4.12c-d, the average dewatering flux of composite hydrogels is slightly higher than those of pure hydrogel particle. Surprisingly, PSA showed the highest dewatering flux among the pure hydrogel particles, but not for PNIPAM. PNIPAM is a temperature-responsive hydrogel, swollen PNIPAM hydrogel particle dewateres most of the water absorbed easily by heat it over its lower critical solution temperature (LCST); however, it is difficult to dewater all the water from it. When PNIPAM is heated above the LCST, a hydrophobic layer will be formed at the surface of hydrogel that limits the outward

diffusion of water molecules. TPU-PNIPAM showed the best dewatering performance among the hydrogels.

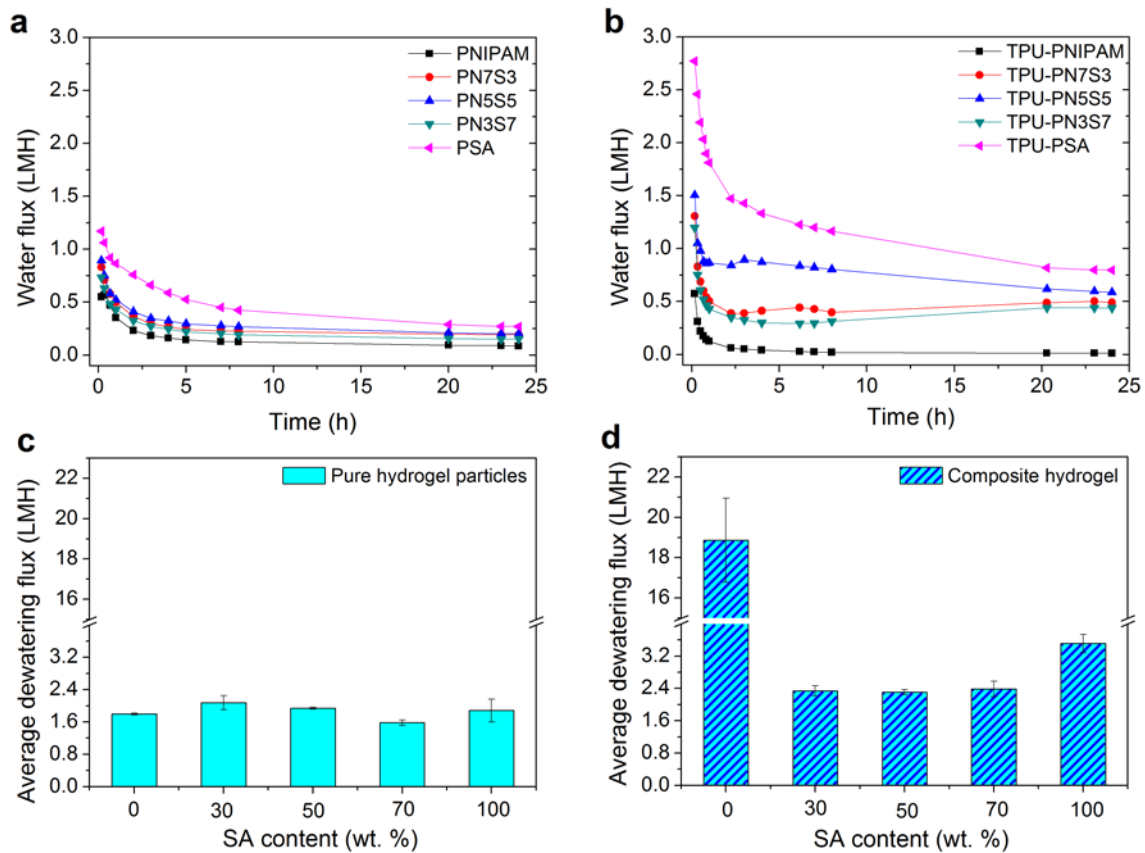


**Figure 4.12** 24 hours forward osmosis water flux of (a) pure hydrogel particle and (b) composite hydrogels with 50 wt. % initial water content; average dewatering flux of (c) pure hydrogel particle and (d) composite hydrogels as a function of SA content. 2000 ppm NaCl solution was used as feed as feed in the FO process. 0.5 g dry pure hydrogel particle and 1 g composite hydrogel (composed of 0.5 g hydrogel and 0.5 g TPU microfibre) were used as the initial draw agent in the test.

This is caused for two reasons: 1) only a very small amount of water was absorbed by TPU-PNIPAM in the FO process; 2) the initial water content of TPU-PNIPAM was 50 wt. %, so it was easy for TPU-PNIPAM to release a small amount of water before the formation of hydrophobic layer. Figure 4.13 shows the weight of water absorbed in the 24 hours FO process and desorbed in the dewatering process by hydrogels. Except for TPU-PNIPAM, the weight of water absorbed by the composite hydrogels is about 3 times as much as those of relevant pure hydrogel particle. 1 g of TPU-PSA (0.5 g of TPU microfibre and 0.5 g of hydrogel) absorbed 9.4 g of water in 24 hours test, while 0.5 g of dry PSA only absorbed 3.2 g of water. TPU-PNIPAM only absorbed a small amount of water in the 24 hours FO test, because the swelling

pressure generated by wet TPU-PNIPAM is small. The initial water content of composite hydrogels used in the test was 50 wt. %, and the relevant swelling ratio was 1 g/g, while the equilibrium swelling ratio of TPU-PNIPAM is 3.9 g/g. It takes a few days for the TPU-PNIPAM to reach swelling equilibrium by immersing it in water. Thus, it is difficult for wet TPU-PNIPAM to generate high FO fluxes. After the FO test, all the water absorbed in the FO process was desorbed in the dewatering process. The percentage of liquid water recovery is shown in Figure 4.14, after combining the TPU microfibre and hydrogel, it is slightly increased.

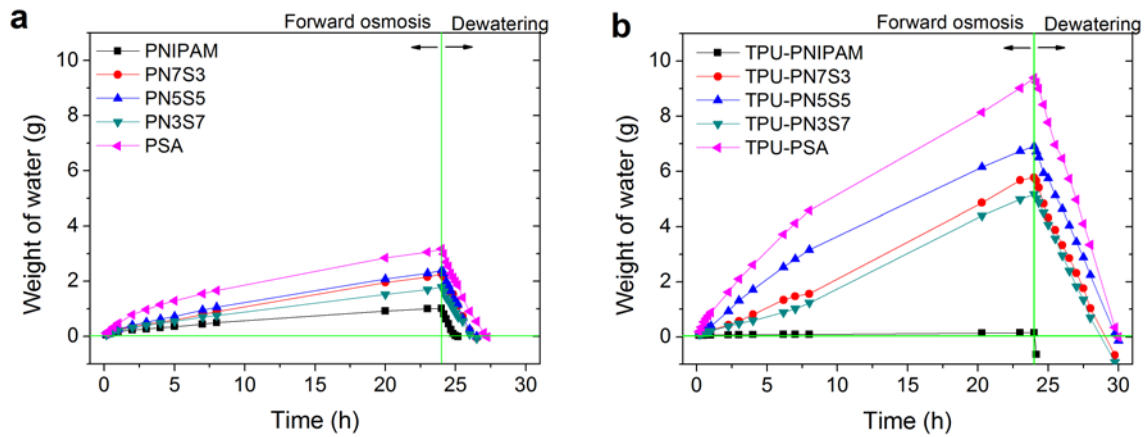


**Figure 4.13** Forward osmosis and solar dewatering performance of pure hydrogel particle and composite hydrogels. 2000 ppm NaCl solution was used as feed in the FO process. The dewatering process was tested under  $1 \text{ kW} \cdot \text{m}^{-2}$  incandescent lamp. (a) Weight of water absorbed or desorbed by the pure hydrogel particles in the FO and dewatering process. 0.5 g dry pure hydrogel particle was used in the test. (b) Weight of water absorbed or desorbed by the composite hydrogels in the FO and dewatering process. 1 g composite hydrogel (composed of 0.5 g hydrogel and 0.5 g TPU microfibre) with 50 wt. % initial water content was used in the test.

The temperature change of hydrogels in one hour dewatering process was measured, as shown in Figure 4.15. 2.5 g of water was added to 0.5 g of hydrogel particle or 1 g of composite hydrogel to obtain a swollen hydrogel before this test. The water content of hydrogel particle and hydrogel of the composite were the same. The test was conducted under  $1 \text{ kW} \cdot \text{m}^{-2}$  incandescent lamp. After 6 minutes, the composite hydrogels reached their highest temperature. Thereafter, the temperature of composite hydrogel decreased with time, likely due to the decreasing water content of hydrogels. However, the temperature of swollen pure hydrogel particles increased in the first 20 minutes, and then remained constant. The highest temperatures of composite hydrogels were greater than those of relevant pure hydrogel

particles. The temperature increase and decrease of TPU-hydrogel composite were both faster than those of pure hydrogel particles, which indicated that heat transfer is more efficient in the composite hydrogel. This is consistent with the data of average dewatering flux.

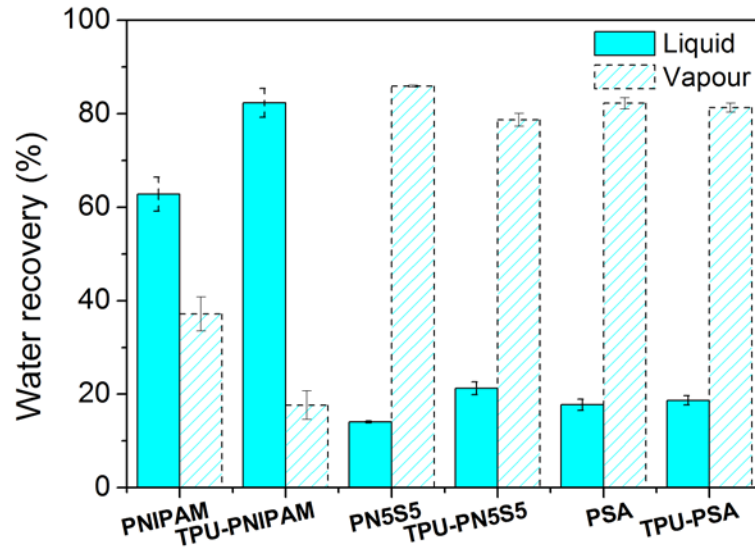


**Figure 4.14** Liquid and vapour water recovery of hydrogels in the dewatering process.

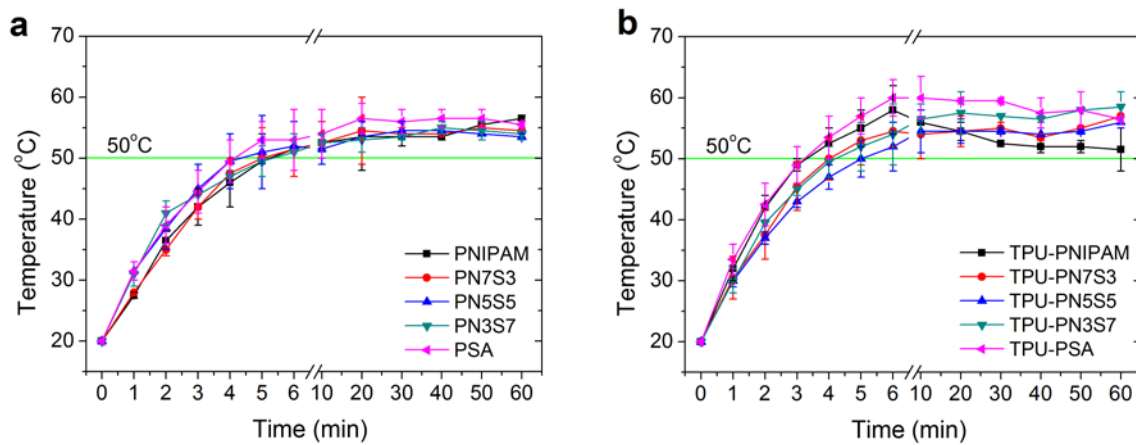


**Figure 4.15** Temperature changes of (a) pure hydrogel particle and (b) composite hydrogels under a  $1 \text{ kW}\cdot\text{m}^{-2}$  incandescent heat dewatering process. The hydrogel particles used in this test contained 0.5 g dry pure hydrogel particle and 2.5 g water. The composite hydrogels used in this test contained 1 g composite hydrogels (composed of 0.5 g hydrogel and 0.5 g TPU microfibre) and 2.5 g water.

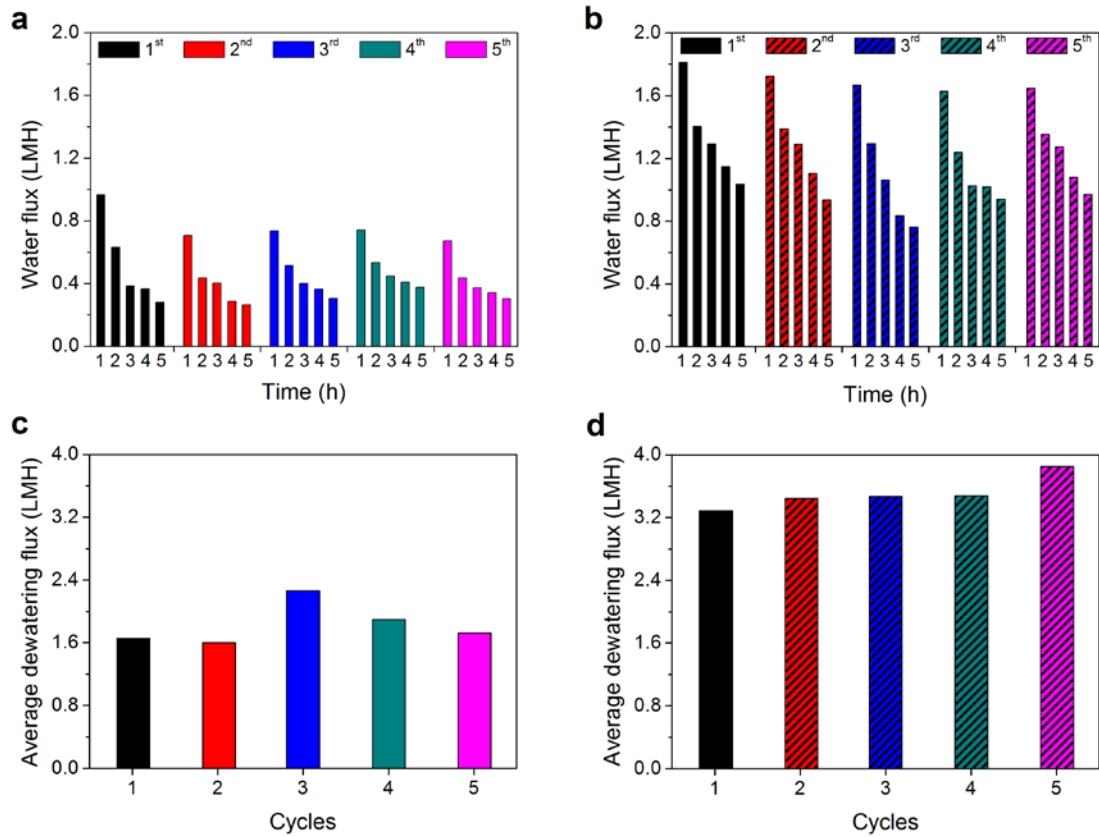


**Figure 4.16** Reusability of (a) PSA particles and (b) TPU-PSA. 5 cycles of forward osmosis and dewatering performance were tested. In the FO test, 5 hours water flux was measured in each cycle. 2000 ppm NaCl solution was used as feed. Average dewatering flux of (c) PSA particles and (d) TPU-PSA were measured under  $1 \text{ kW}\cdot\text{m}^{-2}$  incandescent lamp. 0.5 g of dry pure hydrogels and 1 g of composite hydrogels with 50 wt. % water content were used in the tests.

Figure 4.16 shows the reusability of PSA and TPU-PSA. Both PSA and TPU-PSA showed good reusable performance after 5 cycles, but TPU-PSA generated much higher FO water flux, as well as average dewatering flux. The water flux of PSA decreased from 0.97 (1<sup>st</sup> hour) to 0.28 LMH (5<sup>th</sup> hour) in the first cycle, while these decreased from 0.67 to 0.30 LMH in the fifth cycle. In contrast, the relevant water fluxes of TPU-PSA were 1.81 (1<sup>st</sup> hour) and 1.03 LMH (5<sup>th</sup> hour) in the first cycle, and they were 1.65 and 0.97 LMH in the fifth cycle. The FO water flux of TPU-PSA decreased slightly in 5 cycles. The swelling pressure, which is the driving force of the FO process, was estimated (Figure 4.17). The result shows that the osmotic pressure of PSA hydrogel (SR=5) is 6.3 MPa, while that of TPU-PSA (SR=5) is 8.2 MPa. These are both larger than that of seawater (2.34 MPa at 298 K), and TPU-PSA is greater.

Regarding dewatering performance, the average dewatering flux didn't change significantly in 5 cycles. The average dewatering flux of PSA particle was 1.83 LMH, while that of TPU-PSA composite was 3.51 LMH. Both the FO water flux and dewatering flux of TPU-PSA are twice as high as that of PSA. When the hydrogel is dehydrated by temperature stimuli in air, the water content of hydrogel surface reduces rapidly as a glassy rigid skin is formed at the surface as the water content keeps decreasing; this can significantly limit further water release due to "case hardening". [39, 40] This increase of dewatering flux of TPU-PSA, compared to PSA particles, may be due to the ease with which "case hardening" can occur due to the transport of water out through TPU microfibrils and the micro-channels.

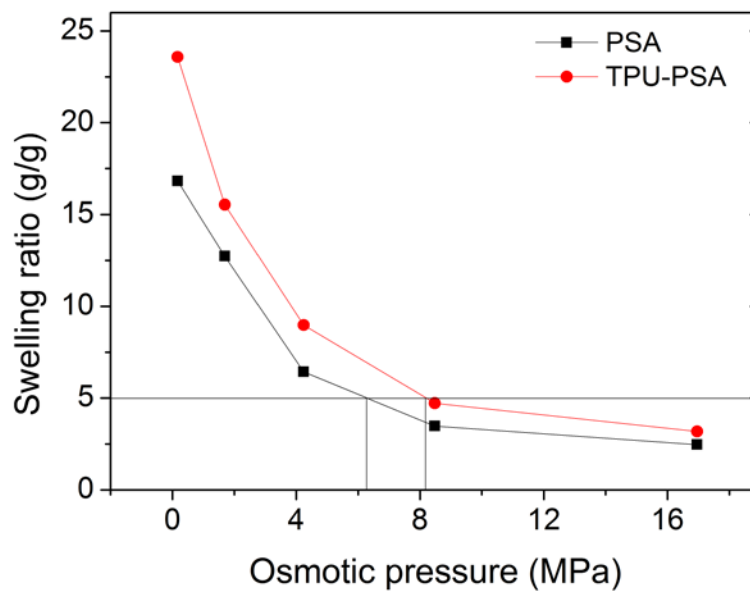


**Figure 4.17** The swelling ratio of PSA and TPU-PSA under different osmotic pressure (different concentration of NaCl solution). The data was measured according to [13].

Hydrogel (Swelling ratio = 5) was placed on the active side of a FO membrane, while NaCl solutions with different concentrations were used as feed on the other side of membrane. The NaCl concentrations used in the experiment are 2, 20, 50, 100, and 200 g/L. The measurement lasts 24 hours at room temperature.

## 4.3.5 Swelling mechanism of hydrogels

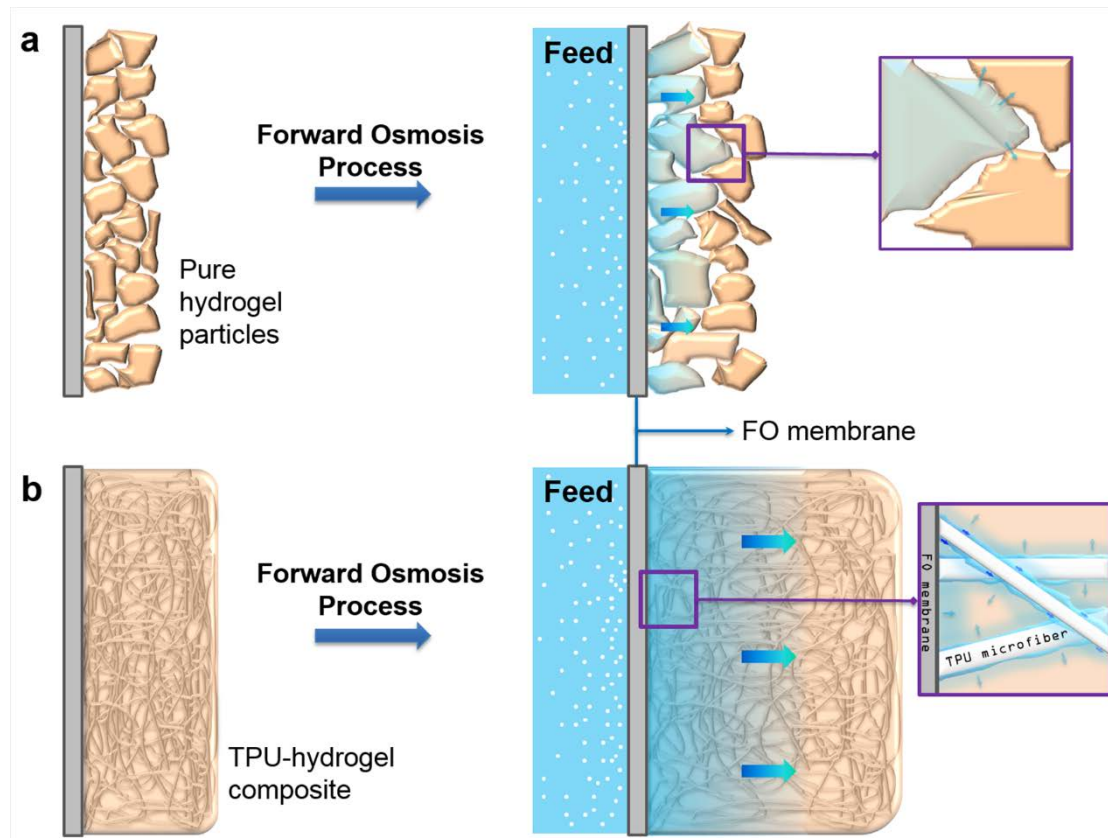


**Figure 4.18** The proposed swelling mechanisms of (a) pure hydrogel particle and (b) TPU-hydrogel composite.

Figure 4.18 shows the proposed swelling mechanism of pure hydrogel particles and TPU-hydrogel composite. For pure hydrogel particles, the first particle layer next to FO membrane absorbs water from the feed; followed by the second layer of particles absorbing water from the swollen hydrogels. There are two problems in this process: 1) it is not easy for the second layer hydrogel particles to absorb water from the swollen particles, because the water absorbed is mostly bound to hydrogel during the early stage of swelling, and the contact between them may not be good. 2) The swelling pressure generated by swollen hydrogel particles (first layer) is lower than when they are dry, resulting in a rapid decrease of water flux in the FO process. In this study, wet composite hydrogels (50 wt. % water content) are used as draw agents, which mean that the TPU microfibre is wet and hydrophilic. Thus, water would spread rapidly on the TPU microfibre. As shown in Figure 4.18b, the proposed swelling process of the composite hydrogel is that the hydrogel on the membrane surface absorbs water from the feed solution, then, water transports through microchannel around TPU microfibre to the inner part of the composite until it is absorbed by the hydrogel near the microfibre. Better water transport helps

to increase initial water flux, and maintain the high water flux in the FO process. On the other hand, the TPU microfibre also helps to transport the water or water vapor outward during the dewatering process. In summary, better water transport of the composite hydrogel improves the FO water flux when being swollen and also increases the dewatering flux, by simply constructing a hydrophilic fibre-hydrogel composite system.

#### **4.4 Summary**

In conclusion, the swelling pressure of polymer hydrogels was enhanced by incorporating TPU microfibrils, and thus improving water transport into the inner part of the composite monolith. The hydrophilicity of wet TPU microfibrils and the capillary effect generated by microchannels around them resulted in greatly enhanced water absorption ability and water diffusion rate, and sustained swelling pressure of the polymer hydrogels. The composite hydrogel therefore induced significantly higher forward osmosis water flux and dewatering flux compared to pure hydrogel particles. TPU-PSA generated a water flux of 2.77, 1.28 and 0.80 LMH in the first 10 minutes, 5 hours, and 24 hours, respectively, which are about twice of those of PSA hydrogel particle (1.17, 0.53, and 0.27 LMH). In terms of the dewatering performance, the dewatering flux of TPU-PSA was 3.51 LMH, which is almost two times of that of PSA particles (1.83 LMH). This study provides a simple and effective strategy for improving water transport through the hydrogel structure and sustaining swelling pressure of stimuli-responsive polymer hydrogels, which is very promising for designing high-performance draw agents for forward osmosis application.

#### **4.5 References**

- [1] M. Hamidi, A. Azadi, P. Rafiei, Hydrogel nanoparticles in drug delivery, *Advanced drug delivery reviews*, 60 (2008) 1638-1649.
- [2] W.A. Laftah, S. Hashim, A.N. Ibrahim, Polymer hydrogels: A review, *Polymer-Plastics Technology and Engineering*, 50 (2011) 1475-1486.
- [3] C. Chang, B. Duan, J. Cai, L. Zhang, Superabsorbent hydrogels based on cellulose for smart swelling and controllable delivery, *European Polymer Journal*, 46 (2010) 92-100.
- [4] A.P. Rokhade, S.A. Agnihotri, S.A. Patil, N.N. Mallikarjuna, P.V. Kulkarni, T.M. Aminabhavi, Semi-interpenetrating polymer network microspheres of gelatin and sodium

- carboxymethyl cellulose for controlled release of ketorolac tromethamine, *Carbohydrate Polymers*, 65 (2006) 243-252.
- [5] B. Adhikari, S. Majumdar, *Polymers in sensor applications*, *Progress in polymer science*, 29 (2004) 699-766.
- [6] J. Kim, K.-W. Lee, T.E. Hefferan, B.L. Currier, M.J. Yaszemski, L. Lu, Synthesis and evaluation of novel biodegradable hydrogels based on poly (ethylene glycol) and sebacic acid as tissue engineering scaffolds, *Biomacromolecules*, 9 (2007) 149-157.
- [7] H. Omidian, K. Park, J.G. Rocca, Recent developments in superporous hydrogels, *Journal of pharmacy and pharmacology*, 59 (2007) 317-327.
- [8] A. Pourjavadi, H. Hosseinzadeh, M. Sadeghi, Synthesis, characterization and swelling behavior of gelatin-g-poly (sodium acrylate)/kaolin superabsorbent hydrogel composites, *Journal of composite materials*, 41 (2007) 2057-2069.
- [9] D. Li, X. Zhang, J. Yao, G.P. Simon, H. Wang, Stimuli-responsive polymer hydrogels as a new class of draw agent for forward osmosis desalination, *Chemical Communications*, 47 (2011) 1710-1712.
- [10] T.Y. Cath, A.E. Childress, M. Elimelech, Forward osmosis: principles, applications, and recent developments, *Journal of membrane science*, 281 (2006) 70-87.
- [11] D. Li, X. Zhang, G.P. Simon, H. Wang, Forward osmosis desalination using polymer hydrogels as a draw agent: Influence of draw agent, feed solution and membrane on process performance, *Water research*, 47 (2013) 209-215.
- [12] A. Razmjou, G.P. Simon, H. Wang, Effect of particle size on the performance of forward osmosis desalination by stimuli-responsive polymer hydrogels as a draw agent, *Chemical Engineering Journal*, 215 (2013) 913-920.
- [13] Y. Zeng, L. Qiu, K. Wang, J. Yao, D. Li, G.P. Simon, R. Wang, H. Wang, Significantly enhanced water flux in forward osmosis desalination with polymer-graphene composite hydrogels as a draw agent, *Rsc Advances*, 3 (2013) 887-894.
- [14] H. Wang, J. Wei, G.P. Simon, Response to Osmotic Pressure versus Swelling Pressure: Comment on “Bifunctional Polymer Hydrogel Layers As Forward Osmosis Draw Agents for Continuous Production of Fresh Water Using Solar Energy”, *Environmental science & technology*, 48 (2014) 4214-4215.
- [15] Y. Hartanto, S. Yun, B. Jin, S. Dai, Functionalized thermo-responsive microgels for high performance forward osmosis desalination, *Water research*, 70 (2015) 385-393.

- [16] Y. Cai, W. Shen, S.L. Loo, W.B. Krantz, R. Wang, A.G. Fane, X. Hu, Towards temperature driven forward osmosis desalination using Semi-IPN hydrogels as reversible draw agents, *Water research*, 47 (2013) 3773-3781.
- [17] D. Li, X. Zhang, J. Yao, Y. Zeng, G.P. Simon, H. Wang, Composite polymer hydrogels as draw agents in forward osmosis and solar dewatering, *Soft Matter*, 7 (2011) 10048-10056.
- [18] A. Razmjou, M.R. Barati, G.P. Simon, K. Suzuki, H. Wang, Fast deswelling of nanocomposite polymer hydrogels via magnetic field-induced heating for emerging FO desalination, *Environmental science & technology*, 47 (2013) 6297-6305.
- [19] F. Ganji, S. Vasheghani-Farahani, E. Vasheghani-Farahani, Theoretical description of hydrogel swelling: a review, *Iran Polym J*, 19 (2010) 375-398.
- [20] A. Razmjou, Q. Liu, G.P. Simon, H. Wang, Bifunctional polymer hydrogel layers as forward osmosis draw agents for continuous production of fresh water using solar energy, *Environmental science & technology*, 47 (2013) 13160-13166.
- [21] X.-Z. Zhang, Y.-Y. Yang, T.-S. Chung, K.-X. Ma, Preparation and characterization of fast response macroporous poly (N-isopropylacrylamide) hydrogels, *Langmuir*, 17 (2001) 6094-6099.
- [22] J. Chen, K. PARK, Superporous hydrogels: fast responsive hydrogel systems, *Journal of MACROMOLECULAR SCIENCE—PURE AND APPLIED CHEMISTRY*, 36 (1999) 917-930.
- [23] L.-W. Xia, R. Xie, X.-J. Ju, W. Wang, Q. Chen, L.-Y. Chu, Nano-structured smart hydrogels with rapid response and high elasticity, *Nature communications*, 4 (2013).
- [24] H. Cong, L. Li, S. Zheng, Poly (N-isopropylacrylamide)-block-poly (vinyl pyrrolidone) block copolymer networks: Synthesis and rapid thermoresponse of hydrogels, *Polymer*, 54 (2013) 1370-1380.
- [25] J. Song, R. Yu, L. Wang, S. Zheng, X. Li, Poly (N-vinylpyrrolidone)-grafted poly (N-isopropylacrylamide) copolymers: synthesis, characterization and rapid deswelling and reswelling behavior of hydrogels, *Polymer*, 52 (2011) 2340-2350.
- [26] H. Hayashi, K. Kono, T. Takagishi, Temperature-dependent associating property of liposomes modified with a thermosensitive polymer, *Bioconjugate chemistry*, 9 (1998) 382-389.
- [27] R. Yoshida, K. Uchida, Y. Kaneko, K. Sakai, A. Kikuchi, Y. Sakurai, T. Okano, Comb-type grafted hydrogels with rapid deswelling response to temperature changes, *Nature*, 374 (1995) 240-242.

- [28] J. Zhang, R. Xie, S.-B. Zhang, C.-J. Cheng, X.-J. Ju, L.-Y. Chu, Rapid pH/temperature-responsive cationic hydrogels with dual stimuli-sensitive grafted side chains, *Polymer*, 50 (2009) 2516-2525.
- [29] M.R. Badrossamay, H.A. McIlwee, J.A. Goss, K.K. Parker, Nanofiber assembly by rotary jet-spinning, *Nano letters*, 10 (2010) 2257-2261.
- [30] T.B. Mîndru, L. Ignat, I.B. Mîndru, M. Pinteala, Morphological aspects of polymer fiber mats obtained by air flow rotary-jet spinning, *Fibers and Polymers*, 14 (2013) 1526-1534.
- [31] J. Siepman, N. Peppas, Modeling of drug release from delivery systems based on hydroxypropyl methylcellulose (HPMC), *Advanced drug delivery reviews*, 64 (2012) 163-174.
- [32] G. Rathna, D.M. Rao, P. Chatterji, Water-induced plasticization of solution cross-linked hydrogel networks: energetics and mechanism, *Macromolecules*, 27 (1994) 7920-7922.
- [33] K.B. Keys, F.M. Andreopoulos, N.A. Peppas, Poly (ethylene glycol) star polymer hydrogels, *Macromolecules*, 31 (1998) 8149-8156.
- [34] D. Brown, Y.H. Bae, S.W. Kim, Hydrophilic solute release from a hydrophobic elastic matrix, *Macromolecules*, 27 (1994) 4952-4959.
- [35] A. Domján, C. Fodor, S. Kovács, T.s. Marek, B.l. Iván, K.r. Süvegh, Anomalous swelling behavior of poly (N-vinylimidazole)-l-poly (tetrahydrofuran) amphiphilic conetwork in water studied by solid-state NMR and positron annihilation lifetime spectroscopy, *Macromolecules*, 45 (2012) 7557-7565.
- [36] G. Gerlach, K.-F. Arndt, *Hydrogel sensors and actuators: engineering and technology*, Springer Science & Business Media, 2009.
- [37] W. van Dijk-Wolthuis, J. Hoogeboom, M. Van Steenberg, S. Tsang, W. Hennink, Degradation and release behavior of dextran-based hydrogels, *Macromolecules*, 30 (1997) 4639-4645.
- [38] M. Torres-Lugo, N.A. Peppas, Molecular design and in vitro studies of novel pH-sensitive hydrogels for the oral delivery of calcitonin, *Macromolecules*, 32 (1999) 6646-6651.
- [39] A. Bar, O. Ramon, Y. Cohen, S. Mizrahi, Shrinkage behaviour of hydrophobic hydrogel during dehydration, *Journal of food engineering*, 55 (2002) 193-199.
- [40] S. Khalloufi, P. Bongers, Mathematical investigation of the case hardening phenomenon explained by shrinkage and collapse mechanisms occurring during drying processes, *Comput.-Aided Chem. Eng*, 30 (2012) 1068-1072.

## Chapter 5 Improvement of the swelling properties of ionic hydrogels by the incorporation of hydrophobic, elastic microfibrils for forward osmosis applications

### Overview

In this chapter, the swelling property of hydrogels are improved by the introduction of structural inhomogeneity and compressive forces in an ionic hydrogel for the purpose of increasing forward osmosis water flux. This is achieved by incorporating a hydrophobic, elastic polyester (PET) hollow microfibre into an ionic hydrogel under a compressive force during the preparation of the composite hydrogel monolith, as shown in Figure 5.1, the swelling pressure was improved. The forward osmosis water flux of the composite hydrogels increased with increasing microfibre loading and compression pressures. The water flux of the composites was twice as high as that of the pure hydrogel. The composite hydrogels were also better at maintaining high water fluxes for a long period. The water flux of PSA-PET-0.5/0.5-18 decreased from 3.5 to 1.4 LMH after 24 h forward osmosis test. The combination of hydrophilic ionic hydrogel and hydrophobic PET microfibre resulted in an extended, porous structure within the hydrogel because of their different wettabilities, whilst an additional relaxation force was preserved in the composites because of the compression pressure applied during the preparation. Both of these worked together to enhance the FO water flux and maintain it for an extended long period.

This chapter has been published as a journal article: Ranwen Ou, Huacheng Zhang, George P. Simon, Huanting Wang, *Ind. Eng. Chem. Res.*, **2017**, 56 (2), pp 505–512

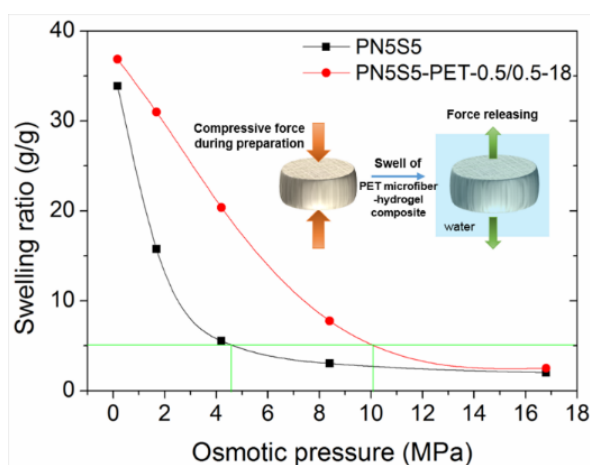


**Figure 5.1** Illustration of the swelling pressure improvement of PET-hydrogel composite.

## 5.1 Introduction

One of the most pervasive problems afflicting the world is water scarcity; by 2025, nearly two-thirds of the world's population are projected to face water shortage [1]. Tremendous efforts have been made to search for environmental and cost friendly solutions to this problem. Among many other technologies, forward osmosis (FO) desalination is gaining growing attention. Such a process shows great potential to lower the costs of production of fresh water from saline water because solar energy and other low-grade heat can be directly used [2, 3]. In the FO process, a semi-permeable membrane is used as the separation medium, and the osmotic pressure difference on two sides of membrane acts as the driving force. The draw agent possesses a higher osmotic pressure than the feed solution which determines the performance of the FO process apart from the FO membrane. A number of materials have been investigated as draw agents, including salts, polar solvents, saccharide solutions, hydrophilic nanoparticles, polyelectrolytes and hydrogels [4]. Of the materials studied to date, the stimuli responsive hydrogel draw agent which was originally reported by our group [2, 3, 5-10], shows great potential in the forward osmosis application because of the easy recovery of water and easy regeneration.

The swelling property of hydrogels and the effective contact between FO membrane and hydrogel are key parameters for achieving high water flux [3, 7, 9]. The degree of contact between the membrane and hydrogel can be enhanced by decreasing the hydrogel particle size [9], increasing the softness of hydrogel [3], or *in situ* preparation of hydrogel monolith on the FO membrane itself [7]. The swelling properties of hydrogels include the swelling kinetics and pressure. The swelling kinetics determine the swelling pattern of solvent diffusion and polymer chain relaxation, while the swelling pressure reveals the driving force of the hydrogel in the FO process. A simple and useful empirical equation is used to describe the swelling kinetics, the so called power law [11, 12]:

$$\frac{M_t}{M_\infty} = kt^n \quad (1)$$

where  $M_t$  and  $M_\infty$  are the amount of water absorbed at time  $t$  and equilibrium, respectively.  $k$  is the characteristic constant of the water-polymer system, and  $n$  is the characteristic exponent of the transport mode. The characteristic exponent  $n$  reveals whether the swelling process is a solvent diffusion controlled or polymer chain relaxation controlled process. The swelling pressure of polymer hydrogel originates from polymer-water mixing, elastic reaction force of

the network, and the osmotic pressure of ionizable groups. The swelling pressure ( $\Pi$ ) of an ionic gel can be expressed as the sum of three contributions from each component [12-14]:

$$\Pi = \Pi_{mix} + \Pi_{el} + \Pi_{ion} \quad (2)$$

where  $\Pi_{mix}$ ,  $\Pi_{el}$ , and  $\Pi_{ion}$  are the mixing, elastic, and ionic contributions, respectively.

The swelling behavior of the hydrogel is strongly dependent on the crosslinking density, and the interactions between the solvent molecules and the polymeric chain segments [12]. Note that the swelling property of hydrogel can be modified by changing the crosslinking density [15], introduction of ionic groups [8] and structural inhomogeneity [16-18]. Firstly, the crosslinking density plays a major role in determining the absorption properties of hydrogel. The water molecules cannot be held in a polymer network with a low crosslinking density, while a highly crosslinked polymer network does not allow the entrance of water. Secondly, the introduction of ionic groups is good for polymer-water mixing and the mixing of ions with solvent, and thus the configurational change of gel structure. Consequently, the solvent diffusion rate and the polymer chain relaxation rate are enhanced accordingly. Thirdly, introducing structural inhomogeneity such as hydrophilic tunnels or porosity accelerates the water diffusion in the hydrogel, which improves the polymer-water mixing, and thus enhances the solvent diffusion rate. In addition, a capillary force can be harnessed if microscale, connected pores can be generated in the hydrogel, and can act as an additional driving force to accelerate the solvent diffusion.

In this paper, the swelling properties of hydrogels are modified by the introduction of structural inhomogeneity and compressive forces in the hydrogel. The structural inhomogeneity is introduced by addition of a hydrophobic microfibre (made of polyester) into an ionic hydrogel. The combination of hydrophobic, elastic polyester (PET) microfibre and hydrophilic hydrogel generates a porous structure, which is expected to be favorable for water transport. In this study, N-isopropyl acrylamide (NIPAM) and sodium acrylate (SA) were selected for preparing the hydrophilic hydrogel, while NIPAM offers the hydrogel thermal responsive ability, and SA endows the hydrogel higher ionic strength. In the preparation process, the mixture of PET microfibre and monomer solution is compressed during polymerization, so that part of the compression force due to the deformed fibres can be stored in the composite. We hypothesize that the addition of PET microfibrils in hydrogel changes the swelling pattern from polymer chain relaxation controlled process to solvent diffusion controlled process, allowing it to attain a swelling equilibrium much more rapidly. In addition,

because of elasticity of PET microfibre, the compressive force is released during the hydrogel swelling, enhancing polymer chain relaxation. The actual effects of the addition of PET microfibrils and the introduction of compressive forces on the swelling pressure of the polymer hydrogel and the forward osmosis water flux are studied in detail.

## 5.2 Experimental

### 5.2.1 Materials

N-isopropyl acrylamide (NIPAM, 97 %), Sodium acrylate (SA, 97 %), N, N-methylenebis (acrylamide) (MBA, 99 %), ammonium persulfate (APS,  $\geq 98$  %), and N, N, N', N' - tetramethyl ethylenediamine (TEMED, 99 %) were purchased from Sigma-Aldrich Australia, and used without further treatment. The polyester (PET) microfibre was the filler of Biozone Polyester Pillow (High & Firm, Biozone). The PET microfibre was washed with ethanol (99.7 %, Merck) and pure water for 3 times, followed by drying in a 45 °C oven before use. The average diameter of the PET microfibre was about 34  $\mu\text{m}$ , which was determined by analyzing the SEM images using Nano Measurer 1.2. Pure water was used in all experiments.

### 5.2.2 Experimental Procedures

*Preparation of pure ionic hydrogel:* Monomer (NIPAM, SA), crosslinker (MBA), and initiator (APS) were dissolved in pure water to form a 16.67 wt. % monomer solution. The weight ratio of NIPAM, SA, MBA, and APS was fixed at 25:25:1:0.5. The ionic hydrogel contained 50 wt. % NIPAM and 50 wt. % SA (PN5S5). In order to get better contact between hydrogel and membrane, a monolithic sample was used in this study [7]. 3 g of monomer solution containing 0.5 g of monomer was transferred into a FO cell after deaeration via flowing  $\text{N}_2$  gas through the solution for 10 min, and a drop of TEMED was then added into the solution under mild shaking to accelerate the polymerization. The monolithic hydrogel was formed on the FO membrane (CTA membrane, Hydration Technologies Inc., Albany, OR) in a few minutes, followed by rinsing with pure water 3 times.

*Preparation of composite hydrogels:* 3 g of monomer solution after deaeration was added into a FO cell, and a drop of TEMED was added as above. Then, a given amount of PET microfibre was added to the solution, followed by pressing the fibre and solution with weight, as shown in Figure 5.2. The amount of the PET microfibre and the compression pressure applied in the

polymerization process are shown in Table 5.1. A polydopamine-coated PET (D-PET) microfibre was also prepared [19]. The hydrogel-D-PET composite was compared with hydrophobic microfibre – hydrogel composite in terms of their microstructure and FO performance. The hydrogel-D-PET composite was prepared using the same procedure described above.

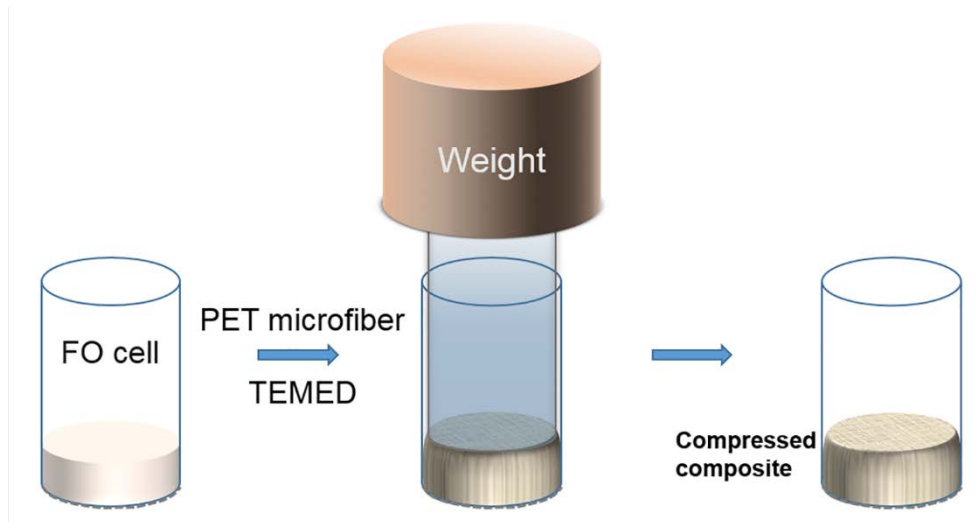


**Figure 5.2** The preparation process of hydrogel-PET microfibre composite.

**Table 5.1** Composition of pure hydrogel and composite hydrogels.

Hydrogel	NIPAM+SA /g	PET microfibre /g	Compression pressure /kPa
PN5S5	0.5	0	0
PN5S5-PET-0.5/0.15	0.5	0.15	18
PN5S5-PET-0.5/0.5	0.5	0.5	0, 8, 18
PN5S5-PET-0.5/1.0	0.5	1.0	18

*Characterization:* The morphology of the pure hydrogel and hydrogel- PET composites was probed using a scanning electron microscope (Nova NanoSEM 450 FESEM, FEI, USA). The wettability of PET microfibre and hydrogels was determined by a contact angle goniometer (Dataphysics OCA15, Dataphysics, Germany). An industrial incandescent lamp (IR 250C, 230 V, 250 W, Philips) was used as light / heat source for dewatering the swollen hydrogel draw agent, and a radiometer (FZ-A) was applied to determine the light intensity. A true-rms digital multimeter (38 XR-A, Amprobe, USA) measured the temperature change of hydrogel during the dewatering.

A gravimetric method was utilized to investigate the swelling behaviors of hydrogels with different PET microfibre loading and compression pressure. A dry monolith hydrogel was put

into 2 L of pure water. The weight of swollen hydrogels was weighed until it reaches an equilibrium. The swelling ratio ( $Q$ ) of hydrogels as a function of time was calculated as follows:

$$Q(t) = \frac{w_t - w_d}{w_d} \quad (3)$$

where  $w_t$  (g) is the weight of swollen hydrogel at time  $t$  and  $w_d$  (g) is the weight of dry hydrogel before the test.

The forward osmosis water flux was determined in a home-made FO cell (Figure 5.2). In the FO mode, the active surface of the FO membrane faced the feed solution, while the hydrogel monolith was prepared on the bottom surface. The monolith contained 0.5 g of hydrogel with different amounts of water, while the composites had different amounts of PET microfibre. The initial swelling ratio of the hydrogel was calculated based on the 0.5 g hydrogel in each monolith. 2000 ppm NaCl solution was used as the feed solution for all measurements. FO water flux,  $F$  ( $L \cdot m^{-2} \cdot h^{-1}$ , or LMH) were determined by the weight change of FO cell with hydrogel over a period of time, as follows:

$$F = \frac{V}{A \times t} \quad (4)$$

where  $V$  (L) is the volume change of hydrogel over a period of time  $t$  (h). The effective area  $A$  ( $m^2$ ) of the FO membrane is  $4.91 \text{ cm}^2$ .

The swelling pressure was estimated according to the method described elsewhere [3]. The hydrogel (swelling ratio = 5) was placed on the active side of a FO membrane in the FO cell, and NaCl solution (2, 20, 50, 100, and 200 g/L) was put on the other side of the membrane. The hydrogel was allowed to absorb water for 24 h at room temperature to reach equilibrium. The initial swelling ratio of the hydrogel is 5 because it is relatively soft and shows good contact with the FO membrane. The final swelling ratio of the hydrogel under a specific NaCl concentration is irrelevant to the initial swelling ratio, the hydrogel may absorb or desorb water after the measurement.

In the dewatering process, the swollen hydrogel monolith was put under an incandescent lamp with a light intensity of  $1 \text{ kW} \cdot m^{-2}$ , the weight loss of the hydrogel as a function of time was recorded. The average dewatering flux was calculated according to Equation (4). In order to recover the liquid water released during the solar dewatering, a setup in Figure 5.3 was used. The swollen hydrogel was put on a microfiltration membrane (Sterlitech, 100 nm pore size) above the funnel. The microfiltration membrane was used to separate the hydrogel from water recovered. When liquid water was observed on the membrane during the dewatering process,

it was collected by turning on a vacuum pump (140 mL piston syringe pump, Monoject™) for a few seconds. The liquid water recovery ( $R_l$ , %) was calculated as follows:

$$R_l = \frac{w_l}{w} \times 100 \quad (5)$$

where  $w_l$  (g) is the weight of liquid water recovered, and  $w$  (g) is the total water recovered, including vapor and liquid.

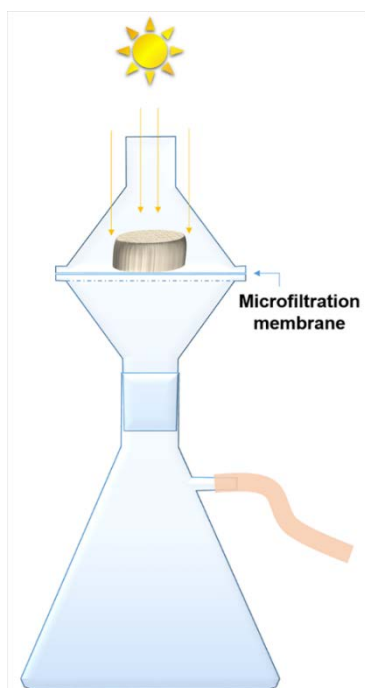


**Figure 5.3** The solar dewatering setup for measuring the liquid water recovery. A microfiltration membrane (Sterlitech, 100 nm pore size) is applied to block the hydrogel from water recovered. Vacuum is applied few times when liquid water can be found on membrane during the dewatering process. A 140 mL piston syringe (Monoject™) is used to produce a vacuum inside the filtering flask in order to drive the liquid water into this receptacle.

## 5.3 Results and Discussion

### 5.3.1 Morphology of PET-hydrogel composites

The SEM image of PN5S5 hydrogel (Figure 5.4a) shows that the dry monolith hydrogel has a dense and continuous polymer network structure. Figure 5.4b demonstrates that the PET microfibre is hollow. The surface and cross-sectional morphology of composite hydrogels are shown in Figure 5.5. The addition of PET microfibrils into NIPAM-SA hydrogel endows the composite with pores, the composite roughly become more porous with increasing amount of

PET microfibre, as observed in Figure 5.5d-f. The formation of the porous structure can be explained by the distinct wettability of ionic hydrogel and PET microfibrils. The hydrophobic PET microfibrils are partially wetted by the monomer solution initially, and then the pores result produced after the polymerization.

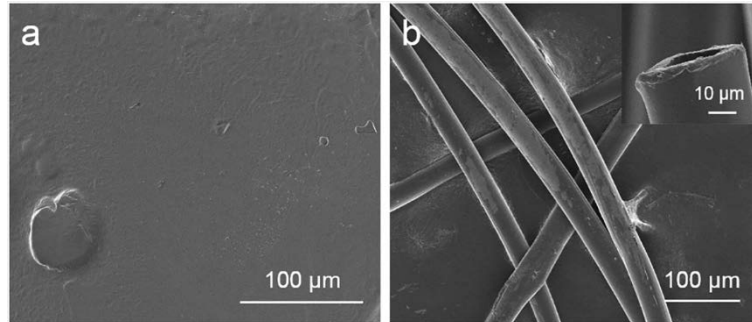


**Figure 5.4** SEM images of (a) PN5S5 hydrogel and (b) PET microfibrils. The inset in (b) shows the hollow structure of PET fibres.

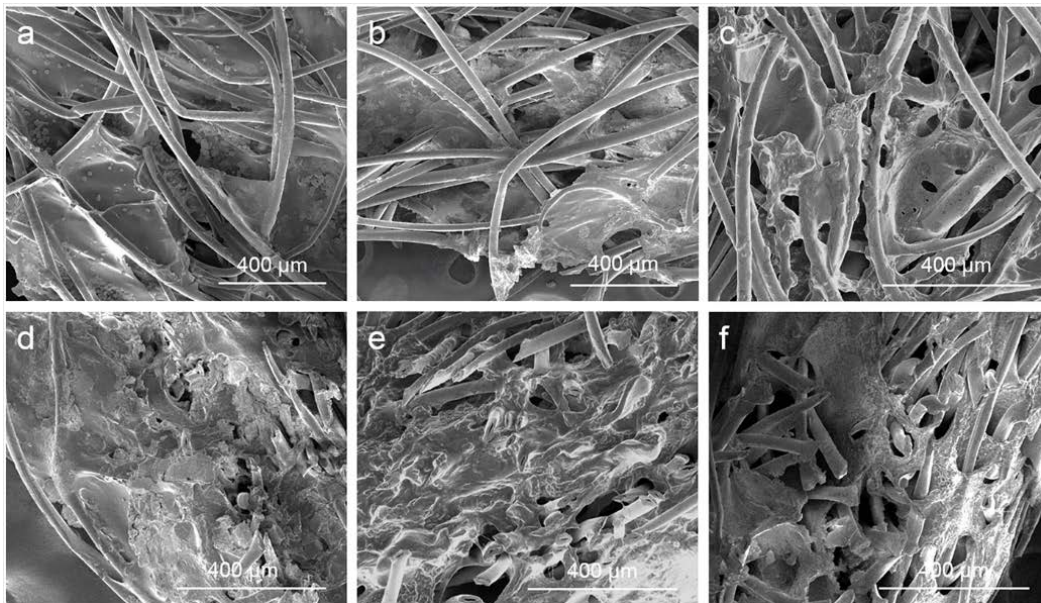


**Figure 5.5** (a-c) Surface and (d-f) cross-sectional SEM images of composite hydrogels. (a, d) PN5S5-PET-0.5/0.15, (b, e) PN5S5-PET-0.5/0.5, (c, f) PN5S5-PET-0.5/1.0. The compressive pressure applied is 18 kPa.

### 5.3.2 Swelling behaviour of hydrogels

The effect of the PET microfibre loading and compression pressure on the swelling properties of hydrogel was studied. In general, a swelling process involves the diffusion of a solvent into a polymer, with the polymer chains changing their conformation to form a rubbery (swollen) polymer material. The equilibrium swelling ratio of PN5S5 and PN5S5-PET-0.5/0.5-18 are 64 and 37 g/g, respectively. The equilibrium swelling ratio of PN5S5-PET-0.5/0.5-18 is about half of PN5S5, because it contains 50 wt. % of PET microfibre which cannot swell in water. As shown in Figure 5.6a, the sigmodal swelling curves implied three distinct stages of swelling: the movement of swelling front until meeting at the rigid core, the acceleration of swelling kinetics, and reaching of equilibrium swelling [9, 20]. In the first stage, when a hydrogel in its initial state is in contact with solvent, the latter attacks the hydrogel surface and penetrates into the polymeric network. Thus, the unsolvated glassy phase is separated from the rubbery hydrogel region with a moving boundary. The unsolvated glassy core in the middle of the hydrogel is the “rigid core”. The initial parts of the sigmodal curves of PN5S5 and its composite were distinctly different, owing to the difference of microstructure. Pure PN5S5 hydrogel was dense and continuous, while the hydrogel-PET composite showed porous structure. The porous structure caused a rapid water uptake, causing the composites to reach a much higher swelling ratio compared to PN5S5, in first 0.5 h. At 0.5 h, PN5S5-PET-0.5/0.5-18 showed higher swelling ratio than PN5S5-PET-0.5/1.0-18, possibly due to the fact that the higher concentrations of hydrophobic PET microfibres may hinder water transport. On the other hand, water was able to reach the core of PN5S5 hydrogel by diffusion in the polymer network and through the pores. The hydrophobic microfibre and pores led to the formation of a disconnected polymer hydrogel network, and decreased hydrogel size. Thus, the advancing swollen front in the composite hydrogel reached the rigid core much more rapidly than the large pure hydrogel monolith, being in the second stage of swelling; the network relaxation rate becoming greater than the rate of solvent diffusion. The acceleration of swelling kinetics of composite hydrogel occurred earlier at 1<sup>st</sup> h, while that of PN5S5 hydrogel alone occurred after 2.5 h of swelling. PN5S5, PN5S5-PET-0.5/0.5-18, and PN5S5-PET-0.5/1.0-18 took 24, 6.5, and 11 h to reach equilibrium, respectively.

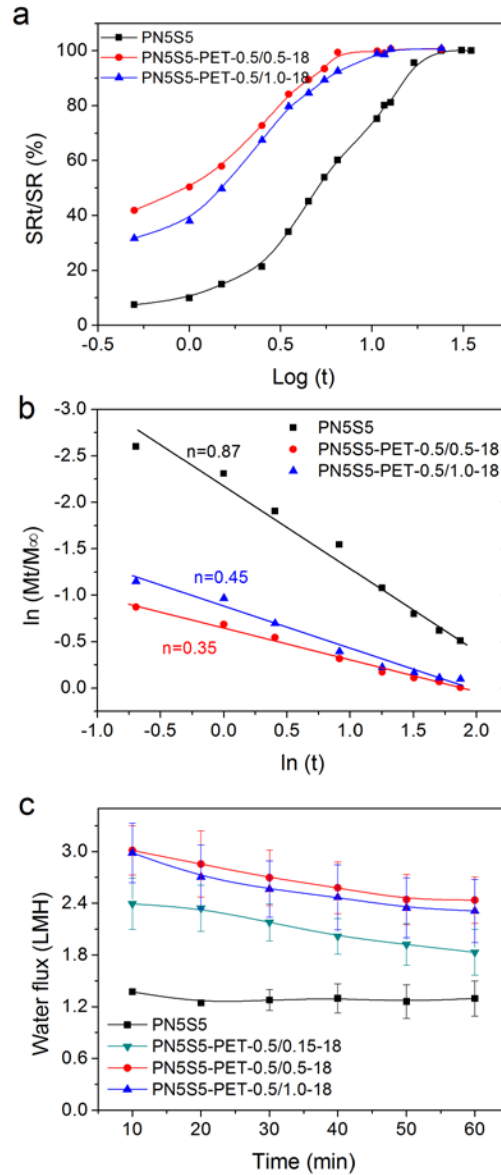
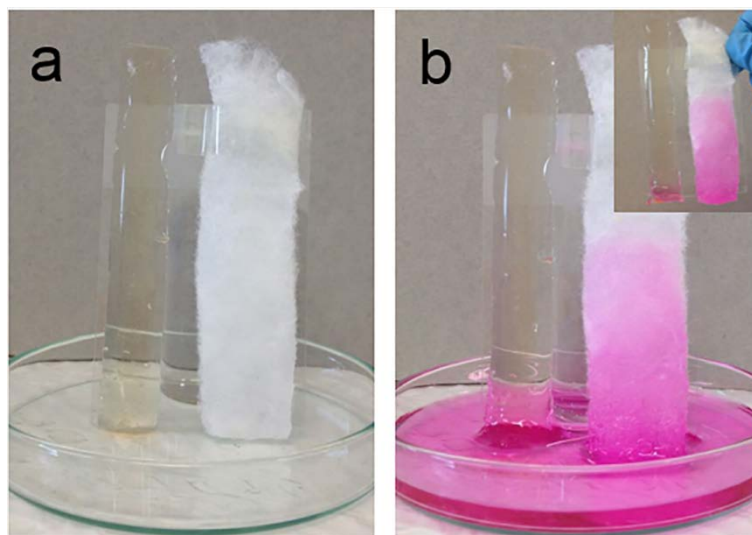


**Figure 5.6** (a) Swelling ratio and (b) swelling kinetics of hydrogels with different loadings of PET microfibres, and (c) forward osmosis water flux induced by the hydrogel and its composites. The unit of  $t$  on the x-axis of (a) and (b) is hour. The initial swelling ratio of hydrogels was 4 for the FO water flux test. The composites used in this measurement were prepared under 18 kPa pressure.

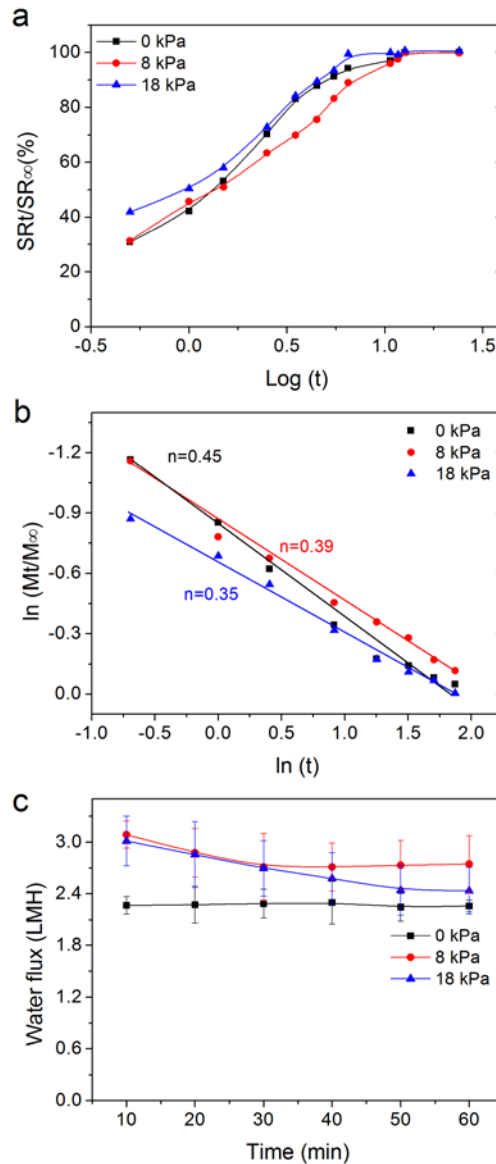
The relation between solvent diffusion rate and polymer chain relaxation rate distinguishes the swelling pattern of the hydrogel. The simplest equation describing the swelling of a polymer is the power law (Equation (1)), where  $n$  is the characteristic exponent of the transport mode. For a slab sample,  $n=0.5$  indicates Fickian diffusion,  $n=1.0$  indicates Case II transport, while  $0.5 < n < 1.0$  implies anomalous transport [9, 11]. Fickian diffusion is a solvent diffusion-controlled process, whilst Case II transport is a polymer chain relaxation controlled process.

However, when the water penetration rate is much smaller than the polymer chain relaxation rate, it is possible to achieve  $n$  values less than 0.5, which is still regarded as Fickian diffusion, but known as “Less Fickian” behavior [21]. As shown in Figure 5.6b,  $n=0.87$  means that the swelling of PN5S5 in water is mainly controlled by the polymer chain relaxation. After blending with PET microfibre, the values of  $n$  for PN5S5-PET-0.5/0.5-18 and PN5S5-PET-0.5/1.0-18 decrease to 0.45 and 0.35, respectively. These  $n$  values are lower than 0.5, which means that the swelling of composite hydrogels exhibit Less Fickian diffusion, and that the polymer chain relaxation rate is much faster than the solvent diffusion rate. This is caused by the porous structure of composite and the decreased hydrogel size, and thus the acceleration of swelling kinetics. Figure 5.6c shows the forward osmosis water flux of hydrogels, the composite hydrogel showed higher water flux than the pure one, while PN5S5-PET-0.5/0.5-18 performed best, which was about twice as high as that of PN5S5. The FO water flux of hydrogels is well consistent with the swelling kinetics.

As shown in Figure 5.7, the strips of PN5S5 and PN5S5-PET-0.5/0.5 were put vertically on rhodamine B aqueous solution to observe the swelling process. After 2 min, the height of RhB solution in the composite was 6.5 times as high as that of PN5S5. This confirms that the porous structure generated by addition of PET microfibre provides an extra driving force for the water absorption.



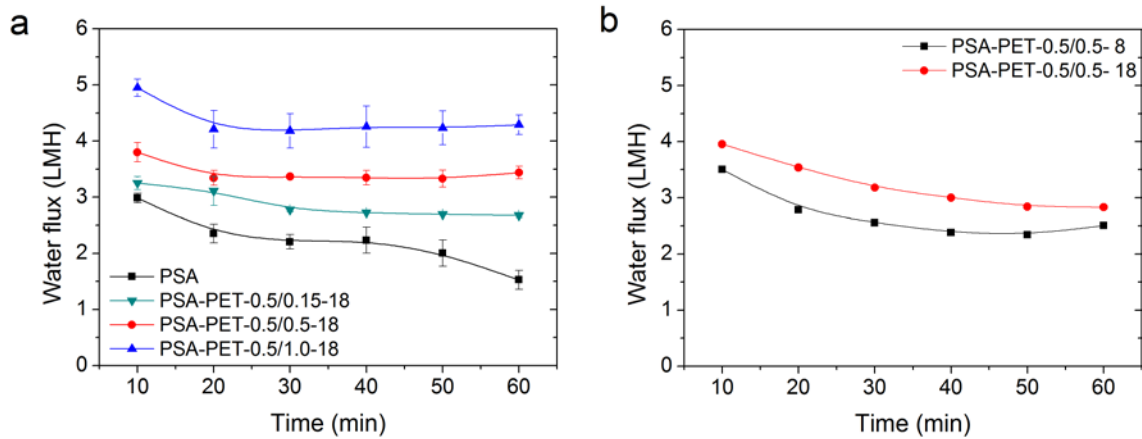
**Figure 5.7** The optical images of pure PN5S5 hydrogel and PN5S5-PET-0.5/0.5 composite hydrogel (a) before and (b) after swelling in aqueous rhodamine B (RhB) solution. The image (b) was taken after 2 mins of absorption.



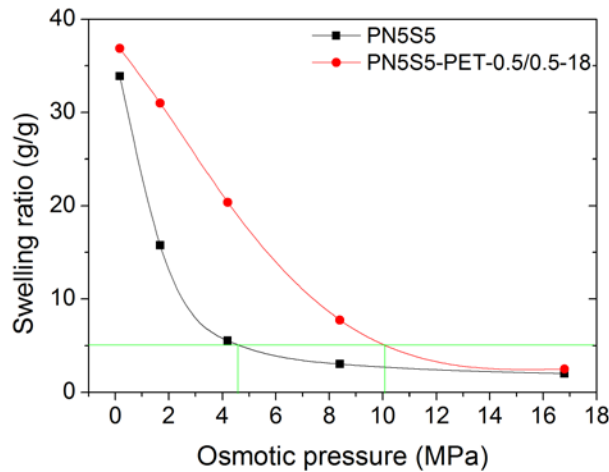
**Figure 5.8** (a) Swelling ratio and (b) swelling kinetics of PN5S5-PET-0.5/0.5 hydrogels prepared with different compression pressure, and (c) forward osmosis water flux induced by the hydrogel draw agent. The unit of  $t$  on the x-axis of (a) and (b) is hour. The initial swelling ratio of hydrogels was 4 for the FO water flux test.

Figure 5.8 shows the effect of compression pressure on the swelling kinetics and FO water flux. In this study, 0, 8, and 18 kPa were applied during the preparation of PN5S5-PET-0.5/0.5. The values of  $n$  in the composites prepared at 0, 8, and 18 kPa were 0.45, 0.39, and 0.35, respectively, which decreases with greater compression pressure applied. The composites prepared under different compression pressure all exhibit Less Fickian diffusion. With greater compression pressure, the composites become more compact and denser, thus the relaxation force generated by the compressed microfibre is higher, which drives the composite swelling faster. The FO water flux generated by the composites prepared at 8 and 18 kPa is higher than

that of with no pressure applied, which is consistent with the swelling kinetics. PSA hydrogel and the PSA-PET composite were also prepared and tested as draw agents; the FO water flux of PSA composite decreased with decreasing PET microfibre loading, and increased with increasing compression pressure. This result is similar to the PN5S5 one, as shown in Figure 5.9. The highest water flux of PSA-PET-0.5/1.0-18 reached 5.0 LMH in the first 10 min, decreasing slowly to 4.3 LMH after 1 h of testing.



**Figure 5.9** The 60 mins forward osmosis water flux of PSA composite with (a) different PET fibres loading, and (b) different compressed pressure loading.



**Figure 5.10** Plot of swelling ratio of PN5S5 and PN5S5-PET-0.5/0.5-18 as a function of osmotic pressure of NaCl solution at equilibrium.

Figure 5.10 shows the swelling ratio of pure hydrogel PN5S5 and the composite hydrogel PN5S5-PET-0.5/0.5-18 at different osmotic pressures. When the swelling ratio is 5, the addition of 50 wt. % PET microfibre and the 18 kPa compression pressure increased the osmotic pressure from 4.6 MPa (PN5S5) to 10.1 MPa. The swelling ratio of the composite hydrogel is always higher than the pure hydrogel under different osmotic pressures. The

increase might be due to three effects: (1) part of the compression pressure existing in the composite hydrogel acted as a driving force; (2) the microscale, porous structure endowed the composite with capillary forces, which also becomes part of the swelling pressure. (3) The difficulty of dewatering composite hydrogel. During the measurement, the hydrogel may absorb water from the NaCl solution or dewater, unsuccessful dewatering may result in higher water content in the hydrogels. The decreasing trend of swelling ratio – osmotic pressure curve of PN5S5-PET is different from that of PN5S5, with the former decreasing slower and showing relatively high swelling ratio in NaCl solution with a higher osmotic pressure. This indicated that the compression pressure and capillary forces that existed in the composite hydrogel were gradually reduced with the swelling of hydrogel, which helped sustain the high water flux for a longer period of time.

### 5.3.3 Forward osmosis and dewatering performance

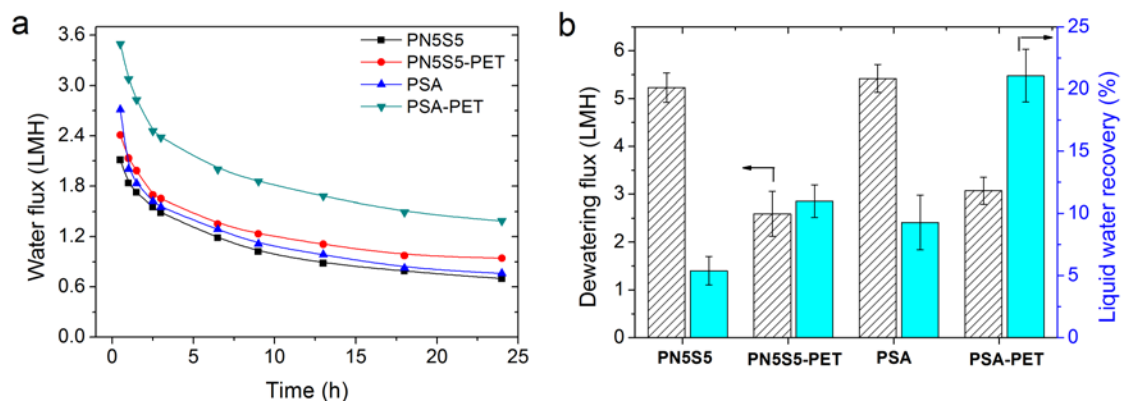


**Figure 5.11** (a) 24 hours FO water flux, and (b) dewatering performance of hydrogels. PN5S5-PET-0.5/0.5-18 and PSA-PET-0.5/0.5-18 were used in this test. The initial swelling ratio of the hydrogels is 2 based on the amount of hydrogel.

The 24 h water flux of PN5S5, PSA, and their PET microfibre composite was also measured. As shown in Figure 5.11a, generally, the composite hydrogel showed a higher water flux than the pure hydrogels, whilst PSA-PET-0.5/0.5-18 performed better than PN5S5-PET-0.5/0.5-18. The water flux of PN5S5-PET-0.5/0.5-18 was 2.4 LMH for the initial 0.5 h, and then decreased to 0.94 LMH after 24 h. In contrast, the water flux of PN5S5 was 2.1 and 0.70 LMH at 0.5 and 24 h, respectively. The water flux of PSA-PET-0.5/0.5-18 decreased from 3.5 to 1.4 LMH in 24 h measurement, which demonstrated that this hydrogel – hydrophobic microfibre composite was able to maintain a relatively high flux over a long period. Figure 5.11b shows the dewatering performance of hydrogels. The composite hydrogels exhibited lower average dewatering fluxes than hydrogel alone. The dewatering flux of PN5S5-PET-0.5/0.5-18 and

PSA-PET-0.5/0.5-18 were about half of that of PN5S5 and PSA, respectively. In addition, the low thermal conductivity of PET ( $0.2 \text{ W m}^{-1} \text{ K}^{-1}$ ) likely reduced the rate of heat transfer. Figure 5.12 demonstrated that the temperature of PN5S5-PET-0.5/0.5-18 and PSA-PET-0.5/0.5-18 increased more slowly than the relevant pure hydrogel. However, the liquid water recovery from composite hydrogels is twice as much as those of the corresponding pure hydrogel. That may be caused by the lower temperature of hydrogel during dewatering, which decreased the evaporation rate of recovered liquid water. What's more, the PET composite hydrogel showed good cycle performance as a draw agent in the FO process, as shown in Figure 5.13. For the 3 cycles, the water flux decreased from 2.1 – 2.2 to 1.4 – 1.5 LMH in 3 hours.

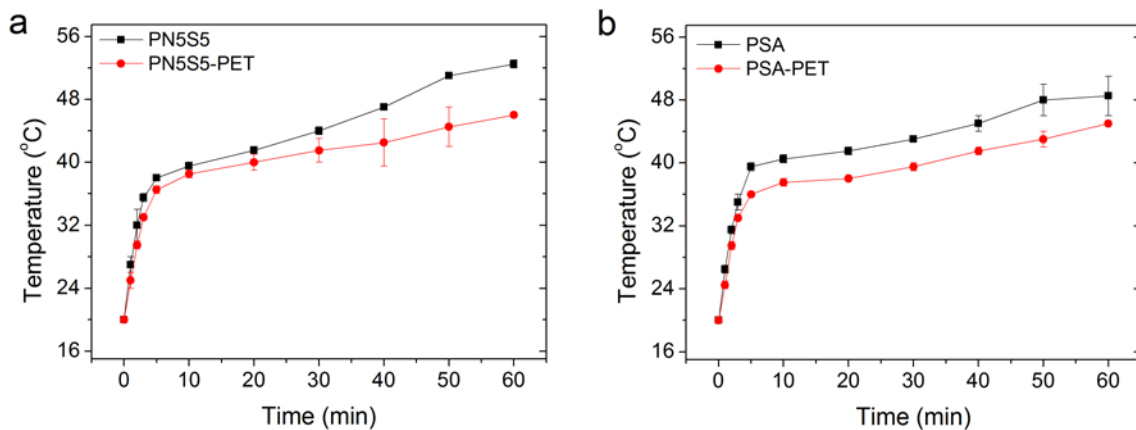


**Figure 5.12** The temperature change of pure hydrogel and composite hydrogel during 60 mins solar dewatering under  $1 \text{ kW/m}^2$  incandescent lamp: (a) PN5S5 and PN5S5-PET, (b) PSA and PSA-PET. PN5S5-PET-0.5/0.5-18 and PSA-PET-0.5/0.5-18 were used in this test.

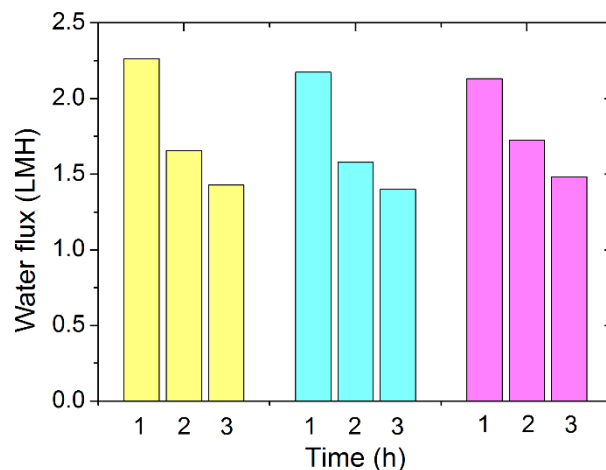


**Figure 5.13** The cycle performance of PN5S5-PET-0.5/0.5-18 composite. Three hours water flux was measured in each cycle. 2000 ppm NaCl solution was used as feed.

## 5.3.4 Effect of hydrophilic or hydrophobic fibres on FO performance of hydrogels

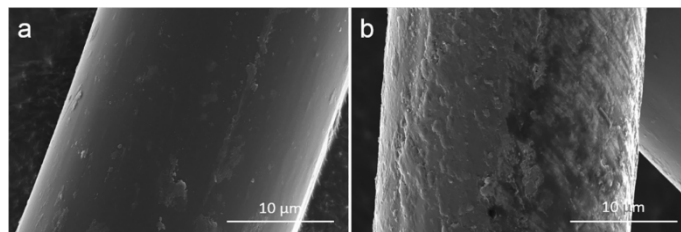


**Figure 5.14** SEM images of (a) PET microfibre and (b) polydopamine coated PET microfibre.

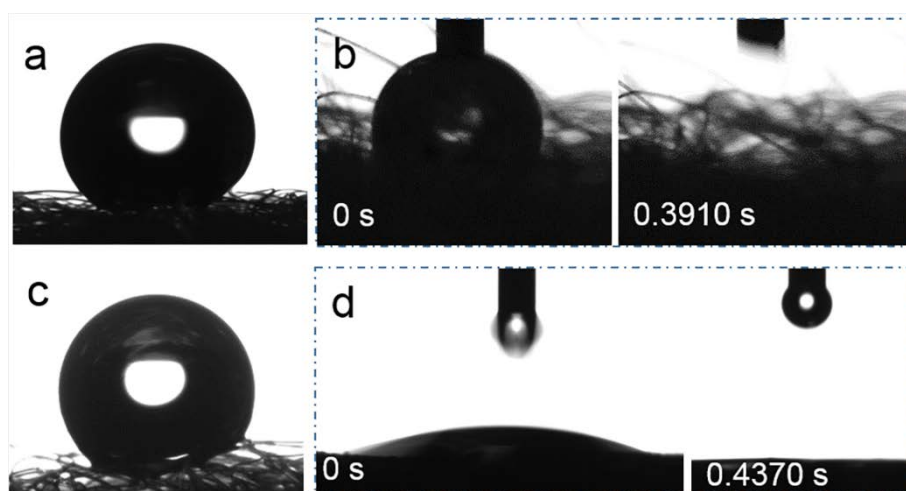


**Figure 5.15** Wettability of PET microfibre, polydopamine coated PET microfibre and their composite hydrogels. Water contact angle of (a) PET microfibre and (b) PN5S5-PET-0.5/0.5-18, (c) D-PET microfibre and (d) PN5S5-D-PET-0.5/0.5-18.

In the previous study, the addition of a hydrophilic thermoplastic polyurethane (TPU) microfibre introduced channels around the fibres into composite hydrogels, which facilitated water transport [7]. In this study, to further investigate how the surface wettability of the microfibre affects the properties and performance of composite hydrogel, PET microfibrils were coated with polydopamine to modify their surface properties. Polydopamine is selected because it can be easily deposited on virtually all types of inorganic and organic substrates, and can form a hydrophilic coating firmly adhering to the bulk materials under mild polymerization conditions. The resulting polydopamine-coated PET microfibrils are denoted as D-PET. Hydrogel composites incorporated with the same amounts of D-PET were prepared and compared with those hydrogel composites prepared with unmodified PET microfibrils. Figure 5.14 shows the SEM images of surface of PET and D-PET microfibrils. The fibre surface became rougher after being coated with polydopamine, while the contact angle decreases from  $151.2^\circ$  to  $127.5^\circ$ , as shown in Figure 5.15a&c. Even though the D-PET microfibre is still

hydrophobic, NIPAM solution can spread into the microfibrils in 3 s (Figure 5.16b), while the contact angle of PET microfibrils containing NIPAM solution is  $132.3^\circ$ . After incorporating these microfibrils into composite hydrogels, the water droplets are instantly absorbed by PN5S5-PET; however in the case of PN5S5-D-PET, they initially spread on the surface, and are subsequently absorbed by the composite, as shown in Figure 5.15 and Figure 5.17. For the PN5S5-PET composite, the hydrophobic PET microfibre penetrates throughout the hydrogel monolith, leading to a porous structure. The D-PET microfibre was more compatible with the hydrogel, and the resulting D-PET/polymer hydrogel monolith showed a similar microstructure observed in the TPU-hydrogel monolith in previous study [7]. It was reported that a hydrogel with many micron to millimetre scale pores could absorb a considerable amount of water in a very short period to fill the whole space [22].

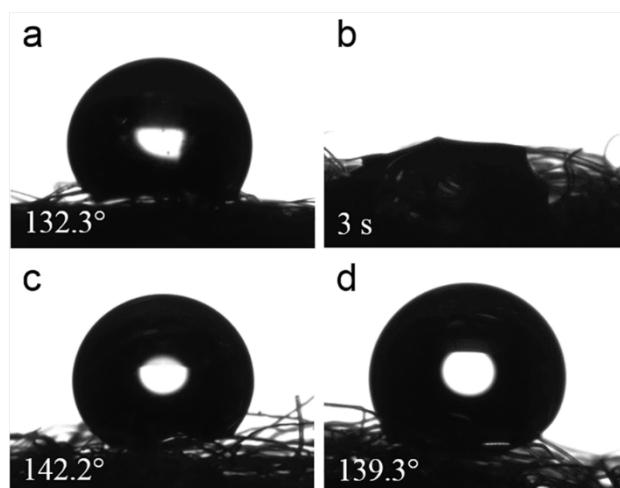


**Figure 5.16** Contact angle of PET (a, c) and D-PET (b, d) microfibrils with NIPAM solution (a, b) and SA solution (c, d) as testing medium.

The forward osmosis and dewatering performance of PN5S5-PET-0.5/0.5-18 and PN5S5-D-PET-0.5/0.5-18 were studied, and the result is shown in Figure 5.18. When the swelling ratio of composite was 4, the water flux of PN5S5-PET-0.5/0.5-18 decreased from 3.0 to 2.4 LMH in 60 mins of testing, while that of PN5S5-D-PET-0.5/0.5-18 decreased from 3.5 to 2.0 LMH. When the swelling ratio of composites decreased to 0, the water flux result showed a similar trend. This demonstrated that the compact structure (PN5S5-D-PET) is good for higher initial water flux; whereas the porous structure (PN5S5-PET) is beneficial to maintaining a higher flux level for a longer period. This can be observed in the swelling ratio – osmotic pressure curves in Figure 5.10.

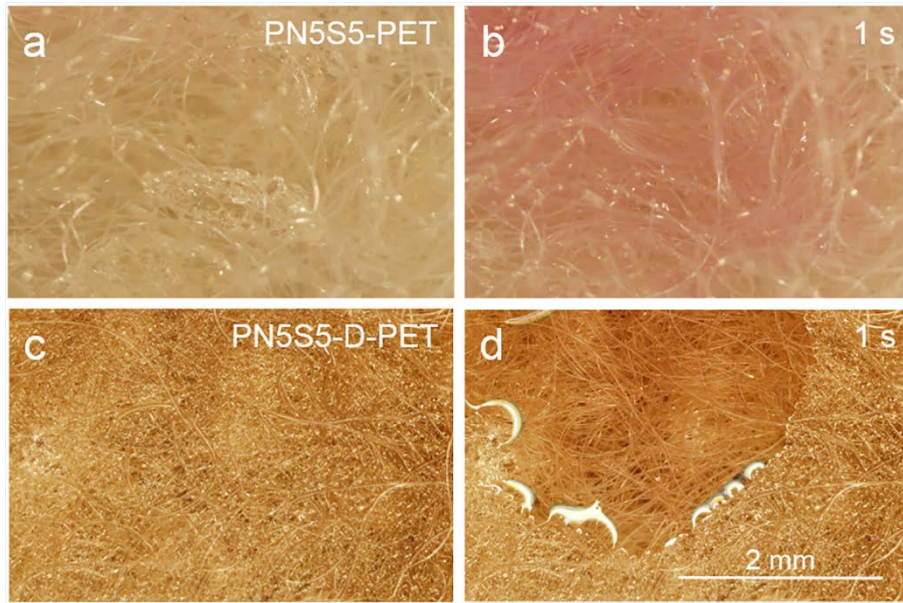


**Figure 5.17** Optical images of (a, b) PN5S5-PET and (c, d) PN5S5-D-PET hydrogel before and after dropping a drop of 100 ppm RhB solution.

With regards the dewatering performance, the average dewatering flux of PN5S5-D-PET-0.5/0.5-18 was twice as high as that of PN5S5-PET-0.5/0.5-18, and the liquid water recovery of PN5S5-D-PET-0.5/0.5-18 was 3 times greater compared with PN5S5-PET-0.5/0.5-18. An explanation for this is that the channels around polydopamine-modified microfibrils more favorably transported water out of the monolith during the dewatering, which increased the dewatering flux and the liquid water recovery [7].

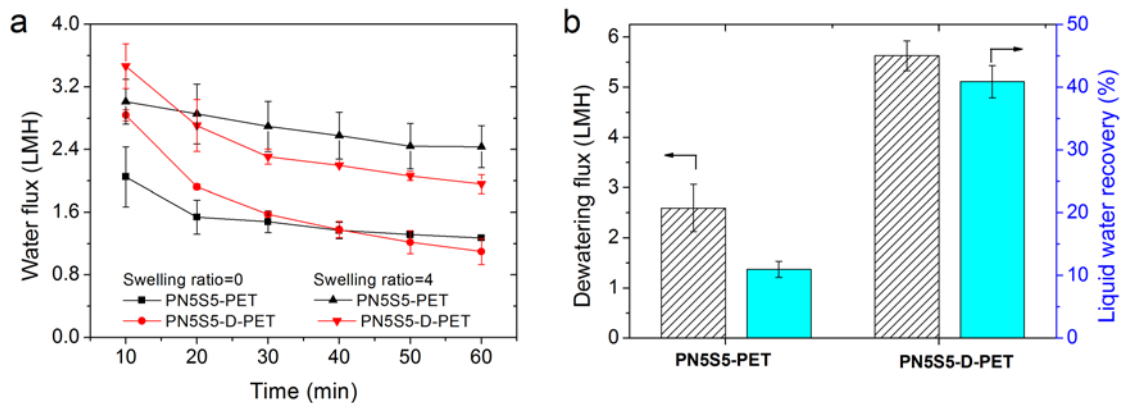


**Figure 5.18** (a) Forward osmosis water flux and (b) dewatering performance of PN5S5-PET-0.5/0.5-18 and PN5S5-D-PET-0.5/0.5-18.

## 5.4 Summary

The swelling properties of an ionic hydrogel-polyester microfibre composite prepared whilst compressing the fibre web during synthesis has been studied in an effort to provide an additional mechanism to improve the properties of hydrogels as a forward osmosis draw agent. The combination of a hydrophilic ionic hydrogel and a hydrophobic PET microfibre mesh imparted to the composite hydrogel porosity, due to the different wettabilities, whilst at the same time providing an additional relaxation force during swelling because of the compression pressure applied to the web during the preparation. The characteristic exponent  $n$  of the composites decreased with increasing PET microfibre loading and increasing amount of compression. The hydrogel-PET composites exhibited Less Fickian diffusion, indicating that the polymer chain relaxation rate is much faster than the solvent diffusion rate. On the other hand, the porous structure and the PET microfibre decreased the sizes of hydrogel domains, increasing solvent diffusion; the swelling equilibrium of PN5S5-PET-0.5/0.5-18 and PN5S5-PET-0.5/1.0-18 being reached after 6.5, and 11 h, which is much faster than that of PN5S5 (24 hours). Further, when the equilibrium swelling ratio is 5, the osmotic pressure of PN5S5-PET-0.5/0.5-18 was increased significantly from 4.6 MPa (PN5S5) to 10.1 MPa. With regards the forward osmosis application, the water flux of hydrogels is consistent with the swelling kinetics result, i.e., it increased with increasing PET microfibre loading and increasing compression pressure. The highest water flux of PN5S5-PET-0.5/0.5-18 was reached 3.0 LMH in the first 10 min, while that of PSA-PET-0.5/0.5-18 was 5.0 LMH. Compared to the composite prepared with a polydopamine-modified microfibre (PN5S5-D-PET), PN5S5-PET was better at maintaining higher water flux in a long period test. The water flux of PSA-PET-0.5/0.5-18 decreased from 3.5 to 1.4 LMH in a 24 h measurement.

The dewatering flux of PN5S5-PET-0.5/0.5-18 was not as rapid as PN5S5, because of the low thermal conductivity of PET ( $0.2 \text{ W m}^{-1} \text{ K}^{-1}$ ) (since the hydrogel is made hydrophobic by application of heat, and thus the rate of its transmission is important). However, the liquid water recovery of composite was twice that of the pure hydrogel. This work demonstrates that the performance of forward osmosis hydrogel draw agent is closely related to the swelling properties of hydrogel, and the draw agent performance can be effectively improved by tailoring its swelling properties.

## 5.5 References

- [1] M. Elimelech, W.A. Phillip, The future of seawater desalination: energy, technology, and the environment, *science*, 333 (2011) 712-717.
- [2] A. Razmjou, M.R. Barati, G.P. Simon, K. Suzuki, H. Wang, Fast deswelling of nanocomposite polymer hydrogels via magnetic field-induced heating for emerging FO desalination, *Environmental science & technology*, 47 (2013) 6297-6305.
- [3] Y. Zeng, L. Qiu, K. Wang, J. Yao, D. Li, G.P. Simon, R. Wang, H. Wang, Significantly enhanced water flux in forward osmosis desalination with polymer-graphene composite hydrogels as a draw agent, *Rsc Advances*, 3 (2013) 887-894.
- [4] R. Ou, Y. Wang, H. Wang, T. Xu, Thermo-sensitive polyelectrolytes as draw solutions in forward osmosis process, *Desalination*, 318 (2013) 48-55.
- [5] D. Li, X. Zhang, J. Yao, G.P. Simon, H. Wang, Stimuli-responsive polymer hydrogels as a new class of draw agent for forward osmosis desalination, *Chemical Communications*, 47 (2011) 1710-1712.
- [6] D. Li, X. Zhang, J. Yao, Y. Zeng, G.P. Simon, H. Wang, Composite polymer hydrogels as draw agents in forward osmosis and solar dewatering, *Soft Matter*, 7 (2011) 10048-10056.
- [7] R. Ou, H. Zhang, G.P. Simon, H. Wang, Microfiber-polymer hydrogel monolith as forward osmosis draw agent, *Journal of Membrane Science*, 510 (2016) 426-436.
- [8] A. Razmjou, Q. Liu, G.P. Simon, H. Wang, Bifunctional polymer hydrogel layers as forward osmosis draw agents for continuous production of fresh water using solar energy, *Environmental science & technology*, 47 (2013) 13160-13166.
- [9] A. Razmjou, G.P. Simon, H. Wang, Effect of particle size on the performance of forward osmosis desalination by stimuli-responsive polymer hydrogels as a draw agent, *Chemical engineering journal*, 215 (2013) 913-920.
- [10] J. Wei, Z.-X. Low, R. Ou, G.P. Simon, H. Wang, Hydrogel-polyurethane interpenetrating network material as an advanced draw agent for forward osmosis process, *Water Research*, 96 (2016) 292-298.
- [11] F. Ganji, S. Vasheghani-Farahani, E. Vasheghani-Farahani, Theoretical description of hydrogel swelling: a review, *Iran Polym J*, 19 (2010) 375-398.
- [12] M. Grassi, G. Grassi, Mathematical modelling and controlled drug delivery: matrix systems, *Current drug delivery*, 2 (2005) 97-116.
- [13] E. Vasheghani-Farahani, J.H. Vera, D.G. Cooper, M.E. Weber, Swelling of ionic gels in electrolyte solutions, *Industrial & engineering chemistry research*, 29 (1990) 554-560.

- [14] H. Wang, J. Wei, G.P. Simon, Response to osmotic pressure versus swelling pressure: comment on “bifunctional polymer hydrogel layers as forward osmosis draw agents for continuous production of fresh water using solar energy”, *Environmental science & technology*, 48 (2014) 4214-4215.
- [15] W.A. Laftah, S. Hashim, A.N. Ibrahim, Polymer hydrogels: A review, *Polymer-Plastics Technology and Engineering*, 50 (2011) 1475-1486.
- [16] H. Cong, L. Li, S. Zheng, Poly (N-isopropylacrylamide)-block-poly (vinyl pyrrolidone) block copolymer networks: Synthesis and rapid thermoresponse of hydrogels, *Polymer*, 54 (2013) 1370-1380.
- [17] L.-W. Xia, R. Xie, X.-J. Ju, W. Wang, Q. Chen, L.-Y. Chu, Nano-structured smart hydrogels with rapid response and high elasticity, *Nature communications*, 4 (2013).
- [18] X.-Z. Zhang, Y.-Y. Yang, T.-S. Chung, K.-X. Ma, Preparation and characterization of fast response macroporous poly (N-isopropylacrylamide) hydrogels, *Langmuir*, 17 (2001) 6094-6099.
- [19] H. Lee, S.M. Dellatore, W.M. Miller, P.B. Messersmith, Mussel-inspired surface chemistry for multifunctional coatings, *science*, 318 (2007) 426-430.
- [20] G. Gerlach, K.-F. Arndt, *Hydrogel sensors and actuators: engineering and technology*, Springer Science & Business Media, 2009.
- [21] J. Wang, W. Wu, Z. Lin, Kinetics and thermodynamics of the water sorption of 2 - hydroxyethyl methacrylate/styrene copolymer hydrogels, *Journal of applied polymer science*, 109 (2008) 3018-3023.
- [22] H. Omidian, J.G. Rocca, K. Park, Elastic, superporous hydrogel hybrids of polyacrylamide and sodium alginate, *Macromolecular bioscience*, 6 (2006) 703-710.

## Chapter 6 Functionalized Metal Organic Framework with thermoreversible ion sorption property for efficient water desalination

### Overview

In this chapter, a new strategy is developed for functionalization of a metal organic framework (MOF) by integrating weak acid groups with weak base groups together to achieve thermally reversible ion sorption property, as illustrated in Figure 6.1. A water-stable MIL-121 with free -COOH groups was used as an example to demonstrate this strategy by introducing a tertiary amine monomer, N, N'- dimethylvinyl-benzylamine, into the nanopores. The amphoteric functionalized MIL-121 exhibits excellent adsorption ability for a wide range of ions, and particularly a NaCl adsorption capacity as high as 0.92 meq/g. Importantly it can effectively release the adsorbed ions under thermal stimulus such as in hot water, with excellent adsorption-desorption cycling performance. This study provides a novel, effective strategy for synthesizing amphoteric MOFs for efficient adsorption of both monovalent and multivalent ions, easy recovery of adsorbed salts and chemical-free regeneration for efficient water desalination and purification, and other environmental applications.

This chapter will be submitted as a journal article: Ranwen Ou, Huacheng Zhang, Jing Wei, Li Wan, Yaoxin Hu, George P. Simon, and Huanting Wang, Functionalized Metal Organic Framework with Thermoreversible Ion Sorption Property for Efficient Water Desalination.



**Figure 6.1** Illustration of reversible ion sorption with functionalized MOF.

## 6.1 Introduction

Metal organic frameworks (MOFs) are a class of porous materials built from organic linkers and inorganic metal nodes or metal-based clusters through coordination bonds, and are well known for high surface area, uniform pore size, controllable structures, and readily tailorable functions.[1-5] Among a large variety of MOFs, stimuli-responsive MOFs have attracted increasing attention because of their attractive structures and properties that can change to adapt surrounding environment.[6-9] The introduction of responsive ability endows MOFs with unique functionalities and properties for many potential applications such as controllable adsorption and separation, energy storage and clean energy, sensing and catalysis. [6, 10-13] Therefore, developing stimuli-responsive MOFs and leveraging their properties for novel applications are of great significance.

Ion adsorption has been widely used in many areas such as water desalination and purification, catalysis, food processing, and pharmaceutical industries.[14-16] To date, porous solid materials such as activated carbons, metal oxides, zeolites, clays, and metal organic frameworks have been used as adsorbents for ion removal in various processes.[17] In particular, highly porous and flexible MOFs have been traditionally focused on gas adsorption and storage; only until recently, they been explored for adsorbing cations and anions in liquid phase, which is very promising for separation of molecules and ions.[18-22] Importantly, their diverse framework structure and high surface area show potential advantages in achieving superior ion adsorption kinetics and capacity.[23-28] Until now, the MOFs have been shown to have good properties for adsorbing metal pollutants in oxo-hydroxo anion forms such as perchlorate, chromate, selenite and arsenate in water treatment and purification processes; but they are not effective in adsorbing monovalent metal salts such as NaCl, which are commonly contained in seawater and other saline waters. Furthermore, the regeneration of spent MOFs usually requires the use of chemicals via ion exchange process, which is costly and environmentally unfriendly. Therefore, it is highly desirable to synthesize MOF adsorbents that can efficiently adsorb various ions including monovalent ions and can be regenerated without involving chemicals; it is anticipated that such new adsorbents would represent a major technological advance in the development of functional MOFs for a green and low-energy process for water desalination and purification to address worldwide shortage of fresh drinking water.[29, 30]

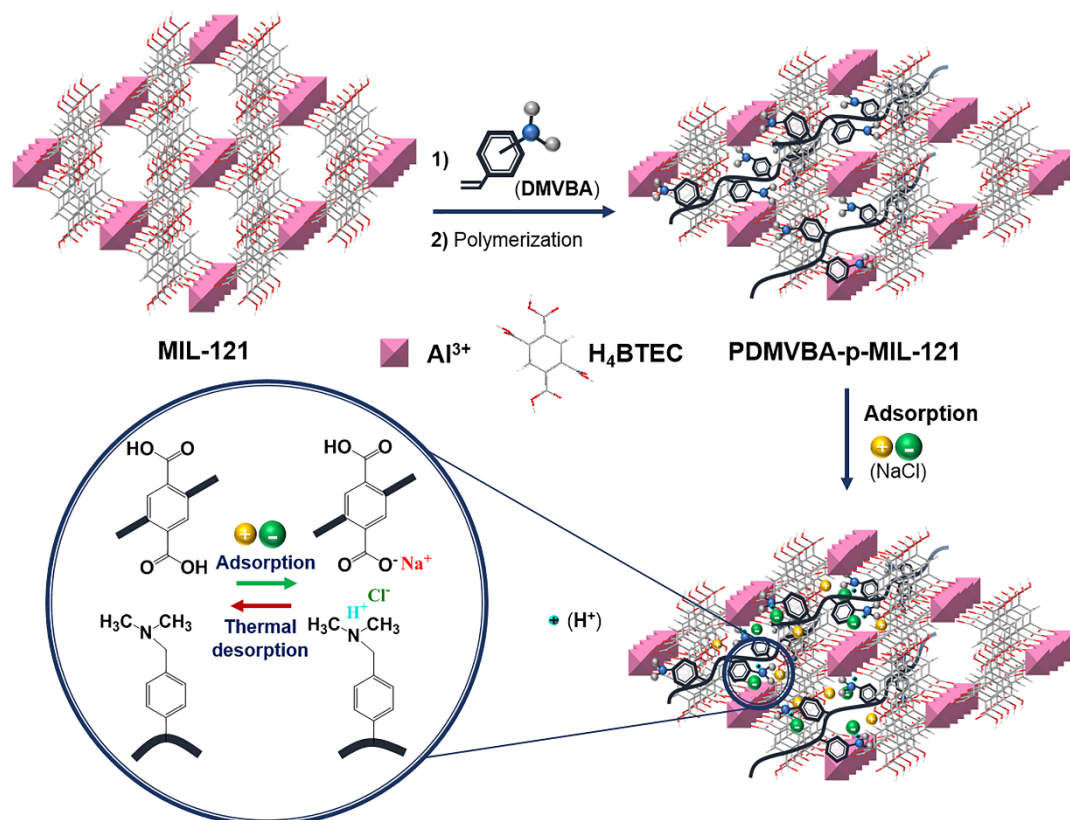


**Figure 6.2** Schematic illustration of the synthesis of amphoteric-functionalized MIL-121 (PDMVBA-p-MIL-121) and its thermoreversible adsorption process.

Here, for the first time, an amphoteric functionalized MOF is applied for highly efficient thermoreversible ion sorption. In particular, the functionalized MOF shows high adsorption capacity of monovalent cations and anions (or their salts), and releases adsorbed ions in hot water. Such thermo-responsiveness enables the chemical-free regeneration of MOF-based ion adsorbents, which is of fundamental, practical, and environmental significance for developing novel stimuli-responsive MOF-based ion adsorbents for water processing. Their thermal regeneration ability can effectively reduce the operating cost of ion adsorption process by using solar heating and industrial waste heat, and is thus also environmentally friendly. The strategy for forming an amphoteric MOF ion adsorbent is to integrate weak acid and base groups inside the MOF unit. Specifically, to make such an adsorbent thermally responsive, a weak-acid polymer or a weak-base polymer is incorporated into the MOF to provide either acid groups or base groups. This concept has been successfully demonstrated by the introduction of amine groups in a water-stable MOF, MIL-121, with free carboxylic groups. Amphoteric functionalization is realized by introducing a tertiary amine monomer (N, N'- dimethylvinylbenzylamine, or DMVBA) into the pores of MIL-121 and subsequent polymerization, as schematically illustrated in Figure 6.2.

Both ion adsorption and thermoreversible properties are achieved by the synergic effect of carboxylic acid groups (cation sites) and tertiary amine groups (anion sites), as further explained in the Results and Discussions. MIL-121 is selected for its excellent stability in water, and its free  $-\text{COOH}$  groups inside the nanochannels,[31] and poly (N, N'-dimethylvinyl-benzylamine) (PDMVBA) is selected for the weaker basicity of tertiary amine group than the primary and secondary amine for easy thermal desorption.[32] The resulting PDMVBA post-synthesis-functionalized MIL-121 is denoted PDMVBA-p-MIL-121.

## 6.2 Experimental

### 6.2.1 Materials

Aluminium nitrate nonahydrate ( $\text{Al}(\text{NO}_3)_3 \cdot 9\text{H}_2\text{O}$ ), pyromellitic acid ( $\text{H}_4\text{BTEC}$ ), N, N'-dimethylvinylbenzylamine (DMVBA), and  $\alpha, \alpha'$ -azoisobutyronitrile (AIBN) were purchased from Sigma-Aldrich. Lithium chloride ( $\text{LiCl}$ ), copper (II) chloride ( $\text{CuCl}_2$ ), and zinc chloride ( $\text{ZnCl}_2$ ) were also supplied by Sigma-Aldrich. Sodium chloride ( $\text{NaCl}$ ), potassium chloride ( $\text{KCl}$ ), calcium chloride ( $\text{CaCl}_2$ ), magnesium chloride ( $\text{MgCl}_2$ ), and ethanol were purchased from Merck.

### 6.2.2 Experimental Procedures

*Synthesis of MIL-121.* The MIL-121 powder was hydrothermally synthesized according to Ref [31]. 1.2 g of  $\text{Al}(\text{NO}_3)_3 \cdot 9\text{H}_2\text{O}$ , 0.4 g  $\text{H}_4\text{BTEC}$ , and 5 mL pure water were put into a Teflon-lined autoclave. The autoclave was heated in an oven for 48 h at 180 °C. The pH values before and after the reaction are 1.41 and 0.26, respectively. The resulting white powder was washed with pure water until the pH value stable ( $\text{pH} \approx 4$ ), and dried in a 60 °C oven. The MIL-121 powder was treated by a heating process at 180 – 380 °C in air for 5 h to empty pores. The free aperture size of MIL-121 is  $8.7 \times 5.7 \text{ \AA}$ .

*Synthesis of PDMVBA-p-MIL-121.* 0.1 g of MIL-121 was dispersed in 2 mL ethanol, following by adding 0.1 g of DMVBA (monomer) and 0.040 g of AIBN (initiator). The solution was stirred for 1 to 14 days with the cap on. Ethanol was then evaporated at room temperature in the fume cupboard until the sample was visibly dry. The mixture was heated at 80 °C for 3 days. The product was washed with ethanol 3 times, and then washed with water until the

conductivity of supernatant was less than 5  $\mu\text{S}/\text{cm}$ . The resultant PDMVBA-p-MIL-121 was dried, ground and used for characterization.

*Characterization.* The X-ray diffraction (XRD) patterns were determined by a Rigaku Miniflex 600 X-ray diffractometer at 40 kV and 25 mA at a scanning rate of 2  $^\circ/\text{min}$  and 2 $\theta$  range of 5 – 40  $^\circ$ . Scanning electron microscopy was undertaken with a Nova NanoSEM 450 and a Magellan 400 microscope (FEG SEM, FEI, USA). Fourier transform infrared spectroscopy was performed using a FT-IR spectrometer (Spectrum 100, PerkinElmer). The conductivity of salt solutions were measured by a laboratory conductivity meter (Cond 730, inoLab). The thermogravimetric data was collected by a Thermal Gravimetric Infra-Red hyphenated system (TGIR, PerkinElmer) performed at a temperature range of 50 – 800  $^\circ\text{C}$ , temperature scanning rate of 40  $^\circ\text{C}/\text{min}$ , in a 20 mL/min  $\text{N}_2$  gas flow.

*Adsorption Capacity Measurement.* 0.1 g of PDMVBA-p-MIL-121 and 20.00 mL salt solution were placed in a 50 mL centrifuge tube, stirred overnight. The conductivity of salt solution before and after adsorption were measured. The adsorption capacity can be calculated as follows:

$$\text{Adsorption Capacity (meq/g)} = \frac{nCV}{M_w \cdot w}$$

where C (g/L) is the concentration difference of salt solution before and after salt adsorption, V (L) is the volume of salt solution,  $M_w$  is the molecular weight of salt, and w is the weight of PDMVBA-p-MIL-121 used. For LiCl, NaCl, and KCl, n equals 1; for  $\text{CaCl}_2$ ,  $\text{MgCl}_2$ ,  $\text{CuCl}_2$ , and  $\text{ZnCl}_2$ , n is 2.

*Desorption of PDMVBA-p-MIL-121-NaCl.* The sample was distributed in 20 mL 500 ppm NaCl solution in a 50 mL centrifuge tube. This centrifuge tube was heated up to 80  $^\circ\text{C}$  for 16 h in an oven, followed by washing and centrifuging with pure water for three times. The sample obtained was then dried in an oven and reused.

## 6.3 Results and Discussion

### 6.3.1 Modification of amphoteric MOFs

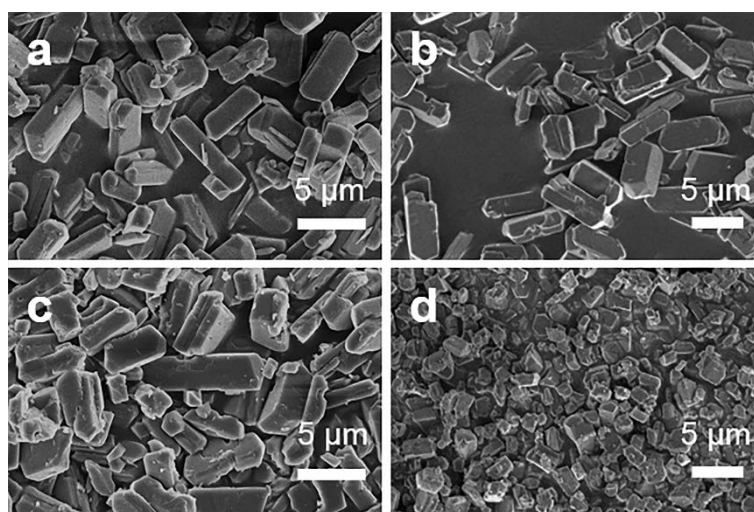


**Figure 6.3** The SEM images of MIL-121 crystals calcined at different temperatures: (a) original - 80 °C, (b) 180 °C, (c) 380 °C, and (d) 530 °C. The scale bar of the images is 5  $\mu\text{m}$ .

The integration of tertiary amine groups in the nanopores of MIL-121 with free carboxylic groups is key to successful amphoteric functionalization for ion adsorption. In this study, MIL-121 is hydrothermally synthesized, and contains free water and pyromellitic acid molecules in the channels.[31, 33, 34] Thus, the as-synthesized MIL-121 is calcined to empty the pores for accommodation of DMVBA. The sorption properties of PDMVBA-p-MIL-121 are optimized by investigating the effect of calcination temperature and the DMVBA impregnation time before polymerization. SEM images, FTIR spectra and XRD patterns of the samples are shown in Figure 6.3, 6.4, and 6.5, respectively, demonstrating how the calcination temperature affects the morphology, chemical and crystal structure of the MIL-121 particles. The morphology and crystal structure of the MIL-121 calcined at 380 °C or below are similar to those of the as-prepared MIL-121. As shown in Figure 6.4, the peak at 1701  $\text{cm}^{-1}$  is assigned to the free –COOH groups in the MIL-121 calcined at 180–350 °C, which will later pair with tertiary amine groups for ion adsorption. Figure 6.6 and 6.7 show the effects of calcination temperature and impregnation time on the NaCl adsorption capacity of PDMVBA-p-MIL-121. The results reveal that the MIL-121 calcined at 300 °C and with incorporated DMVBA for 3 days prior to polymerization has the highest adsorption capacity. This experimental condition was used to prepare PDMVBA-p-MIL-121 for further characterization. Importantly, the MIL-121 calcined at 300 °C (denoted MIL-121-300 °C) was highly water stable. After MIL-121-300 °C was

stirred in water for one month, TEM images (Figure 6.8) show that there were no mesopores formed.

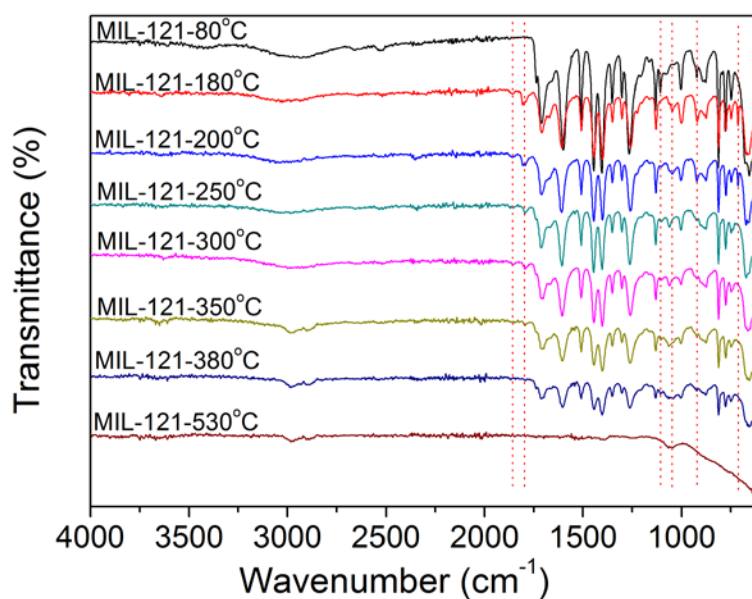


**Figure 6.4** FTIR spectra of MIL-121 powder calcined at different temperatures.

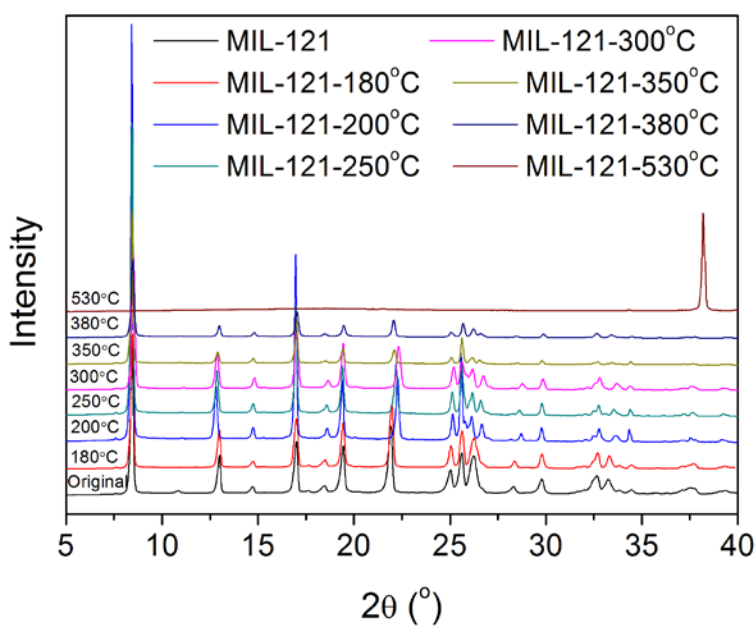


**Figure 6.5** XRD patterns of MIL-121 powders calcined at different temperatures.

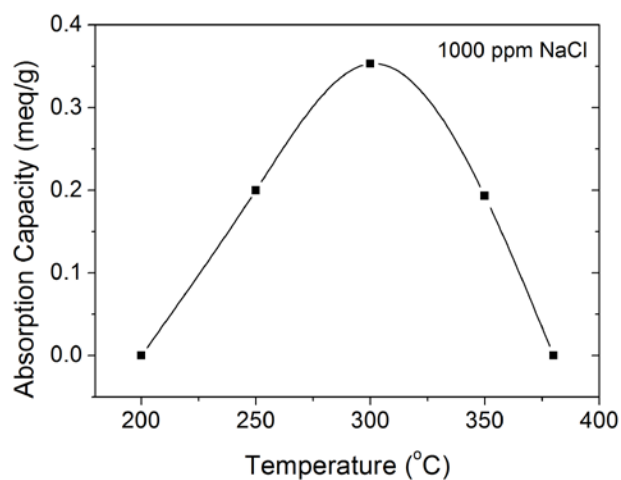


**Figure 6.6** The adsorption capacity (1000 ppm NaCl solution) of PDMVBA-p-MIL-121 prepared with MIL-121 powders calcined at different temperatures, and 3 days of impregnation time before polymerization.

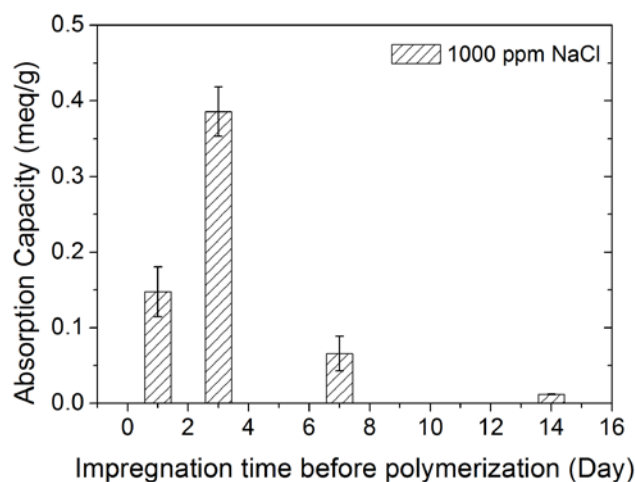


**Figure 6.7** The adsorption capacity (1000 ppm NaCl solution) of PDMVBA-p-MIL-121 prepared with different impregnation time before polymerization and MIL-121-300°C.

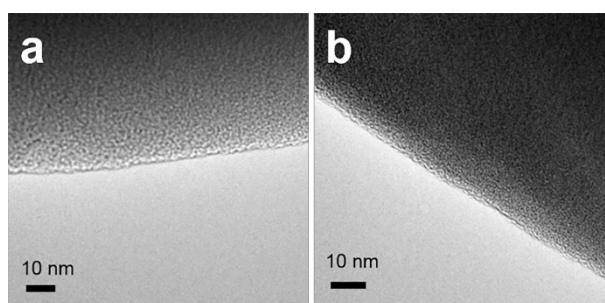


**Figure 6.8** TEM images of (a) as-prepared MIL-121-300 °C and (b) after kept in water under stirring for one month.

## 6.3.2 Morphology salt adsorption of MOFs

As shown in Figure 6.9, MIL-121 crystals demonstrate a smooth surface and clear, distinct edges. However, after the polymerization of DMVBA inside and on the crystals, MIL-121 is covered by the polymer, and the crystal edge becomes smooth and blurred. PDMVBA-p-MIL-121 was also studied for adsorbing ions from 1000 ppm NaCl and MgCl<sub>2</sub> solutions in comparison with pure PDMVBA, MIL-121-300°C, and the result is shown in Figure 6.9c and Figure 6.10. After overnight adsorption, the adsorption capacities of PDMVBA-p-MIL-121 were 0.39 and 0.07 meq/g for NaCl and MgCl<sub>2</sub>, respectively. By contrast, those of pure PDMVBA and MIL-121-300°C powders did not adsorb monovalent and divalent ions at all.

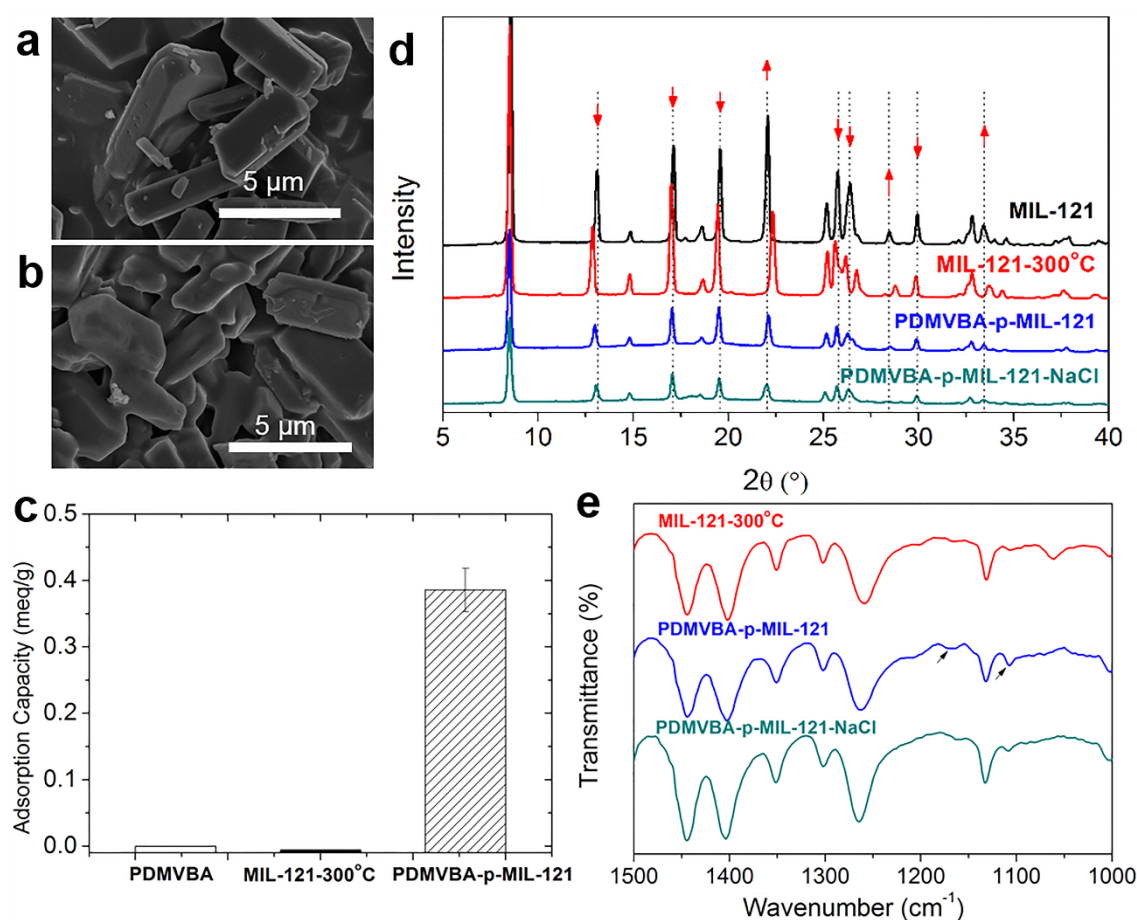


**Figure 6.9** Characterization of MIL-121 and PDMVBA-p-MIL-121. SEM images of (a) MIL-121-300 °C and (b) PDMVBA-p-MIL-121. (c) NaCl adsorption capacity of PDMVBA, MIL-121-300 °C and PDMVBA-p-MIL-121. (d) XRD patterns of as-prepared MIL-121, MIL-121-300 °C, and PDMVBA-p-MIL-121 before and after NaCl adsorption. The red arrows on the peaks show the peak shift of pattern MIL-121-300 °C compared with the XRD pattern of MIL-121. (e) FTIR spectra of MIL-121-300 °C, and PDMVBA-p-MIL-121 before and after NaCl adsorption.

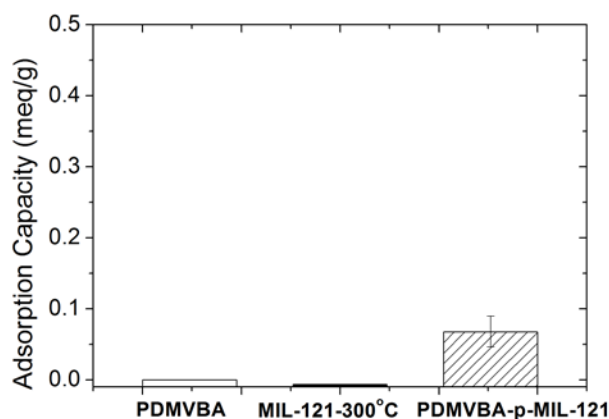


**Figure 6.10** The  $\text{MgCl}_2$  adsorption capacity of PDMVBA, MIL-121-300°C and PDMVBA-p-MIL-121.

### 6.3.3 Adsorption and thermal desorption mechanisms

X-ray diffraction technique (XRD) and Fourier transform infrared spectroscopy (FTIR) were used to study the crystal and chemical structure change of MIL-121 after calcination, incorporation of PDMVBA, and NaCl adsorption.[35, 36] The MIL-n family combines octahedral metal clusters with organic carboxylates to form a range of porous structures, some of which exhibit a remarkable breathing effect upon introduction of guest molecules. MIL-53 (M) has been proven to exhibit breathing behavior.[37-39] The framework structure of MIL-121 is the same as MIL-53, except that MIL-121 has two non-coordinated carboxylic acid groups in the channel of the unit cell. [40] Thus, it is likely that MIL-121 shows the same breathing behavior as MIL-53. Figure 6.9d shows the XRD patterns of as-prepared MIL-121, MIL-121-300°C, and PDMVBA-p-MIL-121 before and after salt adsorption. Compared to the XRD pattern of as-prepared MIL-121, most of peaks of MIL-121-300°C shift to lower  $2\theta$  angles after calcination. On the contrary, after the impregnation of PDMVBA, the peaks mainly shift to higher  $2\theta$  angles compared to MIL-121-300°C; whereas the adsorption of NaCl shifted the peaks to even greater  $2\theta$  angles, indicating that the adsorbed NaCl is located inside the framework. According to the Bragg's Law ( $2d \cdot \sin\theta = n\lambda$ ), the peaks shifting to higher  $2\theta$  angles means a decreased interplanar distance  $d$ , and structure contraction after the introduction of PDMVBA (Figure 6.2). By contrast, emptying the pores leads to expansion of the MIL-121 framework. This breathing behavior of MIL-121 (Al) is exactly same as that of MIL-53 (Al).[41, 42] In the FTIR spectra (Figure 6.9e), the peaks at 1107 and 1168  $\text{cm}^{-1}$  are the characteristic peak of tertiary amine, demonstrating the existence of PDMVBA. After

adsorbing NaCl, these two peaks weakened because most of the tertiary amine groups became tertiary amine hydrochloride that do not have these two characteristic peaks.

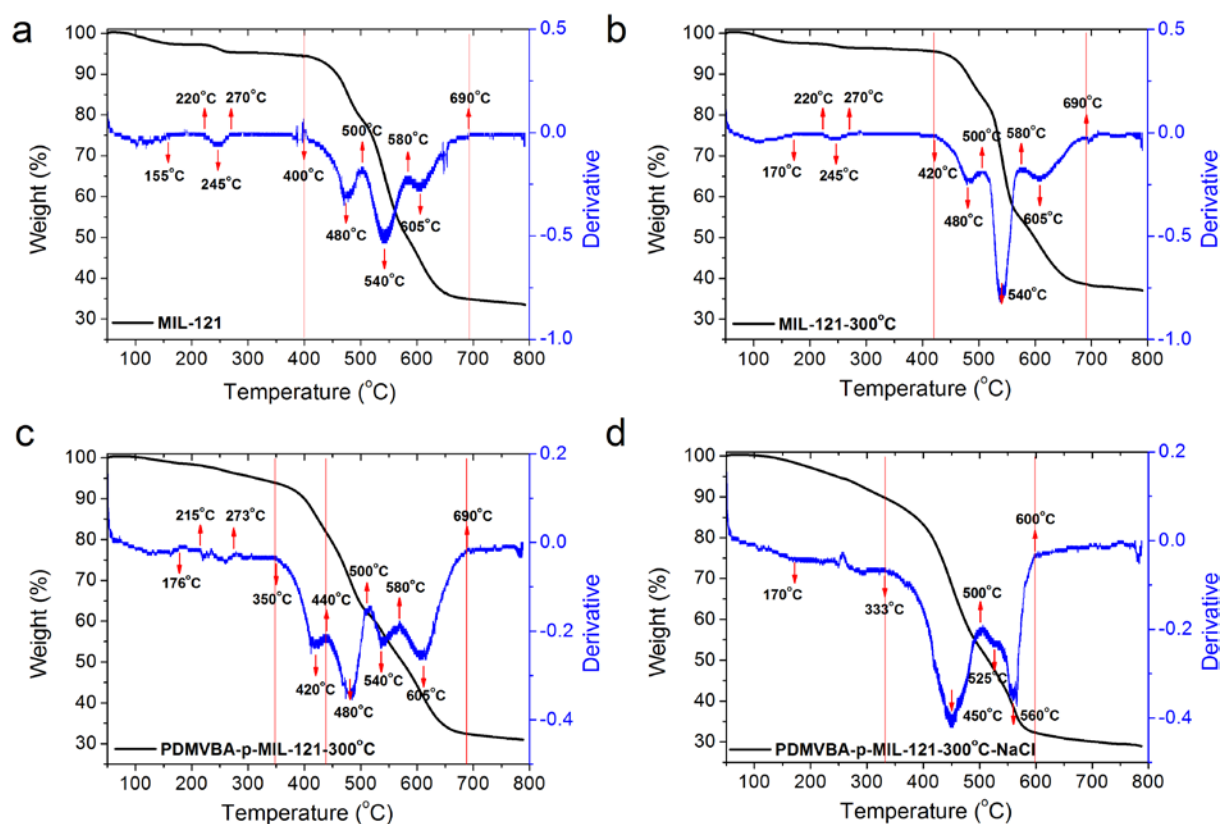
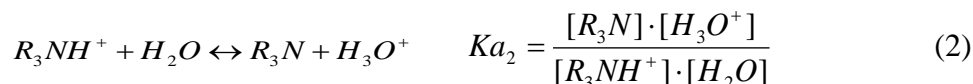
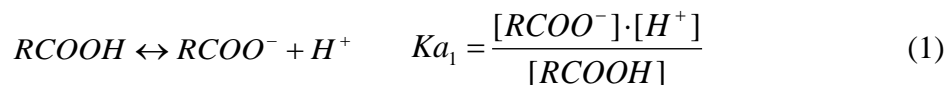


Figure 6.11 Thermogravimetric analysis curves and the relevant derivative of (a) MIL-121, (b) MIL-121-300°C, (c) PDMVBA-p-MIL-121-300°C, and (d) PDMVBA-p-MIL-121-300°C-NaCl. The TGA was conducted under N<sub>2</sub> gas flow.

The thermal behavior of MIL-121-300 °C, PDMVBA-p-MIL-121, and PDMVBA-p-MIL-121-NaCl were characterized to further understand their structure, as shown in Figure 6.11. TGA results indicate that the pyrolysis of PDMVBA-p-MIL-121 involves the pyrolysis of PDMVBA at 350 – 440 °C, and the decomposition of MIL-121 in the temperature range of 440 – 690 °C that is similar to the decomposition of pure MIL-121 (420 – 690 °C). After the adsorption of NaCl, as shown in Figure 6.11d, the pyrolysis of the composite mainly involves two stages, 333 – 500 °C and 500 – 600 °C, which is distinctly different from that of PDMVBA and MIL-121, demonstrating that the adsorption of NaCl changes the chemical composition of MIL-121 framework and PDMVBA. This is because the non-coordinating –COOH becomes –COONa, while the R<sub>3</sub>N becomes R<sub>3</sub>NHCl.

In the aqueous solution, the carboxylic acid and protonated tertiary amine exhibit the following equilibrium: <sup>3,4</sup>



At 30 °C or above, the pKa value of carboxylic acid increases with increasing temperature,[43, 44] while the pKa value of protonated tertiary amine decreases.[45, 46] At lower temperatures, the dissociation of RCOOH and protonation of R<sub>3</sub>N facilitate mutually, which may strengthen the acidity of carboxylic acid group and the basicity of tertiary amine group, giving rise to the ability to adsorb monovalent ions; however, at elevated temperature, the protonation of RCOO<sup>-</sup> and the deprotonation of R<sub>3</sub>NH<sup>+</sup> promote mutually, resulting in the release of adsorbed salts, as shown in Figure 6.2. As a result, the adsorption and thermal regeneration mechanism can be described as follows:



#### 6.3.4 NaCl adsorption capacity of amphoteric MOFs

The amphoteric PDMVBA-p-MIL-121 exhibits high NaCl adsorption capacity. The loading of PDMVBA in the PDMVBA-p-MIL-121 is determined to be 19.3 ± 2.3 wt. % based on the change of sample weight, which is consistent with 17.9 wt. % obtained from the TG analysis. The ratio of the polymer (PDMVBA) penetrated and coated on surface was calculated to be 79:21 on the basis of the thickness of polymer coating, confirming that the majority of the polymer was incorporated into the porous channels of MIL-121. The theoretical maximum adsorption capacity of PDMVBA-p-MIL-121 is calculated to be 1.20 meq/g on the basis of 19.3 wt. % of PDMVBA loading. The adsorption experiments show that the ion adsorption capacity of PDMVBA-p-MIL-121 is dependent on the ion concentration. As shown in Figure 6.12, upon the increase of NaCl concentration, the adsorption capacity of PDMVBA-p-MIL-121 increases and reaches equilibrium at 10000 ppm NaCl aqueous solution after overnight adsorption. The equilibrium NaCl adsorption capacity is 0.92 meq/g, accounting for 77 % of the theoretical maximum value; this indicates most of the ion adsorption sites accessible to ions. When NaCl concentration decreases to 500 ppm, the adsorption capacity drops to 0.13 meq/g. Given < 600 ppm of total dissolved solids in good quality drinking water according to

the Australian drinking water guidelines,[47] PDMVBA-p-MIL-121 can be potentially used to desalinate water in water treatment process.

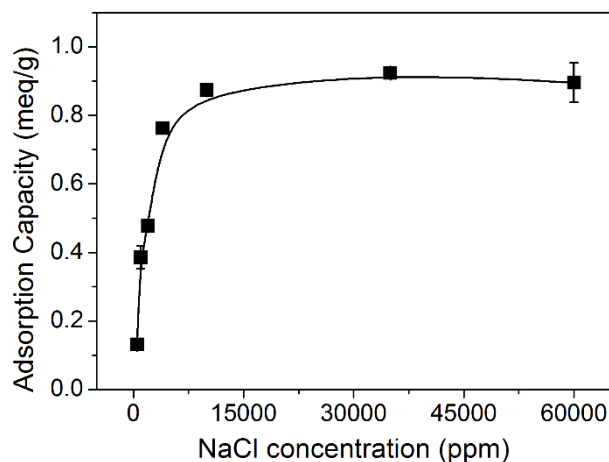


**Figure 6.12** The adsorption capacity of PDMVBA-p-MIL-121 at different NaCl concentrations.

### 6.3.5 Cycling performance of amphoteric MOFs

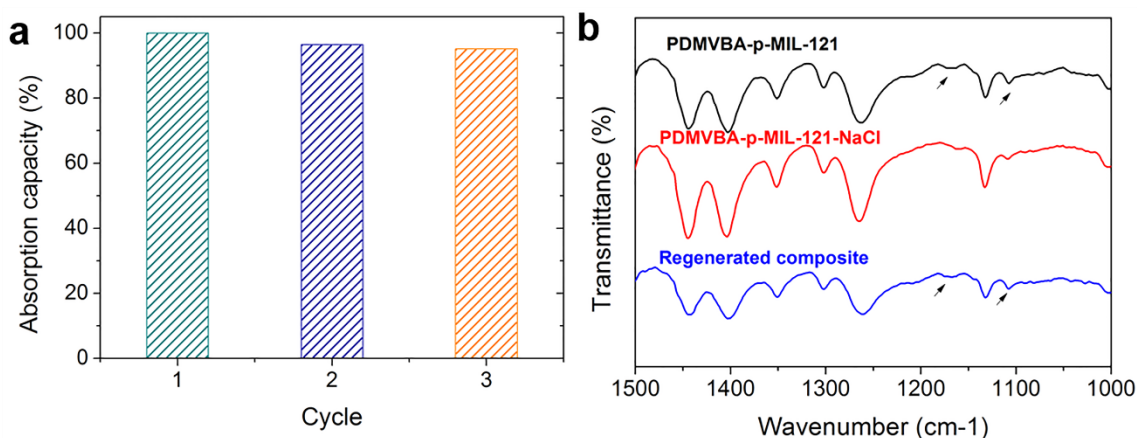


**Figure 6.13** a) The cycling performance of PDMVBA-p-MIL-121 for thermoreversible sorption of 10000 ppm NaCl solution. The PDMVBA-p-MIL-121 was thermally regenerated at 80 °C in 500 ppm NaCl solution. b) FTIR spectra of PDMVBA-p-MIL-121 before and after NaCl adsorption, and after thermal desorption.

Furthermore, PDMVBA-p-MIL-121 exhibits excellent cycling performance, as shown in Figure 6.13. Desorption of the PDMVBA-p-MIL-121-NaCl was achieved by heating it at 80 °C in 500 ppm NaCl solution for 16 hours. In three cycles, the adsorption capacity of PDMVBA-p-MIL-121 decreased gradually from 100 % to 96 %, and then 95 %, demonstrating

the successful thermal regeneration of PDMVBA-p-MIL-121 and the excellent cycling performance. As mentioned above on the FTIR spectra (Figure 6.13 and Figure 6.14), the characteristic peaks of tertiary amine are located at 1107 and 1168  $\text{cm}^{-1}$ , these two peaks weakened after adsorbing NaCl, while they strengthened after thermal desorption, further demonstrating the reversible adsorption mechanism.

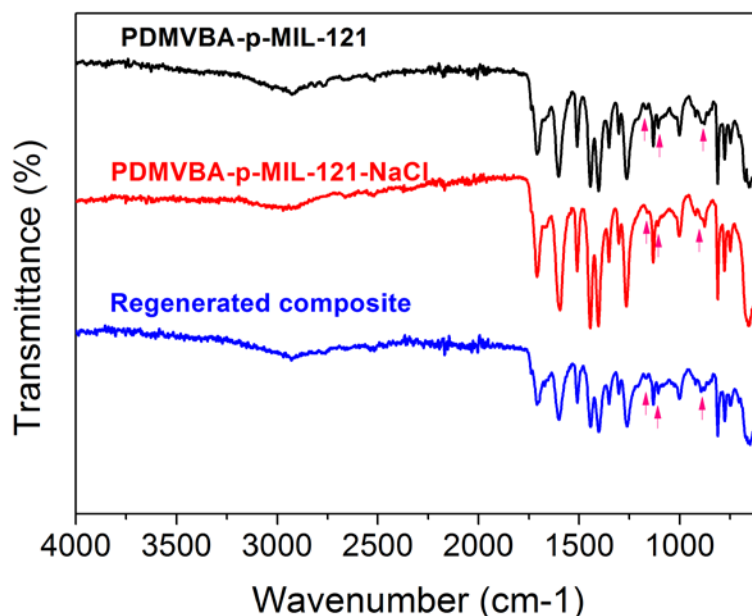


**Figure 6.14** The FTIR spectra of PDMVBA-p-MIL-121 before and after the adsorption of NaCl, and after thermal regeneration.

### 6.3.6 Adsorption of other ions

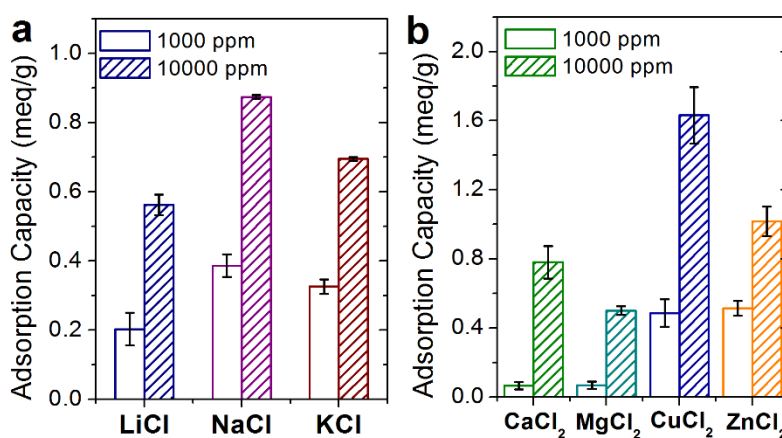


**Figure 6.15.** The adsorption capacity of PDMVBA-p-MIL-121 for adsorption of different monovalent and divalent cations.

In addition to NaCl, PDMVBA-p-MIL-121 is capable of adsorbing other monovalent cations and divalent cations (Figure 6.15). In Figure 6.15a, when salt concentration was 1000 ppm, the adsorption capacities of PDMVBA-p-MIL-121 for LiCl, NaCl, and KCl were 0.20, 0.39, and 0.33 meq/g, respectively. If the salt concentration increased to 10000 ppm, they became 0.56, 0.88, and 0.70 meq/g, respectively. The amount of NaCl adsorbed by PDMVBA-p-MIL-121 is the largest, followed by KCl, and then LiCl. The ionic radius of Li<sup>+</sup>, Na<sup>+</sup>, and K<sup>+</sup> gradually increase, but their hydrated radius gradually decrease, and the absolute values of their Gibbs Free energy of hydration progressively decrease, as shown in Table 6.1.[48-50] Thus, compared to Na<sup>+</sup> and K<sup>+</sup>, hydrated Li<sup>+</sup> has the most difficulty entering the channel of MIL-121, and it takes greatest energy to overcome the hydrated form before combining with –COOH group inside the channel in the aqueous solution. In addition, PDMVBA-p-MIL-121 was applied to adsorb divalent cations, including Ca<sup>2+</sup>, Mg<sup>2+</sup>, Cu<sup>2+</sup>, and Zn<sup>2+</sup> in 10000 ppm CaCl<sub>2</sub>, MgCl<sub>2</sub>, CuCl<sub>2</sub>, and ZnCl<sub>2</sub> aqueous solution. The adsorption capacities for Ca<sup>2+</sup>, Mg<sup>2+</sup>, Cu<sup>2+</sup>, and Zn<sup>2+</sup> are 0.78, 0.50, 1.63, and 1.02 meq/g, respectively. The different adsorbed amounts of these divalent salts are closely related to the solubility of their benzoic acid salt (Table 6.1), while the benzoic acid copper salt and zinc salt are insoluble in water. The PDMVBA-p-MIL-121 adsorbed 1.63 and 1.02 meq/g CuCl<sub>2</sub> and ZnCl<sub>2</sub>, which are equivalent to 0.82 and 0.51 mmol/g, respectively. As a result, the amphoteric PDMVBA-p-MIL-121 shows great potential for adsorbing a range of ions such as in desalination treatments.

**Table 6.1** The radius, hydration energy, and solubility of relevant benzoic acid salt of cations.

Ion	Ionic radius (Å)	Hydrated radius (Å)	Water molecules	Enthalpy of hydration (kJ·mol <sup>-1</sup> )	Gibbs Free energy of hydration (kJ·mol <sup>-1</sup> )	Solubility of relevant benzoic acid salt (g/100 mL) at 30 °C
Li <sup>+</sup>	0.60	3.82	5.2	-531	-475	53.8
Na <sup>+</sup>	0.95	3.58	3.5	-416	-365	62.9
K <sup>+</sup>	1.33	3.31	2.6	-334	-295	76.7
Ca <sup>2+</sup>	0.99	4.2	7.2	-1602	-1505	2.72
Mg <sup>2+</sup>	0.65	4.4	10.0	-1949	-1830	5 (40 °C)
Cu <sup>2+</sup>	0.72	4.2	9.9	-2123	-2010	--
Zn <sup>2+</sup>	0.74	4.3	9.6	-2070	-1955	--

## 6.4 Summary

The feasibility of using an amphoteric MOF as high-performance ion adsorbent for reversibly adsorbing a wide range of ions have been successfully demonstrated. The amphoteric-functionalized MIL-121 (PDMVBA-p-MIL-121) exhibited a high adsorption capacity of NaCl of 0.92 meq/g. PDMVBA-p-MIL-121 was able to adsorb a wide range of other salts including monovalent metal salts (LiCl and KCl) and divalent metal salts (CaCl<sub>2</sub>, MgCl<sub>2</sub>, CuCl<sub>2</sub>, and ZnCl<sub>2</sub>). Importantly, PDMVBA-p-MIL-121 could be thermally regenerated such as at 80 °C in 500 ppm NaCl solution to release the adsorbed salts, and exhibited excellent cycling performance. This study has extended the functional diversity of MOFs to highly efficient ion adsorption and thermal desorption. In particular, the chemical-free regeneration ability provides a unique functionality for developing high-performance MOF-based ion adsorbents to potentially lower operating costs of water desalination and purification and minimize the environmental impact.

## 6.5 References

- [1] H. Fei, C.S. Han, J.C. Robins, S.R. Oliver, A Cationic Metal–Organic Solid Solution Based on Co (II) and Zn (II) for Chromate Trapping, *Chemistry of Materials*, 25 (2013) 647-652.
- [2] H. Furukawa, K.E. Cordova, M. O’Keeffe, O.M. Yaghi, The chemistry and applications of metal-organic frameworks, *Science*, 341 (2013) 1230444.
- [3] A.J. Howarth, M.J. Katz, T.C. Wang, A.E. Platero-Prats, K.W. Chapman, J.T. Hupp, O.K. Farha, High Efficiency Adsorption and removal of selenate and selenite from water using metal–organic frameworks, *Journal of the American Chemical Society*, 137 (2015) 7488-7494.
- [4] X. Li, H. Xu, F. Kong, R. Wang, A Cationic Metal–Organic Framework Consisting of Nanoscale Cages: Capture, Separation, and Luminescent Probing of Cr<sub>2</sub>O<sub>7</sub><sup>2-</sup> through a Single-Crystal to Single-Crystal Process, *Angewandte Chemie International Edition*, 52 (2013) 13769-13773.
- [5] X. Zhao, X. Bu, T. Wu, S.-T. Zheng, L. Wang, P. Feng, Selective anion exchange with nanogated isorecticular positive metal-organic frameworks, *Nature communications*, 4 (2013).
- [6] F.o.-X. Coudert, Responsive metal–organic frameworks and framework materials: under pressure, taking the heat, in the spotlight, with friends, *Chemistry of Materials*, 27 (2015) 1905-1916.

- [7] J. Park, D. Yuan, K.T. Pham, J.-R. Li, A. Yakovenko, H.-C. Zhou, Reversible alteration of CO<sub>2</sub> adsorption upon photochemical or thermal treatment in a metal–organic framework, *Journal of the American Chemical Society*, 134 (2011) 99-102.
- [8] M.A.C. Stuart, W.T. Huck, J. Genzer, M. Müller, C. Ober, M. Stamm, G.B. Sukhorukov, I. Szleifer, V.V. Tsukruk, M. Urban, Emerging applications of stimuli-responsive polymer materials, *Nature materials*, 9 (2010) 101-113.
- [9] X. Meng, B. Gui, D. Yuan, M. Zeller, C. Wang, Mechanized azobenzene-functionalized zirconium metal-organic framework for on-command cargo release, *Science Advances*, 2 (2016) e1600480.
- [10] D. Chen, D. Yang, C. Dougherty, W. Lu, H. Wu, X. He, T. Cai, M.E. Van Dort, B.D. Ross, H. Hong, In Vivo Targeting and Positron Emission Tomography Imaging of Tumor with Intrinsically Radioactive Metal-Organic Frameworks Nanomaterials, *ACS nano*, (2017).
- [11] K. Mandel, T. Granath, T. Wehner, M. Rey, W. Stracke, N. Vogel, G. Sextl, K. Mueller-Buschbaum, Smart Optical Composite Materials: Dispersions of Metal-Organic Framework@ Superparamagnetic Microrods for Switchable Isotropic-Anisotropic Optical Properties, *ACS nano*, (2016).
- [12] S.S. Nagarkar, A.V. Desai, S.K. Ghosh, Stimulus-Responsive Metal–Organic Frameworks, *Chemistry–An Asian Journal*, 9 (2014) 2358-2376.
- [13] S.-L. Li, Q. Xu, Metal–organic frameworks as platforms for clean energy, *Energy & Environmental Science*, 6 (2013) 1656-1683.
- [14] A. Dąbrowski, Adsorption—from theory to practice, *Advances in colloid and interface science*, 93 (2001) 135-224.
- [15] S.D. Alexandratos, Ion-exchange resins: a retrospective from industrial and engineering chemistry research, *Industrial & Engineering Chemistry Research*, 48 (2008) 388-398.
- [16] M.E. Davis, Ordered porous materials for emerging applications, *Nature*, 417 (2002) 813-821.
- [17] J. Rouquerol, F. Rouquerol, P. Llewellyn, G. Maurin, K.S. Sing, Adsorption by powders and porous solids: principles, methodology and applications, Academic press, 2013.
- [18] P. Li, S.-Y. Moon, M.A. Guelta, L. Lin, D.A. Gómez-Gualdrón, R.Q. Snurr, S.P. Harvey, J.T. Hupp, O.K. Farha, Nanosizing a Metal–Organic Framework Enzyme Carrier for Accelerating Nerve Agent Hydrolysis, *ACS nano*, 10 (2016) 9174-9182.
- [19] V. Stavila, R.K. Bhakta, T.M. Alam, E.H. Majzoub, M.D. Allendorf, Reversible hydrogen storage by NaAlH<sub>4</sub> confined within a titanium-functionalized MOF-74 (Mg) nanoreactor, *ACS nano*, 6 (2012) 9807-9817.

- [20] M. Carboni, C.W. Abney, S. Liu, W. Lin, Highly porous and stable metal–organic frameworks for uranium extraction, *Chemical Science*, 4 (2013) 2396-2402.
- [21] A.J. Howarth, T.C. Wang, S.S. Al-Juaid, S.G. Aziz, J.T. Hupp, O.K. Farha, Efficient extraction of sulfate from water using a Zr-metal–organic framework, *Dalton Transactions*, 45 (2016) 93-97.
- [22] C. Wang, X. Liu, J.P. Chen, K. Li, Superior removal of arsenic from water with zirconium metal-organic framework UiO-66, *Scientific reports*, 5 (2015).
- [23] H. Fei, D.L. Rogow, S.R. Oliver, Reversible anion exchange and catalytic properties of two cationic metal– organic frameworks based on Cu (I) and Ag (I), *Journal of the American Chemical Society*, 132 (2010) 7202-7209.
- [24] H.-R. Fu, Z.-X. Xu, J. Zhang, Water-stable metal–organic frameworks for fast and high dichromate trapping via single-crystal-to-single-crystal ion exchange, *Chemistry of Materials*, 27 (2014) 205-210.
- [25] P.-F. Shi, B. Zhao, G. Xiong, Y.-L. Hou, P. Cheng, Fast capture and separation of, and luminescent probe for, pollutant chromate using a multi-functional cationic heterometal-organic framework, *Chemical Communications*, 48 (2012) 8231-8233.
- [26] H. Fei, M.R. Bresler, S.R. Oliver, A new paradigm for anion trapping in high capacity and selectivity: Crystal-to-crystal transformation of cationic materials, *Journal of the American Chemical Society*, 133 (2011) 11110-11113.
- [27] N. Zhang, X. Yang, X. Yu, Y. Jia, J. Wang, L. Kong, Z. Jin, B. Sun, T. Luo, J. Liu, Al-1, 3, 5-benzenetricarboxylic metal–organic frameworks: A promising adsorbent for defluoridation of water with pH insensitivity and low aluminum residual, *Chemical Engineering Journal*, 252 (2014) 220-229.
- [28] X.-P. Zhou, Z. Xu, M. Zeller, A.D. Hunter, Reversible uptake of HgCl<sub>2</sub> in a porous coordination polymer based on the dual functions of carboxylate and thioether, *Chemical Communications*, (2009) 5439-5441.
- [29] D. Li, Y.S. Yan, H.T. Wang, Recent advances in polymer and polymer composite membranes for reverse and forward osmosis processes, *Prog. Polym. Sci.*, 61 (2016) 104-155.
- [30] D. Li, H.T. Wang, Recent developments in reverse osmosis desalination membranes, *J. Mater. Chem.*, 20 (2010) 4551-4566.
- [31] C. Volkringer, T. Loiseau, N. Guillou, G.r. Férey, M. Haouas, F. Taulelle, E. Elkaim, N. Stock, High-Throughput Aided Synthesis of the Porous Metal– Organic Framework-Type Aluminum Pyromellitate, MIL-121, with Extra Carboxylic Acid Functionalization, *Inorganic chemistry*, 49 (2010) 9852-9862.

- [32] J.J. Christensen, R.M. Izatt, D.P. Wrathall, L.D. Hansen, Thermodynamics of proton ionization in dilute aqueous solution. Part XI.  $pK$ ,  $\Delta H^\circ$ , and  $\Delta S^\circ$  values for proton ionization from protonated amines at  $25^\circ$ , *Journal of the Chemical Society A: Inorganic, Physical, Theoretical*, (1969) 1212-1223.
- [33] J.-N. Hao, B. Yan,  $Ag^{+}$ -sensitized lanthanide luminescence in  $Ln^{3+}$  post-functionalized metal-organic frameworks and  $Ag^{+}$  sensing, *Journal of Materials Chemistry A*, 3 (2015) 4788-4792.
- [34] J.-N. Hao, B. Yan, Highly sensitive and selective fluorescent probe for  $Ag^{+}$  based on a  $Eu^{3+}$  post-functionalized metal-organic framework in aqueous media, *Journal of Materials Chemistry A*, 2 (2014) 18018-18025.
- [35] C. Volkringer, T. Loiseau, N. Guillou, G. Férey, E. Elkaim, A. Vimont, XRD and IR structural investigations of a particular breathing effect in the MOF-type gallium terephthalate MIL-53 (Ga), *Dalton Transactions*, (2009) 2241-2249.
- [36] C. Serre, F. Millange, C. Thouvenot, M. Noguès, G. Marsolier, D. Louër, G. Férey, Very Large Breathing Effect in the First Nanoporous Chromium (III)-Based Solids: MIL-53 or  $Cr^{III}(OH)\{O_2C-C_6H_4-CO_2\}\{HO_2C-C_6H_4-CO_2H\}_x \cdot H_2O_y$ , *Journal of the American Chemical Society*, 124 (2002) 13519-13526.
- [37] G. Férey, C. Serre, Large breathing effects in three-dimensional porous hybrid matter: facts, analyses, rules and consequences, *Chemical Society Reviews*, 38 (2009) 1380-1399.
- [38] F. Millange, C. Serre, N. Guillou, G. Férey, R.I. Walton, Structural effects of solvents on the breathing of metal-organic frameworks: an in situ diffraction study, *Angewandte Chemie*, 120 (2008) 4168-4173.
- [39] C. Serre, C. Mellot-Draznieks, S. Surblé, N. Audebrand, Y. Filinchuk, G. Férey, Role of solvent-host interactions that lead to very large swelling of hybrid frameworks, *Science*, 315 (2007) 1828-1831.
- [40] T. Loiseau, C. Serre, C. Huguenard, G. Fink, F. Taulelle, M. Henry, T. Bataille, G. Férey, A Rationale for the Large Breathing of the Porous Aluminum Terephthalate (MIL-53) Upon Hydration, *Chemistry-A European Journal*, 10 (2004) 1373-1382.
- [41] F. Millange, N. Guillou, R.I. Walton, J.-M. Grenèche, I. Margiolaki, G. Férey, Effect of the nature of the metal on the breathing steps in MOFs with dynamic frameworks, *Chemical Communications*, (2008) 4732-4734.
- [42] T.K. Trung, P. Trens, N. Tanchoux, S. Bourrelly, P.L. Llewellyn, S. Loera-Serna, C. Serre, T. Loiseau, F. Fajula, G. Férey, Hydrocarbon adsorption in the flexible metal organic

frameworks MIL-53 (Al, Cr), *Journal of the American Chemical Society*, 130 (2008) 16926-16932.

[43] T. Matsui, H.C. Ko, L.G. Hepler, Calorimetric Heats of Ionization of Aqueous Benzoic Acid from 5-100° C and Derived Thermodynamic Quantities, *Canadian Journal of Chemistry*, 52 (1974) 2912-2918.

[44] J.K. Sa'ib, Titrimetric Study of the Solubility and Dissociation of Benzoic Acid in Water: Effect of Ionic Strength and Temperature, *American Journal of Analytical Chemistry*, 6 (2015) 429.

[45] E.S. Hamborg, G.F. Versteeg, Dissociation constants and thermodynamic properties of amines and alkanolamines from (293 to 353) K, *Journal of Chemical & Engineering Data*, 54 (2009) 1318-1328.

[46] M. Gupta, E.F. da Silva, H.F. Svendsen, Modeling temperature dependency of amine basicity using PCM and SM8T implicit solvation models, *The Journal of Physical Chemistry B*, 116 (2012) 1865-1875.

[47] Australian Drinking Water Guidelines 6, Australian Government: National Health and Medical Research Council, National Resource Management Ministerial Council, (2004).

[48] M.H. Abraham, Y. Marcus, The thermodynamics of solvation of ions. Part 1.—The heat capacity of hydration at 298.15 K, *Journal of the Chemical Society, Faraday Transactions 1: Physical Chemistry in Condensed Phases*, 82 (1986) 3255-3274.

[49] Y. Marcus, The thermodynamics of solvation of ions. Part 2.—The enthalpy of hydration at 298.15 K, *Journal of the Chemical Society, Faraday Transactions 1: Physical Chemistry in Condensed Phases*, 83 (1987) 339-349.

[50] Y. Marcus, Thermodynamics of solvation of ions. Part 5.—Gibbs free energy of hydration at 298.15 K, *Journal of the Chemical Society, Faraday Transactions*, 87 (1991) 2995-2999.

---

## Chapter 7 Conclusion and Future Work

### 7.1 Conclusion

In this thesis, thermo-responsive ability is successfully introduced to the materials for water treatment, including responsive membrane, responsive draw agent, and responsive ion adsorbent. Through the exploration in this thesis, it can be concluded that: 1) introduction of thermally responsive polymer endows the responsive membrane with controllable separation ability and high separation efficiency due to the switchable wettability and the hierarchical structure that enlarged them to superhydrophilicity and superhydrophobicity for improved treatment performance. 2) The swelling behavior / kinetic study efficiently reveals the swelling pressure and FO performance of thermally responsive hydrogel draw agent, advancing the development of desired draw agent. 3) Thermally reversible ion sorption is achieved inside the metal organic framework by amphoteric functionalization, showing high adsorption capacity, accessibility of ion adsorption sites, and excellent cycling performance.

In chapter 3, a robust thermo-responsive polymer membrane with switchable superhydrophilicity and superhydrophobicity was successfully fabricated by evenly coating poly (N-isopropylacrylamide) (PNIPAM) on a thermoplastic polyurethane (TPU) microfibrils mat. In addition, other polymeric micro- or nanofibrils membranes could be used as the substrates for fabricating superwetting materials, which broadens the methods of preparation of such materials. Among the polymer composite membranes prepared in this study, the TPU-PNIPAM-3.6 material performed best, exhibiting excellent mechanical properties, switchable superwettability, fast swelling – deswelling behaviour, and best oil water emulsion separation capacity. Driven by gravity only, the TPU-PNIPAM-3.6 membrane could separate 1 wt. % silicone oil-water emulsion at room temperature with a separation efficiency of  $\geq 99.26\%$ , and separate 99 wt. % silicone oil-water emulsions at 45 °C with a separation efficiency of  $\geq 99.85\%$ . This membrane is a good candidate for not only oil-water emulsion separation, but also for fabricating smart materials for rapidly responsive drug delivery systems and sensors.

In chapter 4, the swelling pressure of polymer hydrogels was enhanced by incorporating TPU microfibrils, and thus improving the forward osmosis performance of hydrogel composites. This study is based on our group's previous study, by modifying the pure responsive hydrogel, and applied in the process as a monolith. TPU-hydrogel composite monolith generated a water flux that are about twice of those of pure hydrogel particle. In terms of the dewatering

performance, the dewatering flux of TPU-hydrogel composite almost two times of that of pure hydrogel particles as well. Further study indicated that the hydrophilicity of wet TPU microfibrils and the capillary effect generated by microchannels around them resulted in greatly enhanced water absorption ability and water diffusion rate, and sustained swelling pressure of the polymer hydrogels. The composite hydrogel therefore induced significantly higher forward osmosis water flux and dewatering flux compared to pure hydrogel particles. This study provides a simple and effective strategy for improving water transport through hydrogel structure and sustaining swelling pressure of stimuli-responsive polymer hydrogel, which is very promising for designing high-performance draw agent for forward osmosis application.

In chapter 5, a hydrogel-PET microfibre composite is prepared by compressing the PET microfibrils added during polymerization of hydrogel, and studied as a forward osmosis draw agent. The combination of a hydrophilic ionic hydrogel and a hydrophobic PET microfibre imparted to the composite hydrogel porosity, due to different wettabilities, whilst at the same time providing an additional relaxation force during swelling because of the compression pressure applied during the preparation. As observed in the experiment, the porous structure and the PET microfibre decreased the sizes of hydrogel domains, increasing solvent diffusion. On the other hand, the characteristic exponent  $n$  of the composites decreased with increasing PET microfibre loading and increasing amount of compression. The hydrogel-PET composites exhibited Less Fickian diffusion, indicating that the polymer chain relaxation rate is much faster than the solvent diffusion rate. With regards the forward osmosis application, the water flux of hydrogels is consistent with the swelling kinetics result, i.e., it increased with increasing PET microfibre loading and increasing compression pressure.

In order to study the effect of hydrophilic or hydrophobic microfibrils on the composite draw agent, a relatively hydrophilic polydopamine-modified microfibre (hydrogel-D-PET) was prepared and fabricated with hydrogel to obtain a composite. The composite with hydrophobic microfibre was better at maintaining higher water flux in a long period test, but the dewatering performance reduced. While the addition of hydrophilic microfibre improved both FO water flux and dewatering flux.

This work demonstrates that the performance of forward osmosis hydrogel draw agent is closely related to the swelling properties of hydrogel, and the draw agent performance can be effectively improved by tailoring its swelling properties.

In chapter 6, an amphoteric MOF is fabricated by integrating weak acid groups with weak base groups together in a porous metal organic framework (MOF) to achieve thermally reversible ion sorption property. The feasibility for reversibly adsorbing a wide range of ions has been successfully demonstrated. PDMVBA-p-MIL-121 could adsorb a wide range of other salts including monovalent metal salts (LiCl and KCl) and divalent metal salts (CaCl<sub>2</sub>, MgCl<sub>2</sub>, CuCl<sub>2</sub>, and ZnCl<sub>2</sub>). The amphoteric-functionalized MIL-121 (PDMVBA-p-MIL-121) exhibited a high NaCl adsorption capacity of 0.92 meq/g. Importantly, PDMVBA-p-MIL-121 could be thermally regenerated such as at 80 °C in 500 ppm NaCl solution to release the adsorbed salts, and exhibited excellent cycling performance. This study has extended the functional diversity of MOFs to highly efficient ion adsorption and thermal desorption. In particular, the chemical-free regeneration ability provides a unique functionality for developing high-performance MOF-based ion adsorbents to potentially lower operating costs of water desalination and purification and minimize the environmental impact.

## 7.2 Further Directions

The introduction of responsive ability endows the raw materials with new functionalities, broadens their application, and enhances the relevant water treatment performance, as illustrated in this study. However, the development of stimuli responsive water treatment system with self-cleaning, self-refreshing, energy-saving, or controllable separation abilities is still in an early stage, further development is challenge but highly desired.

*Smart membrane.* 1) The controllable separation process responds rapidly for selective separation, tunable permeation and / or on-off state management, to achieve biomimetic membrane ultimately. 2) Membrane fouling problems can be relieved by improving wettability and the oscillation of responsive component to release attachments. The final objective is self-cleaning membrane and anti-fouling membrane.

*Smart forward osmosis draw agent.* Ideal performance includes: 1) high osmotic pressure for high water flux, 2) low back diffusion, 3) minimal toxicity and low cost, 4) easy and energy-efficient regeneration, 5) good reusability. Importantly, the development of relevant theory or mechanism, and a proper FO unit for continuous water production are particularly crucial.

*Smart adsorbent.* Rapid adsorption, high adsorption capacity, rapid regeneration, easy collection, and good reusability constitute a desired adsorbent.